# University of *Leicester*

# IDENTIFYING THE VULNERABLE CAROTID PLAQUE BY MEANS OF DYNAMIC ULTRASOUND IMAGE ANALYSIS

Thesis submitted for the degree of

Doctor of Philosophy

at the University of Leicester

by

Baris Kanber BSc (Leicester), MSc (Leeds)

Department of Cardiovascular Sciences

University of Leicester

2014

# IDENTIFYING THE VULNERABLE CAROTID PLAQUE BY MEANS OF DYNAMIC ULTRASOUND IMAGE ANALYSIS

## BARIS KANBER

## Abstract

Stroke is a global healthcare problem with very high rates of morbidity and mortality; therefore, early diagnosis and prevention are of paramount importance. Many strokes are caused by atherosclerotic plaques in the carotid arteries, and these are often assessed using ultrasound examinations that include the measurement of the degree of stenosis. However, despite the degree of stenosis being an important clinical marker of disease severity, there is an urgent need for additional parameters that can identify high-risk, vulnerable plaques, which may be more likely to cause stroke regardless of the degree of stenosis.

This thesis describes the development of techniques for measuring plaque characteristics from ultrasound image sequences, testing the hypothesis that parameters obtained from these measurements can help identify vulnerable carotid plaques.

Novel methods to track plaque boundaries in ultrasound image sequences were developed (Chapters 2 and 3). This allowed the dynamic assessment of plaque echogenicity (Chapter 3), a novel method of quantifying plaque surface irregularities (Chapter 4), and the investigation of arterial wall (Chapter 5) and plaque (Chapter 6) mechanics. In the penultimate chapter (Chapter 7), these parameters were integrated in the form of a carotid plaque risk index (CPRI) and its efficacy in predicting the presence of patient symptoms was assessed.

The dynamic measures of plaque echogenicity and the novel plaque surface irregularity index correlated significantly with the presence of patient symptoms. The CPRI, which combines these parameters with the degree of stenosis, improved diagnostic accuracy compared to the degree of stenosis on its own, and led to a better separation of the symptomatic and asymptomatic patient groups.

The methods for characterising plaque characteristics developed in this thesis could be valuable for identifying vulnerable carotid plaques. The risk index, if its efficacy is confirmed in subsequent clinical trials, may help reduce the incidence and burden of stroke.

## Acknowledgements

## Disclaimer

## Declaration

The ultrasound scans used in this thesis were performed by the staff of the Transient Ischaemic Attack Clinic at the University Hospitals of Leicester. Patient recruitment was carried out by medical students Miss Sarah Nduwayo, Mr. James Garrard, and Miss Preeya Ummur. I confirm that all the other work described in this thesis is my own except where it may have been stated otherwise in the text.

Table of Contents

## List of Tables

9

## List of Figures

**List of Abbreviations**

| Abbreviation | Meaning |
|---|---|
| 3D | Three dimensional |
| ACAS | Asymptomatic Carotid Atherosclerosis Study |
| ACS | Acute Coronary Syndromes |
| ACST | Asymptomatic Carotid Surgery Trial |
| AIUM | American Institute of Ultrasound in Medicine |
| ARFI | Acoustic Radiation Force Impulse |
| BMUS | British Medical Ultrasound Society |
| CAS | Carotid artery stenting |
| CC | Common carotid method |
| CCA | Common carotid artery |
| COV | Coefficient of variation |
| CPRI | Carotid plaque risk index |
| $CPRI_{logistic}$ | Carotid plaque risk index (logistic regression based) |
| CSI | Carotid Stenosis Index |
| CT | Computed tomography |
| DOS | Degree of stenosis |
| ECA | External carotid artery |
| ECST | European Carotid Surgery Trial |
| FDA | Food and Drug Administration |
| FDG | Fluorodeoxyglucose |
| FFT | Fast Fourier Transform |
| FMD | Flow mediated dilation |
| GSM | Greyscale median |
| HT | Hough Transform |
| ICA | Internal carotid artery |
| IMT | Intima-media thickness |
| $I_{SPTA}$ | Spatial-peak, temporal-average intensity |
| IVPA | Intravascular Photoacoustic Imaging |
| IVUS | Intravascular ultrasound |
| LACI | Lacunar infarct |

| | |
|---|---|
| MDSV | Maximal discrepant surface velocity |
| MI | Mechanical Index |
| MRC | Medical Research Council |
| MRI | Magnetic Resonance Imaging |
| NASCET | North American Symptomatic Carotid Endarterectomy Trial |
| NCC | Normalized correlation coefficient |
| NEMA | National Electrical Manufacturers Association |
| NHS | National Health Service |
| NIH | National Institutes of Health |
| NIHR | National Institute for Health Research |
| NIRS | Near-infrared spectroscopy |
| NRES | National Research Ethics Service |
| OCSP | Oxfordshire Community Stroke Project |
| OCT | Optical Coherence Tomography |
| PACI | Partial anterior circulation infarct |
| PEP | Percentage echolucent pixels |
| PET | Positron emission tomography |
| POCI | Posterior circulation infarct |
| PVDF | Polyvinylidine difluoride |
| PZT | Lead zirconate titanate |
| RF | Radiofrequency |
| ROC | Receiver Operating Characteristic |
| ROI | Region of interest |
| s.d. | Standard deviation |
| SAPPHIRE | Stenting and Angioplasty with Protection in Patients at High Risk for Endarterectomy |
| SII | Surface irregularity index |
| SOM | Self organising map |
| SUV | Standardized uptake value |
| TACI | Total anterior circulation infarct |
| TCD | Transcranial Doppler |
| TDI | Tissue Doppler Imaging |

| | |
|---|---|
| TGC | Time gain compensation |
| TI | Thermal index |
| TIA | Transient Ischaemic Attack |
| TMM | Tissue mimicking material |
| TOAST | Trial of Org 10172 in Acute Stroke Treatment |
| VCR | Volume compression ratio |
| WFUMB | World Federation for Ultrasound in Medicine |

# Chapter 1

# Introduction

Carotid plaques are atherosclerotic lesions of the carotid artery wall (Figure 1.1). Although the exact mechanisms are not fully understood, the initiation, progression, and rupture of atherosclerotic plaques are thought to be promoted by inflammatory processes that may be the result of endothelial damage or, less frequently, other factors such as infection [1-2]. The presence of the carotid plaque can cause arterial stenosis, a narrowing of the lumen of the carotid artery, and disturb blood flow to the head. Carotid plaques can also act as sources of atheroembolic material or thrombus which may detach, or otherwise emanate, from the plaque, travel in the bloodstream, and block blood flow further down the arterial tree. This process, called embolisation, can result in strokes, cerebral infarctions, and ocular ischaemia. Most strokes in patients with carotid stenosis are believed to be embolic in nature [3].
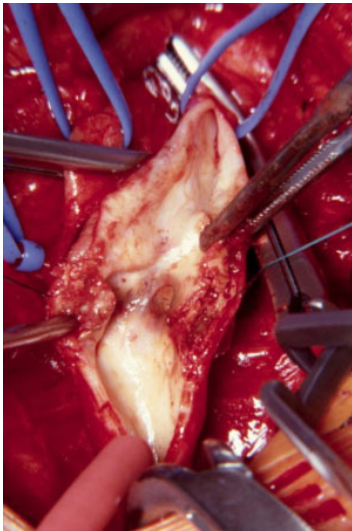


**Figure 1.1** - Plaque in a carotid artery prior to endarterectomy. Used with permission from and courtesy of Professor Brad Johnson of the University of South Florida.

The majority of carotid plaques occur at the bifurcation of the common carotid artery (CCA) into the internal (ICA) and external (ECA) carotid arteries [4]. Having plaques in the carotid arteries increases the risk of stroke and cerebral infarction [3,5]. Hollander et al. found this increase in risk to be approximately 1.5-fold, rising to more than 10-fold when many plaques are present [5]. Although measures such as stenosis severity, maximum plaque thickness, total plaque area are useful and have been associated with increased risk of stroke and other vascular outcomes [6-8], it is recognized that some plaques may be particularly vulnerable or high-risk. Plaque instability, in this respect, is reported to play a major part in the onset of ischaemic events, regardless of the degree of lumen narrowing [9]. Such vulnerable plaques include those which are ulcerated, and those comprising a large lipid pool or necrotic core separated from the bloodstream by a thin fibrous cap. Some of these plaques may already be generating emboli which can be detected using methods such as transcranial Doppler ultrasound (TCD), while others can remain silent and become unstable and rupture suddenly [3,10]. The significance of this thesis is that, if vulnerable plaques can be identified, treatment can be more appropriately tailored, potentially reducing the incidence and burden of stroke.

## 1.1 Stroke

Stroke is a leading cause of death and disability worldwide. It is estimated that 15 million people suffer a stroke each year, with as many as 5 million resultant deaths and 5 million cases of permanent disability [11]. In England, approximately 110,000 strokes occur per year and, according to a report in 2010, there were around 300,000 people living with moderate to severe disabilities as a result of stroke [12]. The cost to the economy has been estimated to be as large as £8 billion[1] per year [12]. In developed countries, stroke accounts for between 2 and 4% of total healthcare expenditure [13].

Stroke occurs when blood flow to or in the head is disturbed, causing cerebral or ocular ischaemia. Depending on the extent of the damage, this can result in transient

---

[1] Direct care costs (cost to NHS), over £3 billion per year.

or permanent symptoms, disability or death. The range of disabilities that may be caused by stroke include paralysis, aphasia, loss of cognitive abilities, partial or complete loss of the visual field, and incontinence [12]. In England, around one in four people who have a stroke die as a result; it is the third leading cause of death, accounting for 10% of all deaths [12]. Globally, 60% of people who suffer a stroke die or become dependent on others [11].

Plaques of the carotid arteries can cause stroke by restricting blood flow to the brain or the eyes, or by being sources of thromboembolic materials which can embolise in the intracranial vascular tree. Some carotid plaques can remain seemingly asymptomatic even when they cause a total obstruction of the artery, yet others cause stroke even when the stenosis severity is low. Therefore, despite a general increase in the risk of stroke with increasing severity of stenosis, some plaques may be more likely to cause cerebrovascular events, and improved identification of such vulnerable plaques could help to prevent stroke.

## 1.2 Classification of Strokes

Strokes are broadly classified into the two types: ischaemic and haemorrhagic. Ischaemic strokes account for approximately 80% to 85% of all strokes [13-15], while haemorrhagic strokes account for the remaining 15% to 20% [13-15]. It is very relevant to the subject matter of this thesis that up to 80% of all ischaemic strokes occur in the areas of the brain supplied by the carotid arteries [4]. In fact, carotid plaques are the underlying cause of the majority of ischaemic strokes [16-17], and the most common source of emboli in stroke originates from the atherosclerotic disease of the carotid bifurcation [18].

There are several classification schemes for further classifying strokes based on the areas of the brain affected, and based on the underlying causes. The Oxfordshire Community Stroke Project (OCSP) classification, for example, categorises strokes as being total anterior circulation infarcts (TACI), partial anterior circulation infarcts (PACI), lacunar infarcts (LACI), or posterior circulation infarcts (POCI). The ending letter I is replaced by the letter H to indicate a haemorrhagic stroke as opposed to an

ischaemic stroke, or the letter S to indicate a stroke of an indeterminate pathogenesis (which may be replaced by the letter I or the letter H following appropriate diagnosis) [19]. The Trial of Org 10172 in Acute Stroke Treatment (TOAST) classification, on the other hand, categorises strokes as being due to either large artery atherosclerosis, cardio-embolism, small-vessel occlusion, other known aetiology, or an undetermined aetiology [20].

## 1.3 Transient Ischaemic Attack

Partial or transient interruption of blood flow to the head, as opposed to a sustained interruption which will typically cause a stroke, can lead to a transient ischaemic attack (TIA) whereby the symptoms normally resolve within 24 hours [11-12]. TIA can manifest itself as a temporary loss of strength or feeling on one side of the body, a transient loss of vision, and other neurological symptoms such as aphasia. It is known that patients who have had a transient ischaemic attack are at an increased risk of having a stroke [21-22]. The early risk of stroke following a TIA is sometimes evaluated using the $ABCD^2$ algorithm [23] where the risk is determined based on clinical features such as age, blood pressure, presence of diabetes and, type and duration of symptoms. The risk of stroke at 2 days can be as large as 8% for $ABCD^2$ scores in the range 6 to 7. However, $ABCD^2$ score cannot identify patients who have significant carotid artery disease or vulnerable plaques [24]. The National Institutes of Health (NIH) Stroke Scale is another scoring technique for risk assessment in patients who present with neurological symptoms, but it is more a measure of stroke severity. Since the risk of stroke is particularly elevated following a TIA, recognition of the symptoms of TIA and stroke are of paramount importance. In the United Kingdom, the Stroke - Act F.A.S.T. campaign (Figure 1.2) aims to raise awareness of stroke/TIA symptoms, which include facial drooping, arm weakness, and speech disturbance; highlighting the significance of seeking urgent medical help.

**Figure 1.2** - A Stroke - Act F.A.S.T. campaign poster (National Health Service, Department of Health).

### 1.4 Stroke Risk Factors

Risk factors for stroke are numerous and include:

- Hypertension;
- Hyperlipidaemia;
- Atrial fibrillation and septal defect (e.g. patent foramen ovale);
- Other heart disease (e.g. coronary heart disease, heart failure, heart attack);
- Impaired glucose tolerance (pre-diabetic hyperglycaemia);
- Diabetes;
- Smoking;
- Previous episodes of TIA/stroke;

- Genetic factors/family history of stroke;
- Alcohol abuse;
- Unhealthy lifestyle (e.g. physical inactivity, obesity) or diet (e.g. high salt intake).

In fact, age is also a risk factor and most strokes affect the elderly. The incidence of stroke doubles with each successive decade over the age of 55, with an overall rate of 0.2 per thousand in those aged 45-54 and 10 per thousand in those aged over 85 [25]. In comparison, the overall incidence rate of stroke is around 2-2.5 per thousand population [25]. However, stroke sometimes occurs in younger patients as well, and is often found to be related to carotid artery stenosis or occlusion [26]. As many as a quarter of strokes that occur in England occur in people under the age of 65, including children [12]. Stroke occurs in about 8% of children with sickle cell disease [11]. Acute ischaemic stroke affects 3.3 of 100,000 children per year [27].

People of African or Caribbean origin and South Asian man are more likely to have a stroke than people from other ethnic groups [12]. African-Caribbean and African men and women have approximately double the risk of stroke compared to the Caucasian population [25]. Hispanics have also been reported to have greater incidence of stroke compared to Caucasians [28].

Stroke is also more common in men than women, but women who have a stroke are more likely to die as a result [12,25]. The latter is largely attributable to the higher mean age of stroke onset in women, but men have an overall 25-30% increased risk of having a stroke [25]. A recent study found that females had significantly more intra-plaque neovascularisation than males [29]. Neovascularisation, the formation of micro-vasculature within plaques, is considered to be a possible cause of plaque instability and a characteristic feature of a more vulnerable plaque type (section 1.7).

The incidence of stroke also appears to be influenced by socio-economic class, with people in the lowest social class having a 60% increased risk of having a stroke compared to those in the highest social class [25].

Other factors that may increase the risk of stroke include antiphospholipid antibodies, hyperhomocysteinemia, inflammation, infection and periodontal disease [28,30-35]. Recently, plaque inflammation (macrophage infiltration) was found to be an independent predictor of recurrent events in stroke patients [36].

Finally, having a carotid plaque is a risk factor for stroke. This is highly relevant to the subject matter of this thesis. In fact, it has recently been reported that patients with carotid plaques may exhibit cognitive decline even when they are seemingly asymptomatic [37]. Therefore, the diagnosis of carotid plaques, particularly those which are vulnerable or unstable, is crucial.

## 1.5 Grading of Carotid Artery Stenosis

Several methods, based on the measurement of arterial lumen diameters in normal and stenosed regions of arteries, are used to quantify the degree of carotid artery stenosis. The North American Symptomatic Carotid Endarterectomy Trial (NASCET) calculated the degree of stenosis as the percentage reduction in the lumen diameter at the stenosed region of the artery, taking the lumen diameter distal to the stenosis as the baseline diameter [38]. The European Carotid Surgery Trial (ECST) employed a similar method but used the estimated normal diameter of the artery, instead of the lumen diameter distal to the stenosis, as the baseline diameter [39]. The common carotid (CC) method is also similar; it uses the diameter of the common carotid artery in the proximity of the carotid bulb as the baseline figure [40]. Another measure that has been developed is the Carotid Stenosis Index (CSI), and is based on the estimation of the proximal internal carotid artery diameter as 1.2 times the diameter of the common carotid artery [41]. It is similar to the other techniques otherwise.

Despite the use of various different methods, the rationale in each case is the same: the degree of stenosis is estimated using a percentage lumen diameter reduction technique whereby the percentage reduction is estimated as the reduction in the lumen diameter of the artery due to stenosis divided by a baseline diameter that would be considered normal. Following the measurement of the degree of stenosis,

arteries are often categorized as normal, mildly stenosed (1-29%), moderately stenosed (30-69%), severely stenosed (70-99%), or occluded [42]. Despite the similarities, there are important discrepancies in stenosis severity measurements made using the individual techniques. These discrepancies are also apparent in the case of the NASCET and ECST methods, which are most widely used in clinical and research practice [43].

In addition to the measurement of the degree of stenosis based on lumen diameter changes, Doppler ultrasound evaluations based on blood velocity criteria and flow characteristics, such as the presence of turbulence and spectral broadening, are also used [44]. In essence, these velocity measures are based on estimating the degree of stenosis by means of stratifying blood flow velocities or velocity-based ratios such as the internal carotid artery peak-systolic flow velocity divided by the common carotid artery end-diastolic flow velocity (St Mary's ratio) or the internal carotid artery peak-systolic flow velocity divided by the common carotid artery peak-systolic flow velocity (PSV ratio) [44-46]. Stenosis severity measures based on blood flow velocity measurements are particularly useful when it is difficult to measure the residual and normal arterial lumen diameters; this is often the case when the percentage diameter reduction is large (e.g. greater than 70%) and there is severe plaque build-up. In fact, Doppler ultrasound based velocity criteria are used more commonly in clinical practice, compared to percentage lumen diameter reduction, to determine the degree of carotid artery stenosis [47]. The use of percentage reduction in the transverse, cross-sectional lumen area, obtained from CT angiography, has also been considered for estimating the degree of stenosis, but this is suggested as an alternative for diameter-based estimations when additional imaging beyond ultrasonography is deemed necessary; for example, if the ultrasonographic assessment does not result in a diagnosis, or if carotid arteries not readily accessible by ultrasound require evaluation [48]. The degree of stenosis is an important parameter that is strongly associated with the risk of stroke in symptomatic patients, and it is often used for clinical decision making [16].

## 1.6 Composition of Carotid Artery Plaques and Histology

The composition of carotid artery plaques can vary greatly; the following are some of the important components that can be found:

- Lipids;
- calcium;
- vascular smooth muscle cells;
- macrophages;
- foam cells;
- other leukocytes (e.g. lymphocytes, neutrophils);
- extra-cellular matrix;
- collagen;
- elastin;
- necrotic cell debris;
- neovascularisation;
- intra-plaque haemorrhage.

Histology is useful for studying plaque specimens that have been collected during carotid endarterectomy and allows an assessment of the composition and morphology of the plaque to be made *ex vivo*. The American Heart Association classification of atherosclerotic plaques is based on the histological assessment of plaque structure and composition [49-50]. Using histological assessment, Salem et al. found that among the TIA clinic patients with severe carotid artery stenoses, who were scheduled to have carotid endarterectomy, those who had recurrent ischaemic events before the scheduled surgery took place, had evidence of large lipid cores in their plaques [51]. Although there is evidence that symptomatic and asymptomatic plaques could have the same histological components [52], their configuration is likely to affect the risk posed by the plaque. Plaques which are fibrotic or calcified, for example, can become vulnerable if they are complex plaques with surface defects or haemorrhage which have so far remained silent [52]. The composition of plaques also evolves over time. A multi-centre study found that symptomatic patients with recent symptoms had more soft tissue content in their plaques than those with distant symptoms, suggesting not

only that plaque composition may change over time after the onset of symptoms, but also that symptomatic patients with more distant symptoms might be regarded as asymptomatic and treated conservatively [53].

Although histology is regarded as the gold standard for studying plaque composition, it does have some important limitations. First is the removal of calcium and lipids during histological preparation which can also affect the structural integrity of atherosclerotic plaques [54]. Secondly, and importantly, histological assessment of plaque composition can only be carried out *ex vivo*; thus is only useful for investigating plaque vulnerability retrospectively.

## 1.7 Causes of Plaque Instability

The exact mechanisms by which plaques become unstable are not fully understood [55]. Ulcerations, intra-plaque haemorrhage, inflammatory processes and the rupture of plaque are amongst the several possible causes of carotid plaque instability [36,56-58]. In the context of inflammatory response, baseline neutrophil count was recently found to be an independent predictor of mortality in neurologically asymptomatic patients with carotid artery stenosis [1]. Plaques which have a large lipid core separated from the bloodstream by a thin fibrous cap may rupture by means of an inflammatory process involving foam-cell infiltration of the fibrous cap [59].

Plaques can also become unstable due to the physical forces present upon them, and it has been suggested that mechanical stresses due to the motion of the plaque and the arterial wall may lead to minor cracks and fissures [60], and any relative motion between the two could cause plaque disruption due to the rupture of the vasa vasorum [60-62]. Shear stress due to blood flow can also influence the stability of plaques [63]. Studies have found that plaque neovascularisation and haemorrhage relate to adverse cardiovascular outcome during follow-up and it has been suggested that plaque vascularisation and haemorrhage are important causes of plaque progression, as well as important mechanisms of plaque disruption leading to atherothrombotic events [64-66]. Dunmore et al. studied carotid plaques collected after endarterectomy and found that symptomatic plaques contained abnormal, immature

microvessels similar to those found in tumours and healing wounds and concluded that such vessels could contribute to plaque instability by acting as sites of vascular leakage and by the recruitment of inflammatory cells [66]. These vessels were dilated, highly irregular and dysmorphic; they lacked vascular smooth muscle cells, and vascular endothelial growth factor colocalized with macrophages were found adjacent to them [66]. Loss of the extracellular matrix in the fibrous cap due to matrix degrading enzymes and the death of matrix synthesizing smooth muscle cells is also thought to play a role in plaque rupture [67].

Apoptosis (programmed cell death) of vascular smooth muscle cells in atherosclerotic plaques in mice has been found to induce features of plaque vulnerability including marked thinning of the fibrous cap, loss of collagen and matrix, accumulation of cell debris (enlargement of the necrotic core), elastin breaks, and intense intimal inflammation [68-70]. Strikingly, low-level vascular smooth muscle cell apoptosis has been found to promote calcification within established plaques in mice, a feature generally considered to be suggestive of plaque stabilisation [69]. Leukocyte mitochondrial DNA damage has also been found to associate with plaque vulnerability in humans [71]. Systemic factors such as infection, autoimmunity, or genes may also be important determinants of plaque instability [63].

## 1.8 Evaluation of the Carotid Plaque

There exists a wealth of techniques for evaluating the carotid plaque. Catheter or conventional angiography is an invasive technique that involves the introduction of an iodine based contrast material into the bloodstream and the subsequent acquisition of x-ray images. Because of the use of contrast materials, it is in contra-indicated in many situations including in patients with impaired kidney function. The procedure of catheter angiography itself is associated with a risk of stroke as large as 1% and a form of neurological complication occurs in as many as 4% of the patients [72]. Although angiography has traditionally been considered the gold standard for diagnosis, it also has several limitations for studying plaque morphology [73]. The degree of stenosis can be adequately assessed using this technique [73-75] but the evaluation of plaque surface ulceration is subject to a high degree of inter-observer

variability [73,76]. The images obtained using this modality reflect the absorption of x-rays by the contrast material in the bloodstream; they show the normal and residual arterial lumens, but do not provide information on the composition of the plaque. Angiography has low discriminatory power to identify the vulnerable plaque, but does provide abundant information on the local arterial tree and can serve as guide for therapy [77]. Computed tomography (CT) angiography uses computed tomography techniques also in combination with x-rays to obtain images of the carotid arteries. Contrast material is injected into a vein and a three dimensional picture is assembled using projection x-ray data provided by a rotating x-ray source/detector gantry. CT angiography shares most of the disadvantages of conventional angiography.

Magnetic resonance imaging (MRI) with or without contrast agents can also be used to evaluate the carotid arteries and plaque [17,78]. MRI can provide image contrast corresponding to plaque composition (e.g. identify and evaluate a fibrous cap, a necrotic core or lipid pool) and does not involve the use of ionizing radiation. MRI can also be used to study intra-plaque haemorrhage [17,56,78-79] and evaluate wall stress which has been shown to be higher in symptomatic patients compared with the asymptomatic [80]. Hatsukami et al. collected MRI data, using a 3-dimensional multiple, overlapping, thin-slab angiography protocol, from 22 patients who were scheduled for carotid endarterectomy, and compared the MRI appearance of the fibrous cap with histological findings [81]. Their results indicated that this MRI angiography protocol was capable of distinguishing intact, thick fibrous caps from the intact and thin, and from disrupted fibrous caps, *in vivo*. Watanabe et al. investigated whether MRI of the carotid arteries can differentiate high-risk soft plaques from solid fibrous plaques more accurately than using ultrasound and found that the sensitivity, specificity, and accuracy for diagnosing high-risk soft plaques were 96, 93 and 94%, respectively for MRI and 75, 63, and 69% for ultrasound [18]. However, the ultrasound assessment in that study was based on a subjective, visual classification system [82]. The disadvantages of MRI based techniques include the high-cost of magnetic resonance imaging and susceptibility to image artefacts. Three dimensional (3D) MRI imaging can improve the characterisation/visualisation of small structures, but sensitivity to motion artifacts is higher with 3D MRI [83].

Angioscopy is also a relevant imaging technology, and involves the direct imaging of the arterial lumen using a miniaturized high resolution camera introduced invasively into the lumen of the blood vessel. The technique is, however, difficult to perform and is limited in terms of applicability [77]. Tissues are significantly opaque to light and angioscopy can only be used to image the internal surfaces of the arterial lumen. Also, since the arterial lumen is blood-filled, other difficulties with the imaging technique arise. Angioscopy can be used to image plaque surfaces and intra-luminal structures like thrombi and tears [77]. Thermography is another catheter based technique involving the formation of images based on local tissue temperatures. It can be used to investigate temperature variations associated with inflammatory processes. Temperature heterogeneity is assessed as an indicator of the metabolic state of the plaque; a coincidence of temperature rises and localisation of vulnerable plaque features is suggested [77]. Optical coherence tomography (OCT) can produce images of very high resolution (10-30 um) but is an intravascular/*ex vivo* imaging technique and the penetration depth is very low (typically 1 to 2 mm) corresponding to the use of near-infrared light sources [84-86]. Several studies have found that OCT images can be highly sensitive for characterizing atherosclerotic plaques [85-86]. Near-infrared spectroscopy (NIRS) is another optical technique which may help identify the lipid content of plaques [77]. Raman spectroscopy can be used to quantify the molecular composition of the plaque, but acquisition times are long with a low penetration depth due to the absorption of light by blood.

Atherosclerotic plaque inflammation can also be studied by the use of radioisotopes, for example, plaque inflammation estimated as the maximum standardized uptake values (SUV) of fluorine-18 radioisotope labelled fluorodeoxyglucose (FDG) using positron emission tomography (PET) [87]. Tawakol et al. found that intensive statin therapy produces significant and rapid, dose-dependent reductions in FDG uptake that may represent changes in atherosclerotic plaque inflammation, concluding that FDG-PET imaging may be useful for detecting early treatment response [88].

Duplex ultrasonography is also extensively used to assess the carotid arteries and the carotid plaque. Like MRI, ultrasonography does not involve the use of ionizing radiation, but, unlike MRI, it is significantly more convenient, costs significantly less

and is more widely available. A wealth of information can be obtained on the carotid arteries and the carotid plaque using duplex ultrasonography (section 1.9) and this thesis is concerned with the identification of vulnerable plaque features using this technique. Other ultrasound-based methods are also available and include intravascular ultrasound (IVUS), an invasive technique involving the introduction of a catheter incorporating an ultrasound transducer into the artery. IVUS allows images of higher resolution to be obtained providing insight into the composition of plaques, and with the use of contrast agents, it can identify surface defects such as ulcerations, the vasa vasorum and neovascularisation. IVUS can also be used to study the mechanical properties of the arterial wall and the plaque by means of an elastography technique termed IVUS elastography. This involves estimating the plaque and vessel wall strain using the depth-gated cross-correlation of radiofrequency IVUS data obtained at varying intraluminal pressures [89-91].

Intravascular palpography is a very similar technique but limits the strain assessment to the surface of the plaque (the first 450 μm layer). This has been reported to be faster, more robust, and easier to interpret than IVUS elastography [90-92]. It can differentiate between deformable and non-deformable tissues, which may enable the detection of vulnerable plaques [77]. Non-invasive assessment of intra-plaque strains in the longitudinal cross-section using radiofrequency ultrasound data and block matching/cross-correlation methods are also active areas of research [93-94]. Acoustic Radiation Force Impulse (ARFI) imaging is another non-invasive ultrasound technique that can characterize the mechanical properties of tissues in terms of tissue strain, potentially differentiating soft and hard plaques [95]. Shearwave elastography, on the other hand, allows the stiffness of tissues in terms of the elastic modulus to be measured. Colour maps indicating local tissue stiffness can be overlaid on top of greyscale ultrasound images, allowing the visualization and measurement of the stiffness distribution in tissue. This technique has already been found to be useful in breast and liver sonography; applicability to vascular ultrasound is under investigation [96]. Earlier forms of elastography were based on the application of a force by the operator (e.g. pushing down on the probe) and measuring of the resulting deformation. In sonoelastography, an externally applied low-frequency vibration was used to generate tissue stress. Tissue Doppler Imaging (TDI) is another, non-invasive

ultrasound technique that may be used to study the carotid arteries and the plaque. TDI has been used to investigate the motion of the arterial wall in healthy individuals and patients with atherosclerotic plaques [97].

Intravascular photoacoustic imaging (IVPA) is a new technique that complements IVUS, and has been shown to provide image contrast corresponding to lipid, calcium, macrophage[1], and matrix metalloproteinase[2] composition of plaques [98-100]. The method is based on the detection[3] of acoustic waves generated within tissue due to thermal expansion as a result of irradiation with a pulsed laser [101-103]. Studies have employed IVUS/IVPA imaging catheters consisting of a single-element ultrasound transducers and a light delivery systems based on a single optical fibres in animal models and *ex vivo* samples of atherosclerotic human aortas and coronary arteries, finding good agreement with histology [99-100,102,104-110]. Another study introduced thermal IVPA, and found that this technique was capable of differentiating between lipid component of plaques and lipid in periadventitial tissues in an *ex vivo* investigation of the atherosclerotic rabbit aorta [111]. The method exploited the temperature dependency of the photoacoustic signal amplitude and differentiated between the two lipid components by comparing photoacoustic signals measured at different temperatures.

Transcranial Doppler (TCD) can be used to monitor emboli entering cerebral circulation; it is widely used during surgery. Barbut et al. found embolic particle diameters ranging from 0.3 to 2.9 mm (mean 0.8 mm) in the aorta during coronary artery bypass grafting [112]. Twenty-eight percent of particles measured 1 mm or more, 44% measured 0.6 to 1.0 mm, 27% measured 0.6 mm or less in diameter [112]. A variable fraction of these emboli (3.9 to 18.1%) was found to subsequently enter cerebral circulation via the middle cerebral artery [112]. Topakian et al. found a significant association between embolic signals in the middle cerebral artery and an increased risk of ipsilateral stroke during their 2 year follow-up study of 435 patients with asymptomatic carotid artery

---

[1] Using contrast agents.

[2] Using contrast agents.

[3] Spectral analysis is performed in the case of spectroscopic intravascular photoacoustic imaging.

stenosis greater than or equal to 70% [113]. In order to characterise plaque composition using ultrasound, some studies have used radiofrequency ultrasound data to calculate parameters such as the integrated backscatter, attenuation coefficient/slope and scatterer size [114-119]. Three-dimensional ultrasound systems are also becoming more widely available with some new display technologies, such as fly-through ultrasound, displaying intraluminal structure in a manner similar to endoscopy [120].

## 1.9 Ultrasound Evaluation

Ultrasound is a widely used diagnostic platform for studying the carotid arteries and plaque (Figure 1.3), permitting the non-invasive evaluation of carotid artery stenosis, plaque characteristics, blood flow, disease progression, and response to treatment [121]. It is relatively low-cost, convenient and does not involve the use of ionising radiation. The procedure is not very time consuming and is relatively comfortable. In the case of the TIA clinic patient, the ultrasonographic assessment of the carotid arteries may include, in addition to the visualisation of any plaques or intimal thickening, the measurement of normal and residual arterial lumen diameters and/or blood flow velocities. This allows the healthcare professional to establish the presence of any apparent carotid artery disease, and measure the degree of stenosis if a narrowing is present.

In addition to the measurement of the degree of stenosis, there has been growing interest in utilizing the additional data available in ultrasound scans, which may help characterise the plaque. This is a sensible avenue for research since two different plaques causing the same degree of stenosis in terms of diameter reduction or blood velocity changes can potentially pose different levels of risk in terms of plaque vulnerability or actual stroke risk.
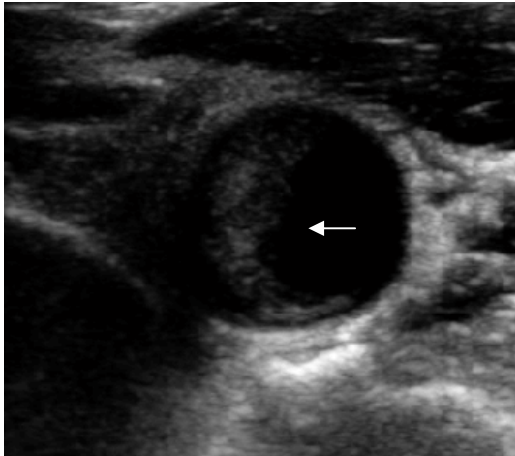
**Figure 1.3** - B-Mode ultrasound image of a carotid artery with plaque (arrow) in transverse cross-section.

Several properties of carotid plaques related to plaque appearance and dynamic behaviour have been studied; there is considerable evidence that ultrasound may be able to detect specific carotid plaque characteristics that relate to vulnerability [122]. Gomez [73], for example, reported that individuals who appear to be at a higher risk of stroke are those with heterogeneous plaques, particularly if the plaque narrows the arterial lumen diameter by more than 70% to 75%. Geroulakos et al. [123], on the other hand, provided a review of the evidence supporting the hypothesis that carotid plaque surface characteristics and internal structure as seen on ultrasound may be independent predictors of the risk of stroke, and concluded that ultrasonographic plaque morphology should be used together with other local risk factors in prospective studies which aim to identify the subgroup of patients at high risk of stroke.

In early studies, plaques were simply and subjectively classified as having a heterogeneous or homogeneous ultrasonographic appearance and as being echolucent/hypo-echoic or echogenic/hyper-echoic. One study, for example, categorised plaques into four groups (Table 1.1) based on the qualitative assessment of sonographic appearance [124]. In fact, many qualitative and quantitative parameters characterising the carotid plaque may be obtained using ultrasonography; these are discussed in the sections that follow.

**Table 1.1** - The four plaque categories described by Gray-Weale et al.

| Type | Description |
|------|-------------|
| 1 | Predominantly echolucent plaques with a thin echogenic cap. |
| 2 | Substantially echolucent lesions with small areas of echogenicity. |
| 3 | Dominantly echogenic lesions with small areas of echolucency. |
| 4 | Uniformly echogenic lesions, equivalent to homogeneous. |

### 1.9.1 Plaque Morphology and Texture

Texture and morphology refer to the sonographic appearance of carotid plaques. This appearance depends on the shape and size, and composition of plaques, and their interaction with the ultrasound beam. Lipids, for example, are relatively weakly scattering and tend to have a darker texture, while calcium rich structures are strongly attenuating with a large acoustic impedance compared to most other structures, giving rise to a bright texture pattern, typically with ultrasonic shadowing. It is, therefore, plausible that parameters obtained from the ultrasonographic appearance of plaques may be useful surrogate markers of the actual plaque morphology and composition and are widely investigated.

Lal et al., for example, performed pixel distribution analysis of the B-Mode ultrasound carotid plaque image by means of determining the echogenicity of specific tissues (e.g. blood, lipids, calcium, and fibro-muscular tissues) in control subjects and using these to quantify tissue types in the ultrasound images of carotid plaques [125-126]. In the control subjects, the following anatomical areas were examined: subcutaneous fat (abdomen), muscle (biceps), fibrous tissue (iliotibial tract), and calcium rich structures (tibia and skull). The plaques were further characterised using histology following carotid endarterectomy. The results of the pixel distribution analysis for blood, lipids, fibro-muscular tissues and calcium correlated significantly with the histological findings [125]. Furthermore, a significantly higher amount of blood (intra-plaque haemorrhage) and lipids were found in symptomatic plaques compared with the

asymptomatic [125-126]. In contrast, larger amounts of calcification were found within asymptomatic plaques. In symptomatic plaques, lipid cores were found to be larger and closer to the boundary between the plaque and the arterial lumen [126]. Plaque morphology can affect blood flow patterns, which may also have a bearing on the risk of stroke and other cerebrovascular events [127]. Thrombus formation, for example, may be accelerated in regions of slow or recirculating flow, high shear and increased turbulence [127].

Some investigators used more abstract methods to characterize the ultrasound appearance of carotid artery plaques. Tsiparas et al., for example, used three multi-scale transforms with directional character to characterise atherosclerotic plaques from their B-Mode ultrasonographic appearance (20 plaques of which 11 were symptomatic); they attempted to discriminate between the plaques that caused symptoms and those that did not [128]. The transforms used were the dual-tree complex wavelet transform, the finite ridgelet transform and the fast discrete curvelet transform. They took the standard deviation and entropy of the transform sub-images as texture features, and used a support vector machine trained using the bootstrap technique to classify the samples. The authors found that the curvelet transform achieved the best classification performance, which was 84.9% for images corresponding to peak systole and 73.6% for images corresponding to end diastole. The different classification performances obtained for the different phases of the cardiac cycle were attributed to the possibility of variations in the allocation of materials within the plaque throughout the cardiac cycle, thus reflecting in the texture analysis. However, it is more likely, as will be shown in Chapter 3, that this may be due to out-of-plane plaque, patient or probe motion, which change the actual two-dimensional plaque cross-section being imaged. The main drawbacks of this study were the limited sample size and its abstract nature.

### 1.9.1.1 Plaque Echogenicity and Heterogeneity

Several studies have found that echolucent plaques, irrespective of the degree of stenosis, may be associated with the presence of cerebrovascular symptoms [61,129-131], an increased risk of stroke [113,132-136], and the presence of ipsilateral

hemispheric brain infarcts [137]. Similar increases in the risk of stroke and perioperative embolic complications in carotid artery stenting have also been reported [138-139]. Græbe et al. found a negative correlation between plaque echogenicity and $^{18}$F-FDG uptake, indicating that echolucent plaques may be more likely to have inflammation; the latter is thought to relate to plaque vulnerability and cap rupture [87]. A study by Biasi et al. found that computerised analysis of plaque echogenicity was better than the degree of stenosis in indentifying plaques associated with brain infarcts [140]. Recently, Salem et al. reported that plaque echolucency had a relationship to recurrent cerebrovascular events in patients scheduled to have carotid endarterectomy, before surgery took place [51]. The echolucent carotid plaque has also been found to be an independent predictor of acute coronary syndromes (ACS), suggesting that ultrasound examination of carotid arteries may be helpful for screening populations at high risk of ACS [141].

Holdsworth et al. studied the relationship between carotid plaque heterogeneity and the degree of stenosis and found that at less than 20% stenosis only 4.4% of plaques were heterogeneous while at 80-90% stenosis 84.5% of the plaques were heterogeneous [142]. AbuRahma et al. also compared carotid plaque heterogeneity with the severity of stenosis and found that the higher the degree of stenosis, the more likely it was to be associated with heterogeneous plaques and symptoms [143]. They also found that plaque heterogeneity was more positively correlated with symptoms than with the degree of stenosis, and pointed out that it may be necessary to consider the plaque heterogeneity during the selection of patients for carotid endarterectomy [143]. In contrast, El-Barghouty et al. reported that symptomatic carotid plaques and plaques associated with cerebral infarctions were less heterogeneous than asymptomatic plaques and plaques not associated with cerebral infarctions [133]. Tegos et al. also found that homogeneous echo-patterns were more prevalent among plaques that were associated with symptoms, compared to asymptomatic plaques [131]. Topakian et al. found a significant association between echolucent plaques and an increased risk of ipsilateral stroke during a 2 year follow-up of patients with asymptomatic carotid artery stenosis.

There appears to be a general consensus that plaque echolucency increases the risk of stroke and other cerebrovascular events, which is broadly in agreement with the expectation that soft plaques (e.g. lipid rich, necrotic or haemorrhagic) may be more vulnerable than hard plaques (calcified or fibrous) [131,133]. It has been reported that fibrous (hard) plaques can sometimes have an echolucent presentation [18], although pathology studies have found fibrous content, in general, to be significantly greater for echogenic plaques compared with the echolucent ones [144-145].

In contrast with plaque echolucency, some studies found the presence of cerebrovascular symptoms to be associated with heterogeneous plaques, while other studies found associations with homogeneous plaques [131,133,143]. These discrepant results may be partly due to the different methods of homogeneity assessment used. AbuRahma et al., for example, used a qualitative assessment scheme in which plaques displaying a mixture of hypoechoic, isoechoic, and hyperechoic regions were categorised as being heterogeneous, while plaques having only one of these qualities were defined to be homogeneous [143]. El-Barghouty et al., on the other hand, evaluated plaque heterogeneity as the difference between the greyscale medians (section 1.9.1.1.1) of the most echogenic and most echolucent regions of plaques, expressed as a heterogeneity index [133].

### 1.9.1.1.1 The Greyscale Median (GSM)

One of the simplest parameters that can be used to quantify the ultrasonographic appearance of carotid plaques is the first-order statistic greyscale median (GSM), the median greyscale intensity of the pixels making up the plaque ultrasound image[1]. The greyscale median has been found to be a potential indicator of carotid plaque vulnerability with several studies finding associations between plaque GSM and plaque inflammation [87], the presence of ipsilateral brain infarcts [129,132-133,137], the presence of cerebrovascular symptoms [146], and an increased risk of stroke during and after carotid artery stenting (CAS) [138]. A brief review of the literature that has been published up to date on plaque GSM/echogenicity is presented in this section.

---

[1] At 8-bit resolution, greyscale intensity has $2^8$ or 256 levels ranging between 0 (the least echogenic) and 255 (the most echogenic).

In one of the earlier studies looking at the echogenicity of carotid plaques, Geroulakos et al. classified 105 carotid artery plaques causing greater than 70% stenosis in the internal carotid artery into four types: echolucent plaques, predominantly echolucent plaques, predominantly echogenic plaques and echogenic plaques and carried out a comparison against brain CT findings [130]. Their results showed an increased incidence of ipsilateral brain infarcts in echolucent plaques (37%) compared with 18% in the other 3 plaque types combined (p less than 0.02). Subsequent to this, Iannuzzi et al. carried out a retrospective analysis of ultrasonographic plaque data from 242 stroke and 336 transient ischaemic attack (TIA) patients and found an association between hypo-echoic carotid plaques (odds ratio=3.0, p=0.005) and ipsilateral brain involvement in TIA patients [61]. El-Barghouty et al. also found a similar relationship: they found that in 87 patients with 148 plaques producing more than 50% internal carotid artery stenosis, who had CT brain scans to establish the presence of any ipsilateral cerebral infarction, plaques with a GSM more than 32 were associated with an incidence of 11% (7/64) CT infarction, while GSM below or equal to 32 were associated with 55% (46/84) incidence of CT infarction (p less than 0.001, relative risk = 22) [132-133]. These results suggested that the assessment of plaque GSM may help identify high-risk lesions, namely lesions associated with ipsilateral brain infarcts. A follow-up study confirming the association between plaque GSM and cerebral infarctions was published a year later; this study involved 190 patients with 329 carotid plaques, in which 161 plaques were from asymptomatic sides and 168 were symptomatic [133].

The earlier studies highlighted an important problem with the measurement of GSM. This was the variability of individual GSM measurements when compared between studies. It was suggested that this was likely to be due to the non-standardized acquisition settings used in different studies. It was possible to change the gain settings on ultrasound equipment, resulting in brighter or darker ultrasound images. Other scanner settings such as the greyscale transfer curve and dynamic range were also likely to have marked effects. In order to reduce this variability, Elatrozy et al. attempted to standardise the ultrasonic images of carotid plaques by means of

specifying certain acquisition settings to be used for carotid artery scanning and normalizing the resultant images [129,147-148]. These settings were:

> **The text in this section has been removed from the electronic version of this thesis due to copyright restrictions. Please refer to the appropriate reference(s) or the full thesis available at the University of Leicester Library.**

Normalization was performed by linearly scaling the resultant images so that the GSM of an operator selected blood region fell in the range 0 to 5 and that of the brightest part of the adventitia on the same side as the plaque fell in the range 185 to 195 [148]. A consensus report had suggested the use the mastoid muscle and cervical vertebrae, in addition to blood, as reference structures but the use of blood and adventitia as reference structures has the benefit that these can normally be selected close to the plaque and are easier to include in the same ultrasound cross-section as the plaque [137,149]. Other studies assessed the echogenicity of plaques using qualitative classification schemes taking blood in the vessel lumen and the far wall of the artery

---

[1] This controls the assignment of greyscale values for image formation.

as reference structures [136,150-151], sometimes using the intima-media complex of the far wall of the artery as a single reference [152].

The results of the study by Elatrozy et al. showed that, upon standardisation, the coefficient of variation among 4 different observers was 4.7% for the plaque GSM [129]. The GSM of symptomatic plaques was lower (21±14.8) than asymptomatic plaques (38±26). They found that the GSM and the percentage echolucent pixels (PEP) were the most significant variables (p=0.001) that were related to the presence or absence of ipsilateral hemispheric symptoms [129].

The study by Polak et al. was not quantitative but investigated the association between incident first stroke and echogenicity of plaques by following a cohort of over 4,000 individuals, who were 65 years of age or older and without symptoms, for an average of 3.3 years [135]. Their results showed that in asymptomatic patients aged 65 years or older, the risk of incident stroke was associated with two ultrasound findings: hypo-echoic carotid artery plaques and a degree of carotid artery stenosis greater than or equal to 50%. In a cohort of 96 patients with carotid stenosis in the range 50-99% (41 symptomatic, 55 asymptomatic), Biasi et al. quantitatively evaluated plaque echogenicity using the GSM [140]. They found that the GSM was better than the degree of stenosis in identifying plaques associated with an increased incidence of CT scan determined brain infarction. The incidence of ipsilateral brain infarctions was 20% when the degree of stenosis was less than 70%, and 25% when the degree of stenosis was greater than 70%. On the other hand, the incidence of ipsilateral brain infarctions was 40% for GSM less than 50 compared with 9% for GSM greater than 50 (p less than 0.001).

Using image normalisation, Sabetai et al. assessed the reproducibility of GSM measurements in 232 asymptomatic carotid plaques (stenosis range 60% to 99%) and correlated their results with the presence of ipsilateral CT-demonstrated brain infarcts. The normalized GSM of plaques associated with ipsilateral, silent, CT-demonstrated brain infarcts was 14, while that of plaques that were not so associated was 30 (p = 0.003). The authors found that the normalization technique used increased the reproducibility of the GSM measurements across different recoding media (e.g. VHS

tape or hard-copy) and (linear) scanner probes used (p<0.001). When Grønholdt et al. tested the hypothesis that stroke development can be predicted by the echolucency of carotid plaques, they found that echolucent plaques causing a degree of stenosis 50% or more, determined using Doppler ultrasound, were associated with risk of future strokes in symptomatic but not asymptomatic patients [134]. In symptomatic patients, the relative risk of ipsilateral ischaemic stroke for echolucent plaques compared to echogenic plaques was 3.1 (95% confidence interval, 1.3 to 7.3). On the other hand, for 80-99% stenosis compared to 50-79% stenosis, the relative risk was only 1.4 (95% confidence interval, 0.7 to 3.0).

In a cross-sectional study involving 127 symptomatic and asymptomatic plaques, Tegos et al. found that the symptomatic status was associated with plaques of low GSM (10.5) and predominant homogeneous echo-pattern, while asymptomatic plaques had high GSM (28) and a less predominant homogeneous echo-pattern (p=0.001 for GSM and 0.003 for homogeneity) [131]. Ruiz-Ares et al. also found that symptomatic plaques had lower GSM than asymptomatic plaques, although they found different mean values for the two groups (20.0 versus 29.0, p=0.002) [146]. Christodoulou et al. collected a total of 230 plaque images which were classified into two types: symptomatic because of ipsilateral hemispheric symptoms, and asymptomatic in the absence of ipsilateral hemispheric events [153]. They extracted ten different texture feature sets and shape parameters (a total of 61 features including the GSM) from manually segmented plaque images and found a high degree of overlap between the symptomatic and asymptomatic groups, making the separation of the two groups difficult. The authors used the extracted feature sets as input for a modular neural network composed of self organising map (SOM) classifiers, achieving an average diagnostic yield of 73.1%. In a study of 418 cases of carotid artery stenting (CAS) from 11 international centres, Biasi et al. found that carotid plaque echolucency (defined in the study as a GSM of 25 or less) increased the risk of stroke during and after CAS [138]. They recommended that, in addition to measures such as the degree of stenosis, plaque GSM should also be taken into account in the planning of endovascular treatments.

Golemati et al. measured GSM at peak systole and at end diastole in 10 symptomatic and 9 asymptomatic plaques and reported that the GSM did not vary significantly between these two phases of the cardiac cycle [154]. They concluded that an image corresponding to any phase of the cardiac cycle may be used to estimate plaque echogenicity. The authors did, however, point out the need for further experiments to support this finding: they suggested that very compliant plaques may change shape during the cardiac cycle and a change in their echogenicity may be observed. However, a limitation of this study was that it had a very small number of plaque samples. Golemati et al. also did not find a statistically significant difference in the various echogenicity descriptors they studied, including the GSM, between symptomatic and asymptomatic plaques, in the small group (19 symptomatic and asymptomatic plaques) they investigated [154]. Lind et al. related the GSM of the intima-media complex of the common carotid artery to the echogenicity of the carotid plaque in 582 subjects and found that GSM of intima-media complex had a correlation to the plaque GSM (r=0.60, p<0.0001) independent of plaque size and the intima-media thickness [155]. GSM of the intima-media complex was also found to correlate significantly with the visually estimated echogenicity of the plaque [155].

In a study looking at plaque inflammation, Græbe et al. compared plaque GSM in 33 patients with plaque inflammation estimated as the maximum standardized uptake values (SUV) of fluorine-18 radioisotope labelled fluorodeoxyglucose (FDG) using PET [87]. A negative correlation between the plaque GSM and the FDG SUV (r=-0.56, p<0.01) was found. Echo-rich plaques had little inflammation, while echolucent plaques exhibited a wide range of inflammatory activity from low to high [87]. It was also reported that while the FDG SUV differentiated asymptomatic plaques from the symptomatic, the GSM values did not. The authors suggested that [18]FDG PET may be useful as a tool for stratifying echolucent plaques, in terms of inflammatory activity, into an active category and an inactive category with the former indicating a potentially more vulnerable group of plaques.

Finally, and more recently, Salem et al. carried out an investigation to determine whether the computerised analysis of ultrasound plaque data could identify features predictive of an increased risk of early recurrent events in symptomatic patients

scheduled to undergo carotid endarterectomy [51]. The plaques harvested during surgery were independently scored for markers of histological plaque instability. It was found that a low plaque GSM (odds ratio 6.21, p=0.003) was independently associated with recurrent cerebrovascular events before surgery. Patients with recurrent cerebrovascular events were the patients (n=20) who suffered a further ischaemic event following admission to hospital and before actually undergoing carotid endarterectomy.

A summary survey of the literature on plaque echogenicity/GSM is provided in Table 1.2. It can be seen that, with the exception of Golemati et al. [154], who measured GSM at systole and diastole, previous studies primarily looked at plaque echogenicity on single frames of ultrasonographic images, which were typically selected at random points during the cardiac cycle. In fact, it appears that most studies simply used the best looking image, determined in a subjective manner, for plaque echogenicity/GSM assessment. In Chapter 2, the foundations for computationally delineating arterial wall boundaries in ultrasound image sequences is laid, which is subsequently extended to a method of tracking plaque boundaries in Chapter 3. In the latter chapter, the variations in plaque GSM that may be observed on a frame-by-frame basis throughout ultrasound image sequences are investigated and highlighted.

**Table 1.2** - A summary survey of the literature related to ultrasonographic plaque echogenicity/GSM assessment. Normalisation indicates whether image normalisation was performed. 'Type of analysis: Qualitative' denotes that a qualitative assessment was carried out, while 'Type of Analysis: Static' denotes that a quantitative analysis was performed on a single frames of ultrasonographic images. 'Post P/C: Nsp' denotes that the post-processing/greyscale transfer curve used on the ultrasound equipment was not specified, while 'Post P/C: Lin' indicates that the post-processing curve used on the ultrasound equipment was linear.

| Investigators | Year | Post P/C | Type of analysis | Normalisation | Findings |
|---|---|---|---|---|---|
| Geroulakos et al. [130] | 1994 | Nsp | Qualitative | None | • An association between echolucent plaques and ipsilateral hemispheric brain infarcts. |
| European Carotid Plaque Study Group [53] | 1995 | Nsp | Qualitative | None | • Plaque echogenicity inversely related to soft tissue content. |
| El-Barghouty et al. [132] | 1995 | Nsp | Static | None | • Low GSM associated with a higher incidence of ipsilateral brain infarction. |
| Iannuzzi et al. [61] | 1995 | Nsp | Qualitative | None | • An association between hypo-echoic plaques and ipsilateral brain involvement in TIA patients. |
| El-Barghouty et al. [133] | 1996 | Nsp | Static | None | • Cerebral infarction more common in echolucent than echogenic plaques. |
| Droste et al. [156] | 1997 | Nsp | Qualitative | None | • Correlation between the plaque echogenicity |

| Investigators | Year | Post P/C | Type of analysis | Normalisation | Findings |
|---|---|---|---|---|---|
| | | | | | and the histological assessment of plaque composition not significant. |
| Grønholdt et al. [157] | 1998 | Nsp | Qualitative | None | • An association between the histological composition of carotid artery plaques and plaque echogenicity. |
| Polak et al. [135] | 1998 | Nsp | Qualitative | None | • Hypo-echoic plaques associated with an increased risk of incident stroke. |
| Elatrozy et al. [148] | 1998 | Lin | Static | Linear | • GSM of plaques with ipsilateral hemispheric symptoms lower than for asymptomatic plaques. |
| Elatrozy et al. [129] | 1998 | Lin | Static | Linear | • GSM found to be a significant variable that relates to the presence of ipsilateral hemispheric symptoms. |
| Golledge et al. [158] | 1998 | Nsp | Qualitative | None | • Echolucent plaques found to be more common in symptomatic patients, compared with the asymptomatic. |
| Biasi et al. [140] | 1999 | Nsp | Static | None | • GSM found to be better than the degree of stenosis in indentifying plaques associated |

| Investigators | Year | Post P/C | Type of analysis | Normalisation | Findings |
|---|---|---|---|---|---|
| | | | | | with ipsilateral brain infarctions. |
| Sabetai et al. [137] | 2000 | Lin | Static | Linear | • GSM of plaques associated with ipsilateral, asymptomatic brain infarcts lower than that of plaques that were not so associated. |
| Mathiesen et al. [136] | 2001 | Nsp | Qualitative | Subjective | • Echolucent plaques found to be associated with an increased risk of ischaemic events. |
| Grønholdt et al. [134] | 2001 | Nsp | Static | Linear | • Echolucent plaques found to be associated with risk of future strokes in symptomatic patients. |
| Tegos et al. [131] | 2001 | Lin | Static | Linear | • Symptomatic plaques found to be associated with a lower GSM than asymptomatic plaques. |
| Liapis et al. [159] | 2001 | Nsp | Qualitative | None | • Presence of echolucent plaques found to be associated with a higher risk of stroke. |
| Lal et al. [125] | 2002 | Nsp | Static | Linear | • Significant correlations between tissue composition predicted by pixel distribution analysis and determined by histological assessment. |
| Christodoulou et al. | 2003 | Lin | Static | Linear | • It may be possible to identify a subgroup of |

| Investigators | Year | Post P/C | Type of analysis | Normalisation | Findings |
|---|---|---|---|---|---|
| [153] | | | | | patients at a high risk of stroke based on texture features. |
| Biasi et al. [138] | 2004 | Lin | Static | Linear | • Plaque echolucency found to increase the risk of stroke during and after carotid artery stenting. |
| Golemati et al. [154] | 2004 | Lin | Static at systole and diastole. | Histogram equalization | • GSM may be used to characterise atheromatous plaques of the carotid artery. |
| Grogan et al. [160] | 2005 | Lin | Static | Linear | • Symptomatic plaques found to be more echolucent and less calcified than asymptomatic plaques. |
| Kalogeropoulos et al. [161] | 2006 | Nsp | Qualitative | None | • Echolucent plaques found to be more prevalent among patients with TIA compared with control subjects. |
| Lind et al. [155] | 2007 | Nsp | Static | Linear | • GSM of the intima-media complex in the common carotid artery had a significant correlation to the plaque GSM. |
| Ding et al. [162] | 2008 | Nsp | Qualitative | None | • Carotid plaques in acute stroke patients found |

| Investigators | Year | Post P/C | Type of analysis | Normalisation | Findings |
|---|---|---|---|---|---|
| | | | | | to be echolucent or predominantly echolucent. |
| Rosenkranz et al. [163] | 2009 | Nsp | Static | None | • Patients who had TCD detected solid cerebral microemboli intra-operatively had lower GSM compared to patients who did not have embolic events. |
| Graebe et al. [87] | 2010 | Lin | Static | Linear | • A negative correlation found between plaque GSM and $^{18}$F-FDG uptake on positron emission tomography. |
| Dósa et al. [164] | 2010 | Nsp | Qualitative | None | • Presence of echolucent femoral artery plaques found to be an independent predictor of recurrent carotid artery stenosis after carotid endarterectomy. |
| Staub et al. [165] | 2011 | Nsp | Qualitative | None | • Plaque echogenicity found to be inversely related to the degree of intra-plaque neovascularisation. |
| Topakian et al. [113] | 2011 | Nsp | Qualitative | None | • Plaque echolucency found to be associated with an increased risk of ipsilateral stroke. |
| Salem et al. [51] | 2012 | Lin | Static | Linear | • Low GSM found to be associated with recurrent |

| Investigators | Year | Post P/C | Type of analysis | Normalisation | Findings |
|---|---|---|---|---|---|
| | | | | | events in recently symptomatic patients. |
| Kolkert et al. [166] | 2013 | Nsp | Static | Linear | • No significant relationship between the GSM of plaques and the patient symptomatic status. |
| Irie et al. [167] | 2013 | Nsp | Static | Linear | • GSM found to improve the prediction of future cardiovascular events in asymptomatic type 2 diabetic patients. |
| Singh et al. [168] | 2013 | Nsp | Qualitative | Subjective | • A significant association between stroke recurrence and carotid plaque echolucency. |

### 1.9.1.2 Plaque Surface Irregularities and Ulceration

Plaque surface irregularities observed on ultrasonographic assessment may be indicative of plaque ulceration, since the latter can appear as excavations, cavities, or caverns of the plaque surface [169]. This has potential applicability to the problem of identifying vulnerable carotid plaques, since ulcerations increase the risk of stroke and are associated with an increased risk of thrombus formation, intra-plaque haemorrhage and downstream embolisation [73,170-173].

Previous studies have found significant relationships between plaque ulceration and plaque surface irregularities, the presence of cerebrovascular symptoms, plaque vulnerability, and the risk of stroke and other cerebrovascular events [55,63,170,172,174-177]. Rothwell et al. found that patients with irregular plaques in the symptomatic carotid artery were more likely to have irregular plaques also in the contralateral carotid artery, suggesting that some individuals may have a systemic predisposition to atherosclerotic plaque surface irregularities that is independent of traditional risk factors [63]. AbuRahma et al. compared ultrasonic plaque morphology in 135 patients who had carotid endarterectomy with pathological assessment of surgical specimens and found that irregular plaques were more often associated with intra-plaque haemorrhage and neurologic events [172]. Handa et al. carried out a follow-up study of 214 patients from nine hospitals and found that patients with ulcerated plaques had a sevenfold higher risk of stroke compared to patients with non-ulcerated plaques [175]. They identified plaque ulceration according to a subjective classification scheme depending on the presence of large, obvious excavations or multiple cavities and/or cavernous appearances [169,175].

Fisher et al. characterized surgically removed carotid artery plaques from 241 patients for ulceration and thrombus, and found that carotid plaque ulceration and thrombosis were more prevalent in the symptomatic patients [170]. Prabhakaran et al. studied the association between carotid plaque surface irregularity and the risk of ischaemic stroke in a multiethnic population of 1,939 patients and found that the unadjusted cumulative 5-year risks of ischaemic stroke were 1.3%, 3.0%, and 8.5% for no plaque, regular plaques, and irregular plaques, respectively. Rosenkranz et al. found the

numbers of solid microembolic signals, detected by means of dual-frequency transcranial Doppler ultrasound, per carotid artery stenting (CAS) procedure and per hour of CAS procedure, were higher in patients with irregular plaques than those with smooth plaques [178]. Molloy and Markus recorded embolic signals for 1 hour in the middle cerebral arteries of 111 patients with greater than 60% carotid artery stenosis and found more embolic signals in patients with plaque ulceration [3]. Their study also found the presence of asymptomatic embolisation to be predictive of future ischaemic events [3]. Sitzer et al. found strong associations between microemboli in the middle cerebral artery monitored preoperatively and plaque ulceration characterised by histology following carotid endarterectomy [171]. Pedro et al. found that plaque surface disruption assessed qualitatively using ultrasound correlated with the presence of symptoms [179]. Carra et al. followed 230 asymptomatic patients for a median duration of 32 months and found that the presence of an irregular plaque surface correlated with plaque progression and the development of neurological events [180]. Recently, Kuk et al. found that carotid plaque ulcer volume assessed by three dimensional ultrasound imaging was predictive of cardiovascular events and subjects with total ulcer volume greater than or equal to 5 $mm^3$ had a higher risk of developing stroke and other vascular events during a five year follow-up period [173]. Ulcers were defined as distinct discontinuities in the surfaces of atherosclerotic plaques with a volume greater than or equal to 1 $mm^3$ in that study [173].

Contrast-enhanced ultrasound can improve the visualisation of plaque surfaces, particularly for hypo-echoic plaques, and may have better diagnostic accuracy for the identification of plaque ulceration and intra-plaque haemorrhage [181]; however, it requires the intravenous administration of a contrast agent.

It is interesting to point out that, although ulcerations can make the ultrasound image of a given plaque irregular, not all of the irregularities of a plaque surface may be due to ulcerations [182]. In other words, some plaques may have inherently irregular surfaces, despite not being ulcerated. In the existing studies, measures of plaque surface irregularities have been mostly qualitative; for example, subjectively classifying plaques as smooth, irregular, ulcerated or not possible to evaluate [53]. Such qualitative assessments lack objectivity, and can fail to differentiate small differences

in surface characteristics of plaques. It can be difficult to classify plaques as being smooth or irregular, beyond the obvious cases. Bluth et al., for example, retrospectively evaluated plaques from 50 patients, but did not find a significant relationship between the qualitative sonographic assessment and the presence or absence of pathologically determined intimal ulcerations [183]. Surface defects having a depth and a length of greater than or equal to 1 or 2 mm with a well defined base, and colour Doppler injection into the recess have also been used for classifying plaque surface irregularities and ulceration [184]. A quantitative method for the dynamic assessment of plaque surface irregularities will be developed in Chapter 4, which will be shown to have a significant relationship to the presence of cerebrovascular symptoms, and increase diagnostic performance when combined with the degree of carotid artery stenosis.

### 1.9.1.3 Other Texture and Morphological Parameters

Other parameters based on plaque morphology and texture that have been investigated include the percentage echolucent pixels, contrast, variance, entropy, texture energy, juxta-luminal black areas, discrete white areas, and fractal dimension. Studies have found evidence that these parameters may help differentiate the symptomatic plaque from the asymptomatic and relate to the future risk of stroke [179,185-187]. Other first- and second-order statistics and texture analysis methods have also been used [54,153,188-190]. In relation to plaque morphology, Thornhill et al. recently carried out a study to determine whether quantitative shape analysis can differentiate free-floating intraluminal thrombus (filling defects resolving with anticoagulant therapy) from atherosclerotic plaques; identifying five potential shape descriptors for this purpose [191]. Stratified GSM analysis and the subsequent colour mapping of the carotid plaque have also been carried out [192]. Plaques which have large lipid or necrotic cores separated from the bloodstream by thin fibrous caps are generally considered to be high-risk; these plaques typically appear predominantly hypo-echoic or echolucent with thin, hyper-echoic surface boundary under ultrasound. In order to identify such plaques, Lal et al. quantified plaque echogenicity on a per-pixel basis taking into account the distance from each pixel to the plaque surface [126]. They found that lipid cores were larger and closer to the arterial lumen in

plaques that had associated cerebrovascular symptoms (p<0.01). It would be reasonable to expect that, for non-homogenous plaques, the configuration of the various, individually homogenous sub-regions making up the plaque, may be important in determining its behaviour and stability. This is certainly the case for the classical model of the vulnerable plaque where a large soft core is contained within a thin fibrous cap. In such a plaque, the rupture of the thin fibrous cap could result in the release of the intra-plaque contents into the bloodstream [193]. This argument is also applicable to any lipid-rich or necrotic region of the plaque, particularly if that region is close to the surface of the plaque (i.e. juxta-luminal). Texture analysis is also used in other areas of ultrasound imaging. Moon et al., for example, analyzed the texture of 137 breast masses by means of log-decompressing the greyscale images and using this to estimate the density of scatterers. They found that a computer-aided diagnosis system based on the first- and second-order statistics could differentiate between malignant and benign masses [194].

Other morphological parameters investigated in relation to plaque vulnerability include the volume compression ratio (VCR), calculated as the percentage reduction in plaque volume from diastole to systole measured using three dimensional ultrasonography [195]. The VCR has been evaluated as a surrogate marker of the elasticity of carotid artery plaques and was found to be related to the echogenicity of plaques, and associated with the presence of ischaemic cerebrovascular events [195].

## 1.9.2 Evaluation of Plaque Motion

Motion of the arterial wall and the atherosclerotic plaque may contribute to plaque destabilisation and relate to the risk of stroke and other cerebrovascular events [196-198]. Several studies have investigated arterial wall and plaque motion from ultrasound image sequences. In the 1990s, Chan described two approaches to track the motion of carotid plaques, namely a 'discrete approach' and a 'continuous approach' [199]. The discrete (modified feature-based) approach involved applying (and using the average of) four 5x5 pixel$^2$ texture masks, optimized for extracting spot and edge features, to a number of points-of-interest selected by the operator and finding the pixels in successive frames which had feature values most similar to those

of the selected points-of-interest. Each template was updated as the tracking of the points proceeded in the image sequence. The continuous (optical flow-based) approach involved tracking the plaque boundary in each frame of the image sequence. A region of interest (ROI) was selected on the first image (the ROI needed to be big enough to enclose the plaque in each image frame) and the boundary of the plaque was detected from this using grey-level histogram thresholding. In order to verify that the movement of plaque was not due to the movement of the transducer or patient respiration, global movement estimation was also carried out. Analysis of two clinical image sequences which had 25 frames each, separated by 1 second intervals, demonstrated differential motion of plaques and the surrounding tissues [199]. However, the study did not establish the presence of any discrepant motion between the plaque and the arterial wall. On the other hand, Iannuzzi et al. found an association between the presence of longitudinal lesion motion ($p=0.02$, odds ratio$=3.0$) qualitatively defined as an apparent distal shift of the plaque axis with ipsilateral brain involvement in transient ischaemic attack patients [61].

Meairs and Hennerici carried out four-dimensional ultrasound assessment of plaque surface deformation in 23 asymptomatic and 22 symptomatic patients with 50-90% degree of stenosis [200]. They used an edge detection algorithm based on the greyscale gradient to detect the plaque surface and a hierarchical motion estimation algorithm to calculate the apparent velocity field. Plaque surface motion estimates were obtained for 18 asymptomatic and 13 symptomatic patients out of the 45 patients examined. Results of motion estimation showed that asymptomatic plaques had surface motion vectors of equal orientation and magnitude to those of the internal carotid artery, whereas symptomatic plaques demonstrated evidence of motion relative to that of the ICA [200]. There were no significant differences in maximum surface velocities between symptomatic and asymptomatic plaques (maximum value 9.4 mm/s). However, maximum discrepant surface velocities (MDSV) in symptomatic plaques was significantly higher than that in asymptomatic plaques (mean and s.d. $3.85\pm1.26$ versus $0.58\pm0.42$ mm/s). MDSV was defined as the maximum of the differences between maximum and minimum plaque surface velocities calculated in successive image volumes [200].

In a radiofrequency study, Bang et al. carried out an analysis of plaque motion in 11 patients by means of two-dimensional cross-correlation of radiofrequency data over a grid spacing of 3 pixels horizontally and vertically [197]. Velocities were calculated relative to the probe (upper image edge) and a reference region directly beneath the plaque. Their study found peak velocities of the order of 5–12 mm/s, which agreed well with the maximum plaque surface velocity of 9.4 mm/s reported by Meairs and Hennerici [200]. Furthermore, spatial analysis demonstrated that different plaque regions may exhibit different motion patterns which may cause internal stress, leading to fissures and plaque disruption [197]. In a B-Mode study looking at arterial wall motion, Golemati et al. showed the expected cyclical motion of the arterial wall in the radial direction, including some axial movement [196]. The technique used was that of region/speckle tracking/matching and the maximum displacement that could be detected was 10 pixels from the initially estimated position in the radial or axial direction. This was a preliminary study and any relationships to cerebrovascular symptoms were not studied [196]. Seven image sequences were investigated, five of which were from healthy subjects and two from patients with atheromatous plaque on the posterior wall. In the latter case, measurements were made at the normal part of the arterial wall [196].

Dahl et al. investigated 29 plaque motion parameters for intra-operator reproducibility, by statistical analysis of data from 12 patients (six patients with a symptomatic carotid stenosis and six asymptomatic patients) [201]. Their results showed that 7 parameters reproduced well while the other parameters did not fit within the assumptions of their statistical model. The parameters that reproduced well described tensional and torsional motion, in addition to the velocity amplitude [201]. Stoitsis et al., on the other hand, carried out motion analysis of plaque surfaces, similar to Meairs and Hennerici but in two dimensions, using block matching/region tracking, with parameters expressed as maximal surface velocity and maximal relative surface velocity [185]. Their study showed that these two parameters were significantly lower in asymptomatic plaques [185]. A total of 10 symptomatic and 9 asymptomatic plaques were assessed. Akkus and Ramnarine used speckle tracking methods, with the normalized correlation coefficient as the similarity measure, to quantify carotid plaque surface movements, vessel wall motion and intra-plaque deformation in one

normal subject and four patients with atherosclerotic disease [202]. However, any relationships to patient symptoms were not studied. Recently, Kashiwazaki et al. found that the motion of intra-plaque contents, a motion they described as one that is not synchronized with the heartbeat, increased the risk of recurrent ischaemic events in a cohort of 115 symptomatic patients with carotid artery stenosis greater than 50% [198].

The existing studies have two main limitations: either qualitative assessments were used, or a small number of samples and/or a limited range of stenoses were investigated. In Chapter 5 a quantitative assessment of arterial wall motion in the stenotic carotid artery is carried out, while in Chapter 6, plaque motion is investigated. In both chapters, the existing literature is extended to a broader range of stenoses and any relationships with the greyscale plaque characteristics are assessed.

### 1.9.3 Plaque Risk Scores

Several studies have previously considered deriving a risk score for atherosclerotic carotid artery disease by means of combining measures of stenosis severity with other parameters characterising the plaque. Prati et al., for example, combined the degree of stenosis with qualitative measures of surface irregularity, plaque echogenicity and texture in the form of a Total Plaque Risk Score [174]. They found that, in 171 subjects with at least one plaque at baseline, the risk score significantly increased the area under the Receiver Operating Characteristic curve for the prediction of cerebrovascular events versus the Framingham risk score alone (0.90 vs. 0.88, p=0.04). Pedro et al. described an Activity Index comprising ultrasound measures of plaque surface disruption (qualitative classification), echogenicity, heterogeneity and the presence of juxta-luminal echolucent areas, in combination with stenosis severity, and found this to be a parameter that positively correlated with patient symptoms [179]. Momjian-Mayor et al., on the other hand, combined the degree of stenosis with a measure of the plaque surface echogenicity, and found that this risk index was significantly higher in the presence of symptoms [203].

Previous studies have developed risk indices either by incorporating qualitative plaque measures, or measurements made on single frames of ultrasound images. In the case of the latter, the final risk indices were constructed using weighting parameters optimised for the particular dataset studied which may limit applicability (Chapter 7). In Chapter 7, a novel risk index will be developed, based solely on parameters dynamically measured from ultrasound image sequences, without incorporating of any dataset-optimised weighting factors.

### 1.9.4 Limitations of the Ultrasound Assessment of Plaque Characteristics

The assessment of carotid artery stenosis and plaque using ultrasonography has certain limitations characteristic of this imaging modality. Due to the presence of bone, only extra-cranial segments of carotid arteries can normally be imaged. Furthermore, imaging of the carotid bifurcation and the distal branches can be difficult in patients whose bifurcations are too high above the level of the mandibular angle and in patients who have short necks [18,204]. Calcium-rich structures such as bone are both highly reflecting (at boundaries with most soft tissues) and absorbing of ultrasound, and acoustic shadowing, if present, can limit ultrasonographic assessment of the carotid plaque further. However, the presence of acoustic shadowing can also be diagnostically useful as shadowing is often an indication of plaque calcification [205]. Abrupt changes in acoustic impedance can cause other problems as well, and it has been reported that the strong reflection of ultrasound waves at interfaces between soft and hard regions of complex plaques can lead to underestimation of plaque vulnerability [18]. It has also been demonstrated that plaques uniformly composed of fibrous tissues could show low echogenicity on ultrasonography, and thus be mistaken for lipid-rich soft plaques [18,204].

Spatial resolution of the ultrasound imaging system is also an important consideration as it can limit the assessment of small structures such as small fissures of the plaque surface. A further limitation arises in relation to totally echolucent plaques, plaques which do not have any echogenicity and cannot be observed without the use of another mode such as Colour Flow Imaging/Colour Doppler. Contrast-enhanced ultrasound can also be used to identify such plaques, and study the surface

characteristics and/or the presence of intra-plaque haemorrhage. However, as discussed in section 1.9.1.2, this requires the intravenous administration of a contrast agent, and thus is an invasive procedure. Despite these limitations, ultrasonography currently remains the most accessible imaging modality that may help identify the vulnerable plaque [206].

## 1.10 Physics of Medical Ultrasound Imaging

Medical ultrasound employs acoustic/mechanical waves with frequencies typically between 1 to 20 MHz which are beyond the range audible to the human ear (approximately 20 Hz to 20 KHz for adults). This frequency range gives an optimal combination of tissue penetration and imaging resolution. Physically, they are longitudinal pressure waves that cause local pressure and particle oscillations without any net displacement of the medium. However, energy is transferred (and dissipated) along the direction of travel. Transverse/shear and other types of wave (such as torsional), including mode conversion, can also occur in solids, but these are not typically used in medical ultrasound, except for the former which, for example, are utilized in Shearwave Elastography. Ultrasound waves are similar to other mechanical waves in nature, such as those produced by earthquakes, except for the differences in wave frequencies. The basic principle of ultrasound imaging is similar to echo-ranging in which the time-of-flight of a received ultrasound wave gives information on the distance to the target, while its amplitude depends on the mechanical properties of the medium it travels in as well as the medium from which it is reflected. Furthermore, any change in wave frequency may be used to gain information on target motion as in Doppler ultrasound (section 1.10.1.4).

### 1.10.1 Ultrasound Wave Propagation

The propagation of ultrasonic waves and their interaction with the medium depend on the mechanical properties of the medium as well as the characteristics of the ultrasonic wave itself[1]. The speed of sound of acoustic longitudinal waves for isotropic media is given by Equation 1.1. This equation implies that the speed of sound is

---

[1] For example, the type of wave, and the wavelength or wave frequency.

greater in media which are less compressible (or more stiff) for a given density. The speed of sound, particularly for gases, and because of changes in the mechanical properties, has a dependence on temperature[1], and in the case of solids/non-homogeneous media, it can vary depending on other factors such as the direction of travel. In tissues, the speed of sound increases with temperature for non-fatty tissues, while it decreases for fatty tissues [207]. The speed of sound can also have a dependence on the wavelength or wave frequency, and wave amplitude, but this dependence is typically small in medical applications. Variations in the speed of sound is less than 1% over the range of frequencies used in medical ultrasound with the exception of bone which may have a larger dependency of the speed of sound on frequency [207].

$$c = \sqrt{1/(\rho\kappa)} = \sqrt{B/\rho}$$

**Equation 1.1** - Speed of sound (c) for isotropic media. $\rho$ is the density of the medium, $\kappa$ is its compressibility and B is the bulk/elastic modulus.

The speed of sound for various biological and non-biological media are listed in Table 1.3. Normally, an average speed of sound of 1540 m/s is assumed for soft tissues at a temperature of $36^{o}$C, but as can be seen from Table 1.3, the speed of sound for different tissues (e.g. bone and lungs) can vary significantly from this value. The product of wave frequency and wavelength equate to the speed of sound; thus, a speed of sound of 1540 m/s and a wave frequency of 7 MHz correspond to a wavelength of 0.22mm.

Longitudinal acoustic waves exhibit as alternating regions of increased pressure (compressions) and decreased pressure (rarefactions) as shown in Figure 1.4. Local

---

[1] The speed of sound in dry air at sea level can be approximated by the formula $c=20.1\sqrt{T+273}$ where T is the temperature in degrees Celcius, and c is the speed of sound in m/s.

particle velocity[1] is given by Equation 1.2 and is typically of the order of several tens of mm/s.

**Equation 1.2** - Local particle velocity (v). p is the local pressure, Z is the characteristic acoustic impedance of the medium, ρ is the density of the medium, and c is the speed of sound.
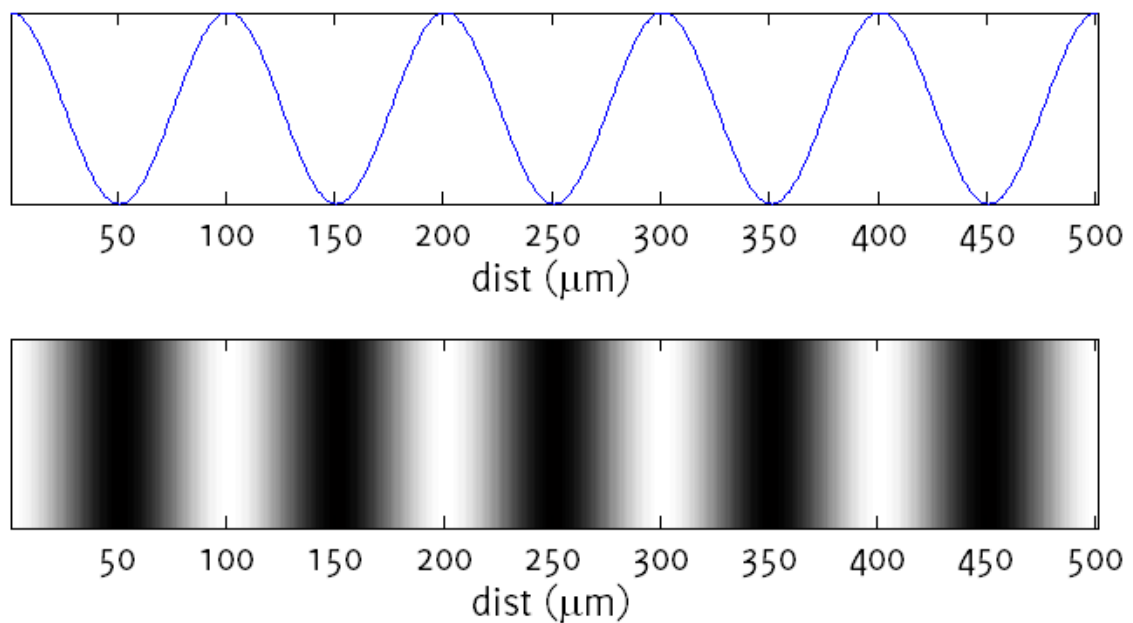


**Figure 1.4** - illustration of an instantaneous pressure profile with distance (dist) along the direction of propagation for an acoustic wave of wavelength 100μm. Bright bands are compressions and dark bands are rarefactions. The vertical axis in the plot shown on the top is the acoustic pressure in arbitrary units, and ranges from -ξ to +ξ, where ξ is the pressure amplitude.

---

[1] This is not to be confused with the acoustic wave (sound) velocity c.

Equation 1.1 indicates that any increase/decrease in the density of the medium will cause a change in the wave propagation speed, unless it is accompanied by a proportional decrease/increase in the bulk modulus. If this is not the case, the propagation is non-linear, and the speed of sound will be different in regions of compression (higher density), compared with regions of rarefactions (lower density). Non-linear propagation results in the generation of the harmonics of the original ultrasound frequency [208], and the second harmonic produced in this way is used in tissue harmonic imaging. The latter gives better image quality due to the higher frequency of the second harmonic at the expense of penetration depth.

### 1.10.1.1 Transmission/Refraction and Specular Reflection

If a sound wave propagating in a medium of acoustic impedance $Z_1$ and speed of sound of $c_1$ is incident on a plane interface with another medium of acoustic impedance $Z_2$ and speed of sound of $c_2$, part of the wave may be reflected and part may be transmitted/refracted depending on the mismatch between the acoustic impedances and the speeds of sound (Figure 1.5)[1].

The acoustic pressure amplitude of the transmitted/refracted ($A_t$) wave is related to the pressure amplitude of the incident wave ($A_i$) by Equation 1.3. Under the assumptions that no energy is dissipated and no mode conversion occurs, the reflected wave amplitude $A_r$ will be such that the reflected wave pressure and the incident wave pressure will sum to the wave pressure of the transmitted/refracted wave at the interface.

$$A_t/A_i = (2Z_2\cos\theta_i) / (Z_2\cos\theta_i + Z_1\cos\theta_t)$$

**Equation 1.3 -** The relationship between the transmitted acoustic wave pressure amplitude ($A_t$) and the incident wave pressure amplitude ($A_i$). $Z_1$ is the acoustic

---

[1] Upon transmission from one medium to another, frequency remains constant, while c and λ may change.

impedance of the first medium, $\theta_i$ is the angle of incidence, $Z_2$ is the acoustic impedance of the second medium, and $\theta_t$ is the angle of transmission/refraction.
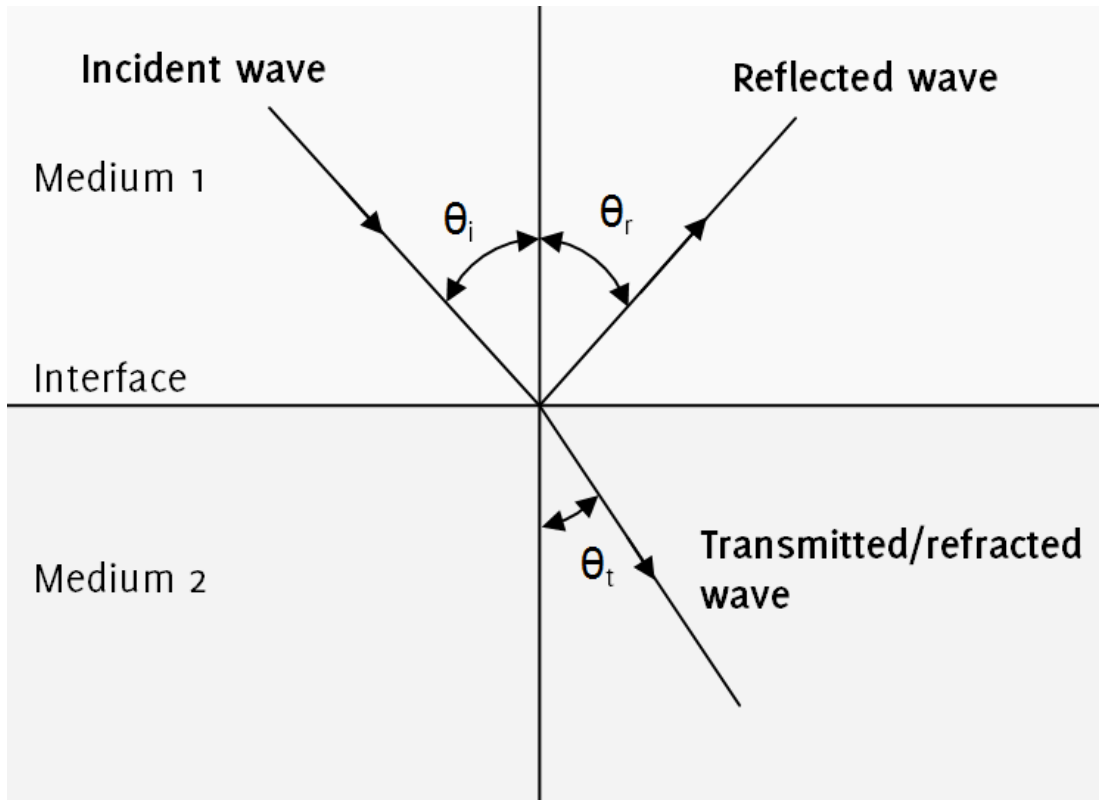


**Figure 1.5** - Illustration of an incident sound wave being partly reflected and partly transmitted (in the form of a refracted wave) at a plane interface between two media. $\theta_i$ is the angle of incidence, $\theta_r$ is the angle of reflection, and $\theta_t$ is the angle of transmission/refraction.

In the case of perpendicular incidence, Equation 1.3 implies that if $Z_1$ and $Z_2$ are equal then $A_r$ is zero and $A_t$ is equal to $A_i$. In other words, there is no reflected wave and the wave is simply transmitted, if the beam is incident perpendicularly on the interface and the acoustic impedances of the two mediums match. If $Z_2$ is greater than $Z_1$ then the reflected wave is in phase with the incident wave, while if $Z_2$ is less than $Z_1$ the reflected wave is $180^0$ out-of-phase with the incident wave [209].

In relation to the direction of propagation of the incident, reflected and transmitted waves, if the incident wave makes an angle $\theta_i$ with the perpendicular to the interface then the reflected wave also makes the same angle with the perpendicular (i.e. $\theta_i$ and $\theta_r$ are equal), while the refracted wave makes angle $\theta_t$ with the perpendicular where $\theta_t$ is given by Snell's law (Equation 1.4).

$$\sin\theta_t/c_2 = \sin\theta_i/c_1$$

**Equation 1.4** - The law of refraction (Snell's law). $c_1$ is the speed of sound in the first medium, $\theta_i$ is the angle of incidence, $c_2$ is the speed of sound in the second medium, and $\theta_t$ is the angle of transmission/refraction (Figure 1.5).

If $c_2$ and $c_1$ are equal then the transmitted wave makes the same angle with the perpendicular to the interface as the incident wave (i.e. $\theta_t$ is equal to $\theta_i$). If $c_2$ is less than $c_1$ then the wave is refracted towards the perpendicular (i.e. $\theta_t$ is less than $\theta_i$). On the other hand, if $c_2$ is greater than $c_1$ then the wave is refracted away from the perpendicular (i.e. $\theta_t$ is greater than $\theta_i$). A special situation occurs if $\theta_t$ is equal to $90^o$, in which case the transmitted wave propagates along the interface and the $\theta_i$ is said to be equal to the critical angle ($\theta_c$). If $\theta_i$ is greater than $\theta_c$ then total internal reflection occurs; there is no transmitted wave or a wave along the interface.

### 1.10.1.2 Scattering and Diffraction

In comparison to the specular reflection and transmission/refraction of ultrasound waves at plane interfaces between media, also called geometric scattering and described in the previous section, non-geometric scattering becomes predominant when the interface between the media exhibits irregularities the dimensions of which are comparable to or smaller than the acoustic wavelength. This type of scattering also occurs when targets smaller than or comparable to the wavelength of the acoustic

wave are present in the path of the ultrasound beam (e.g. cells[1]) and is responsible for the characteristic speckle patterns of tissues observed in ultrasound imaging. Scattering is characterised by a fairly omnidirectional (Rayleigh[2]) or a less omnidirectional (stochastic[3]) reflection/transmission of the acoustic waves. In ultrasonography, interference of the waves produced by the various scatterers cause the characteristic speckle patterns. Diffraction is another process acoustic waves are be subjected to, when sound travels through a medium of non-uniform mechanical properties (e.g. variations in acoustic impedance, density, or speed of sound) or an opening that is comparable to or smaller than the wavelength of the acoustic wave; the process is similar to the diffraction of electromagnetic waves. In fact, the arrays of transducers used in multi-element ultrasound probes (section 1.10.2) can act as a diffraction grating and produce side lobes in addition to the primary beam intended to be produced.

### 1.10.1.3 Attenuation

Attenuation refers to the loss of signal intensity as an acoustic wave propagates through a medium. In biological tissues, the main mechanism is absorption or conversion to thermal energy, with additional contributions from scattering, and mode conversion. Attenuation in terms of the signal amplitude can be written as in Equation 1.5 [210].

$$A(x) = A_0 \exp(-\alpha x)$$

**Equation 1.5** - Attenuation in terms of the signal amplitude $A(x)$ where $A_0$ is the initial signal intensity, x is the distance travelled by the acoustic wave and $\alpha$ is the amplitude attenuation coefficient of the medium.

---

[1] The diameters of red blood cells, for example, are usually in the region 6 to 8 μm.

[2] Rayleigh scattering refers to the type of scattering that occurs when irregularities are smaller than the acoustic wavelength.

[3] Stochastic scattering refers to the type of scattering that occurs when irregularities are comparable to the acoustic wavelength.

Attenuation has a bearing on the penetration depth attainable with ultrasound equipment and takes place both during the outward propagation of the signal away from the transducer and the inward propagation back towards the transducer. Aside from depending on the material properties, attenuation coefficients also have a dependency on wave frequency and are typically modelled as $\alpha = af^b$ where the exponent, for soft tissues, is often assumed to be equal to 1 [207]. Values of the attenuation coefficient, therefore, are usually quoted in decibels per unit length, per unit frequency (e.g. dB cm$^{-1}$ MHz$^{-1}$) and the loss of signal intensity and amplitude in decibels are given by Equation 1.6 and Equation 1.7, respectively.

$$\text{loss of signal intensity (dB)} = 10\log_{10}(I/I_0) = 10\log_{10}(A/A_0)*2$$

**Equation 1.6** - Loss of signal intensity in decibels, where I is the signal intensity and A is the signal amplitude.

$$\text{loss of signal amplitude (dB)} = 10\log_{10}(A/A_0) = 10\log_{10}(I/I_0)/2$$

**Equation 1.7** - Loss of signal amplitude in decibels, where A is the signal amplitude and I is the signal intensity.

Soft tissues are often approximated to have an attenuation coefficient of 0.5 dB cm$^{-1}$ MHz$^{-1}$, but there is considerable variation among different tissue types and propagation trajectories (Table 1.4). In medical ultrasound imaging, time gain compensation (TGC) is applied to compensate for the loss in signal intensity with increasing depth; nevertheless, signal to noise ratio is reduced at greater depths.

### 1.10.1.4 The Doppler Effect

Ultrasound waves reflected from stationary targets do not typically experience a change in frequency. However, as mentioned in section 1.10.1.1, a phase shift may occur. In contrast, when ultrasound waves are reflected by moving targets, a frequency shift does typically occur depending on the angle between the ultrasound beam and the direction of travel of the moving target (Equation 1.8). This is utilized in medical ultrasound to study motion, for example, the measurement of blood flow velocity.

Equation 1.8 implies that no shift in frequency occurs if the angle between the ultrasound beam and the direction of travel of the moving target is $90^0$, while the frequency shift is maximum when the two are parallel (i.e. $\theta=0^0$). Frequency shift is positive if the target is moving towards the probe, and is negative if it is moving away from the probe.

$$f-f_0 = \pm\, (2uf_0\cos\theta)/c$$

**Equation 1.8** - The shift in frequency ($f-f_0$) as a function of the angle ($\theta$) between the ultrasound beam and the direction of propagation of the target moving with velocity of magnitude u. This equation assumes that u is much smaller than the speed of sound (c) in the medium.

**Table 1.3 -** Acoustic properties of various biological and non-biological media [211-212].

| Medium | Density (kg m$^{-3}$) | Speed of sound (m s$^{-1}$) | Acoustic impedance (kg m$^{-2}$ s$^{-1}$) [x10$^6$] (rayls) |
|---|---|---|---|
| Fat | 950 | 1480 | 1.40 |
| Kidney | 1040 | 1560 | 1.63 |
| Breast | 1020 | 1510 | 1.54 |
| Blood | 1060 | 1584 | 1.68 |

| Medium | Density (kg m$^{-3}$) | Speed of sound (m s$^{-1}$) | Acoustic impedance (kg m$^{-2}$ s$^{-1}$) [x10$^6$] (rayls) |
| --- | --- | --- | --- |
| Liver | 1060 | 1595 | 1.69 |
| Bone (cortical) | 1975 | 3500 | 7.38 |
| Bone (trabecular) | 1055 | 1900 | 1.45 |
| Brain | 1040 | 1560 | 1.62 |
| Lung[1] | typically less than 500 | Typically less than 1000 | 0.2 |
| Air (at 0$^0$C and 100 kPa) | 1.2 | 330 | 4X10$^{-4}$ |
| Water (at 20$^0$C) | 1000 | 1480 | 1.5 |
| Castor oil | 950 | 1500 | 1.4 |
| Aluminium (rolled) | 2700 | 6400 | 17 |
| Steel (mild) | 7800 | 5900 | 46 |
| Lead | 11200 | 2200 | 25 |
| Tungsten | 19400 | 5200 | 100 |
| Polyvinylidine difluoride (PVDF) | 1790 | 2300 | 4 |
| Lead zirconate titanate (PZT) | 7500 | 4000 | 34 |

**Table 1.4** - Attenuation coefficients of various human tissues [211].

| Tissue Type | α (dB cm$^{-1}$ MHz$^{-1}$) |
| --- | --- |
| Blood | 0.2 |
| Fat | 0.5 |
| Liver | 0.5 |
| Brain | 0.6 |

[1] Values depend on the degree of inflation (i.e. air content).

| Tissue Type | α (dB cm$^{-1}$ MHz$^{-1}$) |
|---|---|
| Breast | 0.8 |
| Kidney | 1.0 |
| Skeletal muscle (along fibres) | 1.3 |
| Cardiac muscle | 1.8 |
| Skeletal muscle (across fibres) | 3.3 |
| Bone (cortical) | 7 |
| Bone (trabecular) | 10 |
| Lung | 41 |

### 1.10.2 Generation and Reception of Ultrasound Waves

Ultrasound waves are typically generated and received using the inverse and forward piezoelectric effect, respectively, exhibited by polarised lead zirconate titanate (PZT), a ceramic material[1]. PZT, like other materials (e.g. quartz) that exhibit the piezoelectric effect, produce an electric potential when they are deformed (the forward piezoelectric effect), and they deform when an electric potential is applied to them (inverse piezoelectric effect). Application of a periodically varying electric potential, therefore, results in a periodical deformation and relaxation of the material, producing a mechanical wave. Conversely, ultrasound waves produce an alternating electric potential when they are incident on a piezoelectric transducer. Ultrasound waves can be produced using a single element, but transducers used in medical ultrasound imaging typically employ an array of elements. Modern ultrasound probes can have anywhere between 64 to 300 elements, while newer matrix probes used in three-dimensional ultrasound can have as many as 2500. Focusing can be achieved by using a transducer of an appropriate shape, using an acoustic lens, or by means of electronic focusing.

In continuous wave modes, at least two transducer elements are required so that one can be used for generating ultrasound waves, and the other for simultaneous

---

[1] Polyvinylidine difluoride (PVDF), a plastic, is also sometimes used in transducer design but PZT is more commonly used because it has a higher conversion efficiency.

reception. The use of multiple transducer elements is useful for beam steering, dynamic focusing, and parallel processing. In phased array systems, this is achieved by exciting different groups of transducer elements as appropriate with variable delays between them to achieve these goals.

Depending on the acoustic impedance of the piezoelectric elements, a matching layer is often present in ultrasound probes to reduce the impedance mismatch between the elements and tissue, while a backing layer provides mechanical support and absorbs any mechanical energy transmitted into the probe. The latter reduces excessive vibration (ringing) and allows for the generation of shorter pulses, thus improving axial resolution.

### 1.10.2.1 Ultrasound Signal Processing

Figure 1.6 is a simplified block diagram showing the signal processing chain of the received signal for B-Mode ultrasound. The analogue signal produced by each transducer element is amplified, digitized and summed by the beamformer which also delays and weights the output of each transducer element to accomplish receive focusing and apodisation. Signal processing then carries out in-phase/quadrature (I/Q) demodulation. This is followed by envelope detection (Figure 1.7). Finally, log compression, filtering and scan conversion take place. B-Mode greyscale data, as used in this thesis, is obtained after the display and storage process. Data may also be obtained in radiofrequency format or as analogue signals, but it is typically more difficult to obtain these from clinical scanners.

The returned ultrasound signal, summed over all elements, can be written as in Equation 1.9, in other words an amplitude modulated version of the transmit signal with a time dependent phase shift $\theta$. The transmit signal is of no interest and the extraction of the amplitude and phase information can be achieved by demodulating the returned signal. This can be done by multiplying the received signal with a complex signal and low-pass filtering the result (Equation 1.10). An alternative is to use an analytic signal analysis employing the Hilbert transform (Equation 1.11).
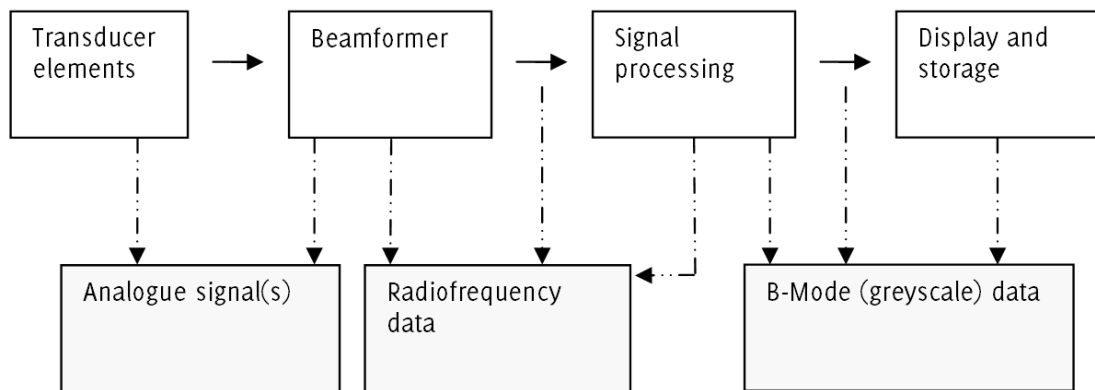
**Figure 1.6** - A simplified block diagram of the received signal processing chain for B-Mode ultrasound where dashed lines show alternative routes for data acquisition.

$$y(t) = A(t)*\cos(2\pi ft+\theta)$$

**Equation 1.9** - The returned ultrasound signal $y(t)$ as an amplitude modulated version of the transmit signal with a time dependent phase shift $\theta$.

Let $f(t) = y(t)*e^{i2\pi ft}$

then, $f(t) = A(t)*\cos(2\pi ft+\theta)*[\cos(2\pi ft)+i*\sin(2\pi ft)]$

thus, $f(t) = A(t)*\cos(2\pi ft+\theta)*\cos(2\pi ft)+A(t)*\cos(2\pi ft+\theta)*i*\sin(2\pi ft)$

thus, $f(t) = A(t)/2*[\cos\theta+\cos(4\pi ft+\theta)]+i*A(t)/2*[\sin(4\pi ft+\theta)-\sin\theta]$

After low-pass filtering, $f(t) = A(t)/2*\cos\theta-i*A(t)/2*\sin\theta$

thus, $f(t) = A(t)/2e^{-i\theta}$

Hence, $A(t) = 2*abs(f(t))$ and phase $\theta = arg(f(t))$

**Equation 1.10** - Demodulation of the returned ultrasound signal $y(t)$ to obtain the signal envelope $A(t)$ and phase $\theta$.

Let f(t) = y(t) + i*z(t) where z(t) is the Hilbert transform of y(t)

thus, z(t) = 1/π * ∫y(t')/(t'-t)dt'

or, z(t) = convolution of -1/(πt) with y(t)

Then, $A(t)=(y(t)^2+z(t)^2)^{1/2}$ and phase θ=tan$^{-1}$(z(t)/y(t))

**Equation 1.11** - Determination of the returned ultrasound signal envelope A(t) and phase θ using the Hilbert Transform/analytic signal method.
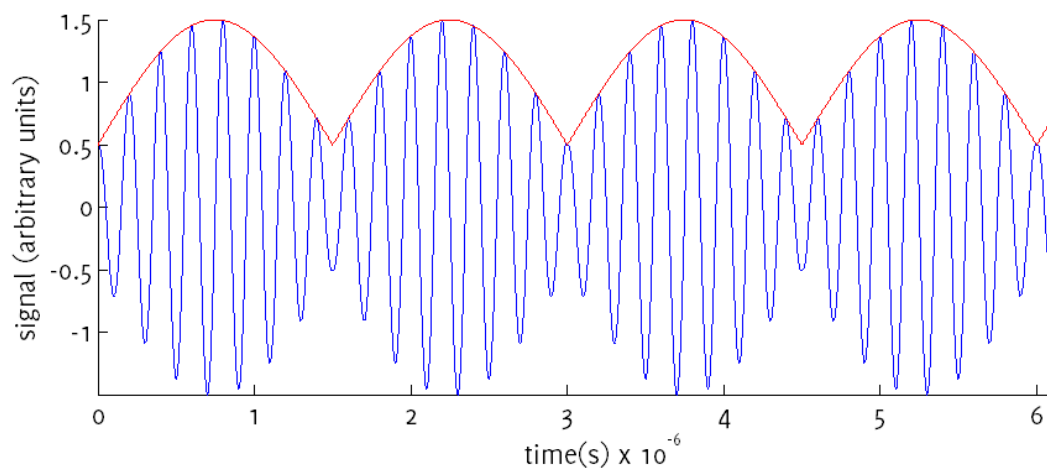


**Figure 1.7** - Illustration of a signal envelope. Blue lines show an amplitude modulated 5 MHz sinusoidal radiofrequency signal while the red curve shows the signal envelope.

### 1.10.3 Biological Effects and Safety

Ultrasound is generally considered to be a safe imaging modality [207-208,213]. However, ultrasound does interact with tissues, and biological effects can become important (and in fact are used in ultrasound therapy) at higher intensities and with certain tissue types such as the eyes, air containing organs (e.g. lungs, intestines), foetuses, embryos, and bone.

Biological effects of ultrasound are generally classified under two headings: thermal and non-thermal effects. Thermal effects refer to the local tissue heating that is caused by ultrasound exposure. However, it is generally believed that at diagnostic levels these are too low to constitute a hazard [207]. On the other hand, higher temperature increases can occur, for example, adjacent to bone surfaces. The most rapid heating takes place in the centre of the beam at the focus, where the beam intensity is highest. Heating is also more likely to be greater with stationary beams (e.g. spectral Doppler), compared with ultrasound modes in which the beam is translated across a region (e.g. B-Mode). Heat produced in this manner is conducted away to nearby cooler tissues and some may be carried away by blood flow. However, there will typically be a steady state increase in local tissue temperature which can be damaging to cells. Human bone marrow cells, for example, will tolerate a raised local tissue temperature of $41^{o}$C for long periods of time (greater than 200 minutes), but survival is very short (less than 20 minutes) at higher temperatures ($45.5^{o}$C) [214]. The World Federation for Ultrasound in Medicine (WFUMB) recommends that a diagnostic exposure which does not produce a temperature rise greater than $1.5^{o}$C above the normal physiological level (e.g. $37^{o}$C) may be used clinically without reservation on thermal grounds [215]. On the other hand, it is also recommended that a diagnostic exposure which increases embryonic or fetal tissues $4^{o}$C above normal temperature (e.g. $41^{o}$C) for 5 minutes or more should be considered potentially hazardous [215].

Non-thermal effects include stable and transient (inertial) cavitation and microstreaming. At low amplitudes, ultrasound can cause breathing oscillation (periodical expansion and compression) of gas bubbles, which may grow by rectified diffusion with long pulses or continuous wave exposures. In the later case, more gas diffuses into the bubble during rarefaction than diffuses out during compression due to differences in surface areas between these two phases. Bubbles with radii of the order of 1μm may resonate at diagnostic frequencies, and at high pressure amplitudes the inertia of the bubble surface can become important. In transient or inertial cavitation, large changes in bubble diameter may occur, resulting in the collapse of the bubble, leading to large increases in local temperatures and pressures. This can cause the sonoporation or lysis of adjacent cells, and can lead to local tissue damage.

Inertial cavitation only occurs in the presence of suitable gas bubbles, and is more likely to occur at higher acoustic pressures and lower frequencies. Inertial cavitation is also more likely to occur in the lungs and intestines (due to the presence of gas in these organs) and in the presence of contrast agents. Tissue damage may occur at diagnostic pressure levels in these situations.

Micro-streaming currents, on the other hand, occur around gas bubbles undergoing breathing oscillations. Large velocity gradients may be present in these micro-streaming currents and can cause shear stresses in cell walls giving rise to membrane rupture or sonoporation.

### 1.10.3.1 Thermal and Mechanical Indices

The American Institute of Ultrasound in Medicine (AIUM)/National Electrical Manufacturers Association (NEMA) Output Display Standard defines two indices related to the biological effects of ultrasound that should be displayed by ultrasound equipment. The Thermal Index (TI) is a measure of the estimated maximum temperature rise that may be expected in tissue and is calculated as the total acoustic power output divided by the power required to raise tissue temperature by $1^{o}$c. However, it does not take into account any additional heating that may be caused by probe heating. Three thermal indices are defined: TIS is the appropriate value for soft tissues, TIB is for bone and TIC is for bone at the surface. British Medical Ultrasound Society (BMUS) advises that below a TI of 0.7 there need not be any restrictions on scanning unless there is noticeable probe heating or if the maternal temperature is elevated [216]. Above a TI of 0.7, it is advised that the exposure of an embryo or foetus should be restricted. Above a TI of 1.0, eye scanning is not recommended, except as part of a foetal scan. At and above a TI of 3.0, scanning of an embryo or foetus, however briefly, is not advised. Maximum exposure time for an adult is advised to be 30 minutes at a TI of 1.0, reducing to 15 minutes at a TI of 1.5, and 1 minute at a TI of 2.5.

The Mechanical Index (MI), given by Equation 1.12, is a measure used to evaluate the likelihood of tissue damage occurring due to non-thermal effects (e.g. cavitation or micro-streaming). Modern diagnostic ultrasound equipment display the TI and the MI, although there is no requirement to display these if they are less than 0.4 and no requirement to display them at all if the equipment can not exceed a TI or MI of 1. BMUS advises that at an MI of less than 0.3 there need not be any restrictions on scanning from a mechanical effects perspective, but at an MI between 0.3 and 0.7 there is a risk of damage to neonatal lung or intestine, and such exposures, if necessary, should be limited as much as possible. At an MI of 0.7 and above, there is an increasing risk of cavitation particularly if contrast agents are used. Food and Drug Administration (FDA) limits for MI in the United States are 1.9 for non-ophthalmic applications and 0.23 for ophthalmic applications. FDA limits for thermal effects are given in terms of the spatial peak temporal average intensity ($I_{SPTA}$) and are 720 mW/cm$^2$ for non-ophthalmic applications and 50 mW/cm$^2$ for ophthalmic applications.

$$MI = p_{r.3}(z_{sptp})/f_c^{1/2}$$

Equation 1.12 - The Mechanical Index (MI) is calculated as the spatial and temporal peak de-rated negative pressure ($p_{r.3}(z_{sptp})$) divided by the square root of the centre frequency of the pulse spectrum ($f_c$). The pressure amplitude must be entered into this equation in MPa and frequency in MHz. As an example, if $p_{r.3}(z_{sptp})$ is 1 MPa and $f_c$=5 MHz, then MI=$1/5^{1/2}$=0.45.

## 1.11 Guide to the Thesis

The rest of the thesis is structured as follows: Chapter 2 introduces a probabilistic algorithm for tracking arterial lumen surfaces in ultrasound image sequences, which is subsequently developed in Chapter 3 into a method for tracking plaque boundaries throughout the cardiac cycle. Chapter 3 also investigates the frame-by-frame variations in the observed plaque GSM and points out that these previously unexplored variations may be partly responsible for the variations in plaque GSM previously found

across centres and studies. Chapter 4 extends the literature by providing a novel method for measuring plaque surface irregularities and shows that by taking into account the surface structure of plaques, measured by objective quantitative means, symptoms can be predicted more accurately compared to the degree of stenosis on its own. Chapters 5 then studies arterial wall motion in the stenotic carotid artery; while Chapter 6 looks at plaque motion throughout the cardiac cycle. Chapter 7 represents the culmination of the thesis, and develops novel risk indices for carotid artery stenosis, incorporating the degree of stenosis, plaque GSM and surface irregularities. It is shown that, unlike the previously developed indices, these risk indices improve diagnostic performance without relying on parameters optimized for the dataset; the latter limit applicability due to variations in measurements across centres. Finally, Chapter 8 summarises and discusses the whole thesis and identifies limitations and future directions for research.

# Chapter 2

# A Probabilistic Approach to Tracking of Arterial Walls in Ultrasound Image Sequences

## 2.1 Overview

This chapter introduces a probabilistic method for tracking arterial walls in ultrasound image sequences, which can be used to study the dynamic behaviour of arteries. This is developed into a method for tracking plaque boundaries in Chapter 3 and is used for the dynamic assessment of greyscale plaque characteristics throughout the rest of the thesis. The novel method of tracking arterial walls introduced in this chapter is also used to study wall motion in the stenotic carotid artery in Chapter 5. In collaboration with the Leicester Diabetes Centre, it is also used for studying the endothelium-dependent, flow-mediated dilation of the brachial artery. A research article based on the contents of this chapter was published in International Scholarly Research Network (ISRN) Signal Processing [217].

## 2.2 Introduction

Greyscale ultrasound imaging (B-Mode) is an established tool for the non-invasive imaging of the human body. Such imaging procedures are often accompanied by measurements that are conveniently performed using the ultrasonic calipers. However, if performed manually, it rapidly becomes a time consuming, difficult task for the operator if the measurements need to be repeated a large number of times, for example over a time series. In B-Mode vascular ultrasound, such a situation arises, when one needs to track the position of the arterial walls over many frames in order to study to distension of the arteries throughout the cardiac cycle. Although specific solutions for tracking the position of the arterial walls using B-Mode ultrasound have been previously described (Table 2.1), for example by region tracking/block matching [196] or computerized edge detection [218], many of these techniques are limited in terms of applicability, while some techniques have a particular vulnerability to image noise. Also, a general purpose segmentation algorithm should be able to track the

position of the arterial walls over a sizeable length of the artery, for any vessel orientation and morphology.

One solution to the problem of arterial wall tracking was by Wendelhag et al. who described a method for measuring the intimate-media thickness and the lumen diameter for the carotid and femoral arteries by means of an analysis system based on dynamic programming [219,229]. However, it was reported that manual corrections were required in a significant portion of the images. Beux et al. presented an automatic procedure to study endothelium-dependent dilation of the brachial artery which involved imposing a threshold on the normalized greyscale intensity to locate the arterial lumen and an intensity gradient criterion to subsequently locate the arterial lumen boundaries [220]. However, this technique worked only in longitudinal cross sectional views of arteries with specific assumptions being made regarding the orientation, curvature, and appearance of the artery. Cheng et al. described a method for detecting the intima-media complex of the far wall of the common carotid artery using active contour models. However, the processing of a single frame of ultrasound image was reported to have taken between 30 seconds and 1 minute which was a major drawback [221].

Newey and Nassiri employed artificial neural networks to detect the anterior and posterior vessel walls of arteries in the longitudinal plane, but it was clear that this technique was directly applicable only to relatively straight, and horizontal sections of arteries [222]. Chen et al. [223], on the other hand, described a cell-competition algorithm for the simultaneous segmentation of multiple objects in a sonogram. The cell-competition algorithm was validated on 13 synthetic images and 71 breast sonograms but applicability to vascular ultrasound image sequences was not investigated.

**Table 2.1 -** A survey of solutions related to the problem of tracking arterial walls in B-mode ultrasound image sequences.

| Reference | Year | Basis of Technique | Applications | Limitations |
|---|---|---|---|---|
| Wendelhag et al. [219] | 1997 | Cost function minimisation. | Measurement of intima-media thickness and arterial lumen diameter. | Extensive manual corrections required. |
| Selzer et al. [218] | 2001 | Edge detection. | Measurement of artery diameter and intima-media thickness. | Operator intervention frequently needed. |
| Beux et al. [220] | 2002 | Greyscale intensity and gradient thresholding. | Endothelium-dependent dilation of the brachial artery. | Dependence on vessel orientation, curvature, and appearance. |
| Cheng et al. [221] | 2002 | Active contours. | Detection of the intima-media complex of the far wall of the common carotid artery. | Long processing times. |
| Newey and Nassiri [222] | 2002 | Artificial neural networks. | Detection of the near and far walls of the artery in the longitudinal plane. | Relatively horizontal and straight vessel assumed. |
| Golemati et al. [196] | 2003 | Region tracking/block matching. | Estimation of carotid artery wall motion. | Limited number of points could be tracked due to computational cost. |
| Chen et al. [223] | 2005 | Cell competition. | Lesion boundary delineation in breast sonograms. | Applicability to vascular ultrasound image sequences not known. |

| Reference | Year | Basis of Technique | Applications | Limitations |
|---|---|---|---|---|
| Hii et al. [224] | 2006 | Normalized correlation coefficient. | Speckle tracking in breast sonograms. | Applicability to vascular ultrasound image sequences not investigated. |
| Cardinal et al. [225] | 2006 | Fast marching algorithm. | Segmentation of intravascular ultrasound images. | Required manual delineation of initial contours. |
| Golemati et al. [226] | 2007 | Hough transform. | Extraction of carotid artery lumen surface. | Arterial cross-sections approximated as straight lines and circles. |
| Mendizabal-Ruiz et al. [227] | 2008 | Polar representation. | Delineation of lumen boundaries in intravascular ultrasound images. | Limitations on the types of contours that could be traced. |
| Yang et al. [228] | 2011 | Edge detection and mathematical morphology. | Delineate vessel lumen boundaries. | Works for transverse cross-sections of arteries. |

The method described by Hii et al. [224] allowed for the normalized correlation coefficient (NCC) to be determined significantly faster then Fast Fourier Transform (FFT) based methods, which is useful for motion tracking as the NCC can be used as a similarity measure in block matching methods. However, speckle decorrelation limits the applicability of region tracking/block matching methods and the absence of unique features along straight segments of arterial walls can cause tracking failure.

The technique described by Cardinal et al. for the segmentation of intravascular ultrasound (IVUS) images worked by detecting a mixture of Rayleigh distributions in the IVUS data followed by a fast marching algorithm which converged on the boundaries of interest [225]. However, the method required the manual delineation of initial contours near the contours of interest to operate. Golemati et al. [226] used the Hough transform to extract the carotid artery lumen surface from longitudinal and transverse sections of arteries, but arterial lumens were modelled as straight lines and circles, respectively, limiting applicability in real-life situations. Mendizabal-Ruiz et al. described a probabilistic segmentation method for IVUS, modelling the lumen contour as a periodic mixture of Gaussians [227], once again placing constraints on the type of contour that can be tracked. Yang et al., on the other hand, employed edge detection and mathematical morphology techniques to delineate vessel lumen boundaries in transverse cross-sections of the common carotid artery but it was not investigated whether the method would also work for longitudinal cross sections of arteries [228].

A recent survey of ultrasound image segmentation methods [230] presented a selection of methods for various clinical applications, including intravascular ultrasound; however, the segmentation of longitudinal cross-sections of arteries was not covered. Thus, although specific methods for B-Mode ultrasound image segmentation have been developed, there appears to be currently no simple solution that can be applied to the diverse range of arterial configurations and imaging conditions encountered, and yet be easily implementable by different centres. Also, some techniques, such as those based on edge detection, are particularly vulnerable to speckle noise as the latter can produce false edge signals. The efficiency of the method is also important as long processing times hinder the practical analysis of long ultrasound image sequences and any possible implementation in real-time. This chapter describes a probabilistic

approach to the segmentation of carotid artery ultrasound image sequences and demonstrates good arterial wall tracking performance, comparable to a more established Tissue Doppler Imaging (TDI) technique [231-232]. This algorithm effectively segments arterial lumens in both longitudinal and transverse cross-sections with little effort on the operator's part.

## 2.3 Methods

First I describe the thought process I used to derive the probabilistic algorithm for arterial lumen segmentation. The process essentially involves simulating the behaviour of the human operator in silico. It is the relatively echo-free (dark) region that draws the attention of the human operator in the first instance when he/she looks at an ultrasound image of the carotid artery. Focusing on any given point in this region, he/she then scans around that point, considering any neighbouring points to be belonging to the same lumen unless there is an abrupt change in the image brightness, in which case he/she may assume that the boundary of the lumen is reached. The brain is, of course, equipped with higher-level decision making processes, but at the low-level, this behaviour may be modelled in three steps: focusing on a lumen of interest, associating neighbouring points in terms of the greyscale similarity between them, and scanning around the point focussed on until the boundaries are found. The rest of this section describes the implementation of this behaviour in silico.

In the probabilistic approach, the probabilities of individual points being within an arterial lumen are associated using a Gaussian relationship. Given a greyscale ultrasound image, a corresponding probability matrix is evaluated where each matrix element represents the probability of that element's respective image pixel being within the artery of interest. The probabilities are computed as follows: given a point B which had a probability $P_b$ of belonging to a certain arterial lumen, the probability $P_a$ that a neighbouring point A also belongs to the same lumen is evaluated as being directly proportional to $P_b$ with a Gaussian dependence on the greyscale contrast between to two points, and an average is taken over the 8 immediate neighbours (Equation 2.1). Here, $G_b$ and $G_a$ are the greyscale intensities of points B and A, and the

constant $\zeta$ is determined by considering the amount of greyscale contrast ($G_{th}$) required to reduce $P_a$ to 1/2 that of $P_b$.

$$P_a = (1/8) \times \sum P_b \, \exp(-(G_b-G_a)^2/\zeta)$$

**Equation 2.1** - The probabilistic algorithm. $\zeta = G_{th}^2/\log 2$ and the sum is taken over the 8 immediate neighbours.

The value of $G_{th}$ is set at 1% of the full range by default but can be altered by the operator if necessary. The operator provides one or more seed points (i.e. points inside the arterial lumen) which are assigned corresponding probabilities of being within the arterial lumen of interest of 1.0, and the probabilities of the remaining points are determined using Equation 2.1. In the case of multiple seed points, the maximum of the probabilities evaluated using each of the seed points is used. The calculation of the probability values starts with the immediate neighbours of each given seed point, and iteratively propagates to more distant neighbours, starting with the nearest, and culminating in the most distant, along a rectangular wavefront.

Finally, the segmentation is performed by passing the probability matrix obtained through the contour function in MATLAB version 7.14 (MathWorks, Natick, Massachusetts, USA) which determines the isolines separating probability values greater than or equal to a user-adjustable probability value $P_{th}$ (set to 0.10 by default) from those that are lower. These isolines represent the segmentation result. An alternative means of using the probability matrix is to construct a binary map, representing the points within the arterial lumen of interest, determined as those which have a probability value greater than or equal to $P_{th}$.

### 2.3.1 Pre-processing

In order to reduce the effects of speckle noise, images are pre-processed, before the above processing takes place, by applying a circular averaging filter of radius 0.425

mm (5 pixels at a reference resolution of 11.77 pixels/mm). The actual filter size in pixels is given by Equation 2.2.

filter size = $0.425\sqrt{(X*Y)}$

**Equation 2.2** - Calculation of the filter size. X and Y are the image resolution in the horizontal and vertical directions, respectively, in pixels/mm.

### 2.3.2 Methods of Evaluation

The efficacy of the algorithm was evaluated by testing it on clinical images of the carotid arteries and the abdominal aorta, and various laboratory, ultrasound test objects. Clinical data included B-Mode carotid artery image sequences from patients acquired using a Philips HDI5000 scanner with an L12-5 probe and a Philips iU22 scanner with an L9-3 probe (Philips Healthcare, Eindhoven, The Netherlands). Image sequences were also obtained from a healthy volunteer using an Aixplorer scanner (Supersonic Imagine, Aix-en-Provence, France) with the L15-4 probe. The use of the data for this purpose was approved by the Leicestershire and Rutland Medical Ethics Committee, and patients and the volunteer gave their informed consent before participating in the study.

Laboratory data included ultrasound image sequences from walled and wall-less flow phantoms and various laboratory test objects acquired using the Philips HDI5000 scanner with the L12-5 probe. The tissue mimicking material used in the construction of the hypo- and hyper-echoic test objects, and the wall-less flow phantom was an agar based formulation [233]. A blood mimicking fluid was circulated [234-235] in the flow circuit of the walled (C-flex™, Cole-Palmer, IL, USA) and wall-less flow phantoms. A computer controlled fluid pump was used to circulate the blood mimicking fluid using a carefully selected input waveform to induce wall dilations in the phantom similar to the dilation characteristics of the carotid artery [236].

Performance was also compared against a conventional region growing technique based on intensity thresholding with a running average region intensity [237]. Images were pre-processed using the same filter, and same seed points and threshold values were used in both the case of the probabilistic algorithm and the conventional region growing technique. The efficiency of the probabilistic algorithm was also evaluated under high image-noise conditions by means of adding Gaussian noise of varying strengths to carotid artery ultrasound images and by testing the method on image sequences with substantial amounts of speckle noise within the vessel lumen from the abdominal aorta, and walled and wall-less flow phantoms.

### 2.3.3 Software and Hardware

Implementation was carried out using MATLAB version 7.14 (MathWorks, Natick, Massachusetts, USA) with portions of the probabilistic algorithm written in the C language for efficiency. The analyses were performed on a self-built personal computer with an Intel Core i5-2500K CPU (Intel Corporation, California, USA) running at 3.30 GHz. The computer was running the 64-bit version of Windows 7 Ultimate (Microsoft Corporation, Seattle, USA).

### 2.4 Results

Setting the algorithm threshold to 2% and choosing a point inside the arterial lumen in a carotid artery with plaque on the posterior wall, the probabilistic algorithm produced the first pass estimate boundary outline and the corresponding probability map seen in Figure 2.1. Adding another seed point produced the overall probability map and segmentation result seen in Figure 2.2. The final arterial boundary outline including that of the plaque surface obtained by adding three more seed points was as shown in Figure 2.3. A close-up view of the segmentation result over the plaque surface can be seen in Figure 2.4.

The result of tracking the arterial lumen for a longitudinal image sequence with one seed point was as shown in Figure 2.5. Investigations made on the processing of this 90 frame image sequence of dimensions 263 (height) x 256 (width) pixels indicated a processing time of approximately 33 milliseconds/frame on the analysis computer

used. However, since the implementation was not designed to take full advantage of the multi-core CPU architecture and was not optimised, it was also observed that the processor as a whole was only running at approximately 30% of full capacity during the analysis. Whole image sequences showing tracking results for this sample under extreme noise conditions can be downloaded from:

https://dl.dropboxusercontent.com/u/13857734/pp/FIG2.5.n1.avi
https://dl.dropboxusercontent.com/u/13857734/pp/FIG2.5.n2.avi
https://dl.dropboxusercontent.com/u/13857734/pp/FIG2.5.n3.avi

Arterial lumens could be effectively segmented with a few seed points in a variety of arterial configurations and image-noise conditions (Figure 2.6). The result of segmentation and tracking of the residual arterial lumen and plaque surface in the transverse plane was as in Figure 2.7. Investigation of segmentation performance in the presence of computationally added Gaussian image-noise produced the results seen in Figures 2.8 to 2.11. In an image sequence from the abdominal aorta, wall tracking in the presence of substantial amounts of image-noise was as in Figure 2.12.

The results of lumen surface tracking for a walled flow phantom with blood mimicking fluid in the flow circuit produced the results Figure 2.13. Tracking results for the laboratory test objects and the comparison between Vernier caliper measured physical dimensions and algorithm-determined dimensions were as in Figure 2.14 and Table 2.2, respectively.

Tracking of the arterial wall diameter for the common carotid artery from the healthy volunteer using an image sequence obtained on the Aixplorer scanner produced the arterial dilation waveform seen in Figure 2.15.

Comparison of algorithm efficacy against the conventional region growing technique showed that the performance of the probabilistic algorithm surpassed that of the conventional region growing algorithm with differences more apparent under high-image noise conditions (Figure 2.16).
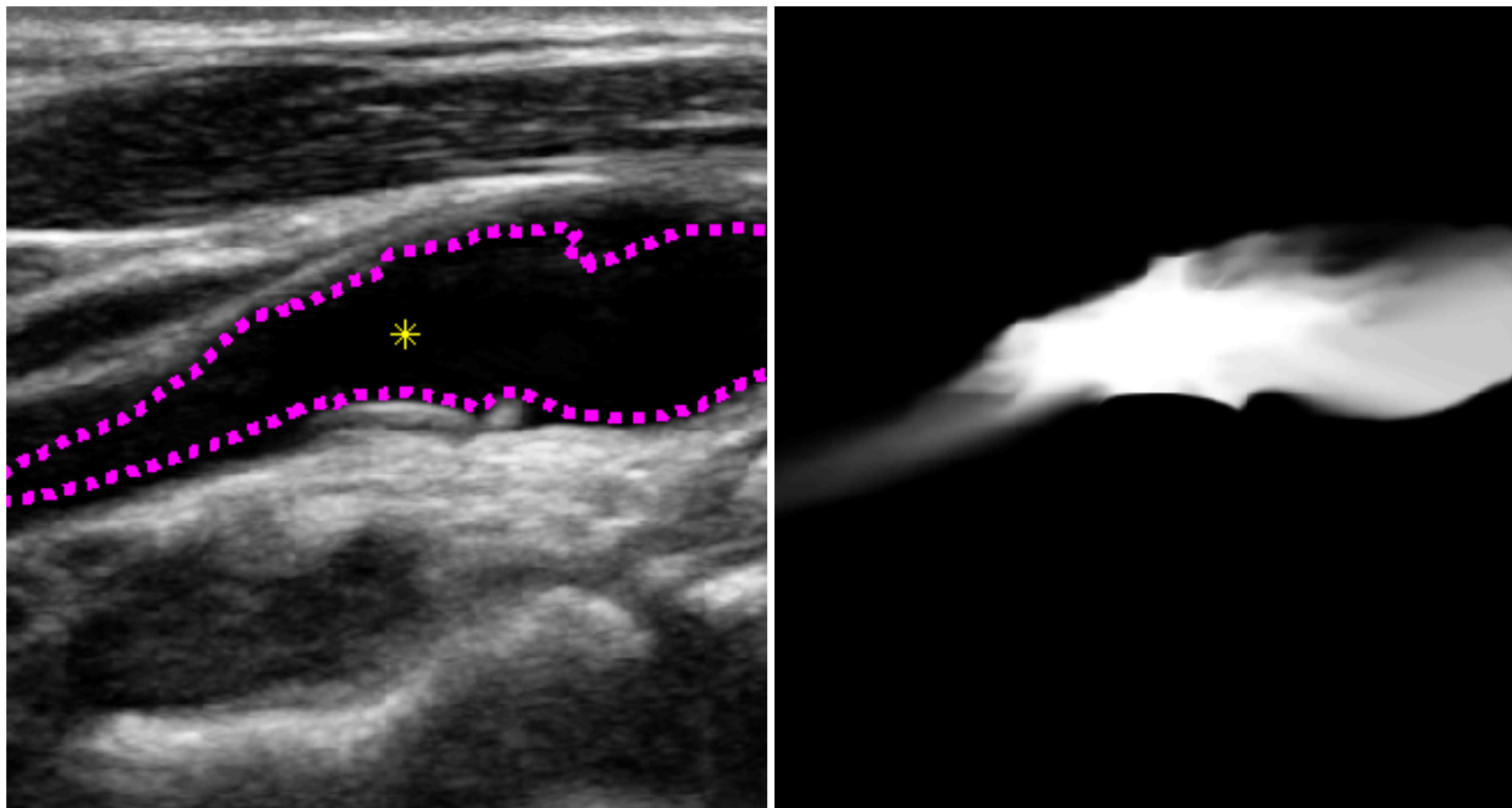
**Figure 2.1** - First pass segmentation result (left) for a carotid artery with plaque on the posterior wall, and the corresponding probability map (right). Probability values range from 0 (black) to 1.0 (white).
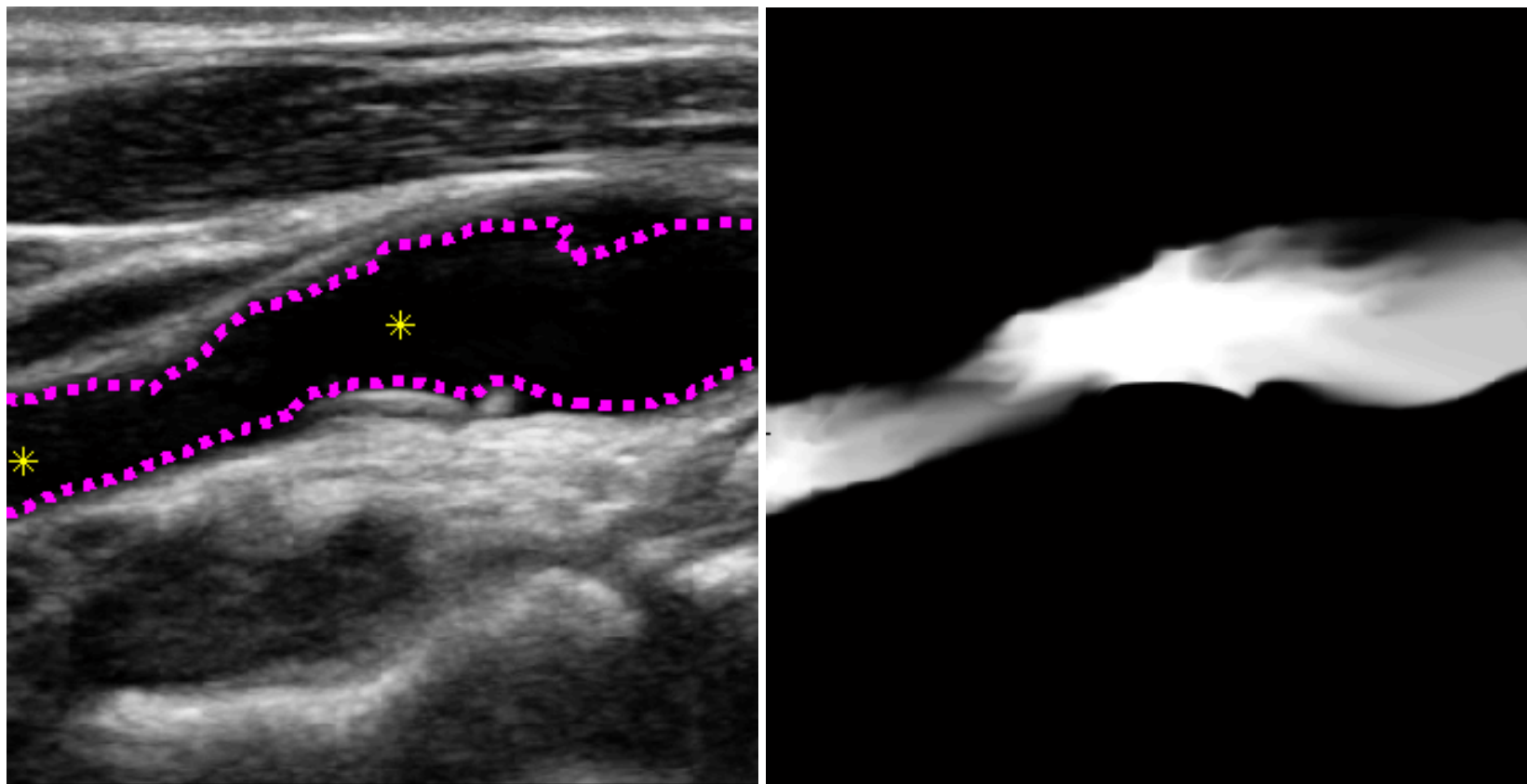
**Figure 2.2** - The effect of adding another seed point. Segmentation result (left) and combined probability map (right).
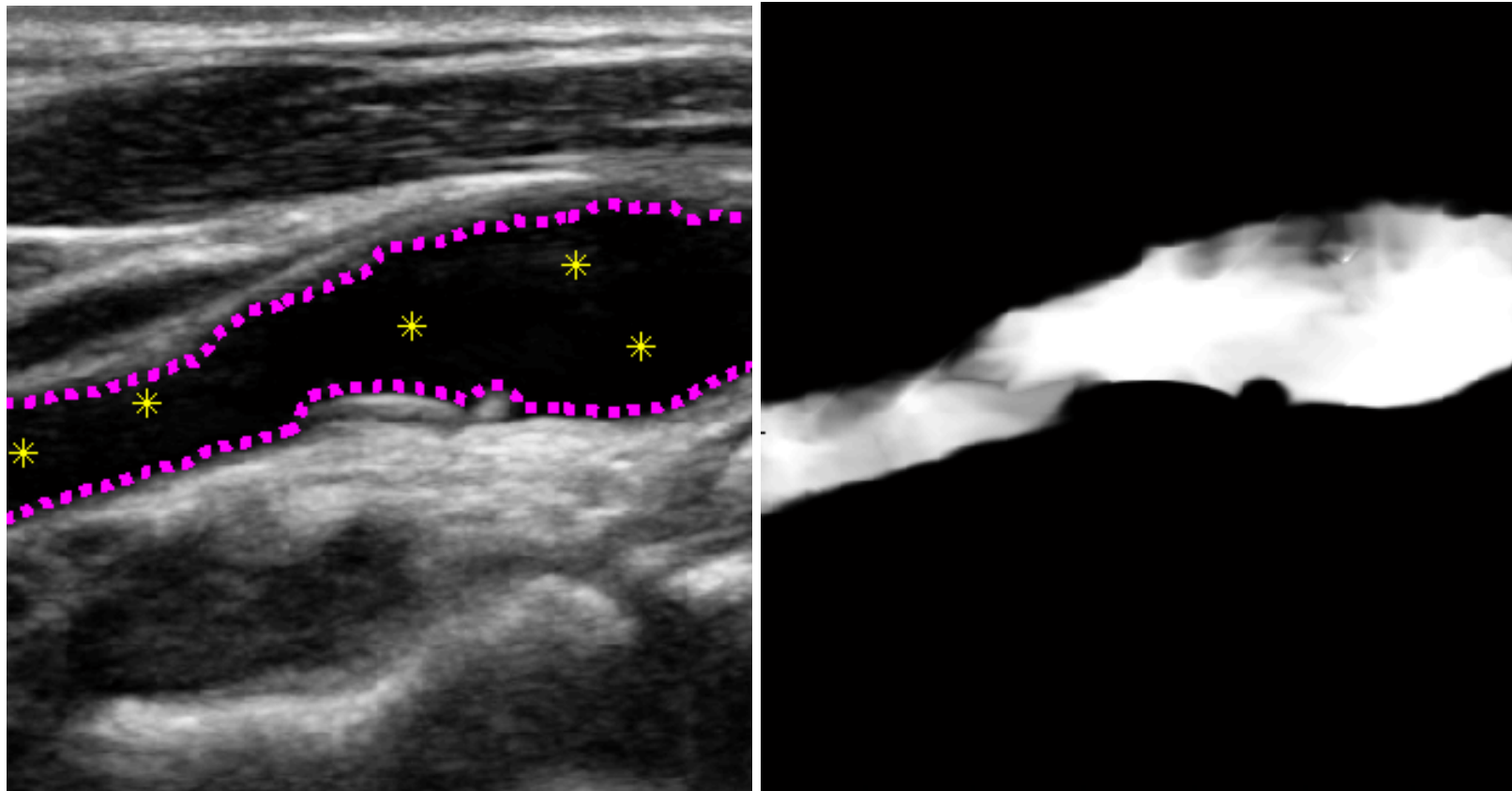
**Figure 2.3** - Final segmentation result (left) and combined probability map (right) with three additional seed points.
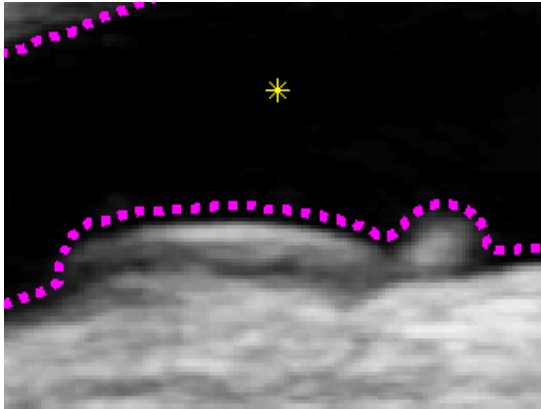
**Figure 2.4** - A close-up view of the segmentation result over the plaque surface.
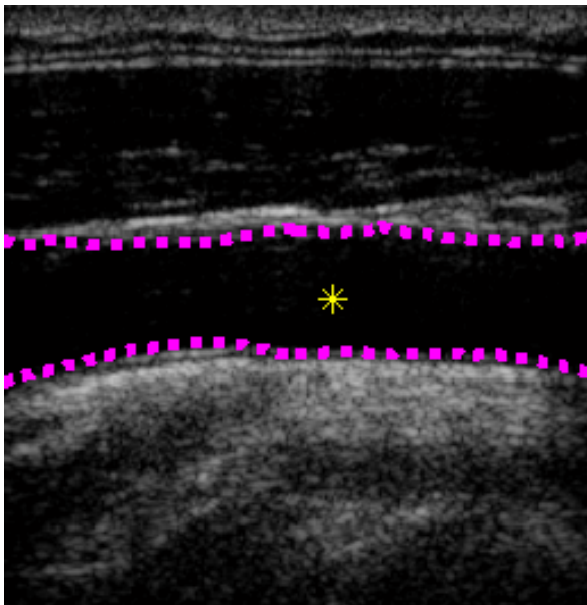


**Figure 2.5** - Tracking of the arterial lumen for a carotid artery image sequence (single frame shown). The whole image sequence is available to download from https://dl.dropbox.com/u/13857734/pp/tt.avi.
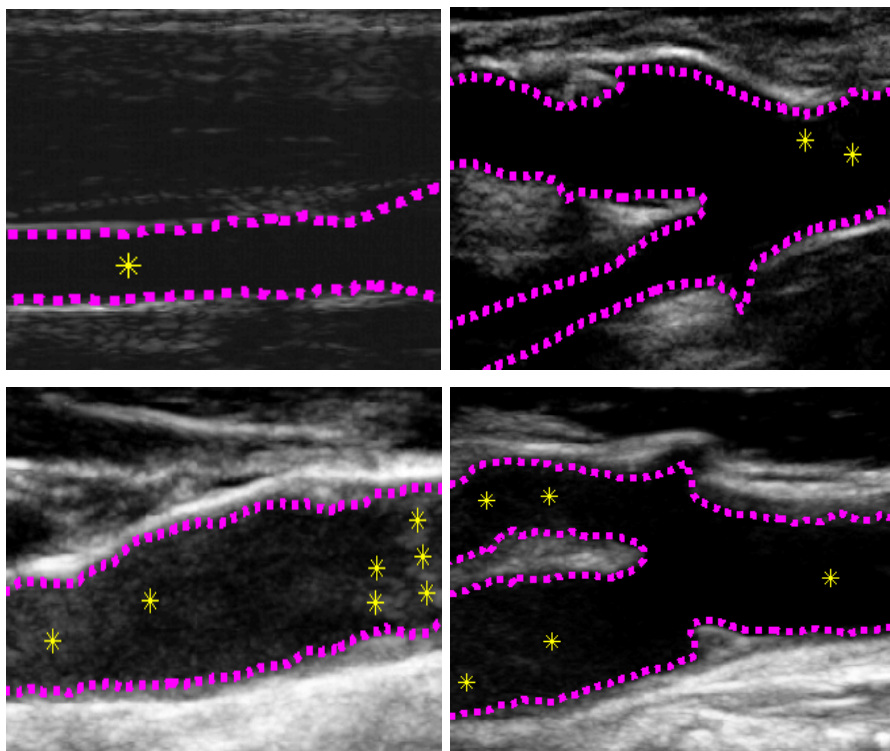
**Figure 2.6** - Arterial lumen segmentation in a variety of vessel configurations and image-noise conditions.
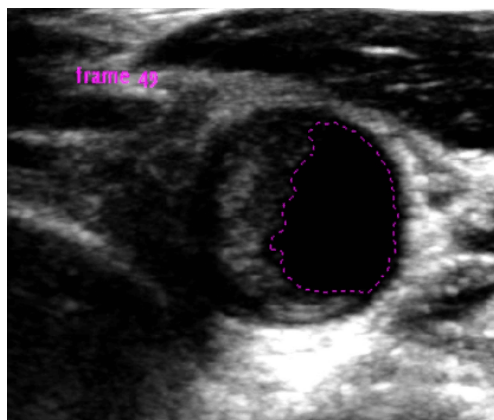


**Figure 2.7** - Tracking of the residual arterial lumen and plaque surface in the transverse plane (single frame shown). The whole image sequence is available for download from http://dl.dropbox.com/u/13857734/pp/t1.avi.
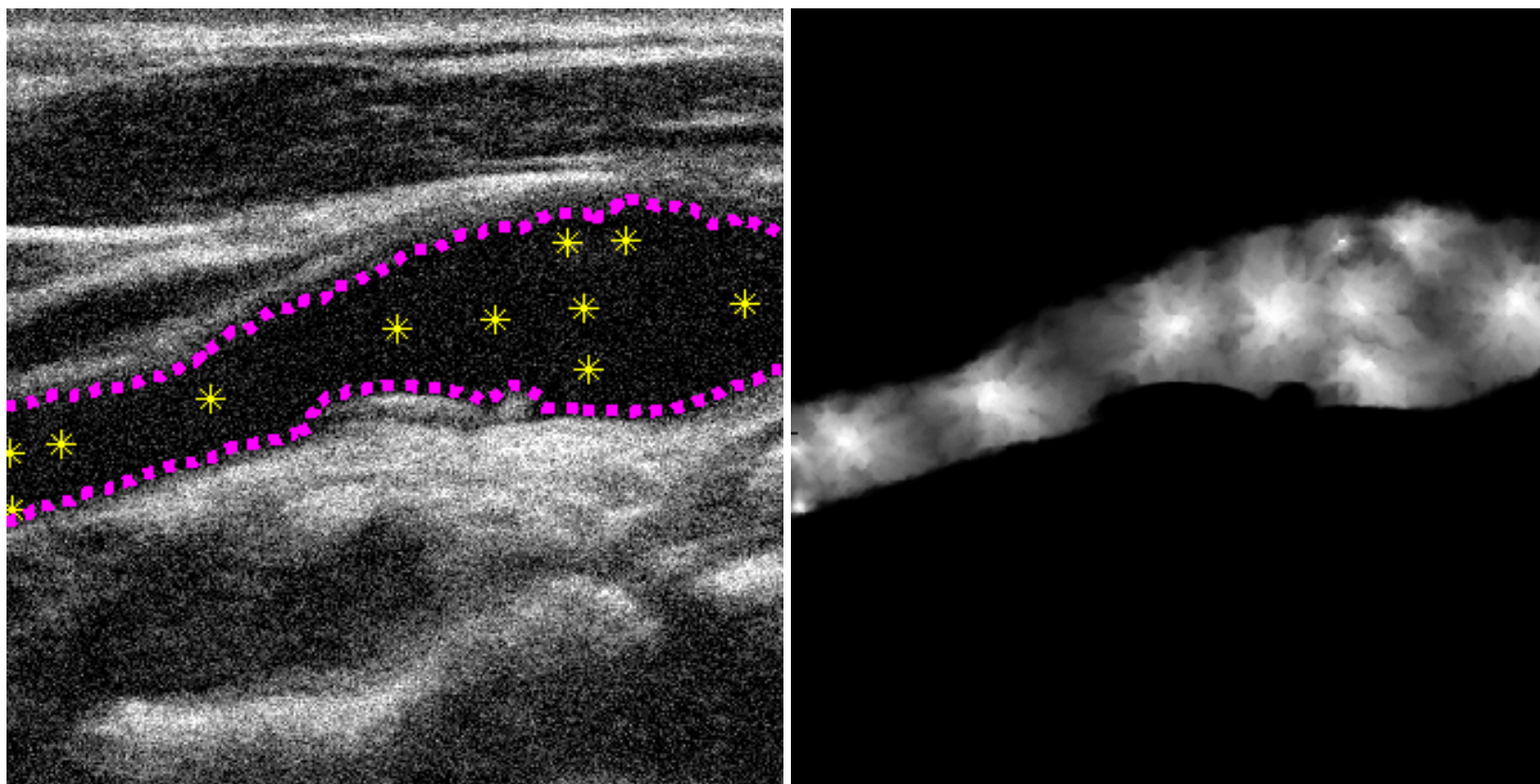
**Figure 2.8** - Segmentation result (left) and probability map (right) in the presence of computationally added Gaussian noise with an approximate standard deviation of 36.1 grey levels, evaluated at an algorithm threshold setting of 2%.
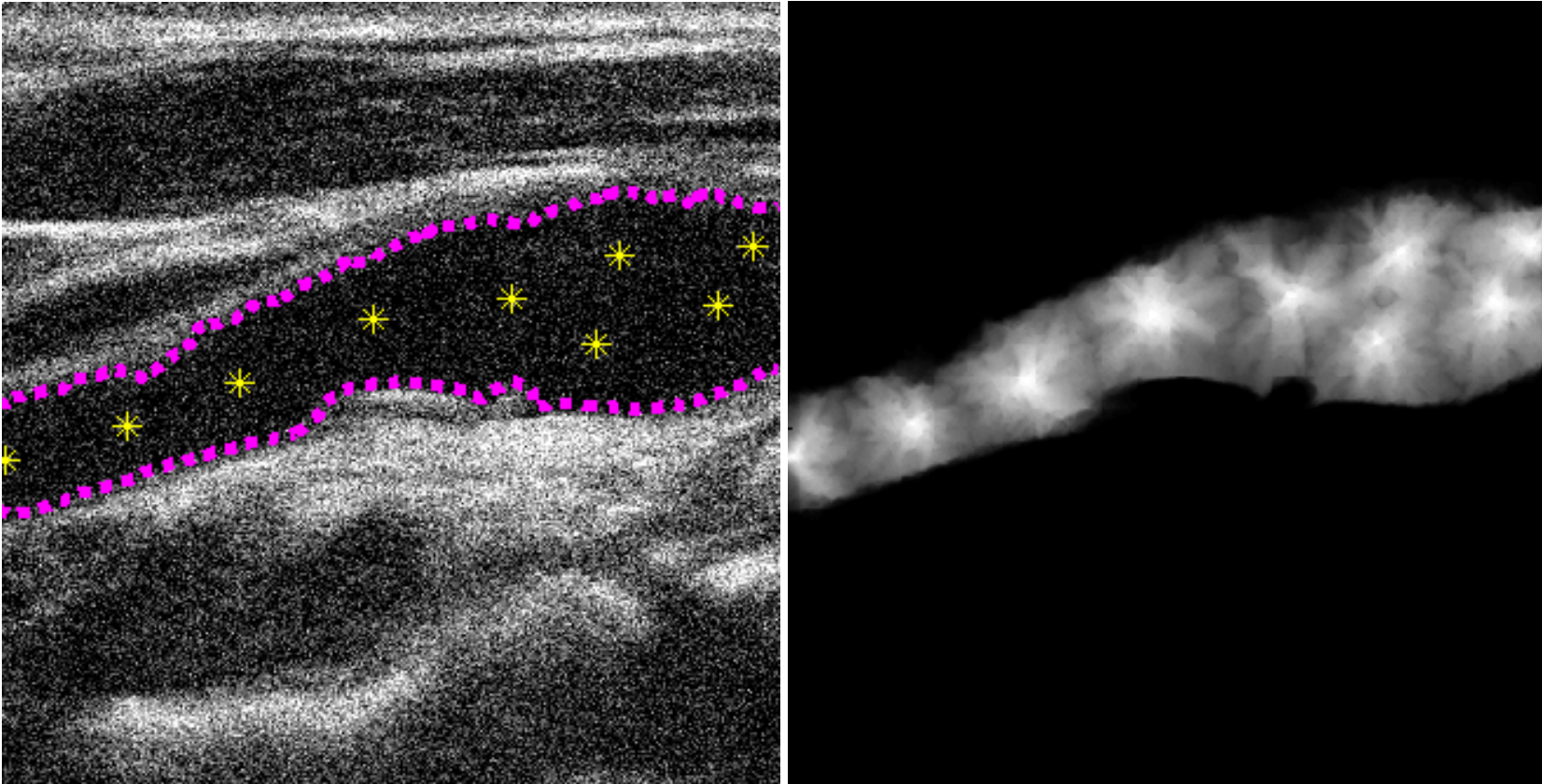
**Figure 2.9** - Segmentation result (left) and probability map (right) in the presence of computationally added Gaussian noise with an approximate standard deviation of 51.0 grey levels, evaluated at an algorithm threshold setting of 4%.
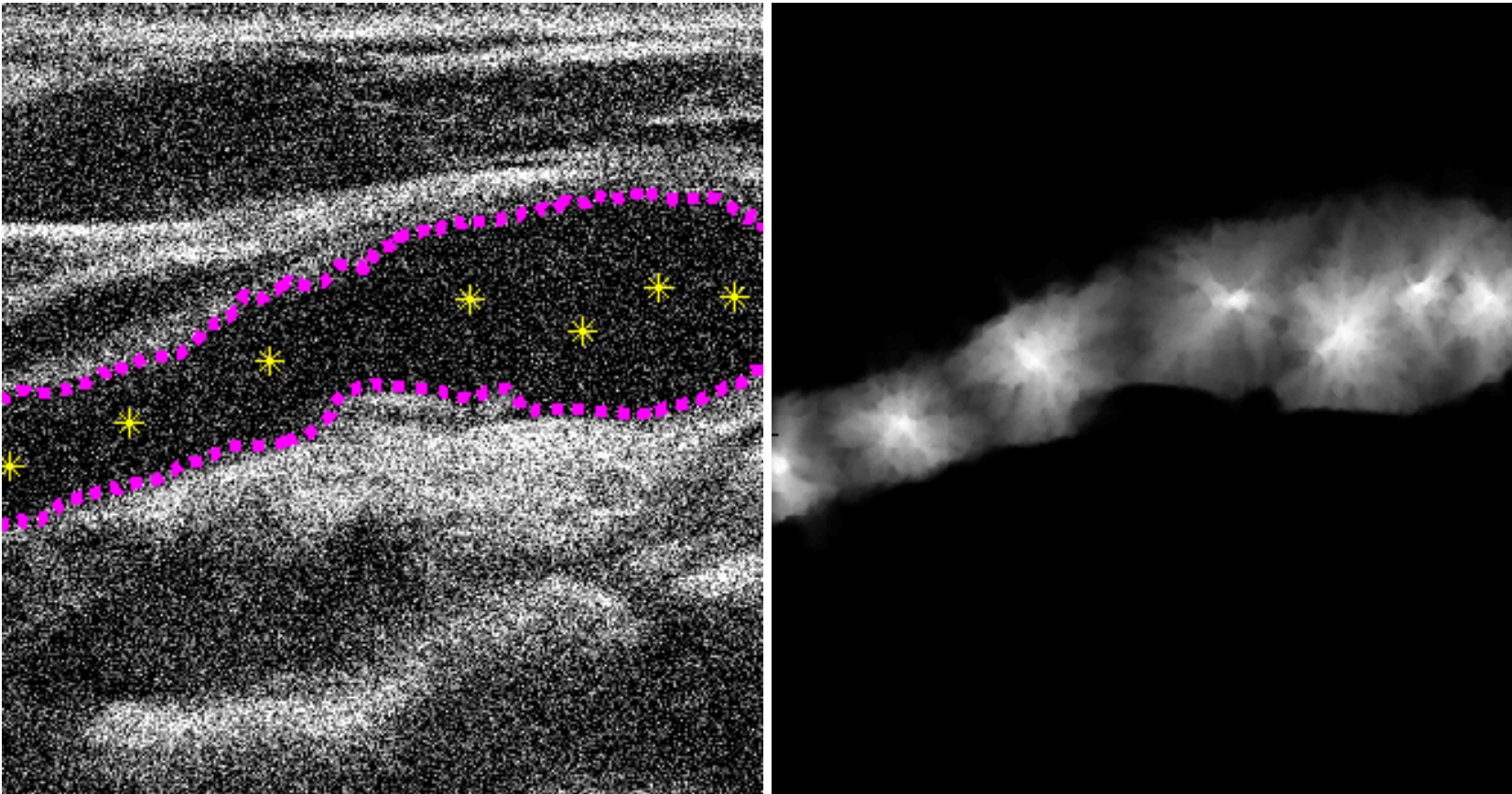
**Figure 2.10** - Segmentation result (left) and probability map (right) in the presence of computationally added Gaussian noise with an approximate standard deviation of 72.1 grey levels, evaluated at an algorithm threshold setting of 4%.
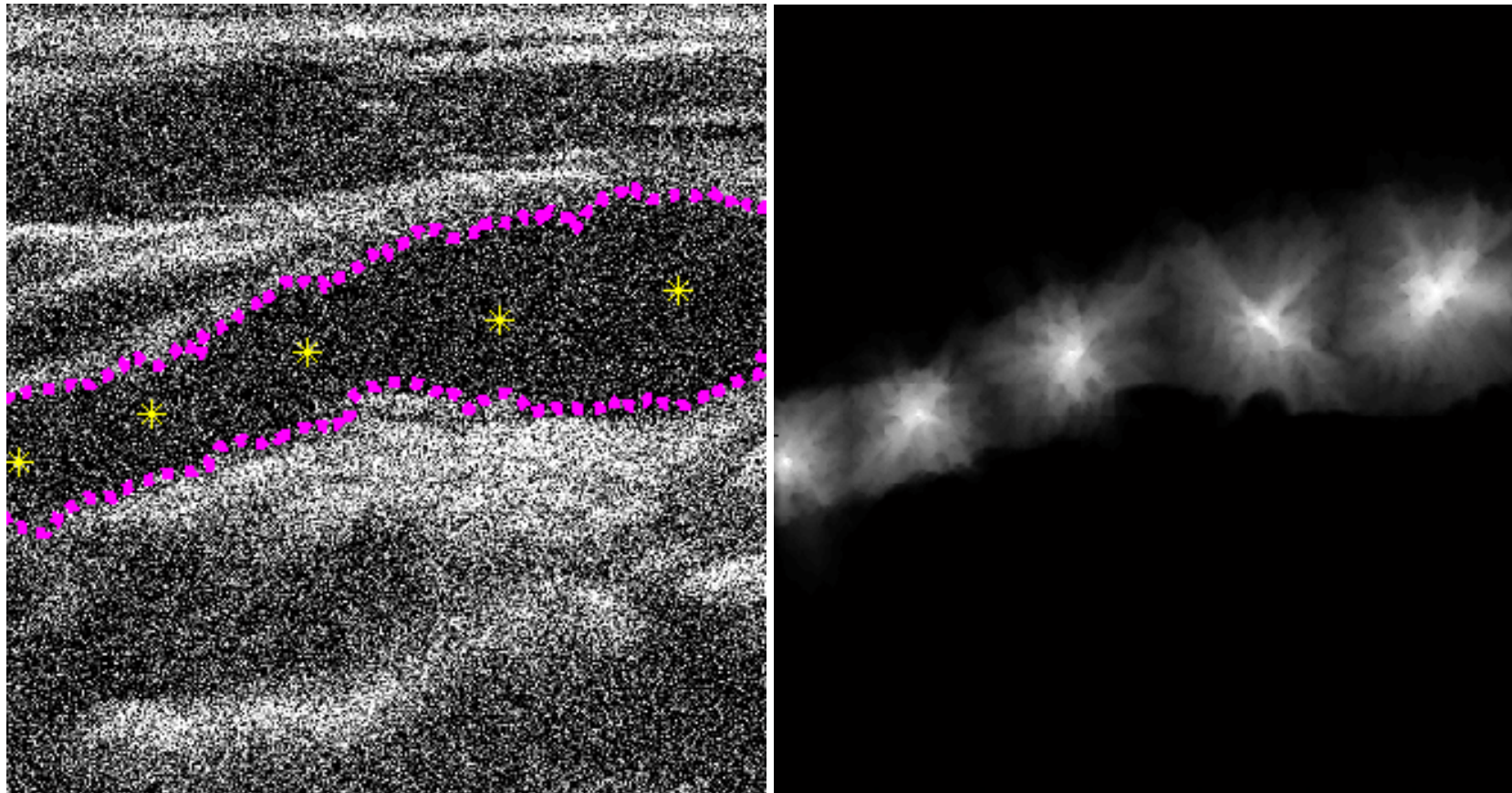
**Figure 2.11** - Segmentation result (left) and probability map (right) in the presence of computationally added Gaussian noise with an approximate standard deviation of 102 grey levels, evaluated at an algorithm threshold setting of 5%.
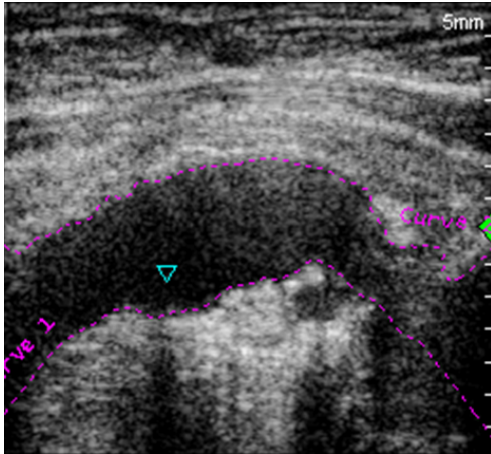
**Figure 2.12** - Tracking of the arterial lumen in the abdominal aorta in the presence of substantial amounts of noise (single frame shown). The whole image sequence is available for download from http://dl.dropbox.com/u/13857734/pp/aa_1.avi.
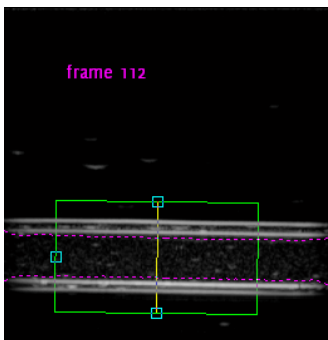


**Figure 2.13** - Tracking of the lumen surface in a walled flow phantom (single frame shown). The whole image sequence available for download from http://dl.dropbox.com/u/13857734/pp/wfp_1.avi.
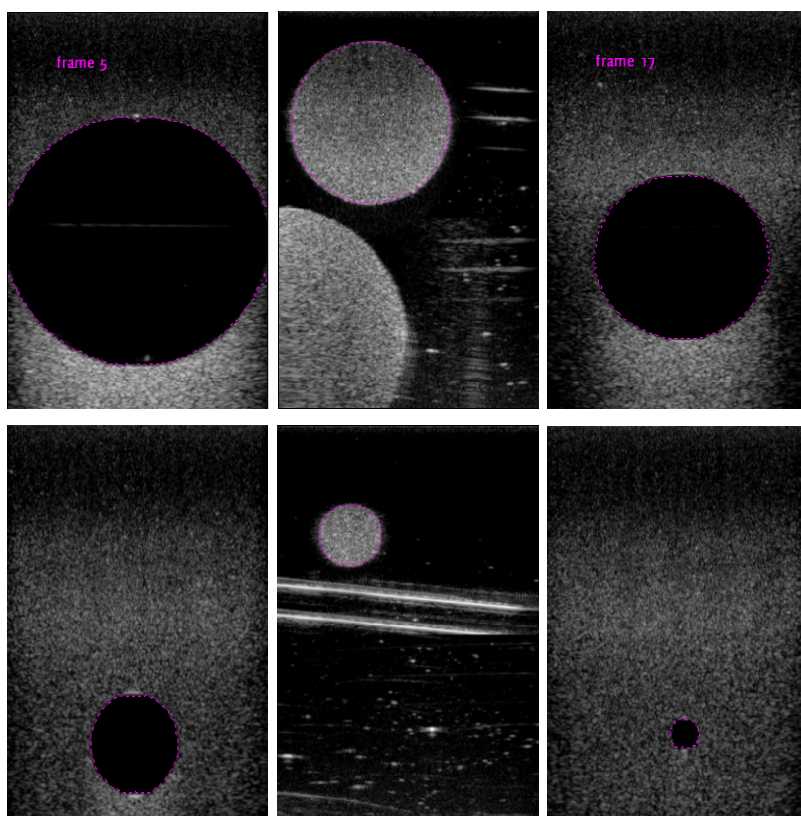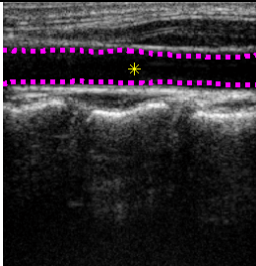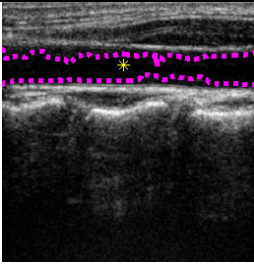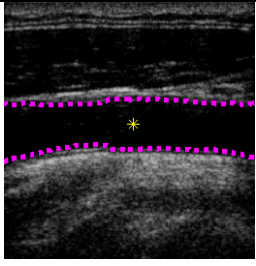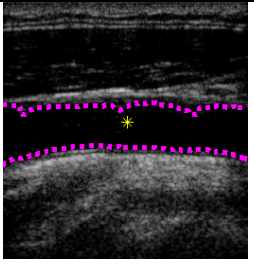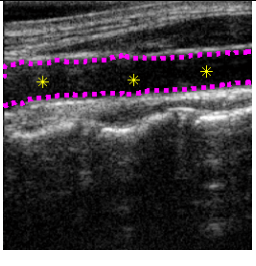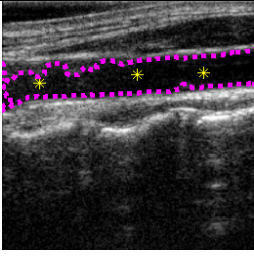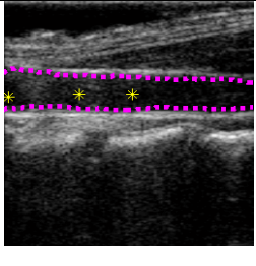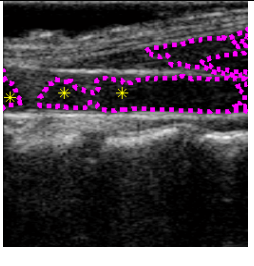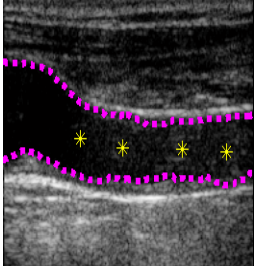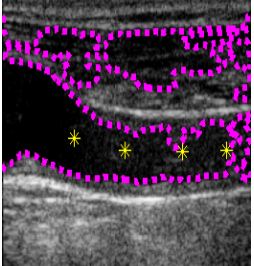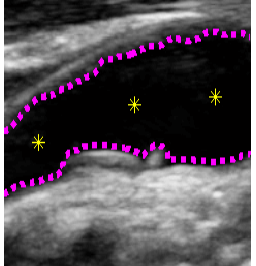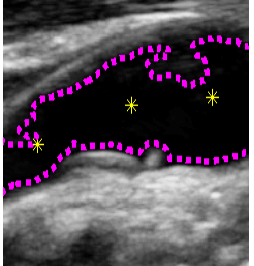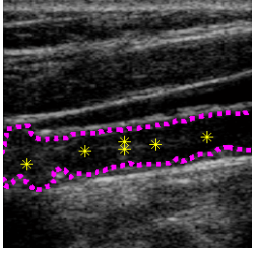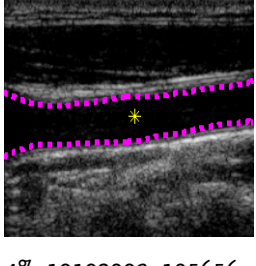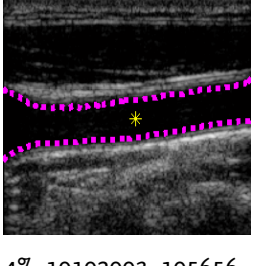
**Figure 2.14** - A selection of segmentation results for the detection of the boundaries of hypo- and hyper-echoic test objects.
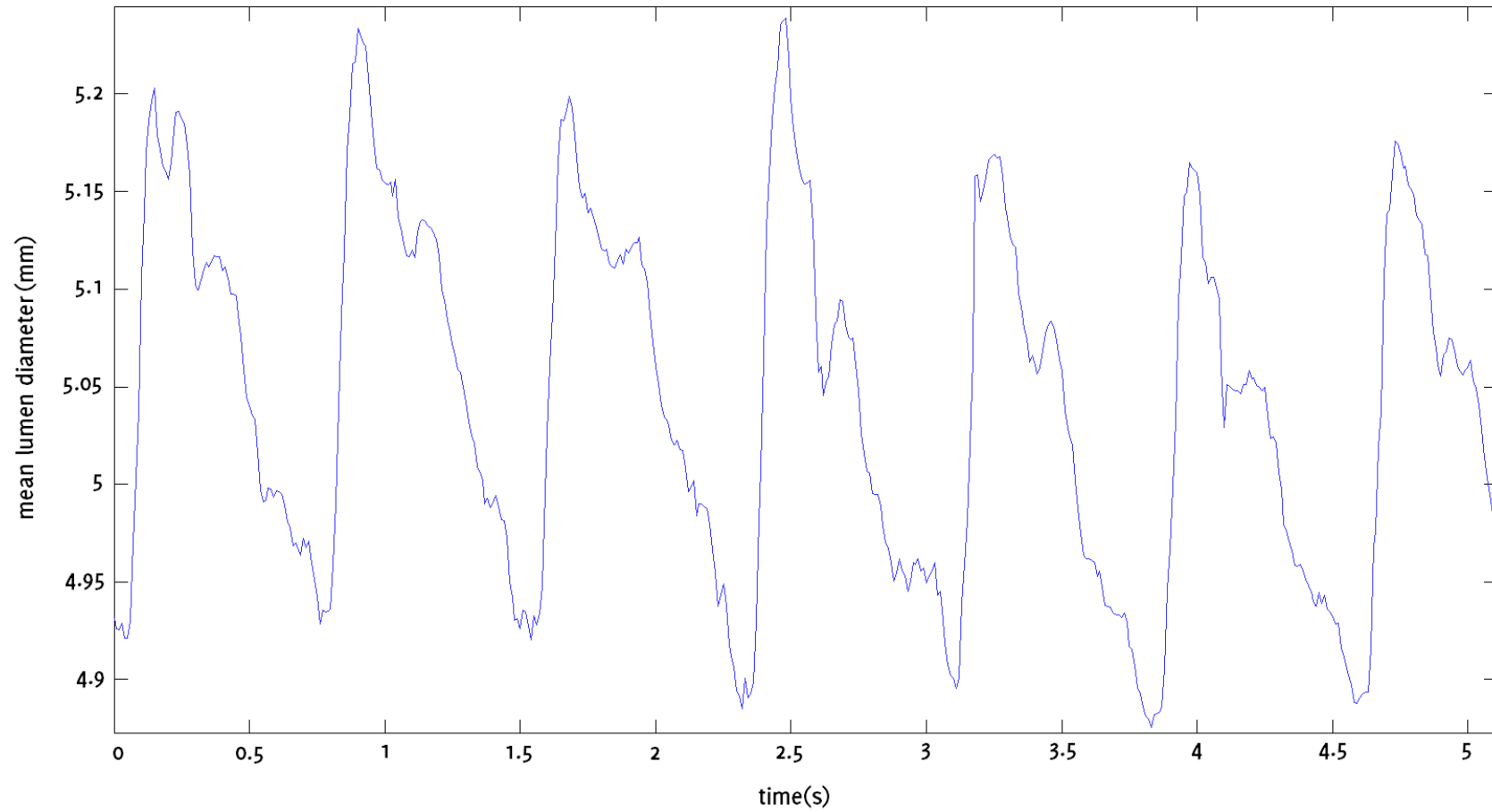
**Figure 2.15** - Variation, over several cardiac cycles, of the lumen diameter of the common carotid artery (averaged over an approximately 1 cm long segment) from a healthy volunteer, determined using the probabilistic algorithm.

| | | | |
|---|---|---|---|
| 3% 02082006_163734 | 3% 02082006_163734 | 3% 01282003_135524 | 3% 01282003_135524 |
| 4% 02082006_164257 | 4% 02082006_164257 | 4% 02082006_165951 | 4% 02082006_165951 |
| 3% 07152005_141346 | 3% 07152005_141346 | 2% 20111205.A_IM41 | 2% 20111205.A_IM41 |
| 3% 07152003_132307 | 3% 07152003_132307 | 4% 10102003_105656 | 4% 10102003_105656 |

| 4% 09012004_143848 | 4% 09012004_143848 | 4% 06172005_145127 | 4% 06172005_145127 |
| 2% 09012004_143034 | 2% 09012004_143034 | 4% 08122005_152103 | 4% 08122005_152103 |
| 4% 06092005_161522 | 4% 06092005_161522 | 4% 06142005_152327 | 4% 06142005_152327 |
| 4% 03102004_180555 | 4% 03102004_180555 | 3% 07312003_132933 | 3% 07312003_132933 |
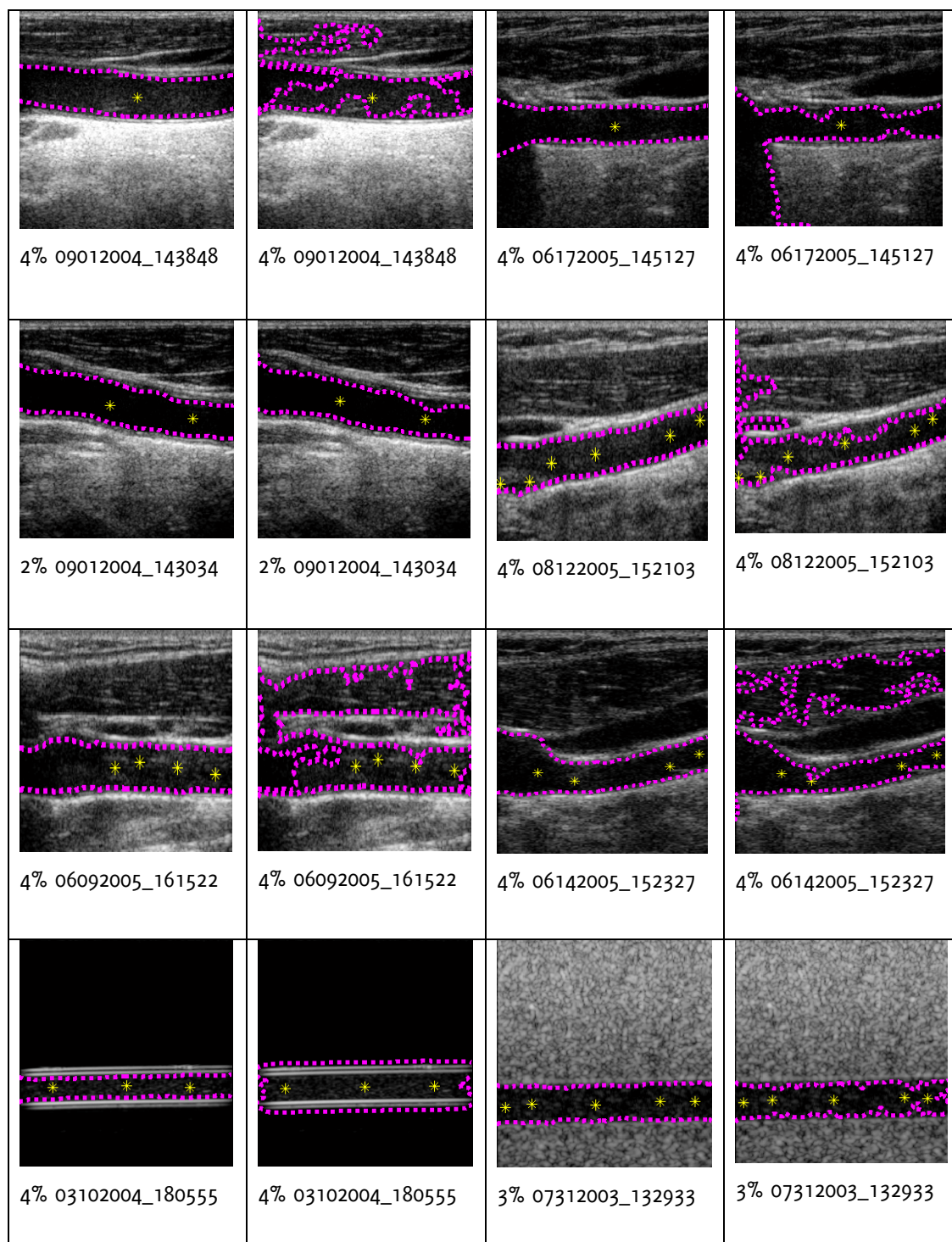
**Figure 2.16** - Comparison between the probabilistic algorithm (first and third columns) and a conventional region growing technique based on intensity thresholding (second and fourth columns). Results are given in pairs and labels indicate file reference and

threshold settings used. The two left-most figures on the bottom-most row are from the walled-flow phantom, and the two right-most figures on the same row are from the wall-less flow phantom.

**Table 2.2** – Comparison between Vernier caliper ($d_{cal}$) and algorithm ($d_{al}$) made diameter measurements for hypo- and hyper-echoic test objects.

| Object | Type | $d_{cal}$ [mm] (±0.5mm) | $d_{al}$ [mm] |
|--------|------|-------------------------|---------------|
| 1 | Hypo-echoic | 4.0 | 3.9 ± 0.2 |
| 8 | Hyper-echoic | 9.0 | 8.8 ± 0.2 |
| 2 | Hypo-echoic | 12.0 | 12.4 ± 0.2 |
| 7 | Hyper-echoic | 14.2 | 14.0 ± 0.3 |
| 3 | Hypo-echoic | 24.0 | 24.3 ± 0.6 |
| 6 | Hyper-echoic | 23.2 | 23.4 ± 0.2 |
| 4 | Hypo-echoic | 37.5 | 37.4 ± 0.2 |
| 5 | Hyper-echoic | 39.0 | 38.9 ± 0.2 |

## 2.5 Discussion

This chapter presented a method based on a probabilistic approach that can be used to efficiently segment out and track blood vessel boundaries in B-Mode ultrasound images and image sequences. The results showed that the technique can be used to track arterial lumens simply and efficiently in both the longitudinal and transverse imaging planes, including in the presence of substantial amounts of speckle noise. Boundary segmentation was robust in the presence of strong, artificially added image-noise and in an ultrasound image sequence from the abdominal aorta with ultrasound artifacts. In the case of the walled and wall-less laboratory flow phantom, good boundary tracking was obtained in the presence of high-intensity reflections within the vessel lumen. Tracking the lumen diameter of the common carotid artery in a healthy volunteer produced a detailed waveform showing the variation of the lumen diameter over several cardiac cycles.

In a separate validation of the method, dimensions of various hyper- and hypo-echoic laboratory, ultrasound test objects measured using the probabilistic method were compared with Vernier caliper measured physical dimensions and similar values were obtained within the error ranges of the measurements. Comparison with a conventional region growing algorithm showed that the probabilistic approach had better immunity to noise and less susceptibility to region overflowing at boundary imperfections.

The method described in this chapter addresses the limitations of the existing arterial lumen detection techniques based on B-Mode ultrasound image analysis. The limitations of the existing techniques included dependence on vessel orientation, curvature and scan plane, and long processing times. The probabilistic method was found to be sufficiently efficient to allow practical analysis of long image sequences, making real-time implementation feasible. The measured average processing time of 33 ms/frame per seed point for an image sequence of dimensions similar to a typical carotid artery scan indicated that frame rates as high as 30 Hz may be achieved in real-time even with the highly un-optimized implementation used in the study.

The advantages of the probabilistic method include its simplicity, and wide area of applicability. This technique was previously found to have good arterial wall tracking performance, comparable to that of Tissue Doppler Imaging [231] which needs access to radiofrequency data. The algorithm can be easily adopted in 3 dimensions and it would be interesting to see what results this would produce in further studies. It is possible that the implementation can be enhanced further, for example by extending the consideration to texture measures (e.g. local greyscale characteristics) or incorporating machine learning into the segmentation process.

## 2.6 Conclusion

The method presented in this chapter, based on a probabilistic approach to the segmentation of B-Mode ultrasound carotid artery images, produces robust segmentation results, including in the presence of substantial amounts of image-noise, and with little effort on the user's part.

# Chapter 3

# Dynamic Variations in the Ultrasound Greyscale Median of Carotid Artery Plaques

## 3.1 Overview

The image contrast provided by B-Mode ultrasound depends on the way ultrasound interacts with tissues and thus is a representation of the ultrasonic properties and structure of tissues. Strongly reflecting structures such as fibrous materials and calcium rich regions generally appear brighter than weakly reflecting tissue components such as lipids, regions of necrosis and haemorrhages. The greyscale median (GSM) of carotid artery plaques succinctly quantifies the B-Mode appearance of plaques and has been widely researched as a surrogate marker of plaque composition and vulnerability. However, existing studies have assessed GSM of plaques on still ultrasound images and ignored any variations that may be present on a frame-by-frame basis. This chapter introduces a novel method of tracking of plaque boundaries in ultrasound image sequences and investigates the nature and extent of the frame-by-frame variations in the plaque GSM. A research article based on the contents of this chapter was published in Cardiovascular Ultrasound [238].

## 3.2 Introduction

The North American Symptomatic Carotid Endarterectomy Trial (NASCET) and the European Carotid Surgery Trial (ECST) have shown that surgery in symptomatic patients with severe internal carotid artery stenosis results in a six-fold reduction of stroke risk [38-39]. However, patients who do not have severe stenoses and patients who are asymptomatic can also go on to develop stroke. It is, therefore, important to be able to determine whether any of these patients have carotid plaques which are high-risk or unstable. Ultrasound greyscale median (GSM) is commonly used to quantify the ultrasound appearance of carotid plaques, and several studies have found that it may be valuable for predicting the risk of cerebrovascular events. In particular, statistically significant associations have been reported between plaque GSM and the presence of

cerebrovascular symptoms [129,131], cerebral infarction in symptomatic and asymptomatic patients [132,137,140], recurrent cerebrovascular events before undergoing carotid endarterectomy [51], and the overall risk of stroke in symptomatic patients [134], asymptomatic patients [135], and during and after carotid artery stenting [138].

GSM measurements have had poor reproducibility across studies. This can be partly attributed to the differences in the acquisition settings used in separate studies. In order to reduce this variability, investigators have attempted to standardise ultrasonic images of carotid plaques by specifying certain acquisition settings to be used for carotid artery scanning and normalizing the resultant ultrasound images [148]. However, existing studies typically measured GSM on still ultrasound images, and thus ignored any variations that may have been observed on a frame-by-frame basis. This chapter establishes the existence of and investigates the nature and extent of any frame-by-frame variations in the plaque GSM using a novel technique for tracking plaque boundaries in ultrasound image sequences.

We hypothesized that variations in the GSM of carotid artery plaques may occur due to deformation of the plaque during the cardiac cycle, and other confounding factors such as out-of-plane plaque, patient or probe motion. Changes in echogenicity between systole and diastole as a result of cardiac contraction, for example, have been shown to occur in sonographic imaging of the myocardium [239]. Furthermore, it was hypothesized that plaques of different composition and morphology may exhibit different inter-frame variations in GSM in otherwise equivalent hemodynamic circumstances and hence the measurement of these variations may give useful insight into the dynamic behaviour of plaques and help identify vulnerable plaques.

## 3.3 Methods

### 3.3.1 Data Acquisition

Frame-by-frame variations in the plaque GSM and area of 27 carotid artery plaques (19 consecutive patients, 11 males, mean age 76, stenosis range 10%-80%) were studied by measuring the GSM and area of plaques on each image frame separately and computing the mean, the standard deviation (s.d.) and the coefficient of variation (s.d./mean) across the frames. The image sequences used were of up to 10 seconds in length (average 4.4 seconds) and were acquired with a mean frame rate of 32 frames per second. The degrees of stenosis of the corresponding arteries were measured using criteria consistent with the NASCET methodology utilizing blood flow velocities in conjunction with the B-Mode and colour flow imaging [38,47,240]. Eleven of the plaques studied were found to be asymptomatic and the remaining sixteen symptomatic after assessment at the University Hospitals of Leicester NHS Trust's Rapid Access Transient Ischaemic Attack (TIA) Clinic. The use of the clinical data for our research had been approved by the National Research Ethics Service (NRES) Committee East Midlands - Northampton (reference 11/EM/0249), and each patient gave informed consent before participating in the study. The ultrasound data were obtained as longitudinal cross-sections using a Philips iU22 ultrasound scanner (Philips Healthcare, Eindhoven, The Netherlands) with an L9-3 probe and included B-Mode (i.e. greyscale) and Colour Doppler image sequences. The vascular carotid preset on the scanner was used (Vasc Car preset, persistence low, XRES and SONOCT on) and the gain was optimized by the operator, an experienced vascular sonographer. In the case of B-Mode acquisitions, the greyscale transfer curve was kept set to Gray Map 2, as this was reported to be the most linear transfer curve on this scanner [241]. Colour Doppler cine-loops were used as a qualitative aid to identifying the location and extent of the plaques, while the B-Mode data were used for the quantitative analyses of the plaque GSM and cross-sectional area.

### 3.3.2 Data Analysis

Quantitative analyses were carried out using MATLAB version 7.14, release 2012a (MathWorks, Natick, Massachusetts, USA) and employed a combination of standard speckle tracking/block-matching techniques and the novel surface tracking algorithm that was introduced in Chapter 2. The latter was used to delineate and track plaque-

arterial lumen boundaries (the plaque surface). Speckle tracking, which was used to track the boundary between the plaque and the underlying tissue, is a standard image analysis technique that involves measuring the similarity between a template and a search image [242]. Given a point to speckle track, a region is defined around the point and used as a template. The process is then essentially to find the position in the search image that has the largest similarity to this template. There are many different measures of similarity between a template and a search image; in this study the normalized correlation coefficient was used since it is invariant to changes in image amplitude [242]. Square regions of approximate area 1.4 x 1.4 cm$^2$ were employed. This template size was found to produce optimum speckle tracking quality in our study as was verified by observing plaque tracking results:

http://www.cardiovascularultrasound.com/content/download/supplementary/1476-7120-11-21-S1.avi

Speckle tracking requires stable speckle patterns to be useful. Speckle patterns at plaque-arterial wall boundaries usually fulfil this requirement but speckle patterns at plaque-arterial lumen boundaries tend to de-correlate rapidly. For this reason, the arterial lumen segmented out using the surface tracking algorithm defining the plaque-arterial lumen boundary, was automatically cut and joined with a polygon comprising the speckle tracked points defining the plaque-arterial wall interface (Figure 3.1). The joining process was carried out by finding the closest points on the arterial lumen surface to the proximal and distal ends of the speckle-tracked plaque-arterial wall boundary and joining these respective points. Regions of plaques that could not be distinguished from the arterial lumen (e.g. echo-free regions) and regions of plaques in areas of acoustic shadowing were excluded from analysis. Plaques for which anechoic regions and regions of shadowing exceeded more than 70% of the total plaque cross-sectional area as observed on Colour Doppler sequences were not included in the study.
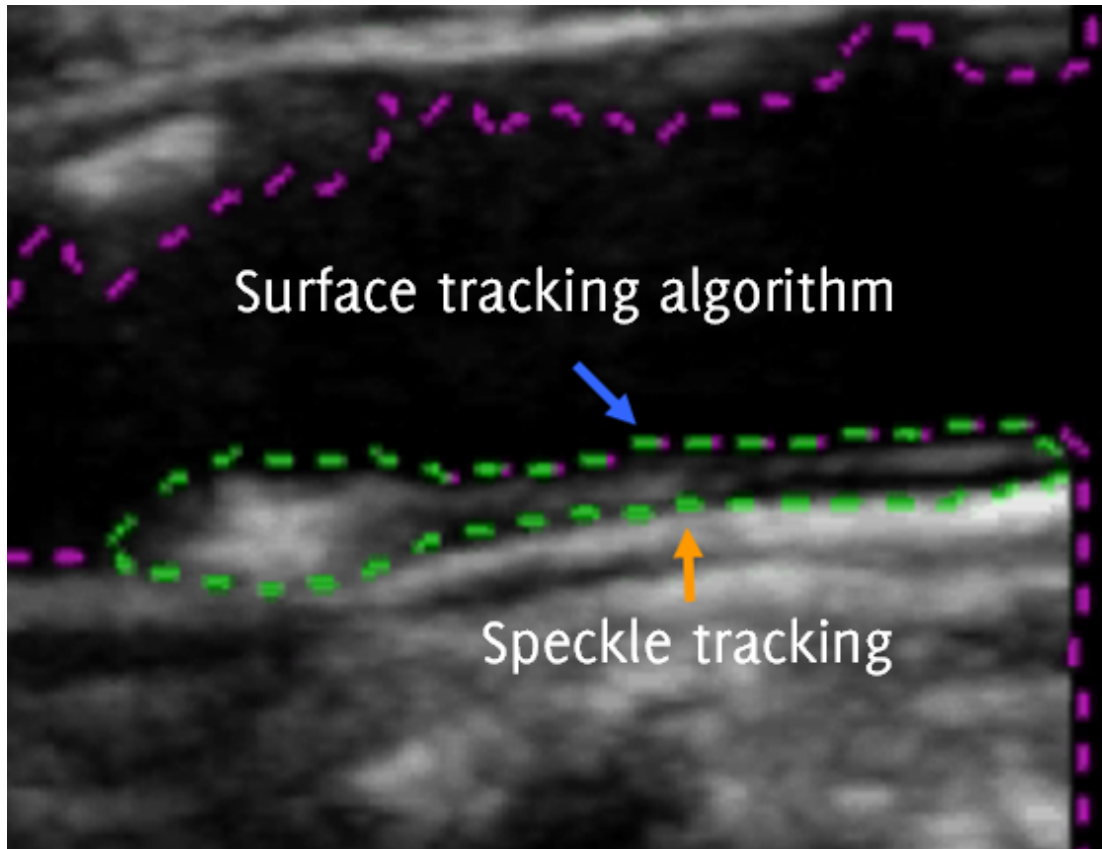
**Figure 3.1** - The plaque region shown by the green dashed lines is defined by two boundaries: the top boundary (blue arrow) defines the plaque-arterial lumen interface and the bottom boundary (orange arrow) defines the plaque-arterial wall interface. The purple lines are the output of the surface tracking algorithm that was introduced in Chapter 2.

Image normalisation was carried out using two different methods in order to observe their effects on the frame-by-frame variations observed. The first normalisation (NORM1) was performed by linearly scaling the ultrasound image intensities so that the GSM of a user-selected blood region inside the vessel lumen was mapped to 0 and the brightest region of the adventitia was mapped to 190. Both of these regions were 5 x 5 pixels$^2$ in size, corresponding to an approximate physical area of 0.4 x 0.4 mm$^2$. The reference regions were selected on the first image of the sequence and the reference GSM values calculated on the first frame were applied to that and all

subsequent images. The second normalisation (NORM2) method involved selecting an adventitia region on each image separately, thus applying separate adventitial reference values to individual images.

From the user's perspective, the procedure for plaque segmentation and tracking was as follows: On the first image of the sequence, the user selected a number of seed points within the arterial lumen for the surface tracking algorithm to track the plaque-arterial lumen boundary. The user, then, manually delineated the plaque-periadventitial tissue boundary using the mouse. The latter were used for speckle tracking and were used to track the plaque-periadventitial tissue boundary in the subsequent images of the sequence. Following the selection of the brightest region of the adventitia, the rest of the process was automated as the plaque-arterial lumen and the plaque-periadventitial tissue boundaries were automatically tracked in the subsequent frames of the image sequence using the surface tracking and speckle tracking algorithms, respectively. An exception to this was the NORM2 normalisation, in which case the user additionally selected the brightest region of the adventitia in each image frame separately.

A semi-qualitative assessment of whether physiologically reasonable (e.g. of the order of 60/min) periodical variations were visually apparent on the GSM and plaque area waveforms was also carried out. This involved measuring the frequency of any periodical variations seen on the GSM and cross-sectional area waveforms and considering frequencies in the range 50/min - 160/min to be potentially attributable to cardiac variations. Conversely, variations with frequencies lower than 50/min or higher than 160/min were not considered to be due to physiological sources and such plaques were placed in the same category as those not showing any apparent, physiologically reasonable, periodical variations in the GSM and cross-sectional area.

### 3.3.3 Statistical Methods

Statistical analyses were carried out using MATLAB version 7.14, release 2012a (MathWorks, Natick, Massachusetts, USA) and SPSS version 20 (IBM Corporation, Armonk, New York, USA). Spearman's test was used to study the correlation between

the inter-frame variations in GSM and area, since neither of these parameters was expected to follow a Gaussian distribution and any correlation between the two was likely to be non-linear. Multi-variable linear regression was used to study the contribution of other plaque GSM and area parameters to the differences observed in the magnitude of the GSM variations for each plaque. The unpaired, non-parametric Mann-Whitney U-test was used to investigate whether the GSM values averaged across all frames, as well as their standard deviations and the coefficients of variation, differed significantly between the asymptomatic and symptomatic plaque groups. Two-tailed values of significance were used in each case.

### 3.3.4 Reproducibility

Intra-observer coefficients of variation for eight selected plaque samples of varying echogenicities were studied by measuring the frame-by-frame variations in the plaque GSM and cross-sectional area five times for each plaque. The measurements were made by the same operator and in sequential order. The same ultrasound acquisition sequences were used for each plaque respectively. The eight plaques were selected from the available dataset to give a wide spectrum of plaque echogenicities for reproducibility analysis.

### 3.3.5 Comparison Against Manual Measurements

In order to compare the plaque GSM and cross-sectional area obtained using our method with those obtained using manual delineation, plaque GSM and cross-sectional area were measured by the same operator using manual delineation for every $5^{th}$ frame, for each of the same eight plaque samples used for our study of reproducibility. This enabled the magnitude of and variation in the plaque GSM and cross-sectional areas to be compared between the two techniques. A Bland-Altman analysis was also carried out to assess the agreement between the GSM measurements made using our method and manual delineation on matching image frames.

### 3.4 Results

Plaque outlines could be tracked successfully in a variety of different configurations (Figure 3.2). Across all plaque samples, the un-normalized plaque GSM, averaged across all frames, ranged between 26 and 112 (mean 47, Table 3.1). Plaque areas ranged between 7 mm$^2$ and 92 mm$^2$ (mean 30 mm$^2$). The mean inter-frame coefficient of variation (s.d./mean) of GSM was 5.2% (s.d. 2.5%) while that of plaque area was 4.2% (s.d. 2.9%). In relation to the normalized GSM obtained using the NORM1 method, the corresponding mean GSM figures ranged between 24 and 96 (mean 46). The mean inter-frame coefficient of variation was the same as without normalization (5.2%) but the standard deviation was slightly larger (2.6%). Normalization using the second normalisation technique (NORM2) for plaques px1, px2, px3, px19 (excluding the region of acoustic shadowing for px19) and px22 resulted in a larger coefficients of variation (values in % were 4.8, 9.7, 6.7, 3.8 and 4.9 for each plaque, respectively) compared to the un-normalized and NORM1 normalized coefficients of variation (Table 3.1).

Periodic variations with frequencies of the order of 60/min in either or both of the plaque GSM or area waveforms were observed for 12 plaques (50%) but not observed for 12 other plaques (Table 3.1). Three plaques were excluded from this analysis because they had short acquisition sequences.

Overall, 13 of the 27 plaques (48%) exhibited inter-frame variations in GSM of greater than 5% measured as the inter-frame coefficient of variation of GSM in both the un-normalized and NORM1 normalized cases. In contrast, only 6 of the 27 plaques (22%) had inter-frame coefficients of variation in plaque area of greater than 5% (Table 3.1, Figure 3.3).
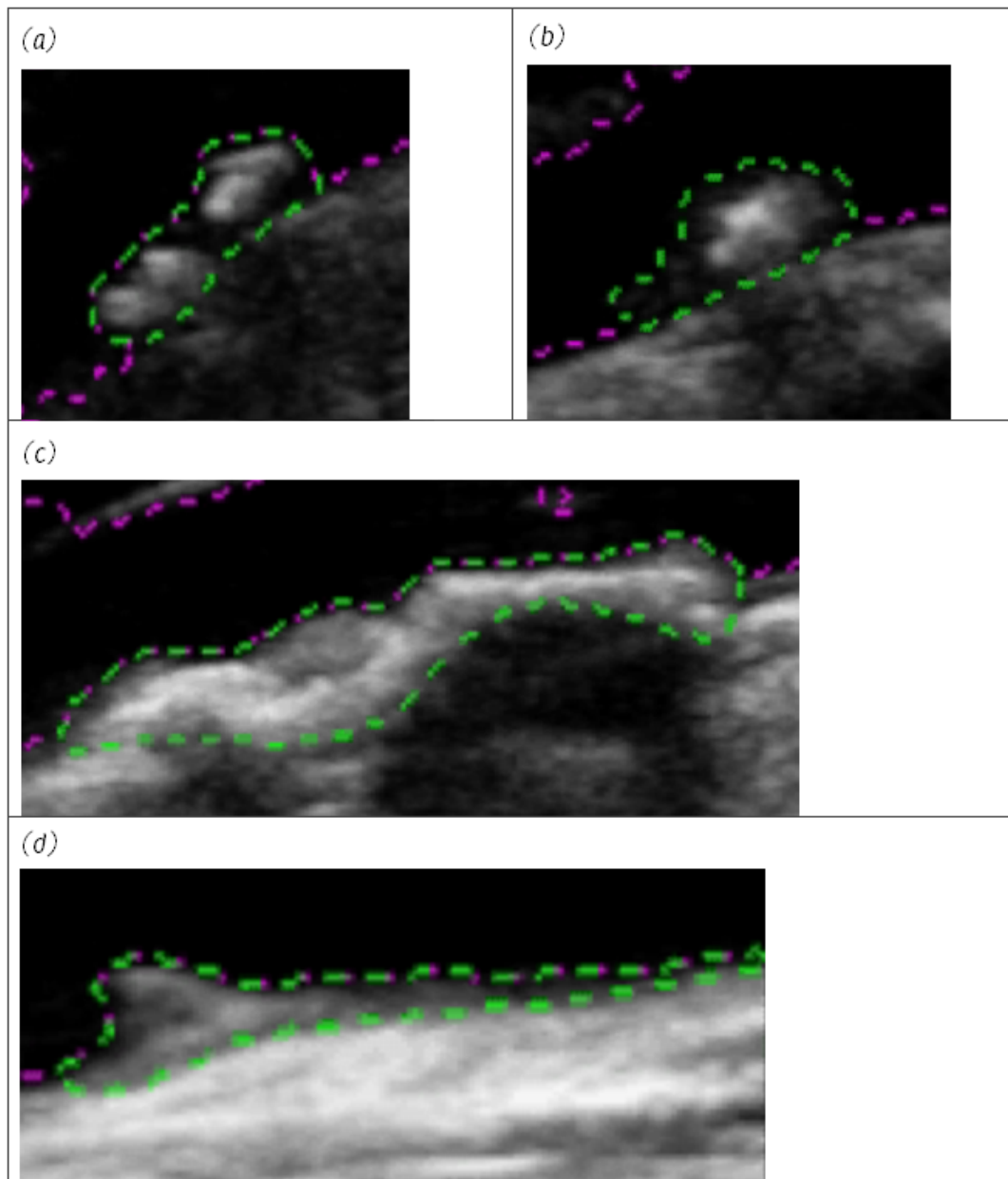
**Figure 3.2** - Close-up views of four plaque samples with varying echogenicities (single frames shown). Plaques (a) px1, (b) px3, (c) px19, (d) px22. The region of acoustic shadowing has been excluded from analysis for px19.
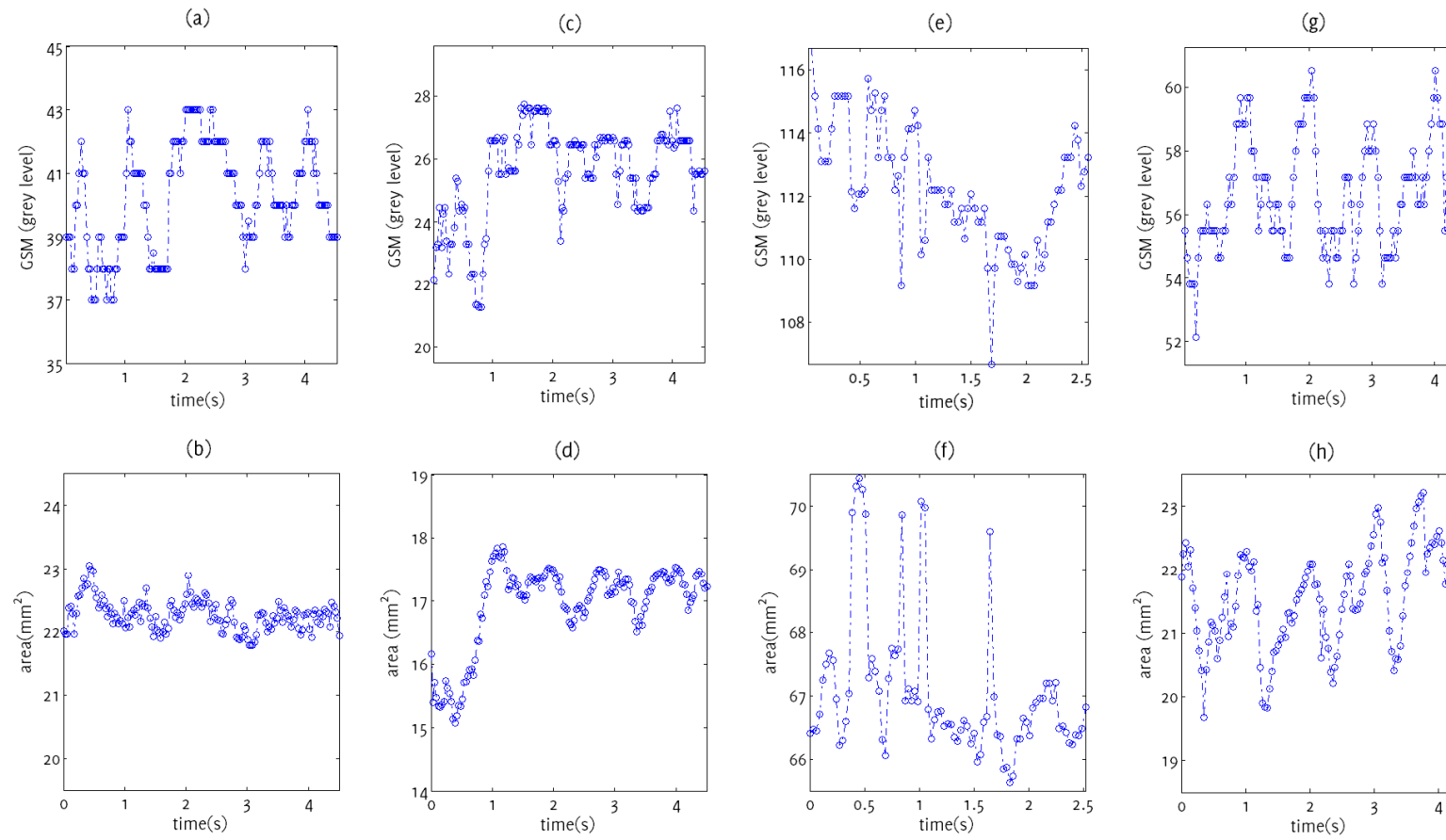
**Figure 3.3** - Variations in the un-normalized plaque GSM (top row), and plaque area (bottom row) for plaques px1 (a,b), px3 (c,d), px19 (e,f), px22 (g,h).

**Table 3.1**- Variations observed in the plaque GSM and area. The last column indicates whether periodical variations of the order of 60/min were observed on the inter-frame GSM and area waveforms. Normalized GSM refers to NORM1. The table has been sorted in terms of the un-normalized, mean plaque GSM.

| Plaque sample | GSM (un-normalized) | | | GSM (normalized) | | | Area | | | Periodical variations observed? |
|---|---|---|---|---|---|---|---|---|---|---|
| | mean | s.d. | COV (s.d./mean) | mean | s.d. | COV (s.d./mean) | mean (mm²) | s.d. (mm²) | COV (s.d./mean) | |
| px3 | 25.6 | 1.52 | 5.9% | 24.4 | 1.45 | 5.9% | 16.9 | 0.69 | 4.1% | Both |
| px10 | 27.6 | 0.74 | 2.7% | 26.3 | 0.70 | 2.7% | 13.1 | 0.80 | 6.1% | |
| px8 | 28.3 | 2.02 | 7.1% | 32.9 | 2.53 | 7.7% | 7.2 | 0.44 | 6.0% | Both |
| px9 | 29.6 | 1.19 | 4.0% | 27.8 | 1.12 | 4.0% | 21.9 | 0.59 | 2.7% | |
| px23 | 30.1 | 0.64 | 2.1% | 25.6 | 0.54 | 2.1% | 49.4 | 1.22 | 2.5% | Excluded |
| px28 | 31.2 | 1.90 | 6.1% | 42.4 | 2.58 | 6.1% | 13.6 | 0.45 | 3.3% | Area |
| px16 | 31.9 | 1.68 | 5.3% | 34.8 | 1.83 | 5.3% | 14.6 | 0.93 | 6.4% | Area |
| px2 | 32.3 | 2.80 | 8.7% | 27.5 | 2.38 | 8.7% | 27.9 | 1.12 | 4.0% | |
| px7 | 33.6 | 0.84 | 2.5% | 35.8 | 0.90 | 2.5% | 52.5 | 1.14 | 2.2% | Both |
| px6 | 33.8 | 2.87 | 8.5% | 36.1 | 3.06 | 8.5% | 28.9 | 3.56 | 12.3% | Both |
| px29 | 33.9 | 2.20 | 6.5% | 27.2 | 1.77 | 6.5% | 91.9 | 1.93 | 2.1% | |
| px24 | 35.5 | 2.52 | 7.1% | 36.9 | 2.62 | 7.1% | 14.4 | 0.37 | 2.6% | Excluded |

| Plaque | GSM (un-normalized) | | | GSM (normalized) | | | Area | | | Periodical variations |
|--------|------|------|---------------|------|------|---------------|------------|------------|---------------|-----------|
| sample | mean | s.d. | COV (s.d./mean) | mean | s.d. | COV (s.d./mean) | mean (mm²) | s.d. (mm²) | COV (s.d./mean) | observed? |
| px5 | 36.9 | 4.31 | 11.7% | 30.9 | 3.60 | 11.7% | 22.0 | 0.96 | 4.4% | Both |
| px13 | 39.3 | 3.12 | 7.9% | 33.5 | 3.05 | 9.1% | 14.6 | 1.65 | 11.3% | GSM |
| px1 | 40.3 | 1.69 | 4.2% | 40.5 | 1.69 | 4.2% | 22.3 | 0.25 | 1.1% | GSM |
| px14 | 40.9 | 1.66 | 4.1% | 38.1 | 1.55 | 4.1% | 30.2 | 1.29 | 4.3% | |
| px26 | 43.4 | 1.49 | 3.4% | 55.3 | 1.90 | 3.4% | 39.5 | 0.94 | 2.4% | |
| px27 | 50.1 | 1.17 | 2.3% | 56.3 | 1.31 | 2.3% | 66.1 | 1.68 | 2.5% | |
| px21 | 52.4 | 2.35 | 4.5% | 51.1 | 2.34 | 4.6% | 22.7 | 1.09 | 4.8% | GSM |
| px15 | 53.7 | 1.97 | 3.7% | 53.1 | 1.95 | 3.7% | 15.9 | 0.71 | 4.4% | |
| px12 | 54.0 | 3.72 | 6.9% | 61.0 | 4.28 | 7.0% | 14.9 | 0.39 | 2.6% | |
| px22 | 67.4 | 2.15 | 3.2% | 56.7 | 1.80 | 3.2% | 21.5 | 0.80 | 3.7% | Both |
| px11 | 70.2 | 1.27 | 1.8% | 71.7 | 1.30 | 1.8% | 38.0 | 0.23 | 0.61% | Area |
| px18 | 73.3 | 5.30 | 7.2% | 58.3 | 4.21 | 7.2% | 25.8 | 0.82 | 3.2% | |
| px4 | 76.9 | 2.22 | 2.9% | 71.0 | 2.08 | 2.9% | 11.3 | 1.05 | 9.3% | |
| px25 | 82.9 | 6.02 | 7.3% | 82.3 | 5.98 | 7.3% | 37.2 | 0.61 | 1.6% | Excluded |
| px19 | 112.3 | 1.98 | 1.8% | 95.7 | 1.72 | 1.8% | 67.0 | 1.14 | 1.7% | |

Normalisation using NORM1 did not appear to change the shape of the GSM variation waveform but caused a translation along the y-axis (Figure 3.4). After normalization, the mean GSM was lower for some plaques, and higher for others (Figure 3.5a). The coefficients of variation were predominantly the same, yet for some plaques, NORM1 also changed the coefficient of variation (Figure 3.5b).
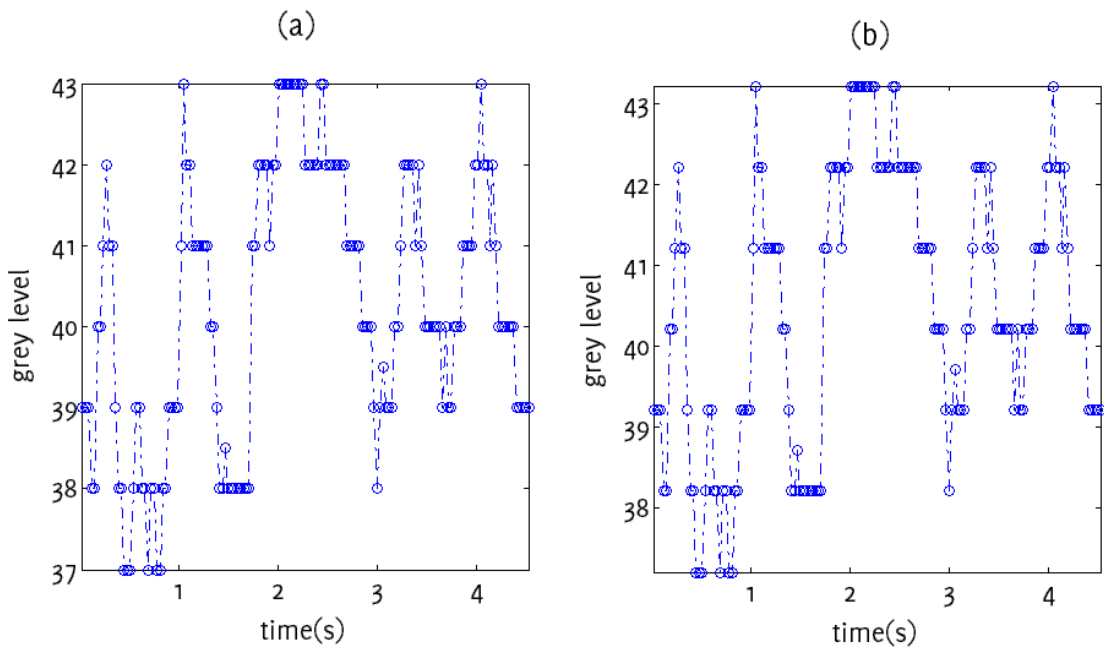


**Figure 3.4** - Variations in GSM for plaque sample px1: (a) un-normalized, (b) normalized (NORM1).

The correlation between the inter-frame coefficients of variation in un-normalized plaque GSM and cross-sectional area (Figure 3.6) was not statistically significant (Spearman's rho 0.36, p=0.07). Testing the influences on the extent of the inter-frame variations seen in the un-normalized GSM, of (a) the mean inter-frame, un-normalized GSM, (b) the mean inter-frame plaque area, and (c) the extent of inter-frame variations seen in plaque area, with the extents taken as the standard deviation of inter-frame values, identified the mean inter-frame GSM as the only statistically significant factor at the 5% significance level (Table 3.2).
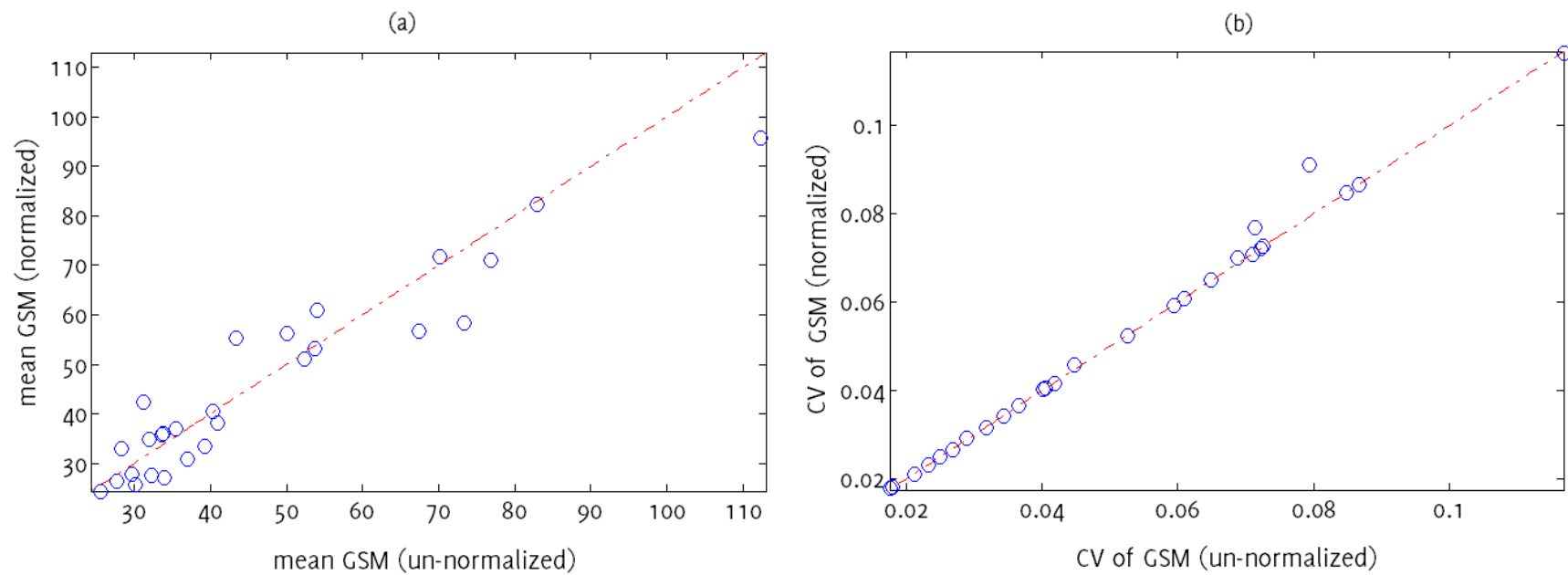
**Figure 3.5** - (a) NORM1 normalized mean GSM versus un-normalized. (b) NORM1 normalized coefficients of variation versus un-normalized. Red dashed lines are the lines of identity and indicate no change upon normalization.
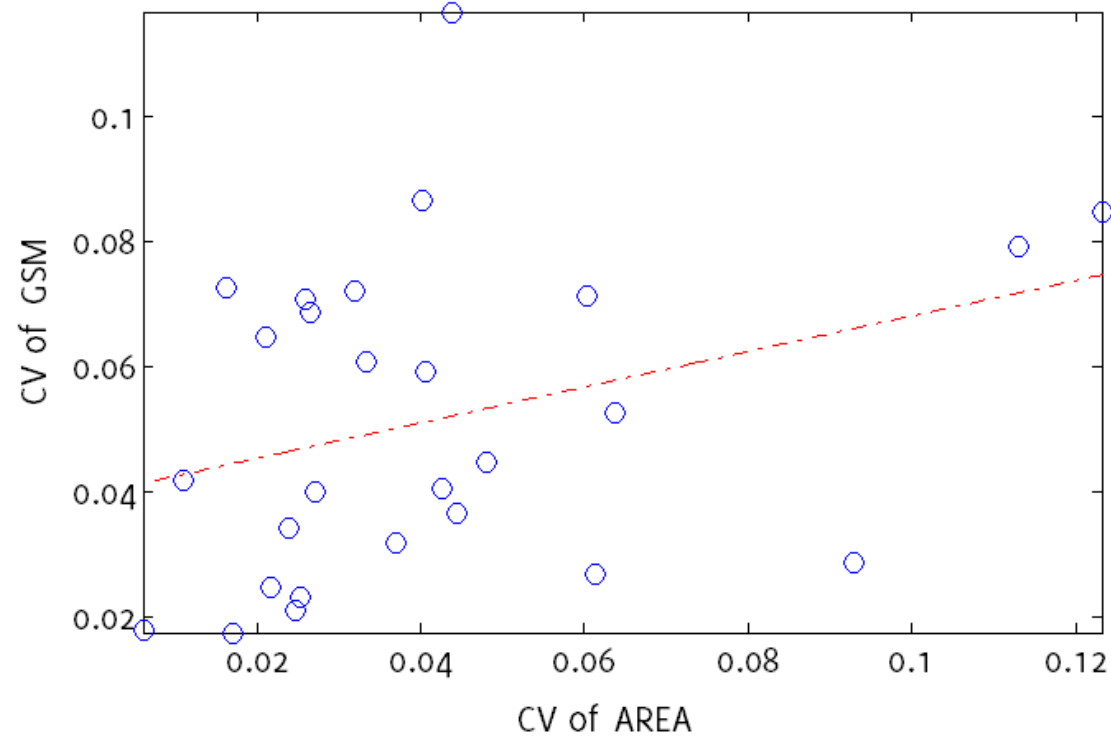
**Figure 3.6** - Scatter plot of inter-frame coefficients of variation for un-normalized GSM versus those for plaque area. The correlation between the two coefficients of variation is weak (Spearman's rho 0.36, p=0.07). The dashed line is a linear fit to the data.

The mean, normalized GSM differed significantly between the symptomatic and asymptomatic plaque groups (p=0.002) but the parameters based on the inter-frame variations in the normalized GSM did not (p=0.48 for the inter-frame standard deviation of normalized GSM and p=0.42 for the coefficient of variation of normalized GSM, Figure 3.7).

**Table 3.2** - Results of multi-variable linear regression, testing for the influences of (a) mean frame-by-frame GSM values, (b) mean frame-by-frame plaque areas, and (c) the standard deviations of the frame-by-frame plaque areas on the standard deviations of the frame-by-frame GSM values. Significant associations are marked with an asterisk (*).

| Factor | a | b | C |
|---|---|---|---|
| Standardized coefficient (β) | 0.48 | -0.33 | 0.19 |
| t statistic | 2.46 | -1.59 | 0.93 |
| Significance (p) | 0.02* | 0.13 | 0.36 |
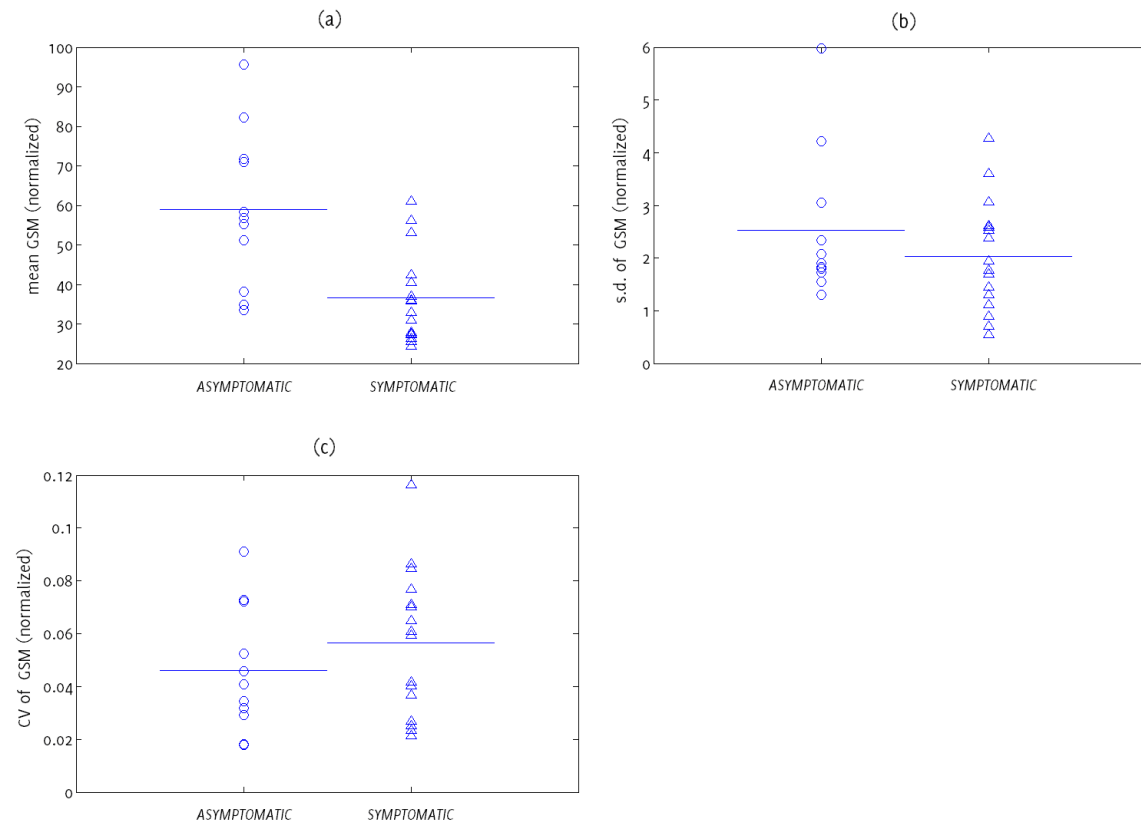
**Figure 3.7** - Distribution of the mean, normalized GSM [a], and the extent of the frame-by-frame variations in GSM (measured as the standard deviations of the inter-frame GSM values [b] and the coefficients of variation [c]), for the symptomatic and asymptomatic plaque groups. The horizontal lines indicate mean values for the individual groups.

Our plaque GSM and area measurements showed good reproducibility (Table 3.3) and were broadly comparable to those obtained using manual delineation (Table 3.4). The mean intra-observer coefficients of variation for the eight selected plaque samples were 1.4% for the measurement of the un-normalized GSM, 2.4% for the plaque area, and 2.8% for the NORM1 normalized GSM (Table 3.3). Manual delineation results showed a greater amount of variation (mean coefficients of variation were 7.7% for the un-normalized GSM and 8.0% for the plaque area compared with 5.4% and 4.0%, respectively, for our method), due to the greater subjectivity of the manual delineation process (Table 3.4). However, the mean difference in GSM measurements between the two techniques was 0.1 grey levels (Figure 3.8) and did not differ significantly from zero ($p=0.77$, t-test). The 95% limits of agreement were -7.9 grey levels to +8.1 grey levels.

Table 3.3 - Intra-observer coefficients of variation (standard errors) for the measurement of the inter-frame mean GSM (un-normalized and NORM1 normalized) and mean area, for eight plaque samples.

| Plaque sample | Plaque GSM | | Cross-sectional area |
|---|---|---|---|
| | Un-normalized | NORM1 normalized | |
| px2 | 1.7% (0.24) | 2.3% (0.29) | 2.9% (0.37) |
| px4 | 0.5% (0.18) | 4.4% (1.39) | 2.3% (0.11) |
| px11 | 1.6% (0.48) | 4.7% (1.53) | 1.4% (0.24) |
| px26 | 1.1% (0.22) | 1.2% (0.30) | 1.5% (0.26) |
| px21 | 1.4% (0.32) | 2.4% (0.56) | 2.5% (0.25) |
| px22 | 1.5% (0.45) | 1.7% (0.43) | 2.9% (0.29) |
| px12 | 1.8% (0.44) | 2.4% (0.66) | 3.3% (0.22) |
| px5 | 1.4% (0.23) | 3.3% (0.46) | 2.3% (0.23) |
| **Column means** | 1.4% (0.32) | 2.8% (0.70) | 2.4% (0.24) |

**Table 3.4** - Comparison with manual delineation for eight selected plaque samples. COV is the coefficient of variation.

| Plaque sample | Our method | | | | | | Manual delineation | | | | | |
|---|---|---|---|---|---|---|---|---|---|---|---|---|
| | GSM (un-normalized) | | | Plaque Area | | | GSM (un-normalized) | | | Plaque Area | | |
| | mean | s.d. | COV (s.d./mean) | mean (mm²) | s.d. (mm²) | COV (s.d./mean) | mean | s.d. | COV (s.d./mean) | mean (mm²) | s.d. (mm²) | COV (s.d./mean) |
| px2 | 32.3 | 2.80 | 8.7% | 27.9 | 1.12 | 4.0% | 28.7 | 3.88 | 13.5% | 27.5 | 2.10 | 7.6% |
| px4 | 76.9 | 2.22 | 2.9% | 11.3 | 1.05 | 9.3% | 78.1 | 4.57 | 5.9% | 11.0 | 2.03 | 18.4% |
| px11 | 70.2 | 1.27 | 1.8% | 38.0 | 0.23 | 0.61% | 73.0 | 3.36 | 4.6% | 37.4 | 0.40 | 1.1% |
| px26 | 43.4 | 1.49 | 3.4% | 39.5 | 0.94 | 2.4% | 45.9 | 2.27 | 4.9% | 36.9 | 1.61 | 4.4% |
| px21 | 52.4 | 2.35 | 4.5% | 22.7 | 1.09 | 4.8% | 51.3 | 2.86 | 5.6% | 22.1 | 1.80 | 8.1% |
| px22 | 67.4 | 2.15 | 3.2% | 21.5 | 0.80 | 3.7% | 67.6 | 3.54 | 5.2% | 21.3 | 1.75 | 8.2% |
| px12 | 54.0 | 3.72 | 6.9% | 14.9 | 0.39 | 2.6% | 52.9 | 4.47 | 8.5% | 15.0 | 1.23 | 8.2% |
| px5 | 36.9 | 4.31 | 11.7% | 22.0 | 0.96 | 4.4% | 36.0 | 4.66 | 13.0% | 22.4 | 1.71 | 7.7% |
| Column means | 54.2 | 2.54 | 5.4% | 24.7 | 0.82 | 4.0% | 54.2 | 3.70 | 7.7% | 24.2 | 1.58 | 8.0% |
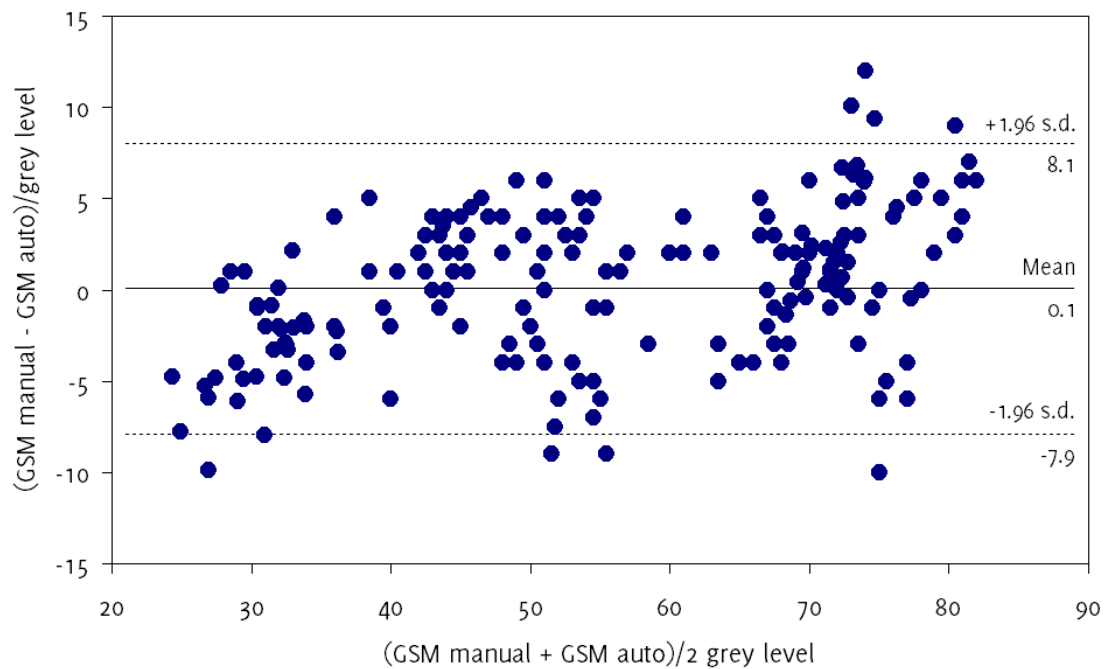
**Figure 3.8** - Bland-Altman plot showing the differences in GSM measurements, on matching image frames, between our method and manual delineation.

## 3.5 Discussion

Our investigation highlighted variations in the GSM and area of plaques when measured on a frame-by-frame basis throughout ultrasound image sequences. Image normalisation did not reduce the extent of the GSM variations and in some cases resulted in greater variation. These results demonstrate that frame-by-frame variations in the plaque GSM cannot be offset by applying normalisation factors based on the selection of blood and adventitia regions in one of the frames. Furthermore, selecting separate reference regions in all images introduced an additional source of variability due to the subjective nature of the process. The reference regions were user-selected and not computerized as they are easily identified by the operator and it would have been difficult to ensure the accuracy of a computerized selection. In NORM1 normalisation, the coefficients of variation for GSM changed after normalization for some plaques. This occurred when the blood reference regions had non-zero GSM,

causing an intercept to be introduced into the linear relationship between the normalized and un-normalized greyscale values. Also, as GSM values are limited to the range 0 to 255, normalization could result in the clipping of the GSM values outside this range, thus affecting the coefficients of variation. The increased coefficient of variation for GSM, in the case of the NORM2 normalisation, provided evidence that the frame-by-frame variations seen in GSM were unlikely to be, at least significantly, due to a general temporal variability in the overall image brightness.

The extent of the GSM variations seen in the study were similar in magnitude to those reported by Elatrozy et al. [148] who found that, after normalisation, the coefficient of variation among 4 different observers was 4.7% for the GSM of plaques. However, the variations captured by that study did not include variations that may have been due to the selection of different still images as each of the four observers appeared to have used the same image to assess the GSM. Therefore, the true inter-observer variabilities may have been greater than that suggested by the results of that study.

The findings of our study have two implications. First, in the case of studies which have considered intra/inter-observer variabilities, the variabilities quoted may have been under-estimated unless the inter-frame variations in the plaque GSM were taken into account. Secondly and conversely, in the case of inter-session or across-study variabilities of GSM measurements, some of these variabilities may have been due to the selection of different image frames corresponding to the differences in the exact cross-sections being imaged.

The variations seen in the plaque GSM and area may be due to a number of different factors. While changes to the acquisition settings during a single acquisition would not be expected, changes in the plaque GSM could occur, for example, if the distance between the plaque and the transducer face changed during an acquisition. Patient or probe motion may also change the location and orientation of the scan plane with respect to the plaque being imaged, affecting both the measured GSM and the observed cross-sectional area. These are likely to be significant contributors to the variations seen in the GSM and area of plaques in this study. Deformation or compression of the plaque under the pulse pressures may also cause changes in the

measured plaque GSM and cross-sectional area and the observation of periodical variations with physiologically reasonable frequencies in the plaque GSM and area for several of the plaques provided evidence to support this hypothesis. However, it should be noted that such cyclic variations could also have been caused by periodic variations in the scan plane location and orientation and due to out-of-plane plaque, patient, or probe motion. The poor correlation between the inter-frame coefficients of variation of GSM and plaque area suggested that at least some of the variations seen in the plaque GSM were likely to have occurred due to factors other than changes in the observed plaque area. This was also supported by the results of the regression analysis, which did not highlight the parameters based on the plaque area as being statistically significant contributors to the variabilities seen, across plaque samples, in the extent of the inter-frame GSM variations.

Other factors that may have caused apparent changes in the plaque GSM and cross-sectional area included unclear plaque boundaries (e.g. poor image quality or substantial image noise), which may have caused fluctuations in the detected plaque boundaries. However, the image sequences used in this study were of sufficiently good quality that any variations due to such fluctuations were not thought to be major contributors to the GSM variations observed.

The statistically significant difference found in the mean GSM of plaques in the symptomatic and asymptomatic groups is in accord with previous findings that have shown symptomatic plaques, in general, as having lower GSM values [129,131]. The differences between the two groups in the case of the parameters describing the inter-frame variations in the GSM were not statistically significant which was plausible as out-of-plane plaque, patient, and probe motion appeared to be a significant sources of variation for GSM measurements.

Manual delineation of the plaque boundaries separately for each image frame was found to increase the extent of the frame-by-frame variations observed in the plaque GSM and area (7.7% and 8.0%, respectively, compared with 5.4% and 4.0% for our method) due to the greater subjectivity of the manual delineation process.

The main limitations of our study were the use of two dimensional ultrasound and the absence of any attempts to fix the scan plane location and orientation with respect to the plaque being imaged, other than those measures normally taken in the clinic (e.g. holding the probe fixed and asking the patient to breath-hold and remain still). It should be remembered that the method of ultrasound acquisition commonly used in carotid plaque GSM studies, namely two dimensional ultrasound, provides only a cross section of the whole plaque volume. Since the plaque GSM measured using two dimensional techniques reflects only a cross-section, these measurements are susceptible to variations due to out-of-plane plaque, probe and patient motion. Studies incorporating three dimensional techniques may overcome this limitation and enable further investigation of the nature of any intrinsic frame-by-frame variations in the plaque GSM or volume. Such follow-up studies may also identify whether any inter-frame variations seen in the GSM and volume of plaques can provide additional insight into the ultrasound characterisation of carotid plaques, thus improving clinical utility.

Another limitation of our assessment of the plaque GSM and cross-sectional area was with regard to anechoic regions of plaques and regions of plaques in areas of acoustic shadowing. These regions were excluded from analysis. The cross-sectional areas of plaques that had such regions were, thus, under-estimated and neither the plaque area nor the GSM reflected the true values. The excluded regions also had an effect on the magnitude of the frame-by-frame variations that were measured for the affected plaques. In the case of anechoic regions of plaques, the inclusion of the anechoic regions would have increased the observed cross-sectional area, while reducing the GSM and the magnitude of the GSM and area variations observed. However, the reduction in the magnitude of the inter-frame GSM variations would have been only because of the absence of echogenicity in these regions. In the case of the regions of acoustic shadowing, these regions need to be excluded from analysis due to the absence of plaque texture information resulting from acoustic shadowing. Although colour Doppler is useful for subjectively defining the plaque-arterial lumen boundary, it is not suitable for quantifying the plaque area throughout the cardiac cycle, since colour filling of the lumen is dependent on blood flow velocity [231]. Nevertheless, our results demonstrated that variations in the plaque GSM and cross-sectional area do

occur, in the visible parts of the plaques that were not in regions of acoustic shadowing. Such variations are important as they could lead to an error in a potential diagnostic test that uses the GSM as the selection criterion, particularly for plaques of intermediate echogenicity where a coefficient of variation of 5% may provide enough bias to move the plaque between high- and low-risk groups. Since the plaque GSM is not generally used to inform clinical decision making, these variations do not currently have a clinical impact. Nevertheless, they should be appreciated for research studies which increasingly utilize the plaque GSM.

Our results did not find the plaque cross-sectional area to significantly affect the extent of the frame-by-frame variations observed in the plaque GSM. A major source of variation in the inter-frame plaque GSM may in fact be the movement of the plaque cross-section with respect to the scan plane and this may be a bigger problem for smaller plaques. However, our results showed that the observed GSM could vary on a frame-by-frame basis substantially for large plaques as well the minor stenoses.

Since previous studies typically quantified GSM on single frames of ultrasound images, the variations found in this study have been previously neglected. Improved attempts to standardise GSM measurements and reduce variability between centres should account for these findings, for example, by performing GSM measurements at peak systolic/diastolic frames or by carrying out an assessment of the average GSM throughout the cardiac cycle. Techniques such as GSM assessment using multiple cross-sectional views of plaques can also be used to improve diagnostic accuracy compared to a single view cross-sectional assessment. The best option would be to carry out the assessment in three dimensions. However, three dimensional ultrasound techniques are still under development and are not widely available. It should be noted that we do not propose the technique we have used in our study as a replacement for the existing methods but we highlight the variations in the plaque GSM and cross-sectional area that may be observed on a frame-by-frame basis using single-view, two dimensional ultrasound.

## 3.6 Conclusions

In conclusion, this investigation found that the GSM of carotid artery plaques can vary when measured on a frame-by-frame basis throughout ultrasound image sequences. These variations affect the reproducibility of studies and have implications for the use of GSM as a predictor of cerebrovascular events. Future studies looking at the GSM of carotid artery plaques may need to take these variations into consideration.

# Chapter 4

# Quantitative Assessment of Carotid Plaque Surface Irregularities and Correlation to Cerebrovascular Symptoms

## 4.1 Overview

Surface irregularities of plaques have long been thought to be potentially useful for identifying vulnerability as it is expected that potentially vulnerable types of plaques such as those with ulcerations or cap ruptures may present with irregular surfaces when imaged using ultrasound (as well as angiography and other imaging modalities). However, three drawbacks exist. First, surface irregularity assessments have been performed on still images, ignoring any variations that may have been present on a frame-by-frame basis. Secondly, the assessments have mainly been qualitative and thus subjective. Thirdly, the scarce quantitative assessments have been based on plaque surfaces manually outlined by the operator, thus introducing subjectivity into the process, and potentially not capturing the full surface structure of the plaque, particularly small fissures or surface disruptions. This chapter contributes to knowledge by providing a novel quantitative method for studying plaque surface irregularities, which is shown to have a significant correlation to symptoms, and presenting the results of the first-ever quantitative study of surface irregularities measured from image sequences in comparison to still image frames. A research article based on the contents of this chapter has been published in Cardiovascular Ultrasound [243].

## 4.2 Introduction

There is growing interest in using ultrasound images of the carotid artery to assess plaque surface irregularities and use this as a surrogate marker of carotid plaque ulceration and vulnerability. Previous studies have investigated plaque surface irregularities using qualitative classification schemes such as smooth vs. irregular or by using specific criteria for classifying ulceration [149,244-247]. Surface structure

determined from ultrasound images has been found to correlate, to some extent, with surface structure found on angiography [248-249], intra-plaque haemorrhage [172], CT/MRI-determined cerebral infarctions [250-253] and the incidence and presence of cerebrovascular events and symptoms [158,172,180,200,248,250,253-254]. Ultrasound-determined surface structure agreed with that found on surgical/autopsy specimens with varying degrees of success [145,182-183,244-245,247,255-261]. A large, prospective study found that the unadjusted, cumulative, 5-year risk of ischaemic stroke was 8.5% when irregular plaques were seen on ultrasound, compared to 1.3% and 3.0% for no plaque and smooth plaques, respectively [262].

Quantitative assessments of plaque surface irregularities may have benefits over qualitative assessments, since they should be more operator-independent. Yet, even with quantitative analyses, manual delineation of the plaque-arterial lumen boundary on ultrasound images introduces some subjectivity into the process and is less likely to capture small defects on the plaque surface. There have been only a few attempts to quantify the surface irregularities of carotid artery plaques. Tegos et al. (263) quantified surface irregularities by calculating the bending energy of the plaque surface. However, plaque surfaces were manually outlined by the operator, and the authors obtained similar bending energies for symptomatic and asymptomatic plaques. More recent studies quantified plaque surface irregularities by measuring the principal curvatures of plaque surfaces in 3 dimensions [264-265]; however, the underlying 3-dimensional ultrasound techniques are still under development, and more difficult to implement in the vascular clinic compared to 2-dimensional techniques.

We hypothesized that an objective, quantitative measurement of carotid plaque surface irregularities using 2-dimensional, cross-sectional ultrasound imaging would correlate with the presence of ipsilateral hemispheric symptoms. This study defined a novel surface irregularity index (SII) and investigated whether it enhances diagnostic performance compared to the degree of stenosis of the carotid artery alone.

## 4.3 Methods

Thirty-two consecutive patients (20 males and 12 females) who attended the University Hospitals of Leicester NHS Trust's Rapid Access Transient Ischaemic Attack (TIA) clinic were recruited. The study was approved by the National Research Ethics Service (NRES) Committee East Midlands - Northampton (reference 11/EM/0249), followed institutional guidelines, and each patient gave informed consent before participating in the study. Patients who did not have carotid stenoses were excluded from the study. In total, surface irregularity indices of 47 carotid artery plaques (stenosis range 10%-95%) were measured. Plaques were classified as either having caused ipsilateral hemispheric cerebrovascular symptoms (i.e. symptomatic) or asymptomatic following specialist medical review. Symptoms included aphasia, transient monocular blindness and hemimotor/sensory symptoms consistent with transient ischaemic attack or stroke.

### 4.3.1 Data Acquisition

Longitudinal cross-sections of the carotid plaque were acquired by experienced sonographers using a Philips iU22 ultrasound scanner (Philips Healthcare, Eindhoven, The Netherlands) with an L9-3 probe. B-Mode (greyscale) and Colour Doppler image sequences were recorded as DICOM files over an average of 5 cardiac cycles (mean frame rate was 32 frames per second) using the vascular carotid preset on the scanner (Vasc Car preset, persistence low, XRES and SONOCT on). Colour Doppler image sequences were used as a qualitative aid to identifying the location and extent of the plaques, and for qualitative assessments, while the greyscale data were used for the quantitative analyses of plaque surface irregularities.

### 4.3.2 Data Analysis

Quantitative analyses were carried out using MATLAB version 7.14, release 2012a (MathWorks, Natick, Massachusetts, USA) and employed a novel technique to track plaques throughout ultrasound image sequences [238]. We measured plaque surface irregularities using a novel surface irregularity index (SII) which was calculated by computationally summing the angular deviations from a straight line, of the luminal plaque surface, and dividing this by the length of the plaque surface. This measures

the degree of irregularity of the plaque surface as opposed to the previous methods which calculated either the bending energy or the curvature of the plaque surface. Although the latter two would be expected to relate to the degree of irregularity of the plaque surface, they are not direct measures of surface irregularities. For example, in the case of the curvature of the plaque surface, positive and negative curvatures can have a cancelling effect, resulting in a zero curvature measurement for an irregular plaque surface. Our surface irregularity index, on the other hand, directly measures the irregularities, which are essentially deviations from a straight line, of the plaque surface, and all irregularities add to the degree of irregularity measured.

The surface irregularity index was also combined with the degree of stenosis of the corresponding artery by taking their product, resulting in a combined risk indicator. The measurements were made without *a priori* knowledge of the patient symptomatic status. Degrees of stenosis were measured using criteria consistent with the NASCET method utilizing blood flow velocities in conjunction with the B-Mode and colour flow imaging [38,47,240] and plaque SII measurements were averaged across all image frames. As Doppler velocity measurements are not able to reliably discriminate degrees of stenosis below 50%, we used B-Mode diameter measurements and colour flow imaging to grade the degree of stenosis into deciles for minor stenoses. We assessed the reproducibility of our surface irregularity measurements by calculating the intra-observer and inter-frame variabilities. Intra-observer variabilities were determined by measuring the surface irregularity indices of nine selected plaques five times using the same carotid file-video for each plaque, respectively. The nine plaques were selected from the available dataset to give a wide range of stenosis severity and plaque echogenicity for reproducibility analysis. Inter-frame variabilities, on the other hand, were assessed for all the plaques included in the study, to give a measure of the magnitude of variations seen in the surface irregularity indices across image frames. A qualitative assessment of plaque surface irregularities was also performed by an experienced vascular scientist, off-line and blinded to patient clinical history, classifying plaque surfaces as either smooth or irregular using the greyscale and Colour Doppler images as a guide.

### 4.3.3 Statistical Methods

Statistical analyses were carried out using SPSS version 20 (IBM Corporation, Armonk, New York, USA). The non-parametric Mann-Whitney U-test was used to determine whether the surface irregularity indices differed significantly between the symptomatic and asymptomatic plaque groups and those plaques qualitatively classified as having an irregular or smooth surface. Kendall's tau was used to establish whether the SII, the degree of stenosis, and the plaque area could be regarded as statistically independent and Receiver Operating Characteristic (ROC) curves were used to investigate the diagnostic performance of the plaque SII on its own and in combination with the degree of stenosis. The correlation between the symptomatic and asymptomatic plaque groups and the qualitative plaque surface assessment was performed using Pearson's $\chi^2$.

### 4.4 Results

Twenty-four of the 47 plaques investigated were found to be not associated symptoms, while the remaining 23 were found to have caused symptoms following expert, specialist stroke physician assessment. The mean age of the symptomatic patients was 75.3 years compared with 77.8 years for the asymptomatic (p>0.05, Mann-Whitney test). None of the patient characteristics sex (20 males), current or past tobacco smoking (63%), hypertension (63%), hypercholesterolaemia (53%), diabetes mellitus (53%), ischaemic heart disease (38%), family history of stroke (34%), previous TIA/stroke (44%), alcohol consumption (28%) and peripheral vascular disease (13%) had a statistically significant relationship to the presence of symptoms (p>0.05 for all, Pearson's $\chi^2$).

Examples of a symptomatic and an asymptomatic plaque, with their corresponding surface irregularity measurements, are shown in Figure 4.1 and Figure 4.2. Across the full data-set, the mean SII of symptomatic plaques was 1.89 radians/mm compared with 1.67 radians/mm for the asymptomatic plaques. Plaque SII (p=0.03), the degree of stenosis (p<0.01), and the product of the two (p<0.01) were all significantly higher in symptomatic plaques compared with the asymptomatic (Figure 4.3). There was no

statistically significant relationship between the plaque surface irregularity index and the degree of stenosis or the plaque area (p=0.30 for both, Figure 4.4).
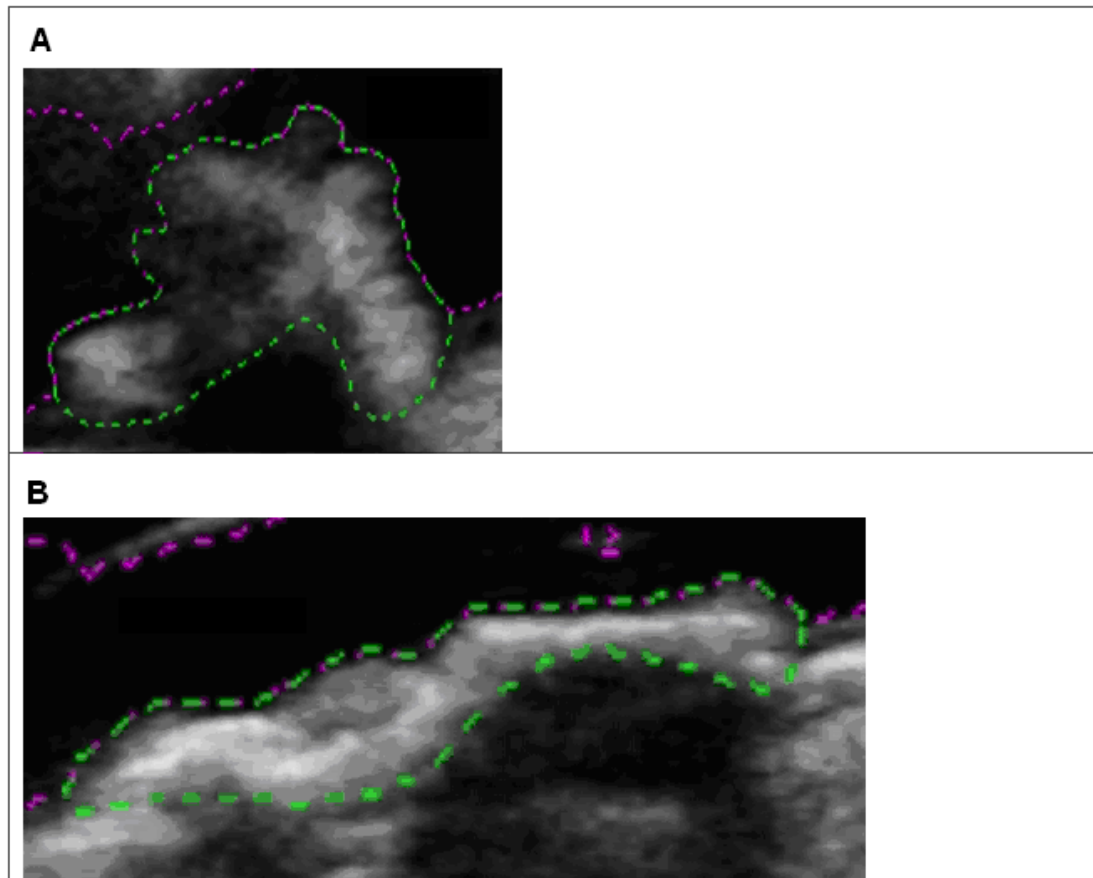


**Figure 4.1** - Two plaques of markedly different surface irregularity indices: (a) a symptomatic plaque with an SII of 2.25 radians/mm; and (b) an asymptomatic plaque with an SII of 1.57 radians/mm. The plaque surface is the boundary between the plaque and the arterial lumen (where the purple and green dashed lines overlap). (a) is also a plaque qualitatively classified as having an irregular surface, while (b) is a plaque qualitatively classified as having a smooth surface.
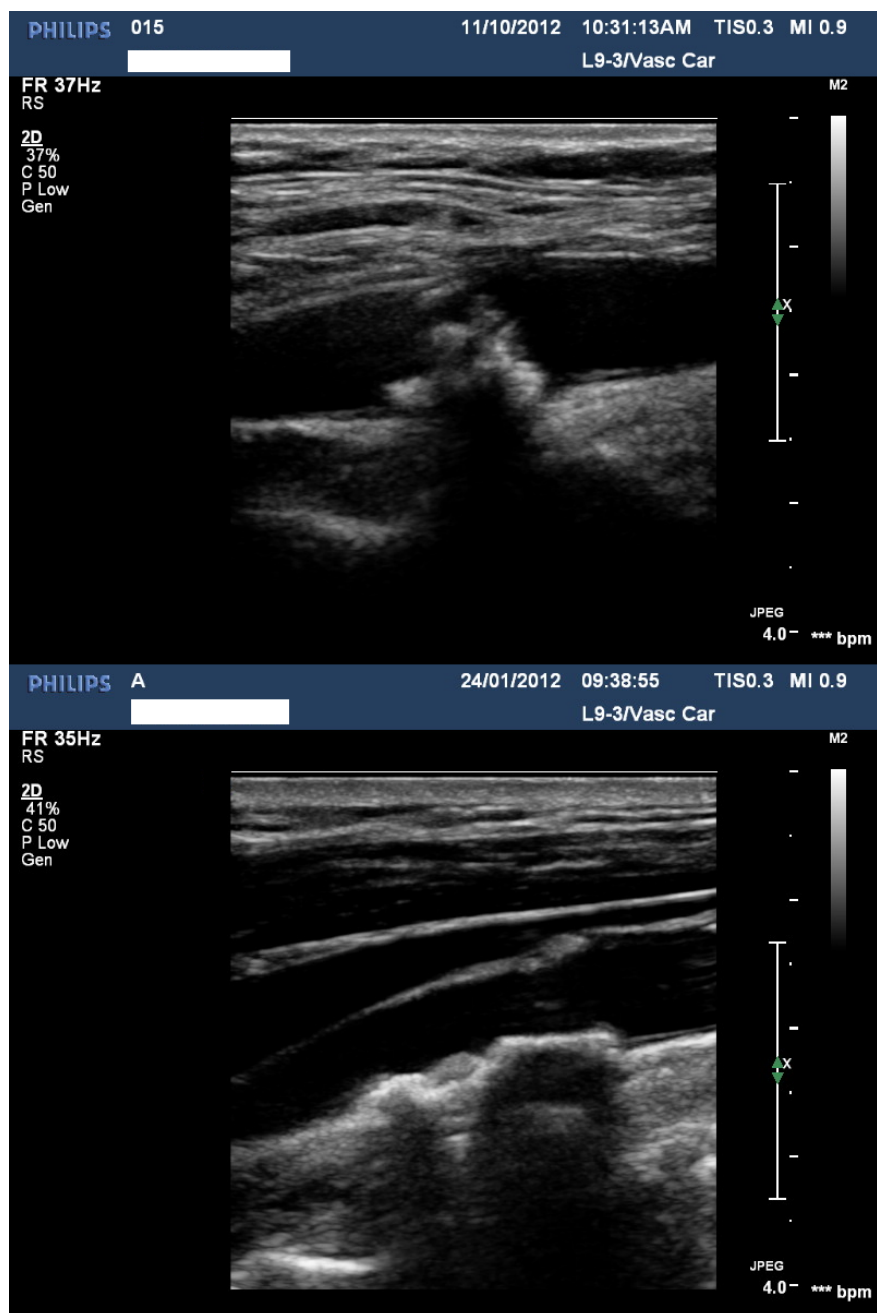
**Figure 4.2** - Full-size ultrasound images corresponding to the close-up plaque views shown in Figure 4.1. The symptomatic plaque (top), and the asymptomatic plaque (bottom).
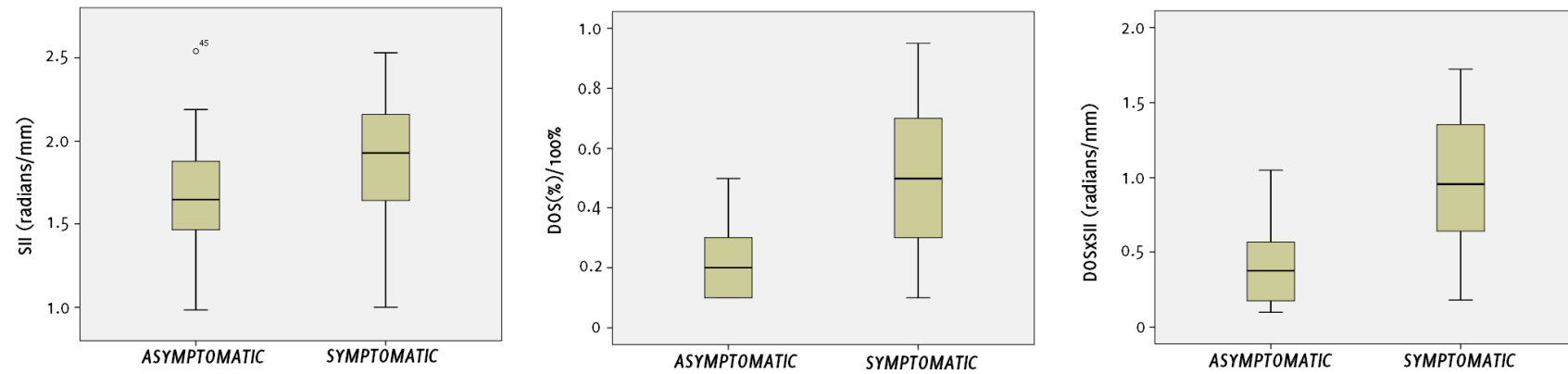
**Figure 4.3** - Distribution of plaque surface irregularity index (SII, left), degrees of stenosis (DOS, middle) and the product of the two (right) among the symptomatic and asymptomatic plaque groups. Degrees of stenosis are given as degree of stenosis(%)/100% (i.e. 0.5 corresponds to 50%, etc.).
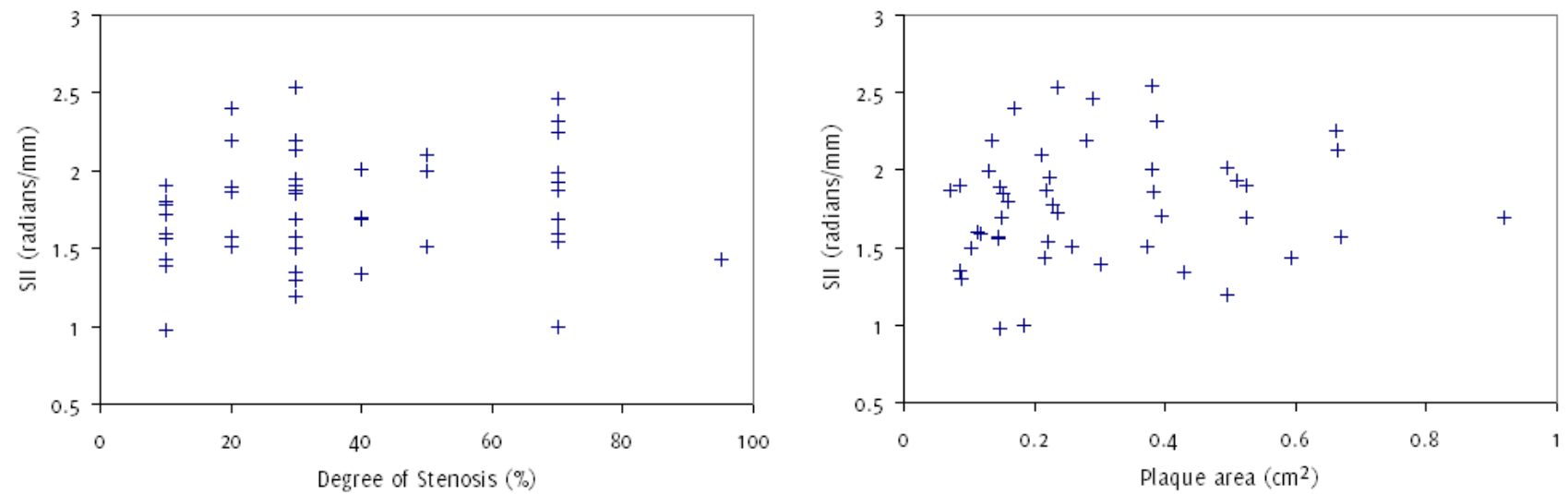
**Figure 4.4** - Scatter plot of the plaque surface irregularity index *versus* the degree of stenosis of the corresponding artery (left) and the plaque area (right), illustrating a lack of association between these parameters.
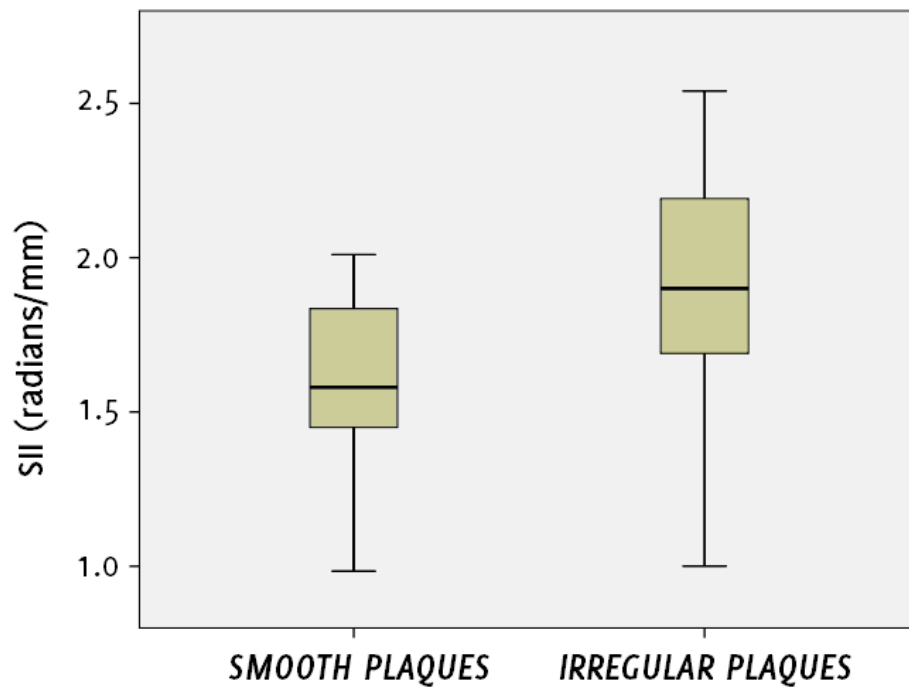
**Figure 4.5** - Distribution of plaque surface irregularity index (SII) among the plaque groups qualitatively classified as having an irregular or smooth surface.

Qualitatively, 27 of the 47 plaques were classified as having an irregular surface, and 20 were classified as being smooth. Figure 4.1 illustrates examples of plaques qualitatively classified as having irregular and smooth surfaces. There were 11 smooth and 13 irregular plaques in the asymptomatic group, and 9 smooth and 14 irregular plaques in the symptomatic group. There was no statistically significant association between the qualitative assessment of surface irregularities and the symptomatic status (p=0.64). However, the SII of the plaques qualitatively classified as having an irregular surface was significantly higher than those classified as having a smooth surface (p=0.01, Figure 4.5).

Receiver operating characteristic (ROC) curve analysis showed that the SII could predict the presence of ipsilateral hemispheric cerebrovascular symptoms with an accuracy of

66% (sensitivity 65%, specificity 67%) on its own and with an accuracy of 83% (sensitivity 96%, specificity 71%) in combination with the degree of stenosis (Figure 4.6). The area under the ROC curve was largest for the product of the degree of stenosis and the SII (0.866) compared to either the degree of stenosis (0.832) or the SII on its own (0.687).

Our study of plaque SII measurement reproducibility showed a mean intra-observer coefficient of variation of 4.4%. The mean intra-observer, inter-frame coefficient of variation was 10.6%.
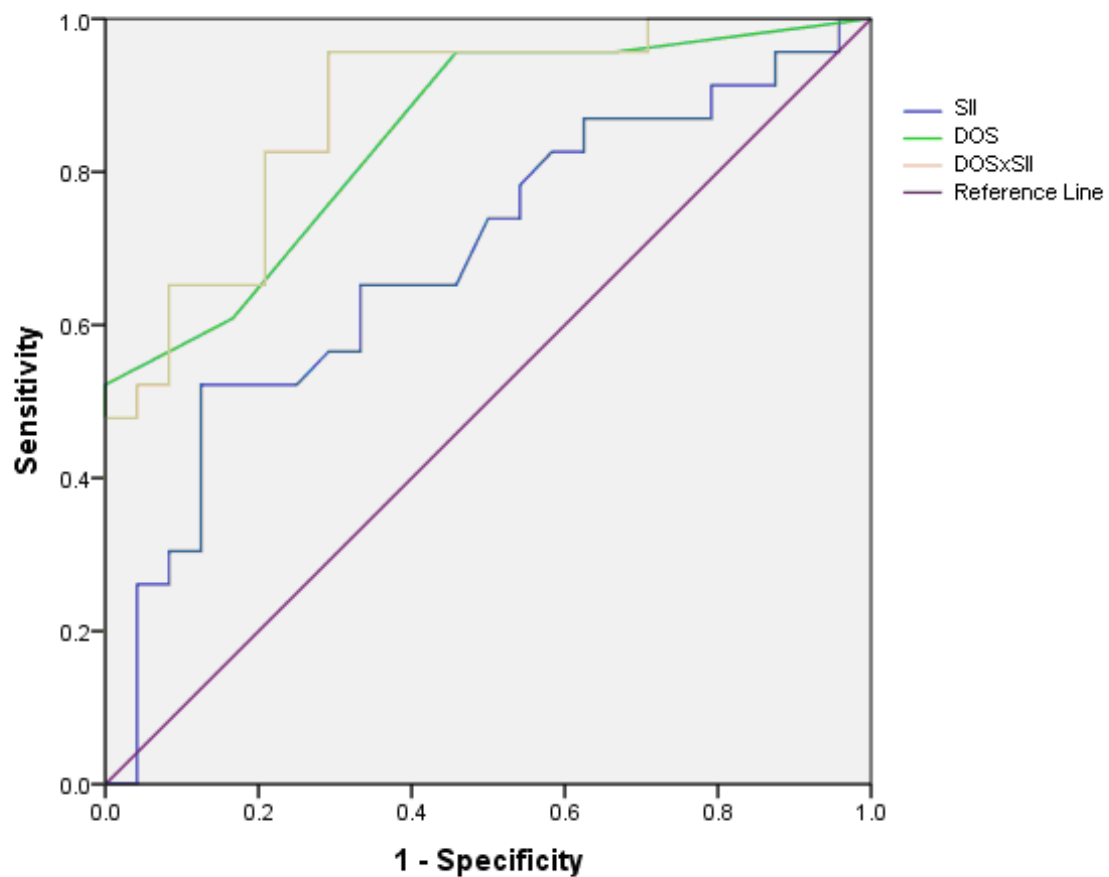


**Figure 4.6** - Comparison between Receiver Operating Characteristic curves for the plaque surface irregularity index (SII), the degree of stenosis (DOS) and their product (DOS×SII).

**4.5 Discussion**

This chapter defined a novel ultrasound plaque surface irregularity index which was found to have potential clinical value for improving the identification of the vulnerable carotid plaque. Ultrasound imaging provides a convenient and non-invasive means of assessing the carotid plaque. Of the characteristics of plaques that can be assessed using ultrasound, plaque surface structure is an interesting potential candidate for inclusion in a stroke risk model. However, there are two major practical problems with the ultrasound assessment of plaque surface structure. First, an irregular surface observed on ultrasound does not necessarily indicate an ulcerated or compromised plaque surface. Barry et al. [182], for example, found that false ultrasound diagnoses of ulceration could be due to culs-de-sac or pits in fibrotic tissue that look like ulcers. Secondly, ulcerations or surface defects may not always be detected, particularly in cross-sectional, 2-dimensional ultrasound imaging. This is due to the limited coverage of 2-dimensional ultrasound. Furthermore, small ulcerations or surface defects may not be revealed if these are smaller than the resolution of the ultrasound imaging system. Despite these difficulties, it is reasonable to expect potentially vulnerable types of plaque, such as plaques with ulcerations or plaques for which the surface integrity has been compromised, to exhibit greater irregularity in general. Irregular plaques could also potentially lead to more disturbed blood flow patterns with local high- and low-velocity flow regions and subsequent increases in plaque stress and increased risks of thrombosis, respectively. We should therefore expect an assessment of the surface irregularities of plaques to bring useful information that relates to plaque vulnerability. However, in a small cohort of patients, a strong correlation to symptoms should not be expected for the surface irregularities on their own, since it is an assessment only of the surfaces of plaques and surface irregularities may or may not be indicative of ulcerations and other surface defects.

In our study, we measured the surface irregularities of plaques in an objective manner and found that these quantitative measurements correlated with a qualitative assessment of surface irregularities. A correlation between surface irregularities and ipsilateral hemispheric symptoms was found for the novel quantitative method but not

for the qualitative measure. The absence of a correlation in the case of the qualitative assessment can be attributed to the increased subjectivity of qualitative measures which may render a weak correlation to symptoms undetectable. The subjectivity of the qualitative assessment is most apparent with plaques that cannot be classified as smooth or irregular with any certainty. In such cases, the assessor may make a highly subjective decision to place the plaque in one or the other group. The alternative is to mark such plaques as having an indeterminate surface characteristic and therefore unclassified.

We found that the combination of the plaque surface irregularity index with the degree of stenosis of the corresponding artery resulted in a more effective diagnostic test compared to the degree of stenosis on its own. This indicates that the objective study of plaque surface irregularities may provide useful additional information for predicting the presence of cerebrovascular symptoms. There was no significant correlation between the plaque SII and the degree of stenosis in our assessment, indicating that the former may provide information that is complementary to the latter.

Our surface irregularity index was combined with the degree of stenosis of the corresponding artery as the latter is an established parameter widely used in clinical practice and associated with an increased risk of cerebrovascular events. We took the product of the two parameters since the presence of ipsilateral hemispheric symptoms was directly related to both the degree of stenosis and the surface irregularity index. Our study found that combining the surface irregularity index with the degree of stenosis results in a more effective risk indicator than the degree of stenosis on its own.

The measurement technique we used had good reproducibility. The intra-observer variations were due to the human operator involvement required for the initial setup of the boundary detection procedure that resulted in the semi-automatic delineation of the plaque-arterial lumen boundaries, while the inter-frame variations were probably chiefly due to out-of-plane plaque, patient, and probe motion.

Further work can be directed towards studying the surface irregularities of plaques taking into account the echogenicity characteristics local to the surface. This would be useful as it may be more likely for surface irregularities to correspond to surface defects such as ulcerations or haemorrhages if the plaque has a less echogenic pattern (e.g. a ruptured fibrous cap or a haemorrhage) compared to being highly echogenic (e.g. fibrous or calcified). The variation of surface irregularities across plaque surfaces should also be explored in a follow-up study since plaque surfaces may contain both smooth and rough segments and their distribution may provide useful additional information that relates to plaque vulnerability.

## 4.6
## Conclusions

This chapter has shown that an objective assessment of plaque surface irregularities using a novel surface irregularity index may correlate with the presence of ipsilateral hemispheric cerebrovascular symptoms. We found an increase in diagnostic performance with the use of the plaque SII versus that provided by the degree of stenosis alone. Plaque SII may therefore be a valuable tool for improving risk assessment, by helping to identify the vulnerable plaques in patients with carotid artery disease. The potential clinical value of this parameter should be explored in follow-up studies.

# Chapter 5

# Wall Motion in the Stenotic Carotid Artery: Association with Greyscale Plaque Characteristics, the Degree of Stenosis and Cerebrovascular Symptoms

## 5.1 Overview

Wall motion characteristics of the stenotic carotid artery may be potentially useful for identifying carotid plaques at risk of rupture since large motions could increase the mechanical stress on the plaque while smaller motions could be indicative of progressive atherosclerotic disease of the arterial wall, which is known to cause the arterial wall to stiffen. Our contributions to knowledge in this chapter include the study of correlation between the wall motion characteristics of the stenotic carotid artery and greyscale plaque characteristics such as the plaque greyscale median and the surface irregularity index. A research article based on the contents of this chapter has been published in Cardiovascular Ultrasound [266].

## 5.2 Introduction

Patients attending transient ischaemic attack (TIA) clinics often undergo ultrasound imaging of their carotid arteries, during which the presence of any atherosclerotic plaques are noted and the corresponding degrees of stenosis are measured. The degree of stenosis is used routinely in clinical practice. However, there is growing demand for additional parameters which can further differentiate high-risk or vulnerable plaques, particularly in those with low to moderate degrees of stenosis. Studies have found that plaque composition in patients undergoing carotid endarterectomy is an independent predictor of future cardiovascular events with plaque neovascularisation and haemorrhage relating to adverse cardiovascular outcome during follow-up [65]. Greyscale plaque characteristics, such as the plaque greyscale median (GSM) and surface irregularities also have the potential to be additional indicators of vulnerable plaques [51,129,131,134-135,140,238,243,262]. Ultrasound assessment of the mechanical properties of the carotid plaque using

shearwave elastography is an emerging technique that may also provide additional benefit [267]. Another potentially useful parameter which can be easily measured from ultrasound scans performed in the TIA clinic is the systolic dilation or distension of the artery with the atherosclerotic plaque. The dilation of the carotid artery from diastole to systole depends on several factors including arterial stiffness, and previous studies have shown that stiffer arteries are associated with atherosclerosis and are risk factors for stroke and other cardiovascular diseases [268-271]. The amount of arterial dilation is a physical parameter that may also affect the stability of the plaque, since greater arterial motion may increase the mechanical stress on the plaque and promote instability [197,200,272-274].

The presence of the atherosclerotic plaque can have a significant effect on arterial wall motion [275-276]. One study found that arterial distensibility was not only significantly lower in the internal carotid artery where there was a plaque, but it was also lower in the common carotid artery of the affected side in comparison with the contralateral common carotid artery, providing evidence that the effect of a plaque on arterial mechanical properties is not limited to the actual plaque site but rather extends to a considerable degree in a proximal direction [275]. Computational models, on the other hand, showed that the non-uniform thickness of the diseased arterial wall can restrict wall motion and re-distribute stress, giving rise to increased stress concentrations at the plaque shoulders [276]. Therefore, an assessment of the wall motion characteristics of the stenosed carotid artery may provide useful indicators that correlate with the risk of plaque rupture and the prevalence of symptoms.

A previous study found that patients with acute symptomatic carotid stenosis had impaired brachial artery flow mediated dilation (FMD) compared to patients with asymptomatic carotid stenosis in a patient population with greater than 50% reduction in the diameter of the carotid artery [277]. That study showed that impaired brachial FMD was an independent predictor of cerebral ischaemic symptoms. However, not many studies have considered whether the physiological dilation of the stenosed carotid artery itself might have any correlation to cerebrovascular symptoms, addressing the question of whether patients presenting with ipsilateral hemispheric symptoms have distinctly different carotid artery dilations compared to patients that

do not. A study by Ramnarine et al. (97) looked at the physiological dilation of atherosclerotic carotid arteries and correlated results with the degree of stenosis, but any relationships to the presence of patient symptoms were not investigated. Another study examined the dilation characteristics of the carotid artery at the level of the plaque and compared this with the adjacent common carotid artery leading to a longitudinal strain gradient estimation, but again, any relationships to the presence of patient symptoms were not studied [278]. More recently, Beaussier et al. (279) studied the longitudinal distension gradient between the plaque and the adjacent common carotid artery with respect to the presence of ipsilateral hemispheric symptoms and found no statistically significant differences. However, their results do not appear to indicate whether there were any significant differences in the degree of arterial dilation at the adjacent carotid segment between the symptomatic and asymptomatic groups. That particular study also involved only a small number of carotid arteries with ipsilateral symptoms (n=9).

It is plausible that wall motion in the stenotic carotid artery may affect the stability of the carotid plaque and consequently, relate to the presence of ipsilateral hemispheric symptoms. Wall motion data along with the degree of stenosis and greyscale plaque characteristics may therefore help identify the vulnerable plaque. The purpose of this study was to test the hypothesis that the systolic dilation of the stenosed carotid artery is related to the presence of ipsilateral hemispheric symptoms and can be used to differentiate between symptomatic and asymptomatic patients. Arterial wall motion was measured before the proximal shoulder of the plaque as this is an ideal, upstream location close to the plaque where a well defined segment of the artery can often be found. The latter is important because arterial wall motion measurements across the plaque can suffer from high variability [97]. Our investigation measured the absolute and percentage dilation of stenotic carotid arteries, from end diastole to peak systole, and explored whether these parameters had any statistically significant associations to the degree of stenosis, greyscale plaque characteristics, and the presence of ipsilateral hemispheric symptoms.

## 5.3 Methods

Forty seven patients who attended the University Hospitals of Leicester NHS Trust's Rapid Access Transient Ischaemic Attack clinic were recruited. Variations in the lumen diameters of 61 stenotic carotid arteries (stenosis range 10%-95%) were measured. The study was approved by the National Research Ethics Service (NRES) Committee East Midlands - Northampton (reference 11/EM/0249) and followed institutional guidelines. Each patient gave informed consent before participating in the study. Patients who did not have carotid artery stenosis were excluded from the study. Carotid arteries for which the ultrasound image quality was poor were excluded from the wall motion analysis. Image sequences which were considered to be of poor quality included those with substantial image noise in the vessel lumen and those with poorly defined vessel wall segments. In the case of patients with stenosed left/right carotid arteries, each side was included and analyzed separately. In total, lumen diameter variations of 45 stenosed carotid arteries were included in the final wall motion analysis. Carotid arteries with atherosclerotic plaque were classified as either having ipsilateral hemispheric cerebrovascular symptoms (i.e. symptomatic) or asymptomatic following specialist medical review. Symptoms included aphasia, transient monocular blindness and hemimotor/sensory symptoms consistent with transient ischaemic attack or stroke.

## 5.3.1 Data Acquisition

Longitudinal cross-sections of the carotid artery and plaque were imaged by experienced sonographers using a Philips iU22 ultrasound scanner (Philips Healthcare, Eindhoven, The Netherlands) and an L9-3 probe. Acquisitions included B-Mode (i.e. greyscale) and Colour Doppler image sequences. B-Mode image sequences were acquired using the vascular carotid preset on the scanner (Vasc Car preset, persistence low, XRES and SONOCT on) and were recorded in DICOM format over an average of 6 cardiac cycles (mean frame rate was 32 frames per second). Gain was optimized by the experienced sonographers. In the case of B-Mode acquisitions, the greyscale transfer curve was set to Gray Map 2, as this was reported to be the most linear transfer curve on this scanner [241]. Colour Doppler cine-loops were used as a qualitative aid to identifying the location and extent of carotid plaques, while the B-

Mode data were used for the quantitative analyses including that of arterial wall motion and greyscale plaque characteristics.

### 5.3.2 Data Analysis

Quantitative analyses were carried out using MATLAB version 7.14, release 2012a (MathWorks, Natick, Massachusetts, USA) and employed the arterial wall tracking algorithm introduced in Chapter 2 to track and measure arterial lumen diameters over time.
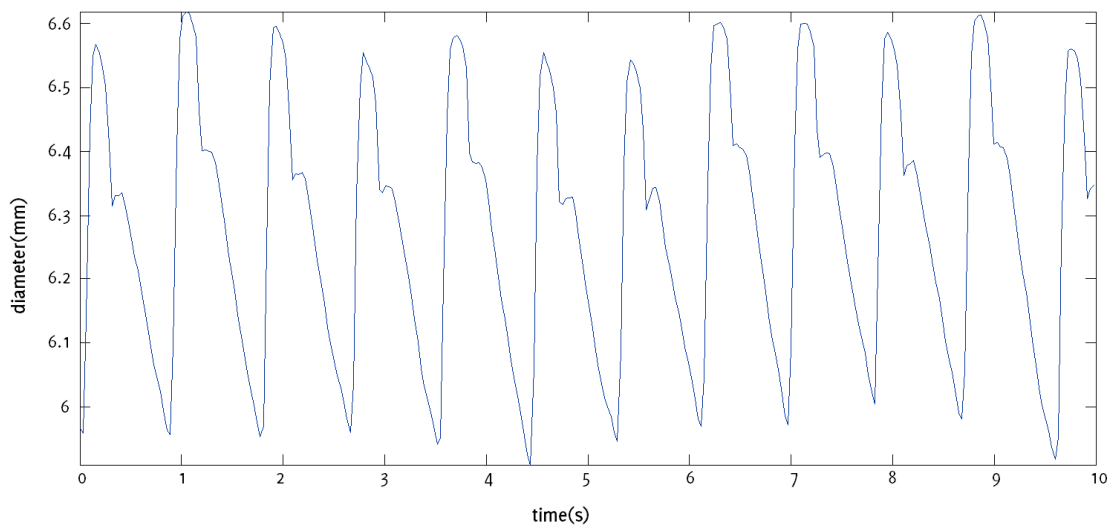


**Figure 5.1 -** Example of an arterial dilation waveform showing lumen diameter variations of a carotid artery throughout several cardiac cycles.

Arterial diameter variation waveforms (Figure 5.1) were obtained before the proximal shoulder of the plaque, but as close to it as possible, and averaged over a region approximately 3 mm long for each image frame (Figure 5.2). The measurements were made without prior knowledge of the patient symptomatic status. The peaks of the diameter variation waveforms (Figure 5.1) were taken to be the (peak) systolic values and the troughs as the (end) diastolic. The absolute value of the systolic arterial dilation was calculated as the increase in the arterial lumen diameter from diastole to

systole and percentage systolic dilation as the same figure divided by the diastolic diameter. The same calculations were carried out for all the cardiac cycles observed on the arterial diameter variation waveforms and averages were calculated. Normalized and un-normalized plaque GSM and surface irregularity indices (SII) were obtained using previously described methods [238,243] while the degree of stenosis of the corresponding arteries were measured using criteria consistent with the NASCET method utilizing blood flow velocities in conjunction with the B-Mode and colour flow imaging [38,47,240].

### 5.3.3 Statistical Analysis

Statistical analyses were carried out using SPSS version 20 (IBM Corporation, Armonk, New York, USA). The non-parametric Wilcoxon-Mann-Whitney test was used to determine whether quantitative measurements such as the absolute and percentage diameter changes, degree of stenosis, and greyscale plaque characteristics differed significantly between patient groups (e.g. symptomatic/asymptomatic, hypertensive/normotensive, etc.). A further ANCOVA test was carried out between the percentage systolic dilation of the artery and symptomatic status, controlling for the effects of the diastolic arterial diameter. Pearson's correlation was used to determine whether the absolute and percentage diameter changes had any statistical relationship to the age of the patient, the degree of stenosis, and the greyscale plaque characteristics. Partial correlations, controlling for the effects of the baseline diastolic diameters, were also carried out for the percentage diameter changes. Finally, logistic regression was carried out to investigate which parameters significantly correlated with the presence of ipsilateral hemispheric symptoms. Two-tailed values of significance were used and p-values less than 0.05 were considered to be statistically significant.
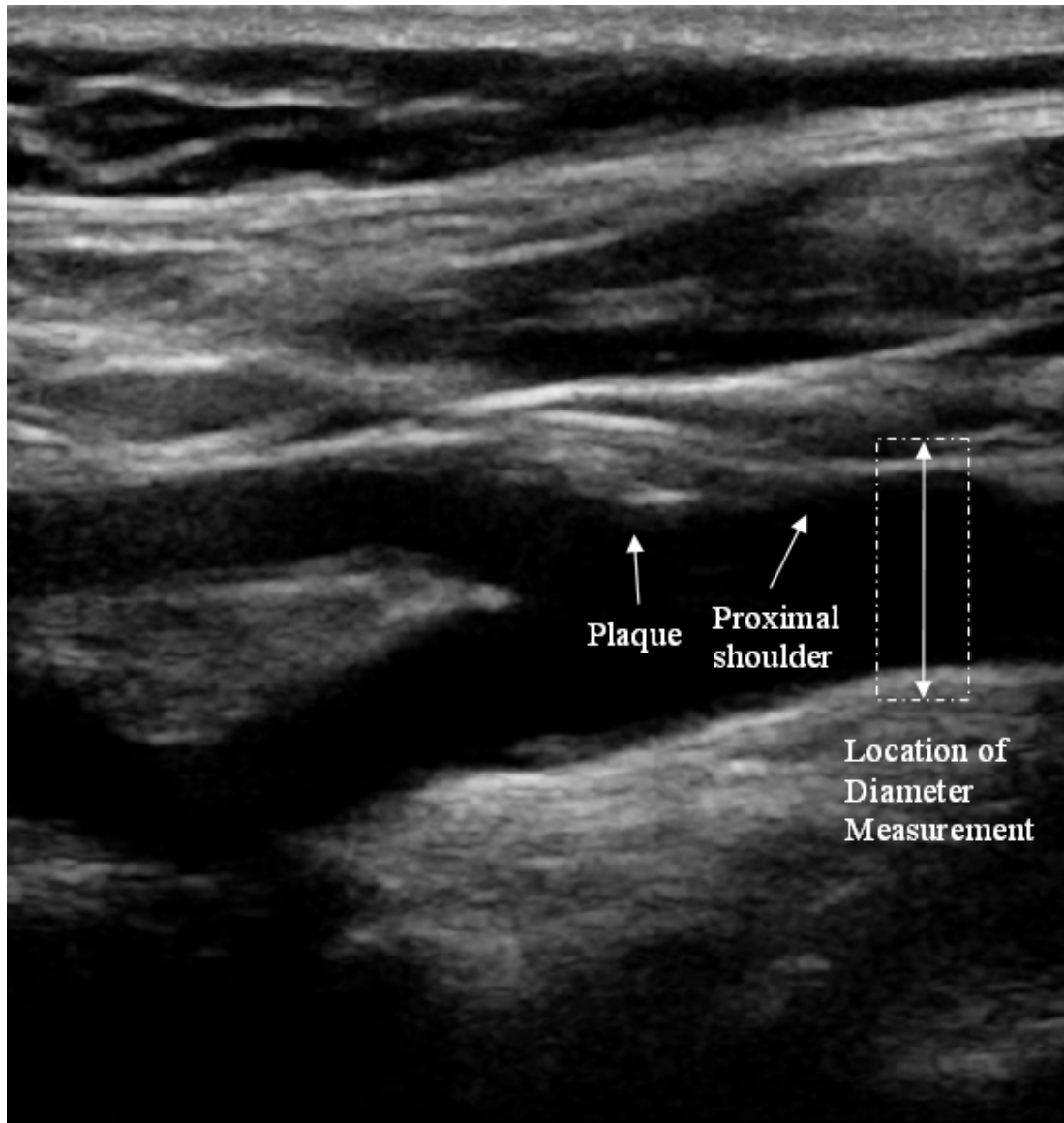
**Figure 5.2** - A carotid bifurcation plaque and illustration of the location of the diameter measurements. In this case, the plaque appears at the carotid bulb, and diameter measurements are taken in the distal common carotid artery immediately before the proximal shoulder of the plaque.

### 5.3.4 Reproducibility

In order to assess the reproducibility of the arterial wall motion detection technique used, we investigated the intra-observer coefficients of variation for the measurement

of the systolic/diastolic diameters, and absolute/percentage diameter changes for 10 arteries. This subset of arteries was selected from the available dataset to give a wide range of stenosis severity, plaque echogenicity and arterial diameters for reproducibility analysis. The measurements were made by the same operator and in sequential order. The same ultrasound acquisition sequences were used for each artery respectively.

## 5.3.5 Comparison against manual measurements

Arterial diameter measurements made using our method were compared against diameter measurements made manually by placing cursors on the ultrasound images and measuring the distances between the near and far walls of the arteries. This was done using a computer program with a graphical user interface written in MATLAB version 7.14, release 2012a (MathWorks, Natick, Massachusetts, USA). Using the same arteries selected for our reproducibility analysis, we manually measured arterial diameters at the same location and on matching image frames as for the automated technique. Approximately 30 diameter measurements per artery spread over the cardiac cycles were compared between the two techniques. Arterial diameters obtained using the manual method were compared with those obtained using the automated technique using Bland-Altman and linear regression analysis.

## 5.4 Results

Mean age was 77.3 years (range 58-95 years); 19 female. The prevalence of cerebrovascular risk factors was: 76% hypertension, 53% hypercholesterolaemia, 33% ischaemic heart disease, 29% diabetes mellitus, 47% previous TIA/stroke, 64% smoking, 44% alcohol consumption and 33% family history of stroke. Thirty one of the 61 arteries studied were found to be associated with ipsilateral hemispheric symptoms, while the remaining 30 were found to be asymptomatic following expert specialist stroke physician assessment.

The mean percentage systolic dilation of the symptomatic arteries (6.6%) was lower than that of the asymptomatic arteries (7.2%), but this difference was not statistically

significant (p=0.16, Figure 5.3). ANCOVA, controlling for the effects of the diastolic diameters, also found the same difference to be not statistically significant (p=0.14). Arteries with ipsilateral hemispheric symptoms also had lower absolute diameter changes on average (0.42 mm) than asymptomatic arteries (0.47 mm) but this difference was also not significant (p=0.17, Figure 5.3). The degree of stenosis (p<0.01), normalized plaque GSM (p=0.021) and the plaque surface irregularity index (p=0.016) differed significantly between the symptomatic and asymptomatic groups while the un-normalized plaque GSM (p=0.14) did not.
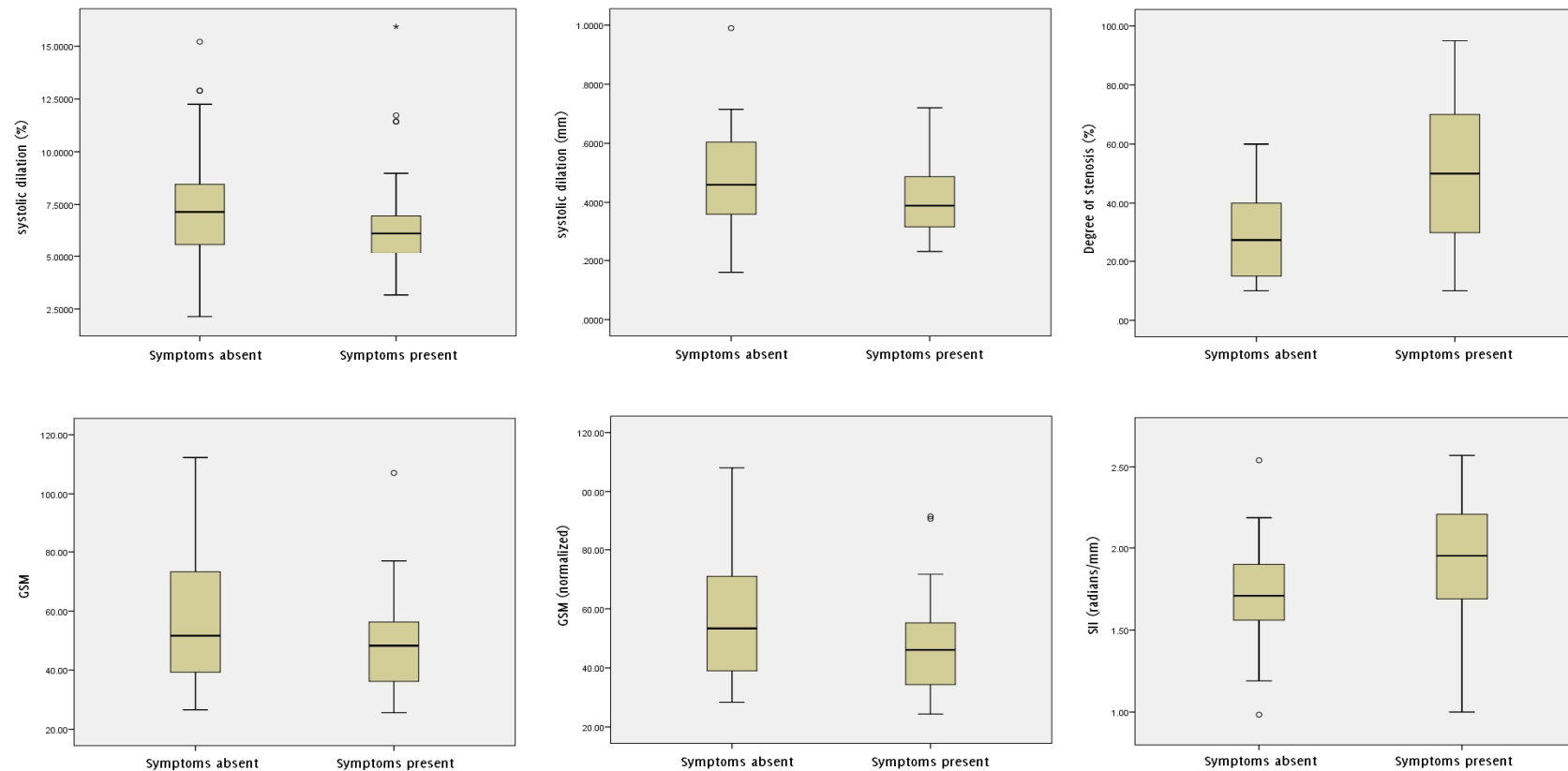
**Figure 5.3 -** Box and whisker plots showing the distribution, versus the presence of ipsilateral hemispheric symptoms, of the absolute and percentage arterial diameter changes, degree of stenosis, normalized and un-normalized plaque GSM, and the surface irregularity index (SII).
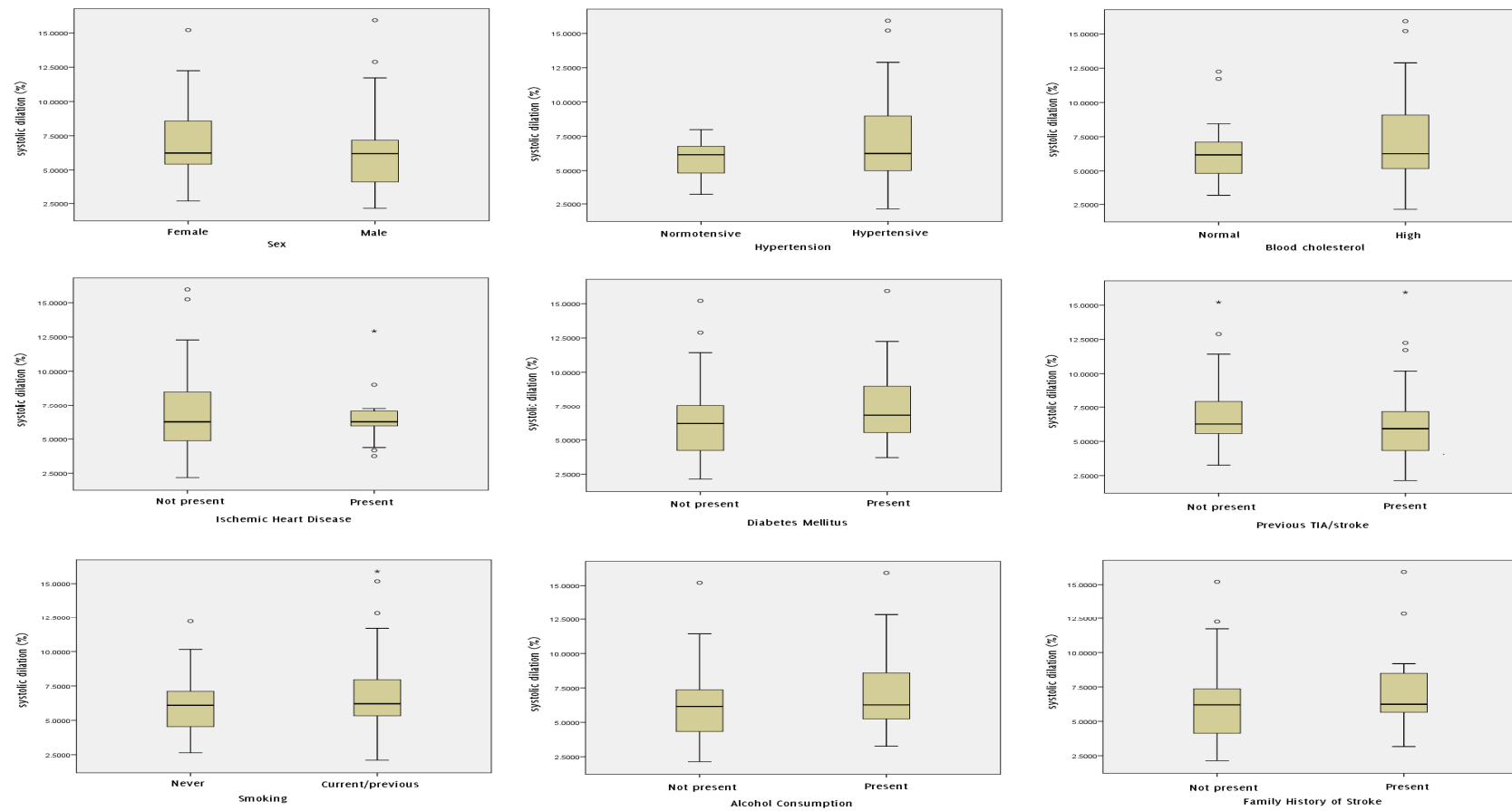
**Figure 5.4 -** Box and whisker plots showing the distribution of the percentage systolic diameter changes versus patient characteristics.

The patient characteristics age, sex, hypertension, high cholesterol, ischaemic heart disease, diabetes mellitus, previous TIA/stroke, smoking, alcohol consumption, and family history of stroke did not show significant differences in the percentage and absolute systolic dilation of the arteries (Table 5.1, Figure 5.4, Figure 5.5). There were no statistically significant correlations between the percentage systolic dilation of arteries and the degree of stenosis (p=0.82), patient age (p=0.14), un-normalized plaque GSM (p=0.29), normalized plaque GSM (p=0.34) or the plaque surface irregularity index (p=0.54, Figure 5.6). Partial correlations, adjusting for the effects of the baseline diastolic diameters, also found no statistically significant relationship between the percentage systolic dilation of the arteries and the degree of stenosis, patient age, or the greyscale plaque characteristics (p>0.05 for all). Absolute diameter changes were also not significantly correlated with the degrees of stenosis (p=0.70), patient age (p=0.68), un-normalized plaque GSM (p=0.78), normalized plaque GSM (p=0.69) or the plaque surface irregularity index (p=0.90, Figure 5.6).

Logistic regression testing found only the degree of stenosis, normalized plaque GSM and the surface irregularity index to be significant predictors of the presence of ipsilateral hemispheric symptoms (Table 5.2). The un-normalized plaque GSM was not found to have a significant correlation to symptoms.

Our assessment of reproducibility showed mean intra-observer coefficients of variation of 1.0%, 1.2%, 11.7%, and 12.4% for the measurement of the systolic diameters, diastolic diameters, absolute systolic diameter changes, and percentage diameter changes, respectively. Comparison against manual measurements showed a mean difference in diameter measurements between the two techniques of -0.016 mm (Figure 5.7) which did not differ significantly from zero (p=0.06, t-test). The 95% limits of agreement were -0.29 mm to 0.26 mm. Linear regression analysis showed a strong correlation between the measurements made using the two methods ($R^2$=0.97, Figure 5.8).
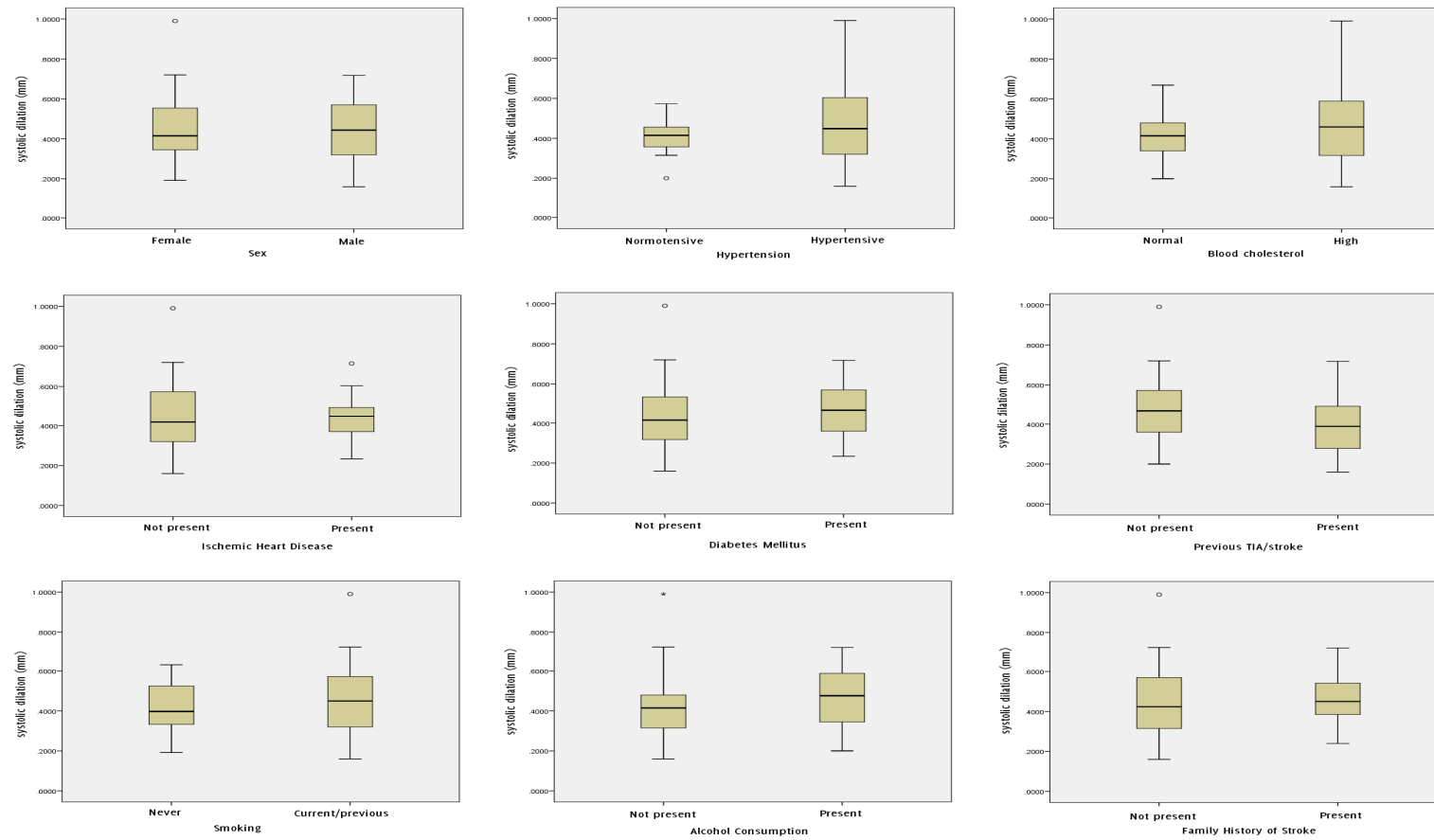
**Figure 5.5 -** Box and whiskers plots showing the distribution of the absolute systolic diameter changes versus patient characteristics.
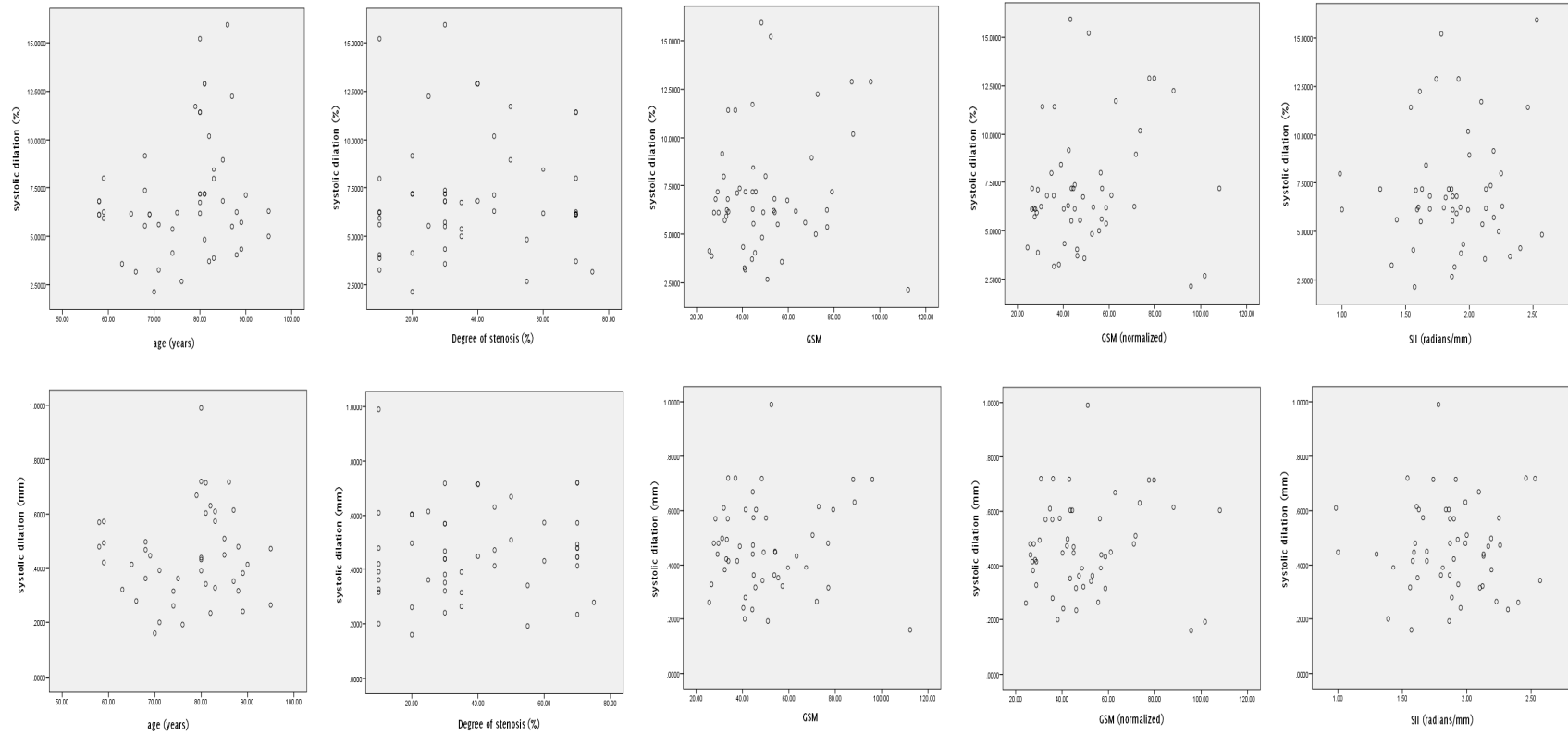
**Figure 5.6 -** Scatter plots of the absolute and percentage systolic diameter changes versus patient age, degree of stenosis, unnormalized and normalized plaque GSM, and the plaque surface irregularity index (SII), illustrating a lack of association between the absolute and percentage systolic dilation of arteries and any of these parameters.
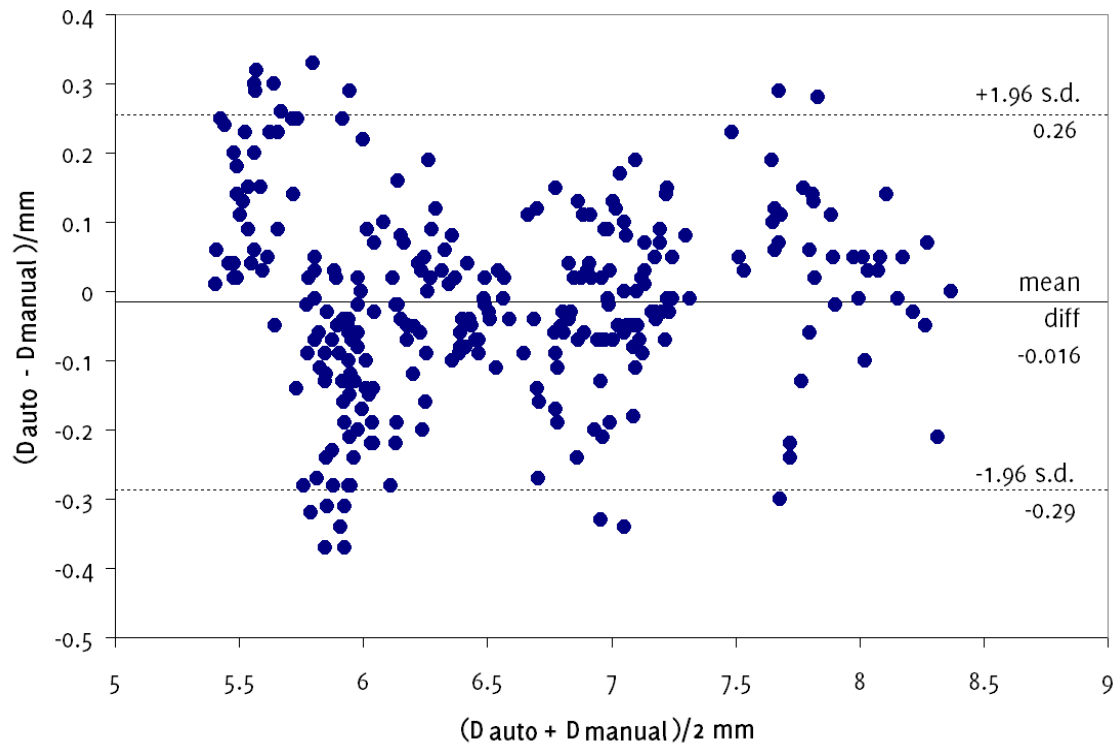
**Figure 5.7 -** Bland-Altman plot showing the differences in arterial diameters, on matching image frames, measured manually ($D_{manual}$) and using our method ($D_{auto}$).

**Table 5.1 -** Non-parametric Wilcoxon-Mann-Whitney associations between the absolute and percentage systolic diameter changes before the proximal shoulder of the atherosclerotic plaque and patient characteristics. Age was dichotomized using the median of the dataset as a cut-off value.

| Patient Characteristic | Significance (p-value) | |
|---|---|---|
| | Absolute Diameter Change | Percentage Diameter Change |
| Age | 0.44 | 0.33 |
| Sex | 0.96 | 0.68 |
| Hypertension | 0.45 | 0.34 |

| Patient Characteristic | Significance (p-value) | |
|---|---|---|
| | Absolute Diameter Change | Percentage Diameter Change |
| Hypercholesterolaemia | 0.54 | 0.41 |
| Ischaemic Heart Disease | 0.94 | 0.90 |
| Diabetes Mellitus | 0.31 | 0.28 |
| Previous TIA/stroke | 0.16 | 0.32 |
| Smoking | 0.34 | 0.49 |
| Alcohol | 0.29 | 0.47 |
| Family history of stroke | 0.35 | 0.41 |
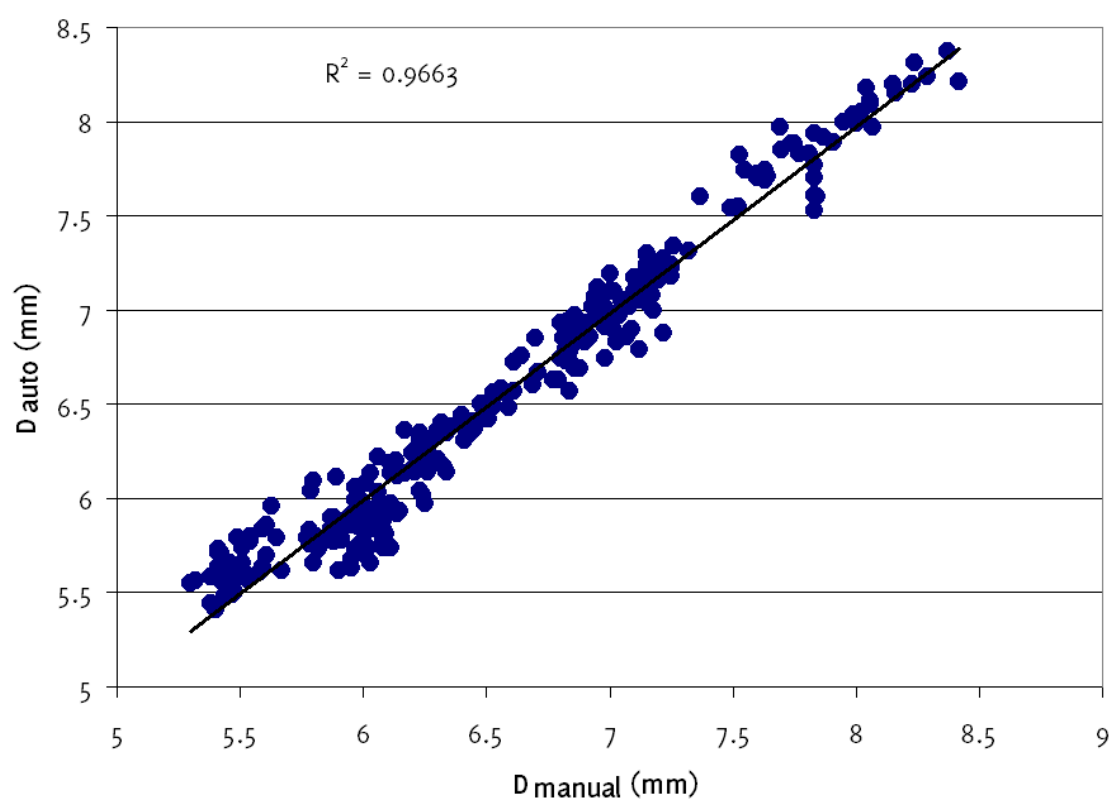


**Figure 5.8** - Scatter plot showing a strong linear relationship between arterial diameters measured manually ($D_{manual}$) and using our method ($D_{auto}$).

**Table 5.2 -** Logistic regression testing for any association between the presence of ipsilateral hemispheric symptoms and the degree of stenosis, greyscale plaque characteristics and the absolute and percentage dilation of the arteries. Significant associations are marked with an asterisk (*).

| Parameter | Significance (p-value) |
|---|---|
| Degree of stenosis | 0.01* |
| Percentage systolic diameter change | 0.20 |
| Absolute systolic diameter change | 0.10 |
| GSM | 0.09 |
| GSM (normalized) | 0.02* |
| SII | 0.02* |

## 5.5 Discussion

This chapter provides new data on wall motion in atherosclerotic carotid arteries and the association with cerebrovascular symptoms, the degree of stenosis, and greyscale plaque characteristics. These data may also be useful for informing computational models of carotid stenosis [280] and experimental phantom replicas [281-282], especially considering the scarcity of distension measurements immediately before the proximal shoulder of the carotid plaque.

One motivation for our study was the plausibility of a relationship between the diastolic to systolic dilation of the carotid artery and the presence of cerebrovascular symptoms, since changes in arterial wall motion behaviour may be indicative of vascular disease and aging, both of which are risk factors for stroke [268-269,283]. However, our study found no significant relationship between the absolute and percentage dilation of the carotid artery before the proximal shoulder of the atherosclerotic plaque and the presence of cerebrovascular symptoms. Diameter changes were also not significantly correlated with the degree of stenosis, in accordance with our previous findings [97].

Arteries which have greater amounts of wall motion may increase plaque vulnerability due to mechanical factors [272-274]. Therefore, with progressive atherosclerotic disease, while the risk of stroke may be raised on a systemic level, a reduction in the amount of arterial wall motion may result in a lower risk of plaque rupture from a mechanical perspective. These considerations complicate the relationship between the dilation characteristics of the carotid artery before the proximal shoulder of the atherosclerotic plaque and the presence of cerebrovascular symptoms, and are likely to be factors that contribute to the absence of a difference in the carotid artery dilations of the symptomatic and asymptomatic patients found in this study.

Arterial lumen diameters measured using our technique were found to be comparable to those measured using a manual method. Our study found good reproducibility for the measurement of the diastolic and systolic diameters but lower reproducibility for the measurement of the absolute and percentage diameter changes. These results are in accordance with previous studies which found derived parameters combining the systolic and diastolic arterial diameters to be considerably less reproducible than the diameter readings on their own [284-285]. It has been reported that even a small variance in arterial diameter measurements may cause a considerable variance in the derived metrics of carotid distension, therefore limiting its potential usability in the clinical setting [285]. Godia et al. attributed the different and sometimes conflicting results reported on the association between carotid distension and cardiovascular outcomes to this variability [285]. In the present study, the greater variabilities associated with absolute and percentage diameter changes may be additional factors contributing to the absence of a difference found in the carotid artery dilations of symptomatic and asymptomatic patients. Studies incorporating larger datasets or more precise methods may be able to find such a difference.

The statistically significant relationship between the presence of ipsilateral hemispheric symptoms and both the normalized plaque GSM and the surface irregularity index confirm our previous findings [238,243]. Interestingly, the un-normalized plaque GSM was not found to be a significant predictor of symptoms. This may be indicative of variations in overall image brightness, due to differences in

ultrasound gain settings or tissue attenuation, and highlights the importance of the normalization procedure for GSM measurements.

A limitation of this study is that we did not have pulse pressure measurements which would have allowed us to quantify arterial distensibility. However, this study focussed on motion aspects rather than stiffness and is part of our broader research aim to develop and define a plaque risk index based on ultrasound measurements. Previously, we have quantified greyscale plaque characteristics such as the plaque GSM and surface irregularities [238,243] as possible indicators of vulnerable plaques and the present study was conducted to investigate the potential of dilation characteristics before the proximal plaque shoulder as an additional parameter to include in a prospective vulnerable plaque-stroke risk model. In this study we did not perform measurements across the plaque to assess any differential wall motion between the plaque and the proximal carotid segment. Our previous study using Tissue Doppler Imaging (TDI) demonstrated a variety of pertinent wall motion features across the plaque site that may be related to the biophysics of arterial disease. However, high variability demonstrated the limitations of arterial wall motion measurements across the plaque, in contrast to more robust measurements that can be performed on well defined segments of vessels [97].

## 5.6 Conclusions

In this chapter we investigated the systolic dilation of stenosed carotid arteries measured before the proximal shoulder of the atherosclerotic plaque. Absolute and percentage diameter changes were lower for the arteries of patients with ipsilateral hemispheric symptoms, but these differences were not statistically significant. Normalized plaque GSM and our novel surface irregularity index were found to be significant predictors of symptoms.

# Chapter 6

# Quantitative Assessment of Plaque Motion in the Carotid Arteries using B-Mode Ultrasound

## 6.1 Overview

This chapter describes a quantitative assessment of carotid artery plaque motion using B-Mode ultrasound. It contributes to knowledge by extending the study of plaque motion to a wider range of stenosis severity (10-95%), compared with the existing literature, and investigating the physical accelerations of plaques. Motion of 81 carotid artery plaques from 51 patients were investigated, relative to the ultrasound probe and relative to the tissues directly underlying the plaque. An *in vitro* study was also carried out, assessing the motion of a test object, comprising tissue mimicking materials, controlled by a programmable actuator device. The latter study validated the motion assessment and demonstrated a lack of motion detection below a displacement of 50 μm, and greater measurement error in the range 50 to 100 μm, compared with the range 200 to 500 μm.

## 6.2 Introduction

Ultrasound imaging is routinely used to assess atherosclerotic plaques in the carotid arteries. Although the processes increasing plaque vulnerability are not fully understood, it is thought that physical motion due to blood flow may play a part, contributing to plaque rupture and subsequent thromboembolisation [60-61,286-287]. Plaque motion [61,197-198,200] and plaque strain [37,93-94] due to blood flow have been previously studied, though the literature is relatively scarce [272]. Previous studies of plaque motion using ultrasound have employed both qualitative and quantitative methods, and some studies reported motion analysis to be potentially useful for identifying the vulnerable carotid plaque [61,185,197-198,200,273-274,288-290]. Although there have been attempts to improve tracking accuracy by using refined methods such as adaptive block matching, sub-pixel interpolation, optical flow and the use of radiofrequency ultrasound data, the limitations arising from the restricted

spatial resolution of the imaging system have been largely overlooked [197,289]. Poor reproducibility has been reported before [201], but the extent to which this may be due to the motion magnitudes being lower than those that can be resolved by ultrasound imaging equipment needs further investigation. This chapter explores carotid plaque motion relative to the ultrasound probe (bulk motion) and relative to the tissues directly underlying the plaque (discrepant motion), investigating any relationships between the motion parameters and the degree of stenosis, greyscale plaque characteristics, and the presence of cerebrovascular symptoms.

## 6.3 Methods

Fifty one patients (61% male, age range 58-95 years) who attended the University Hospitals of Leicester NHS Trust's Rapid Access Transient Ischaemic Attack (TIA) clinic were recruited for this study. The study was approved by the National Research Ethics Service (NRES) Committee East Midlands - Northampton (reference 11/EM/0249) and followed institutional guidelines. Patients gave written, informed consent before participating in the study. Ultrasound image sequences of the carotid plaque in longitudinal cross-section were acquired by experienced sonographers using a Philips iU22 ultrasound scanner (Philips Healthcare, Eindhoven, The Netherlands) and an L9-3 probe. B-Mode (greyscale) image sequences were recorded as DICOM files over an average duration of 5.6 seconds (mean frame rate was 32 frames per second) using the vascular carotid preset on the scanner (Vasc Car preset, persistence low, XRES and SONOCT on). Motion analysis was carried out for 81 plaques (stenosis range 10-95%). Each plaque was classified as either having caused cerebrovascular symptoms relating to the ipsilateral brain hemisphere within the past six-month period (i.e. symptomatic) or as asymptomatic following specialist medical review.

### 6.3.1 *In Vitro* Study

Laboratory experiments were carried out using an actuator device that generated programmable and repeatable periodic displacements of a tissue mimicking material (TMM). The specifications of this precision lead-screw-based linear actuator (T-LA-28S, Zaber Technologies Inc, Richmond, British Columbia, Canada) indicated a typical linear displacement accuracy of 8 μm and a precision of 0.3 μm. The actuator movement was

controlled by a desktop computer through the RS-232 interface and was programmed to produce a more rapid displacement of the posterior wall away from the probe (downward) compared to the displacement towards to probe (upward) in order to mimic the rapid dilation of the carotid artery during systole compared to the less rapid relaxation during diastole [266]. The actuator moved a 4 cm diameter Perspex plate cut-out that formed part of the bottom of a water tank. The bottom was covered with a watertight latex membrane sealed with silicone, which allowed vertical movement of the Perspex plate by the actuator. A test object made of a rectangular block of TMM was placed on the Perspex plate and used for motion analysis. The TMM used was an agar-based formulation, which had good acoustic properties and met the requirements of the IEC 1685 draft report [291-292]. The composition (by weight) was 82.97% water, 11.21% glycerol, 0.46% benzalkoniumchloride, 0.53% SiC powder (400 grain, Logitec Ltd., Glasgow, UK), 0.94% Al2O3 powder (3 µm, Logitec), 0.88% Al2O3 powder (0.3 µm, Logitec), and 3.00% agar (Merck Eurolab). The TMM was prepared by heating the ingredients to $96^{o}C$ ($\pm 3^{o}C$) for 1 hour using a double boiler whilst stirring continuously with a motorised stirrer. The mixture was then allowed to cool down to $42^{o}C$ and cast into shape. DICOM image sequences were recorded with the actuator set to produce maximum displacements of 5, 10, 20, 50, 100, 200 and 500 µm (Figure 6.1).

## 6.3.2 Quantitative Analysis

Quantitative analyses were carried out using MATLAB version 7.14 (MathWorks, Natick, Massachusetts, USA) and SPSS version 20 (IBM Corporation, Armonk, New York, USA). The degree of carotid artery stenosis (DOS) was measured using criteria consistent with the NASCET method utilizing blood flow velocities in conjunction with the B-Mode and colour flow imaging [38,47,240]. Normalized plaque greyscale median (GSM) and surface irregularity index (SII) were measured using previously described methods [238,243] and were averaged over all the ultrasound image frames acquired for each artery.
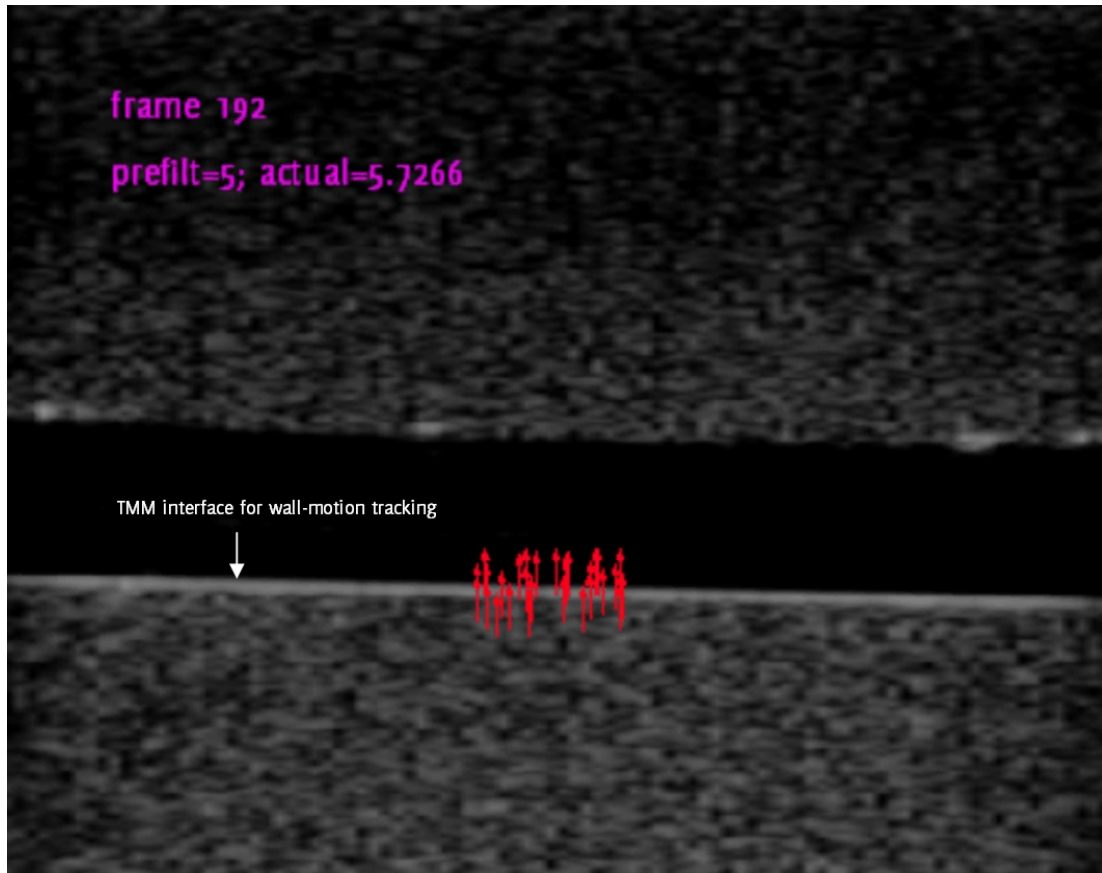
**Figure 6.1** - A still frame from an image sequence of the tissue mimicking material (TMM) with the actuator set to produce a maximum of 500 μm displacement from the initial position. Red arrows show the local TMM displacement at time t relative to the position at frame 1, magnified by a factor of 10. White arrow shows the TMM interface used for wall motion tracking (section 6.3.3).

### 6.3.3 Motion Tracking

Motion tracking was performed using a standard block matching technique with the normalized correlation coefficient as the similarity measure [238]. Several points were manually selected in the first frame of the image sequence at an approximate, uniform grid spacing of 1/2 mm to cover the whole plaque body (or a 1 mm thickness of the tissue in the case of the region of interest directly underlying the plaque) and tracked in the successive image frames by maximizing the values of the normalized correlation

coefficients (Figure 6.2). Template sizes from 20x20 mm$^2$ down to 6x6 mm$^2$ were iteratively searched in decrements of 1x1 mm$^2$ to further maximize the correlation coefficients. Templates sizes smaller than 6x6 mm$^2$ often caused erroneous tracking and were therefore not used. An adaptive block matching technique whereby the individual templates were updated with new ones at every frame was also investigated, but this caused a drift in motion tracking and was not utilized further.

The individual points describing the motion of the plaque and the underlying tissues were separately averaged, resulting in two motion trajectories: one for the plaque ($r_{plaque}$) and one for the underlying tissues ($r_{tissue}$). Motion of the plaque relative to the underlying tissues ($r_{rel}$) was calculated by transforming $r_{plaque}$ to a reference frame the origin of which moved according to $r_{tissue}$. Maximum displacement was calculated as the furthest distance between any two points assessed over all possible pairs of points on a given trajectory. Velocity and acceleration were determined as the first and second numerical derivatives, respectively, of the motion trajectories using the central difference method (gradient function in MATLAB). Reproducibility was assessed by measuring each motion parameter five times for ten plaques, and determining the intra-observer coefficients of variation. In the case of the *in vitro* analysis, motion parameters obtained using the present technique were compared against those obtained using a previously described arterial wall motion assessment method, which tracked the tissue mimicking material interface (Figure 6.1) [217,231].

## 6.3.4 Statistical Methods

The non-parametric Wilcoxon-Mann-Whitney test was used to determine whether motion parameters differed significantly between plaques that were or were not associated with symptoms. Multivariate logistic regressions, one for the motion parameters relative to the ultrasound probe, and one for the motion parameters relative to the tissues directly underlying the plaque, were further employed to assess whether any of the motion parameters were significant predictors of symptoms. Bivariate correlations between the motion parameters and the degree of stenosis, plaque greyscale median and the surface irregularity index were determined using

Spearman's rank correlation coefficient. In all cases, two-tailed p-values less than 0.05 were considered statistically significant.

## 6.4 Results

Motion analysis was successful for 66 plaques (81%) but unsuccessful for 15 (19%). The causes of motion tracking failure were speckle decorrelation (13 plaques), and ultrasonic shadowing (2 plaques). The mean normalized correlation coefficient was 0.95 for the plaques for which motion tracking was successful. Figure 6.2 shows an example of a plaque with successful motion tracking, while Figure 6.3 shows the calculated motion parameters for the same plaque, relative to the ultrasound probe. Cardiac cycles are clearly visible in the plots showing the horizontal and vertical components of plaque position; they are also visible, albeit less clearly, in the plots showing the velocity and acceleration of the plaque. The peaks in the plot showing the plaque acceleration are seen to broadly correspond to the peaks and troughs of the plots showing the horizontal and vertical components of plaque position.

The mean values across all plaques of the motion parameters relative to the probe and the underlying tissues were as shown in Table 6.1 and Table 6.2. For the motion relative to the underlying tissues, average displacement magnitude was low (less than 0.4 mm) and the differences between the symptomatic and asymptomatic groups were not statistically significant (Table 6.2 and Figure 6.4). In the case of the motion of the plaque relative to the probe, the average displacement magnitude was much larger ($>1$ mm) but the differences between the symptomatic and asymptomatic groups were also not statistically significant (Table 6.1 and Figure 6.4). Logistic regression testing further confirmed that none of the motion parameters, either relative to the ultrasound probe or relative to the tissues directly underlying the plaque, were significant predictors of the presence of cerebrovascular symptoms ($p>0.05$). There was no statistically significant association between any of the motion parameters and the degree of stenosis, or the greyscale plaque characteristics (Table 6.3 and Table 6.4).

Measurement reproducibility was good for parameters representing the motion of the plaque relative to the probe (COV < 10%); it was better for mean plaque velocity and

mean plaque acceleration (COV < 5%), than for maximum plaque displacement, maximum plaque velocity, and maximum plaque acceleration (COV >= 5%, Table 6.5). In the case of the motion of the plaque relative to the tissues directly underlying the plaque, reproducibility was poorer for all motion parameters (COV > 15%). *In vitro* assessment showed that motion was not detected below a set displacement of 50 μm, while accuracy was low in the range 50 to 100 μm (Table 6.6). Figure 6.5 and Figure 6.6 show the calculated motion parameters for the case where the actuator was set to produce maximum displacements of 500 and 200 μm, respectively. Periodic, downward displacements of 476 and 188 μm are seen in Figure 6.5 and Figure 6.6, respectively, with a small horizontal motion component in the case of Figure 6.5. In agreement with the programming of the actuator, velocity and acceleration were found to be greater when the motion was away from the ultrasound probe (increasing y values) compared to towards to probe (decreasing y values, Figure 6.5).

**Table 6.1** - Mean values, across plaques, of the motion parameters relative to the ultrasound probe.

| | Max displacement (mm) | Max velocity (mm/s) | Mean velocity (mm/s) | Max acceleration (mm/s$^2$) | Mean acceleration (mm/s$^2$) |
|---|---|---|---|---|---|
| **All plaques** | 1.24 | 4.71 | 1.34 | 69.1 | 21.8 |
| **Symptomatic** | 1.19 | 4.03 | 1.27 | 57.7 | 20.4 |
| **Asymptomatic** | 1.30 | 5.50 | 1.42 | 82.3 | 23.3 |
| **Significance (p-value)** | 0.92 | 0.30 | 0.76 | 0.05 | 0.51 |

**Table 6.2** - Mean values, across plaques, of the motion parameters relative to the underlying tissues.

|  | Max displacement (mm) | Max velocity (mm/s) | Mean velocity (mm/s) | Max acceleration (mm/s$^2$) | Mean acceleration (mm/s$^2$) |
|---|---|---|---|---|---|
| All plaques | 0.35 | 2.38 | 0.70 | 56.6 | 17.6 |
| Symptomatic | 0.35 | 2.29 | 0.67 | 54.7 | 16.8 |
| Asymptomatic | 0.35 | 2.49 | 0.72 | 58.9 | 18.5 |
| Significance (p-value) | **0.67** | **0.82** | **0.67** | **0.65** | **0.26** |

**Table 6.3** - Significance of association (p-values) between motion parameters relative to the ultrasound probe, the degree of stenosis (DOS), plaque greyscale median (GSM) and the surface irregularity index (SII).

|  | Max displacement | Max velocity | Mean velocity | Max acceleration | Mean acceleration |
|---|---|---|---|---|---|
| DOS | 0.62 | 0.65 | 0.54 | 0.29 | 0.71 |
| GSM | 0.57 | 0.52 | 0.92 | 0.55 | 0.95 |
| SII | 0.18 | 0.13 | 0.07 | 0.33 | 0.13 |

**Table 6.4** - Significance of association (p-values) between motion parameters relative to the underlying tissues, the degree of stenosis (DOS), plaque greyscale median (GSM) and the surface irregularity index (SII).

|  | Max displacement | Max velocity | Mean velocity | Max acceleration | Mean acceleration |
|---|---|---|---|---|---|
| DOS | 0.09 | 0.13 | 0.19 | 0.58 | 0.92 |
| GSM | 0.27 | 0.47 | 0.89 | 0.18 | 0.58 |
| SII | 0.17 | 0.16 | 0.24 | 0.75 | 0.45 |

**Table 6.5** - Reproducibility of the motion parameters (intra-observer coefficients of variation).

| Relative to the ultrasound probe | Max displacement | 0.08 |
|---|---|---|
| | Max velocity | 0.07 |
| | Mean velocity | 0.02 |
| | Max acceleration | 0.05 |
| | Mean acceleration | 0.01 |
| Relative to the underlying tissues | Max displacement | 0.20 |
| | Max velocity | 0.16 |
| | Mean velocity | 0.19 |
| | Max acceleration | 0.16 |
| | Mean acceleration | 0.21 |

**Table 6.6** - *In vitro* assessment comparing the measured motion of the tissue mimicking material (TMM) with the set displacement of the actuator and the motion of the TMM-lumen interface measured using wall motion techniques [266].

| | Set displacement (µm) | 5 | 10 | 20 | 50 | 100 | 200 | 500 |
|---|---|---|---|---|---|---|---|---|
| Measured motion of the TMM wall | Max displacement (µm) | 7 | 15 | 26 | 53 | 105 | 201 | 503 |
| | Max velocity (mm/s) | 0.16 | 0.14 | 0.27 | 0.55 | 0.60 | 1.17 | 3.99 |
| | Mean velocity (mm/s) | 0.02 | 0.03 | 0.06 | 0.12 | 0.22 | 0.37 | 0.95 |
| | Max acceleration (mm/s²) | 3.3 | 2.4 | 4.2 | 8.0 | 8.1 | 14.7 | 47.4 |

| | Mean acceleration (mm/s²) | 0.50 | 0.76 | 1.25 | 2.0 | 2.3 | 3.5 | 11.0 |
|---|---|---|---|---|---|---|---|---|
| Measured motion of TMM | Max displacement (μm) [error] | 0 [100%] | 0 [100%] | 0 [100%] | 74 [48%] | 74 [26%] | 188 [6.0%] | 476 [4.8%] |
| | Max velocity (mm/s) | 0 | 0 | 0 | 1.3 | 1.2 | 1.26 | 4.9 |
| | Mean velocity (mm/s) | 0 | 0 | 0 | 0.16 | 0.16 | 0.34 | 0.91 |
| | Max acceleration (mm/s²) | 0 | 0 | 0 | 22.5 | 20.5 | 22.2 | 75.7 |
| | Mean acceleration (mm/s²) | 0 | 0 | 0 | 5.2 | 5.0 | 6.1 | 13.0 |
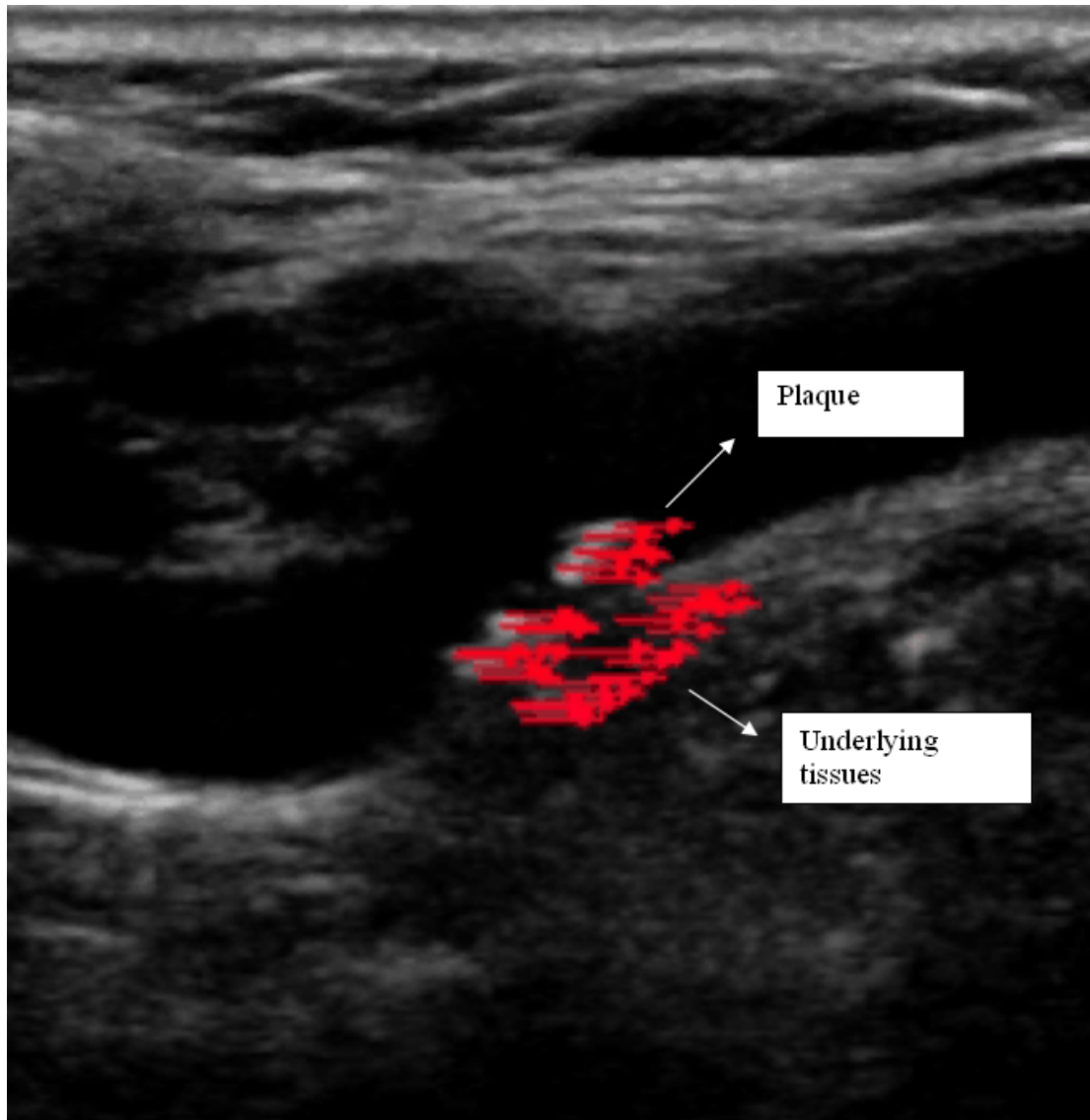
**Figure 6.2** - An example of a plaque and underlying tissues on the opposite sides of the posterior arterial wall at the carotid bulb, with motion tracking. Arrows show the local displacement at time t with respect to the position at frame 1, magnified by a factor of 10.
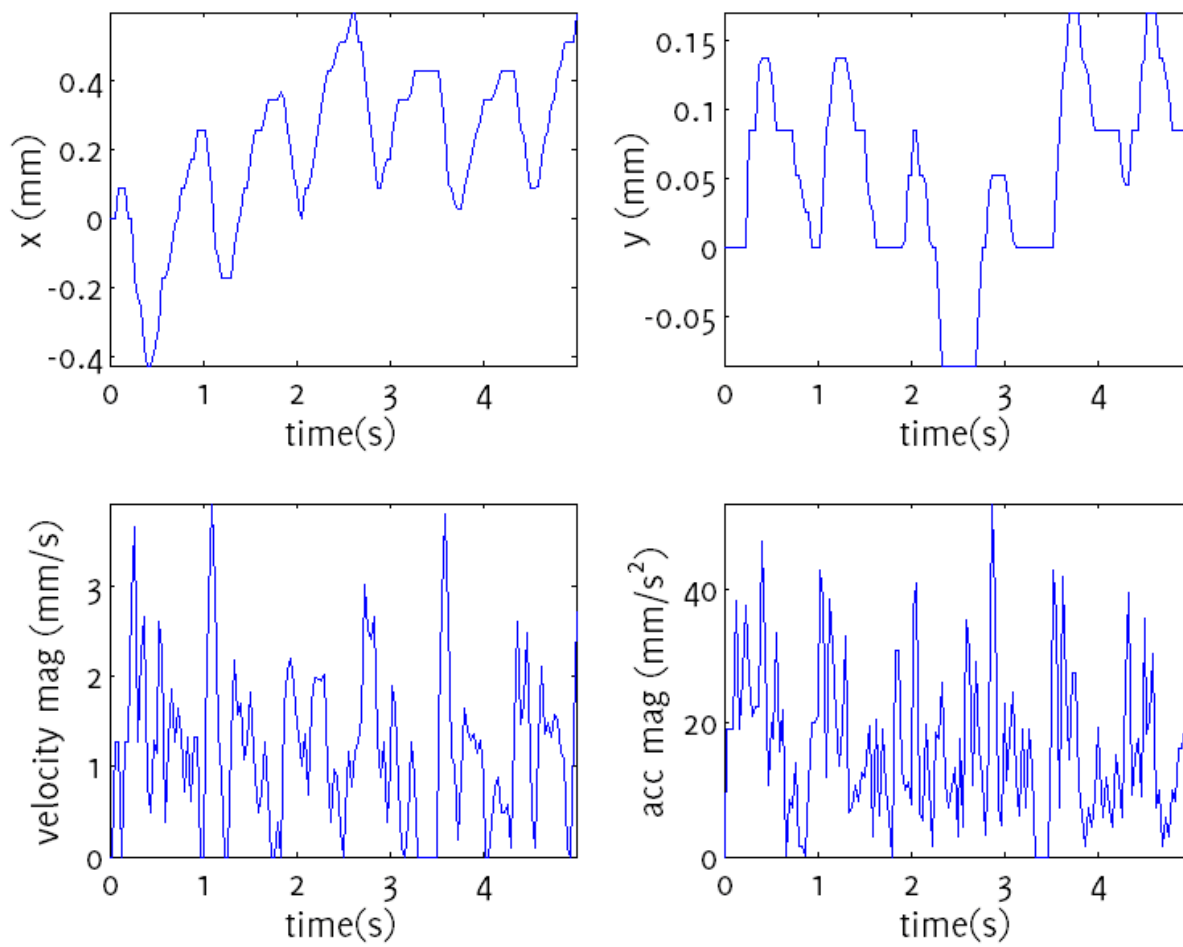
**Figure 6.3** - Calculated motion parameters, relative to the ultrasound probe, for the plaque sample shown in Figure 6.2. The horizontal and vertical components of plaque position are shown in the top-left and top-right plots, respectively. Velocity and acceleration magnitudes are shown in the plots at the bottom.
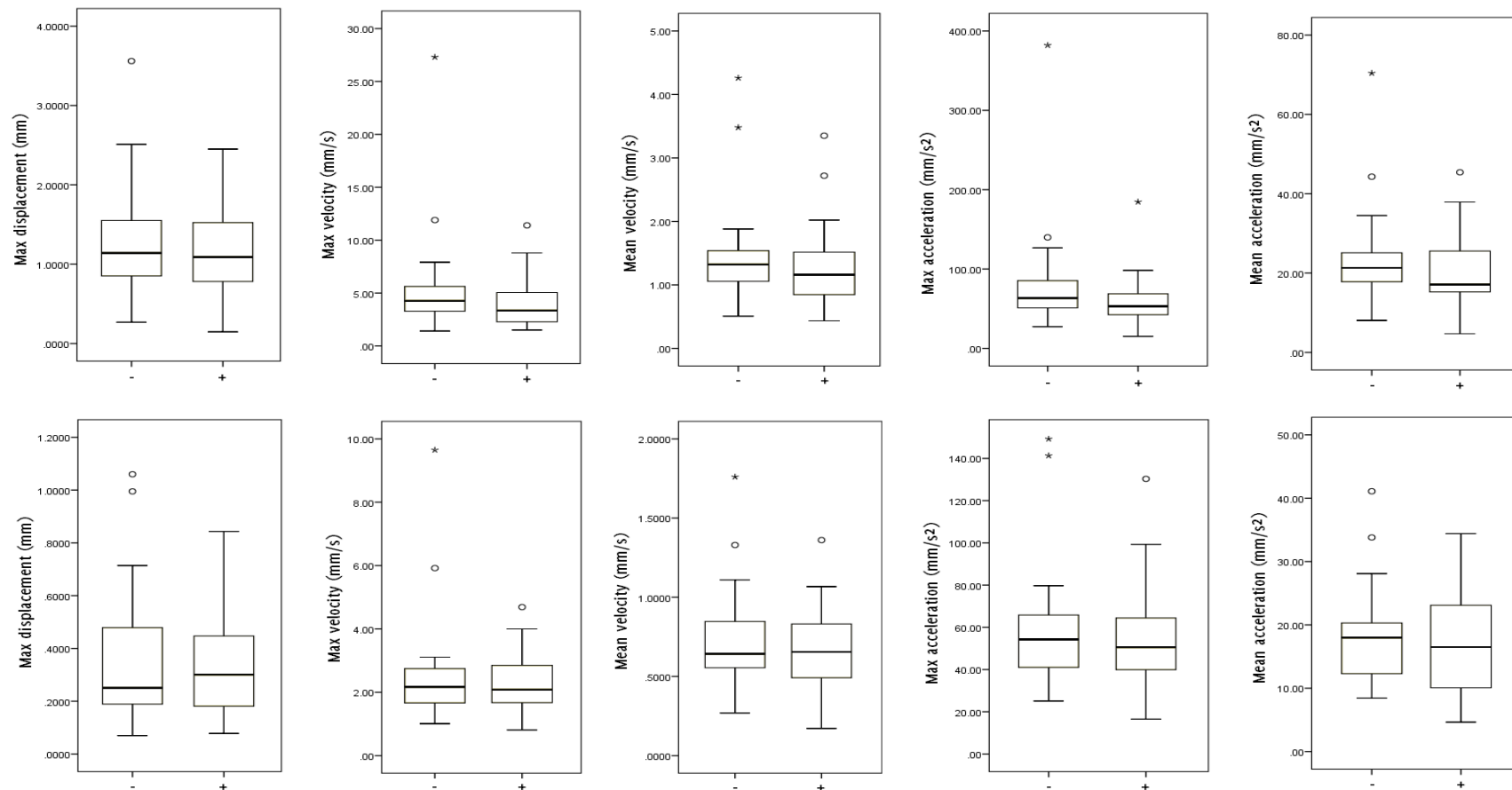
**Figure 6.4** - Box-whisker plots showing the distribution of the motion parameters (relative to the probe: top row, relative to the underlying tissues: bottom row) within the asymptomatic (marked -) and symptomatic (marked +) groups.
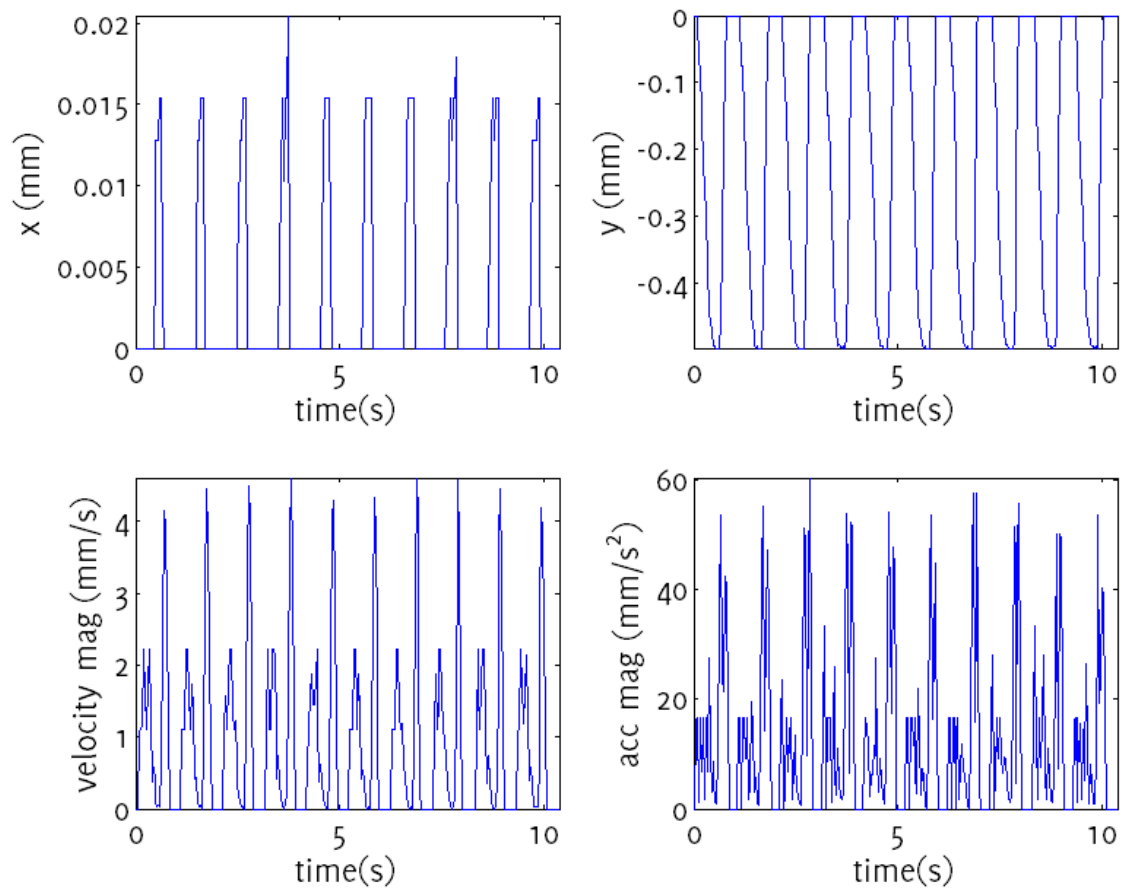
**Figure 6.5** - Calculated motion parameters for the *in vitro* study with the actuator set to produce a maximum displacement of 500 μm. The horizontal and vertical components of position are shown in the top-left and top-right plots, respectively. Velocity and acceleration magnitudes are shown in the plots at the bottom.
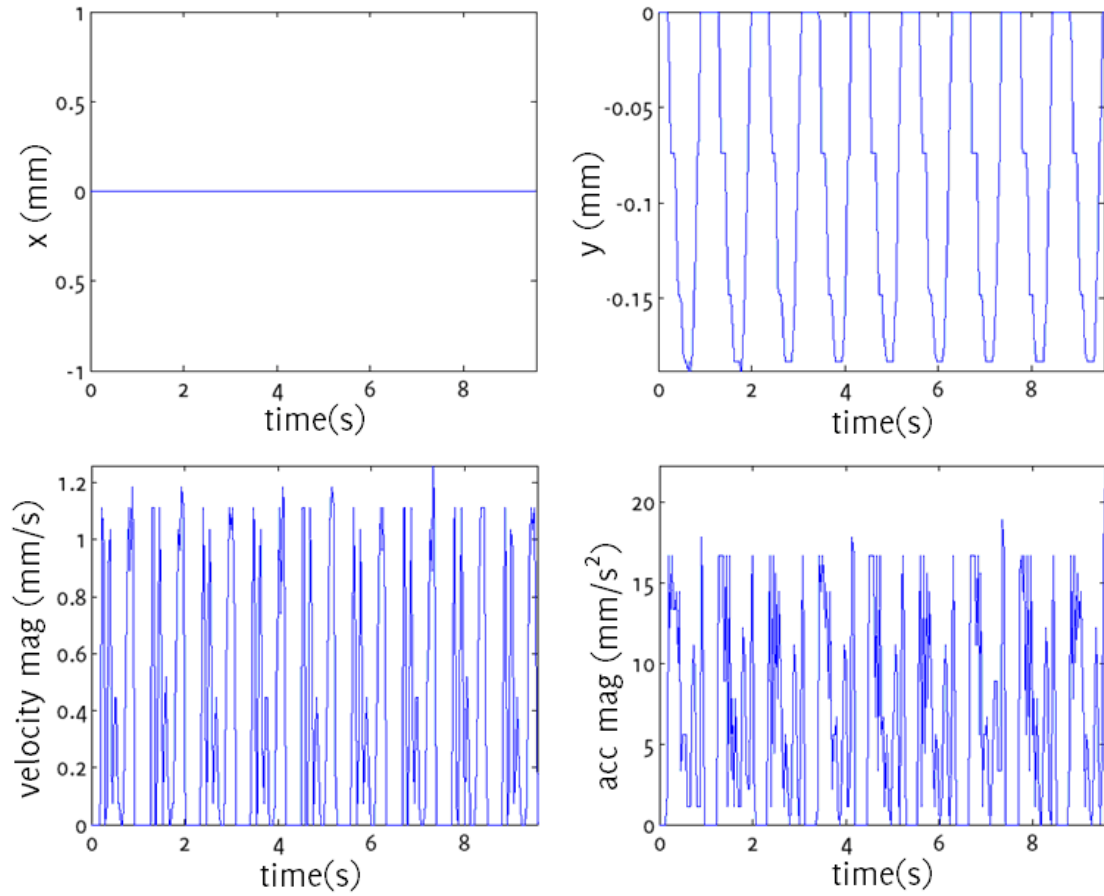
**Figure 6.6** - Calculated motion parameters for the *in vitro* study with the actuator set to produce a maximum displacement of 200 µm. The horizontal and vertical components of position are shown in the top-left and top-right plots, respectively. Velocity and acceleration magnitudes are shown in the plots at the bottom.

## 6.5 Discussion

This chapter investigated plaque motion using B-Mode ultrasound image sequences and contributes new data to the literature on typical plaque displacements, velocities and accelerations that may be encountered when the motion is measured relative to the ultrasound probe and relative to the tissues directly underlying the plaque. Plaque velocities relative to the ultrasound probe have been investigated before, and the results are in accordance with previous findings [197,200]. In relation to the

177

displacement of the plaque relative to the underlying tissues, the results showed motions generally smaller than the resolution of a typical modern ultrasound scanner ($\leq$1mm). From a clinical perspective, the rationale for carrying out this study was that those plaques experiencing larger amounts of motion might be more prone to rupture, and thus more likely to be symptomatic, due to tissue stresses that may be caused by motion. However, the results did not support this hypothesis. There were no significant differences in the motion parameters in relation to the presence of cerebrovascular symptoms, and no significant associations were found between plaque motion and the degree of carotid artery stenosis, or the greyscale plaque characteristics.

Several studies have previously investigated the motion of the atherosclerotic plaque. Chan's early work confirmed the existence of carotid plaque motion when patient or probe motion is taken into account [199]. However, this was a preliminary study looking at only two clinical image sequences at low frame rates, and did not establish the presence of any discrepant motion between the plaque and the underlying tissues. Iannuzzi *et al.* used a qualitative assessment scheme based on an apparent distal shift of the plaque axis, and found that longitudinal plaque motion was associated with ipsilateral brain involvement in transient ischaemic attack patients [61]. However, only a small percentage of the plaques (37%) were found to have longitudinal lesion motion in that study and the analysis was based on 18 plaques having longitudinal plaque motion in the artery ipsilateral to hemispheric damage, compared to 6 plaques which had longitudinal plaque motion in the artery contralateral to hemispheric damage. Other studies, on the other hand, reported that plaques from symptomatic patients had higher maximum discrepant surface velocities compared with plaques from asymptomatic patients [185,200]. Although the results of this chapter are not directly comparable with the results of these studies, since discrepant surface velocities were not studied in this chapter, this study affirms Dahl *et al.*'s finding that maximum velocity may be a parameter that has low reproducibility [201].

The spatial resolution of our imaging equipment was measured to be approximately 1 mm in the axial and lateral directions using a Cardiff Composite Test Object (Diagnostic

Sonar, Edinburgh, United Kingdom). Motion magnitudes as low as 50 μm could be detected using the method described in this chapter, due to the averaging of several block-matched points selected over the plaque body, thus providing sub-pixel resolution. Studies using radiofrequency ultrasound data, such as the one by Bang *et al*. benefit from the additional information provided by the phase of the radiofrequency signal [197], and improved methods of motion tracking, such as adaptive block matching [289], may increase motion tracking accuracy. However, in both radiofrequency studies and studies using improved methods of motion tracking, the intrinsic spatial resolution of the imaging system will still limit precision and accuracy. Therefore, spatial resolution of the imaging equipment needs to be considered in the analysis of plaque motion (i.e. motion magnitudes in comparison to the resolving power of the imaging system) and will determine the clinical applicability of motion assessment using B-Mode ultrasound. Increasing the frame rate of the ultrasound acquisition can help by reducing the amount of speckle decorrelation on a frame-by-frame basis. However, increased frame rates do not help overcome the limitations arising from the restricted, intrinsic spatial resolution of the imaging system.

No significant relationship was found between motion parameters and the presence of cerebrovascular symptoms in this investigation. Intra-plaque strain analysis [37,93-94] and methods assessing the mechanical properties of plaque such as Shearwave Elastography [293-294] may be suggested as future directions for research to help identify the vulnerable plaque.

## 6.6 Conclusions

The study of atherosclerotic plaque motion due to blood flow measured using B-Mode ultrasound found no significant differences in the motion parameters investigated, in relation to the presence of ipsilateral hemispheric cerebrovascular symptoms. Furthermore, no significant associations were found between the motion parameters and the degree of carotid artery stenosis or greyscale plaque characteristics.

# Chapter 7

# A Novel Ultrasound-Based Carotid Plaque Risk Index Associated with the Presence of Cerebrovascular Symptoms

## 7.1 Overview

This thesis has described several ultrasound-based plaque parameters that may help identify the vulnerable plaque. First and foremost, the degree of stenosis is an important measure used in clinical practice, and must be taken into account when other ultrasound parameters are used. However, it is uncertain how such additional parameters should be used in conjunction with the degree of carotid artery stenosis. Previous attempts to combine ultrasound plaque characteristics with the degree of stenosis either involved the introduction of risk indices based on a risk model with parameters optimised to the dataset under study, or the use of machine learning/classification algorithms to classify plaques. However, this has reduced applicability and hindered clinical adoption, since most ultrasound measures of plaques, including the degree of stenosis, are subject to variations across centres and methods of evaluation. This chapter introduces a novel ultrasound-based carotid plaque risk index (CPRI) incorporating the degree of stenosis, the normalized greyscale median, and the surface irregularity index, and shows that CPRI increases diagnostic accuracy compared to the degree of carotid artery stenosis alone, without the use of such optimised parameters.

## 7.2 Background

Clinical trials such as the North American Symptomatic Carotid Endarterectomy Trial (NASCET) and European Carotid Surgery Trial (ECST) have shown endarterectomy to be beneficial for symptomatic patients with severe carotid artery stenosis (i.e. 70-99%) [38-39,295]. However, the selection of patients for surgery is not optimal, and it is

suggested that approximately 70-75% of patients will not have a stroke if treated medically [296]. Some studies reported surgery to be of potential benefit also for patients with lower degrees of symptomatic stenosis [9,297]. In patients with carotid artery occlusion or near-occlusion, the benefit of carotid endarterectomy is marginal in the short-term and uncertain in the long-term [297]. Occlusions or near-occlusions, paradoxically, appear to be associated with a low risk of stroke when treated medically in both symptomatic and asymptomatic patients [298]. In the case of asymptomatic patients, while some studies such as the Asymptomatic Carotid Atherosclerosis Study (ACAS) and the Medical Research Council (MRC) Asymptomatic Carotid Surgery Trial (ACST) have shown that surgery may reduce the risk of stroke in patients with severe carotid artery stenosis, there is about a 3% perioperative stroke or death rate associated with carotid endarterectomy (which may be higher in routine clinical practice outside clinical trials), and the benefit of surgery, particularly in patients with concomitant illnesses, is largely debated [299-306]. In the ACST trial the number needed to treat to prevent 1 disabling or fatal stroke after 5 years was approximately 40 [298]. Carotid stenting is less invasive than endarterectomy, however, it may be associated with a higher (9.6% compared with 3.9% for endarterectomy) 30-day incidence of stroke or death [307]. On the other hand, Stenting and Angioplasty with Protection in Patients at High Risk for Endarterectomy (SAPPHIRE), a randomized trial of endarterectomy versus angioplasty with the use of an emboli-protection device in patients with coexisting conditions that potentially increased the risk posed by endarterectomy, reported a lower 30-day incidence of stroke after stenting (3.6%) and concluded that angioplasty was not inferior to surgery [306,308]. In either case, it has been recently pointed out that even if it was possible to identify and treat every individual with a severe asymptomatic stenosis, 95% or more of all strokes would still occur, and hence the important goal should be to identify the small cohort of patients with vulnerable plaques who would benefit from intervention [301,309-310]. Identifying patients with high-risk or vulnerable plaques is, therefore, paramount so that treatment can be tailored more appropriately.

## 7.3 Introduction

The degree of stenosis (DOS) of the carotid artery is an established parameter that is routinely used in clinical practice [38-39]. However, it is recognized that some plaques may be more vulnerable than others, and their identification would aid clinical decision-making [301]. Previous investigations have shown that ultrasound plaque characteristics such as the greyscale median (GSM) and surface irregularities may be useful for identifying such vulnerable plaques [51,129,131,134-135,140,146,158,172,180,238,243,248,250-251,253-254,262]. Several studies have attempted to combine these and other ultrasound measures with the degree of stenosis to derive a plaque risk index but either qualitative measures have been employed and/or the relevant risk index was based on cut-off values or weighting factors optimised to a particular dataset [174,179,203,311-313]. The incorporation of dataset-optimised factors limits applicability and validity, since the assessment of ultrasound plaque characteristics, including that of the degree of stenosis, can vary depending on the method of assessment used, and can be subject to variation between centres [238,314].

This chapter develops an ultrasound-based carotid plaque risk index (CPRI) that is based on quantitative measurements of plaque echogenicity and surface irregularities, combining these with the degree of stenosis without incorporating any parameters optimised for our dataset. Our study compares the performance of this risk index with DOS and a conventional logistic regression based model with dataset-optimised weighting factors.

## 7.4 Methods

This was a cross-sectional study in which 56 patients (35 male, 21 female) who attended the University Hospitals of Leicester NHS Trust's Rapid Access Transient Ischaemic Attack (TIA) clinic were recruited. Ultrasound image sequences of the carotid plaque in the longitudinal cross-section were acquired by experienced sonographers using a Philips iU22 ultrasound scanner (Philips Healthcare, Eindhoven, The Netherlands) and an L9-3 probe. B-Mode (greyscale) and Colour Doppler image sequences were recorded as DICOM files over an average duration of 5.6 seconds

(mean frame rate was 32 frames per second) using the vascular carotid preset on the scanner (Vasc Car preset, persistence low, XRES and SONOCT on). Colour Doppler image sequences were used as a qualitative aid to identifying the location and extent of the plaques, while the greyscale data were used for the quantitative analyses. The study was approved by the National Research Ethics Service (NRES) Committee East Midlands-Northampton (reference 11/EM/0249) and followed institutional guidelines. Each patient gave informed consent before participating in the study. Eighty-two stenosed carotid arteries (stenosis range 10-95%) were investigated. Plaques were classified as either having caused cerebrovascular symptoms relating to the ipsilateral brain hemisphere within the past six-month period (i.e. symptomatic) or as asymptomatic following the review of patient symptoms and clinical/radiological (CT/MRI) findings.

### 7.4.1 Analysis

Quantitative analyses were carried out using MATLAB version 7.14 (MathWorks, Natick, Massachusetts, USA) and SPSS version 20 (IBM Corporation, Armonk, New York, USA). Degree of stenosis was measured using criteria consistent with the NASCET method utilizing blood flow velocities in conjunction with the B-Mode and colour flow imaging [38,47,240]. As Doppler velocity measurements are not able to reliably discriminate degrees of stenosis below 50%, we used B-Mode diameter measurements and colour flow imaging to grade the degree of stenosis into deciles for minor stenoses. Previously-described methods were employed to evaluate the normalized plaque GSM and the surface irregularity index (SII) [238,243]. GSM and SII were averaged over all the ultrasound image frames acquired for each artery. On average, 180 consecutive frames were analyzed for each artery. The non-parametric Wilcoxon-Mann-Whitney test was used to assess whether quantitative measures differed significantly between symptomatic and asymptomatic groups, and ROC curves were used to assess classification performance. Two-tailed tests of significance were used and p-values less than 0.05 were considered statistically significant. A carotid plaque risk index based on logistic regression methods ($CPRI_{logistic}$) was constructed, similar to Momjian-Mayor et al. [203] in the form of $1/(1+exp(-x))$ where x is equal to $\beta_0+\beta_1*DOS+\beta_2*GSM+\beta_3*SII$ and $\beta_0$, $\beta_1$, $\beta_2$, $\beta_3$ are factors that are optimised for the data. This was done using the

binary logistic regression tool in SPSS, using the symptomatic status as the dependent variable and DOS, GSM, and SII as covariates. Our CPRI, on the other hand, was defined as (DOS*SII)/(GSM+1) with no dataset-optimised parameters. DOS values in this equation were between 0.0 and 1.0 (e.g. 0.5 for 50% stenosis), while the SII were input in radians per metre. The value 1 was added to the GSM to avoid having a mathematical singularity for plaques with a GSM of 0. Box and whisker plots were used to study the distribution of CPRI and CPRI$_{logistic}$ among the plaque groups with and without associated cerebrovascular symptoms.

## 7.5 Results

The mean age of the patients was 76.6 (range 58 to 95) years. Patient age was not significantly different between the asymptomatic (76.9 years) and symptomatic groups (76.4 years, p > 0.05). Patients who had previous TIA/stroke episodes (44.6%) were more likely to be symptomatic (p=0.01), while other patient characteristics did not have a significant association to the presence of symptoms (Table 7.1).

**Table 7.1** - Patient characteristics and the significance of association with cerebrovascular symptoms. The statistical methods used to test the associations were the non-parametric Wilcoxon-Mann-Whitney test for the patient age the $\chi^2$ test for the rest of the patient characteristics. Significant associations are marked with an asterisk (*).

| Patient Characteristic | All patients | Asymptomatic group | Symptomatic group | Significance (p-value) |
|---|---|---|---|---|
| Mean age (years) | 76.6 | 76.9 | 76.4 | 0.80 |
| Sex (males) | 62.5% | 54.5% | 67.6% | 0.33 |
| Hypertension | 64.3% | 63.6% | 64.7% | 0.94 |
| Hypercholesterolaemia | 53.6% | 54.5% | 52.9% | 0.91 |
| Ischaemic Heart Disease | 23.2% | 13.6% | 29.4% | 0.18 |
| Diabetes | 35.7% | 22.7% | 44.1% | 0.11 |
| Previous TIA/stroke | 44.6% | 22.7% | 58.8% | 0.01* |

| Patient Characteristic | All patients | Asymptomatic group | Symptomatic group | Significance (p-value) |
|---|---|---|---|---|
| Peripheral vascular disease | 14.3% | 9.1% | 17.6% | 0.38 |
| Smoking | 67.9% | 68.2% | 67.6% | 0.97 |
| Alcohol consumption | 37.5% | 27.3% | 44.1% | 0.21 |
| Family history of stroke | 33.9% | 22.7% | 41.2% | 0.16 |
| Atrial Fibrillation | 12.5% | 13.6% | 11.8 | 0.84 |
| Stroke (n=8) | 14.3% | Not applicable | 23.5% | Not applicable |
| TIA (n=16) | 28.6% | Not applicable | 47.1% | Not applicable |
| Transient Monocular Vision Loss (n=10) | 17.9% | Not applicable | 29.4% | Not applicable |

**Table 7.2** - Comparison of diagnostic performance between degree of stenosis (DOS), the logistic regression based, optimised risk index (CPRI$_{logistic}$) and our risk index (CPRI).

| Parameter | DOS | CPRI$_{logistic}$ | CPRI |
|---|---|---|---|
| Area under ROC curve (AUC) | 0.771 | 0.845 | 0.849 |
| 95% confidence interval for AUC | 0.670 - 0.873 | 0.757 - 0.932 | 0.765 - 0.934 |
| Sensitivity (%) | 73.8 | 85.7 | 90.5 |
| Specificity (%) | 65.0 | 77.5 | 75.0 |
| Accuracy (%) | 69.5 | 81.7 | 82.9 |
| Positive Predictive Value (%) | 68.9 | 80.0 | 79.2 |
| Negative Predictive Value (%) | 70.3 | 83.8 | 88.2 |

There were 82 carotid arteries with stenoses ranging from 10% to 95%. Forty-two of these arteries were associated with symptoms relating to the ipsilateral brain hemisphere, while 40 were asymptomatic. The degree of stenosis and the SII were significantly higher in the arteries with symptoms, while the normalized plaque GSM was lower ($p < 0.01$ for all). The mean SII of symptomatic plaques was 1970 radians/m compared to 1780 radians/m for the asymptomatic. The corresponding normalized GSM values were 45.1 and 59.5, respectively.

Seven patients had atrial fibrillation present on pre-scan ECG. Three of these patients were asymptomatic since they were not diagnosed to have suffered a cerebrovascular event. The remaining 4 patients had no brain infarcts observed on CT/MRI, but their body symptoms were contralateral to their stenosed carotid arteries.

Examples of a plaque with ipsilateral hemispheric symptoms and a plaque without symptoms are shown in Figure 7.1. The risk index based on optimised logistic regression ($CPRI_{logistic}$) and our CPRI were significantly higher for stenoses that were associated with symptoms ($p < 0.01$ for both), but CPRI showed a better separation of the two groups (Figure 7.2). ROC curve analysis showed that $CPRI_{logistic}$ and CPRI had similar classification performance, better than that of DOS, with CPRI providing a better overall accuracy (Figure 7.3 and Table 7.2). The area under the ROC curve (AUC) was 0.849 for CPRI, 0.845 for $CPRI_{logistic}$ and 0.771 for DOS (Table 7.2). The median CPRI of the symptomatic and asymptomatic groups were 23.2 and 9.2 units compared with 0.71 and 0.30 for $CPRI_{logistic}$. GSM and SII appeared to have similar ROC curves, which were below that of DOS (Figure 7.3). A reduced risk index, not utilizing the plaque surface irregularities, of the form DOS/(GSM+1) also outperformed DOS on its own (Figure 7.4).
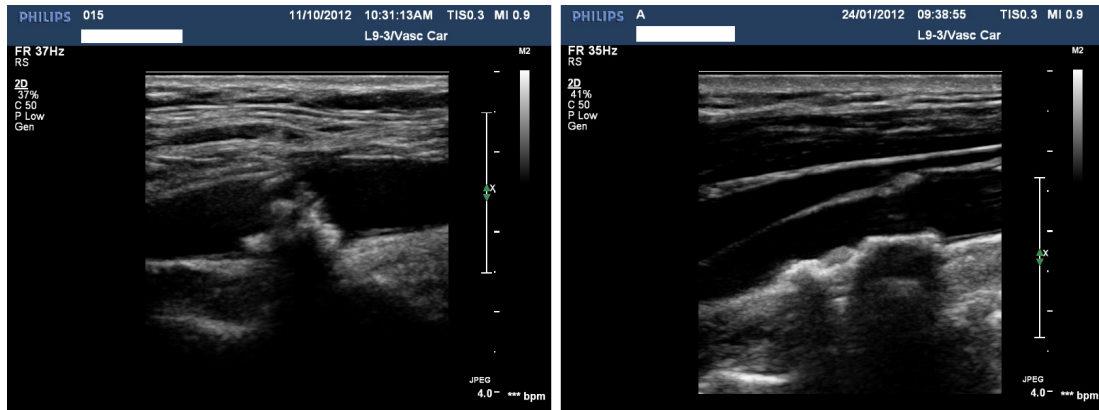
**Figure 7.1** - Example of a symptomatic plaque (left) and an asymptomatic plaque (right) with respective risk indices (CPRI) of 27.5 and 3.25. The degree of stenosis (DOS) caused by the symptomatic plaque was 70%, while it was 20% for the asymptomatic plaque. The difference between the symptomatic and the asymptomatic case was more profound with CPRI than with DOS; the ratio between the two degrees of stenosis was 70/20 (3.5x), while the ratio between the two risk indices was 27.5/3.25 (8.5x).
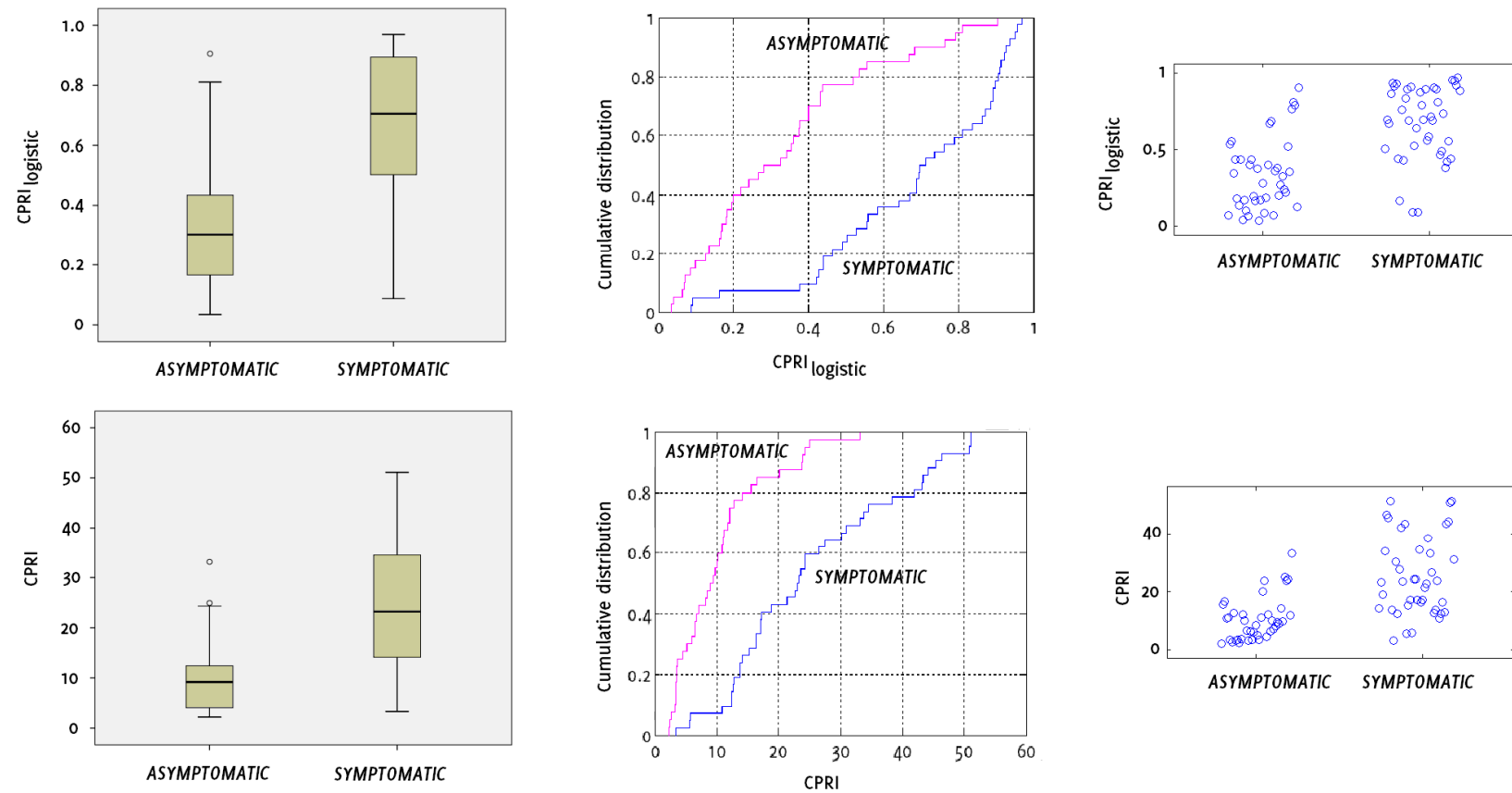
**Figure 7.2** - Box and whisker plots showing the distribution of $CPRI_{logistic}$ (top-left) and CPRI (bottom-left) in carotid artery stenoses with and without cerebrovascular symptoms. The corresponding plots in the middle and on the right further show the distribution of $CPRI_{logistic}$ and CPRI within the two groups in the form of cumulative distribution and scatter plots.
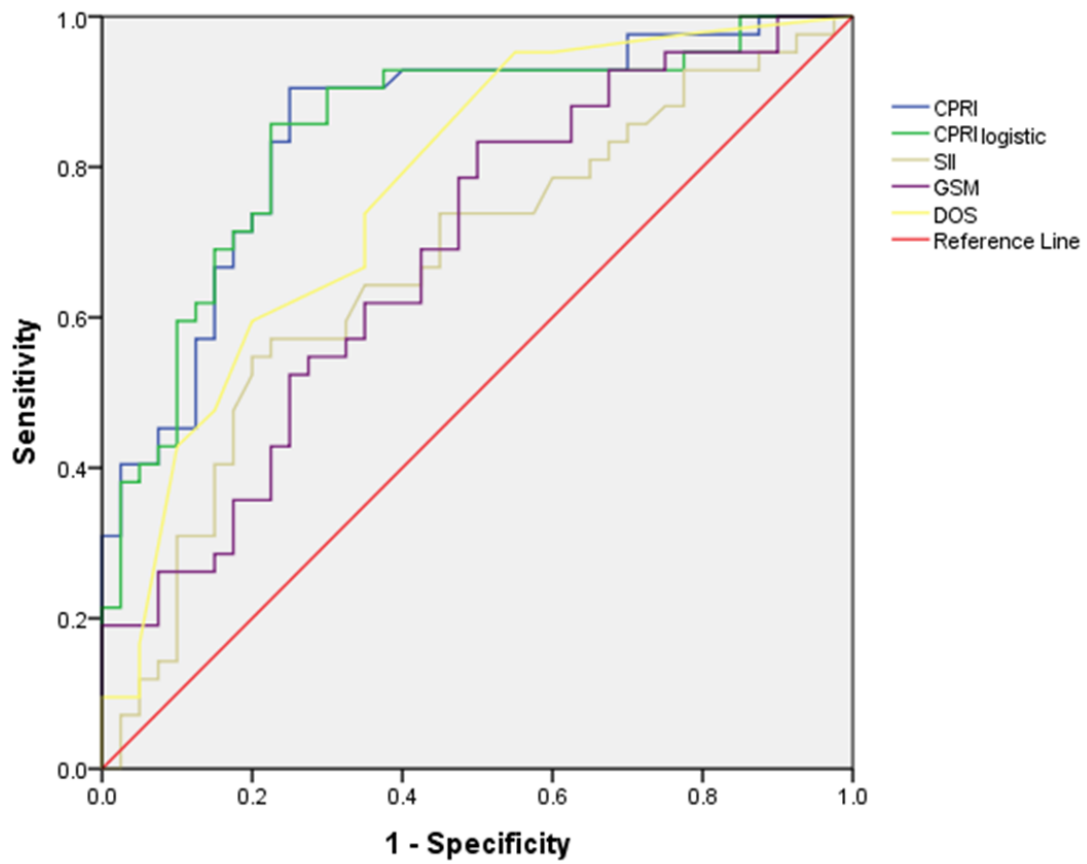
**Figure 7.3** - ROC curves showing the classification performance of the degree of stenosis (DOS), plaque surface irregularity index (SII), the normalized plaque greyscale median (GSM), CPRI$_{logistic}$ and CPRI. 'Reference line' is the line of identity or no discrimination.
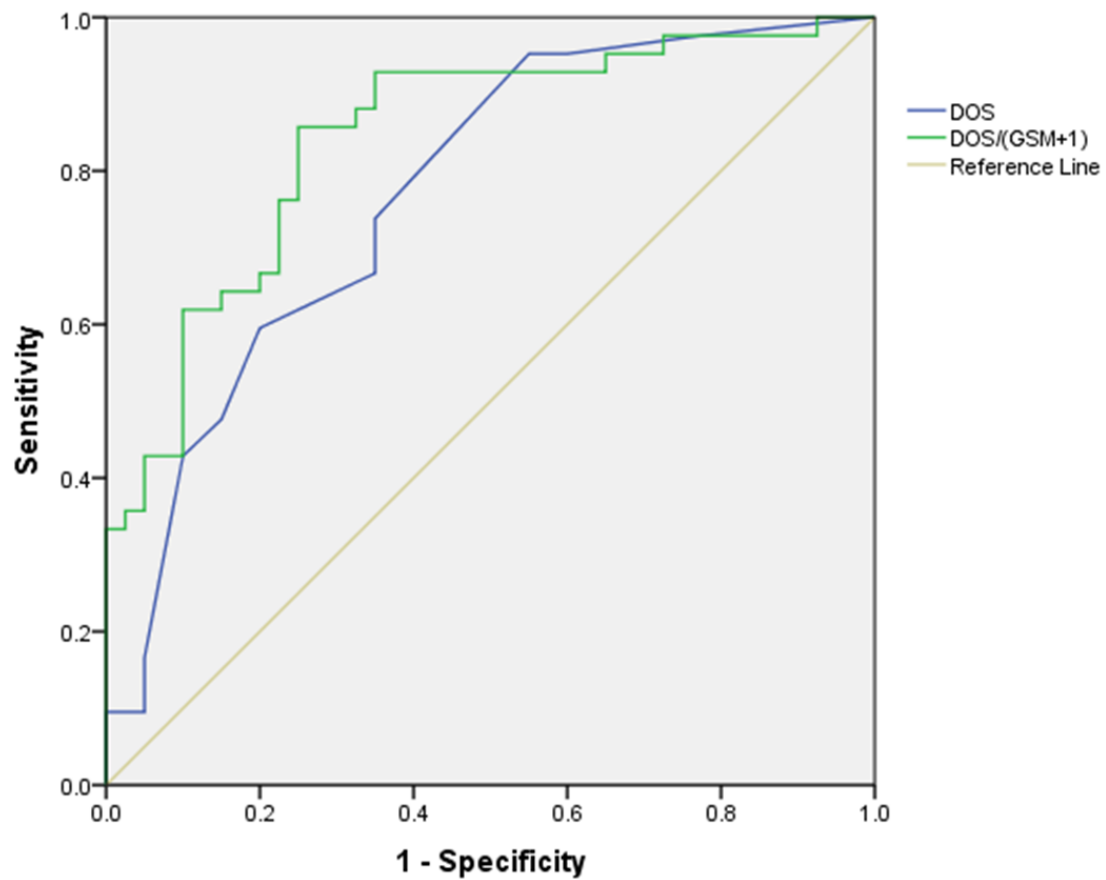
**Figure 7.4** - ROC curves showing the classification performance of the degree of stenosis (DOS), compared with the reduced version of the carotid plaque risk index DOS/(GSM+1). Areas under ROC curve are 0.771 for DOS vs. 0.844 for the reduced index. 'Reference line' is the line of identity or no discrimination.
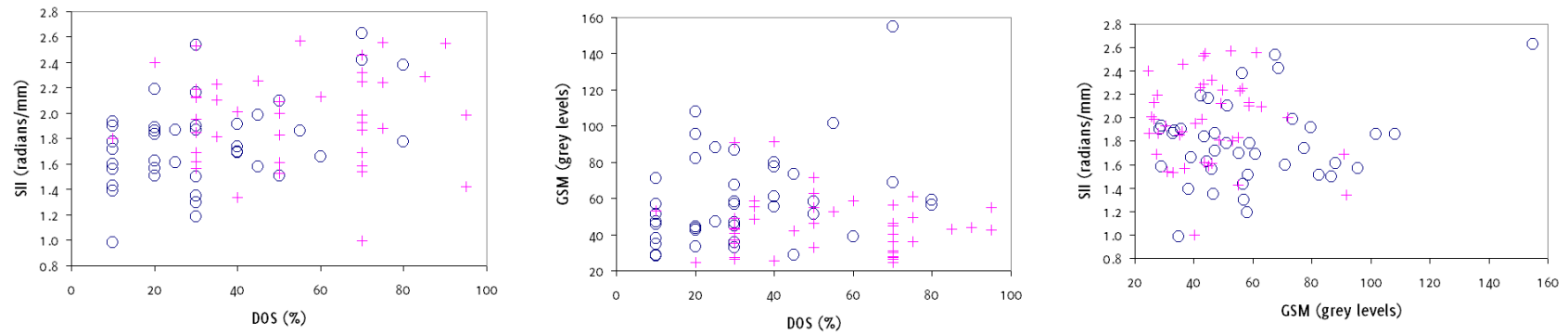
**Figure 7.5** - Scattergrams of SII versus DOS (left), normalized GSM versus DOS (middle), and SII versus normalized GSM (right). Plaques causing symptoms are shown as + in purple, while plaques that have not been associated with symptoms are shown as o in blue.

A general tendency of plaques causing symptoms to cluster around higher degrees of stenosis (DOS) and surface irregularity indices (SII) but lower normalized greyscale medians (GSM) can be observed from the scattergrams of SII versus DOS, normalized GSM versus DOS, and SII versus normalized GSM (Figure 7.5).

## 7.6 Discussion

This chapter described a novel risk index which intuitively combines quantitative measures of plaque echogenicity and surface irregularities with the degree of carotid artery stenosis. This risk index, despite not having any parameters optimizing it for our dataset, was found to have increased diagnostic performance compared to DOS, and a risk index based on logistic regression with such optimised parameters.

Several studies have previously derived risk indices that combine ultrasound plaque characteristics with DOS in order to help identity the vulnerable carotid plaque [174,179,203,311-313]. Prati et al. defined a risk index incorporating DOS, and qualitative measures of surface irregularity, plaque echogenicity and texture [174]. They found that the addition of plaque characteristics significantly increased the area under the ROC curve compared to the Framingham score alone. Momjian-Mayor et al. defined a risk index combining DOS with a quantitative measure of the plaque surface echogenicity and used a logistic regression based statistical model with weighting factors optimised for their dataset [203]. This risk index was found to be significantly higher for plaques with associated symptoms than for plaques without symptoms. Pedro et al. similarly developed an activity index, comprising several measures including that of plaque surface disruption[1], GSM, percentage of plaque area with grey levels less than 40, plaque heterogeneity[2], the presence of juxta-luminal echolucent areas[3] and the degree of stenosis. Weighting scores for various criteria based on these parameters were evaluated and used to assign an activity index to each plaque [179,311]. The activity index correlated positively with the presence of symptoms. This was later extended by Seabra et al. to an enhanced activity index which incorporated

---

[1] Plaque surface disruption assessed qualitatively.

[2] Plaque heterogeneity assessed qualitatively.

[3] Presence of juxta-luminal echolucent areas assessed qualitatively.

additional parameters, including those based on the radiofrequency (RF) ultrasound signal [315]. They used an algorithm based on summing conditional probabilities for individual parameters belonging to the asymptomatic and symptomatic groups [315]. The enhanced activity index was reported to have provided correct identification of all plaques that developed symptoms, while giving a small number of false positives [315]. Nicolaides et al. constructed three risk models based on DOS, clinical and plaque features including GSM, plaque area, plaque type[1], and the presence of discrete white areas [312]. Multivariable, fractional polynomials were used, which were optimised for the dataset, to derive the risk indices. The addition of plaque features increased the area under the ROC curve compared to degree of stenosis alone, and the degree of stenosis and clinical features combined. Kyriacou et al. followed a similar procedure but incorporated several plaque texture features to build a stroke risk model, with weighting factors optimised using their own dataset, and also reported good classification accuracy [313].

A common limitation of the existing methods has been the incorporation of weighting factors and other parameters that were optimised using the particular datasets studied. Ultrasound plaque characteristics such as the GSM, and even DOS, can be subject to variations when measured by different centres and methods [238]. Therefore, regardless of how large the sample size used might be[2], these variations compromise the general validity and applicability of these risk indices. Obtaining good classification accuracy need not mean the model is generally valid, if the model includes parameters that have been optimized for the dataset/assessment method. The incorporation of qualitative measures into some risk models can also be considered a separate limitation since intra- and inter-observer agreement can be low for such subjective assessments [203,314]. Another group of studies have attempted to classify plaques using methods such as pattern recognition, neural networks, support vector machines, and other machine learning algorithms but these do not provide risk indices and suffer from the same limitations [153,185,188-190,316-319].

---

[1] Plaque type assessed qualitatively.

[2] Unless the samples are from multiple representative centres.

Our study has found that a new, intuitive model that does not have any parameters which are optimized for our data has better diagnostic performance than DOS and a dataset-optimised risk index. The area under the ROC curve (0.849 for CPRI vs. 0.771 for DOS and 0.845 for CPRI$_{logistic}$) compared favourably with that of the more complicated risk index defined by Momjian-Mayor et al. [203]. This model, if confirmed in subsequent studies, has the additional benefit that it may be employed by different centres without re-optimisation of the weighting factors. Our intuitive method of risk index construction was based on the observation that the presence of symptoms appears to be directly related to DOS and SII, while being inversely related to GSM [238,243]. In our study, the carotid plaque risk index was defined as (DOS*SII)/(GSM+1), but our investigation also suggested that a reduced risk index of the form of DOS/(GSM+1) also performs better than DOS (AUC 0.771 for DOS vs. 0.844 for the reduced index). The reduced index could be particularly useful at centres where quantitative assessment of surface irregularities is not available. Normalized plaque GSM can be easily measured using widely available software packages such as Photoshop (Adobe Systems, San Jose, California, USA) [129] and the reduced index can be used to obtain an enhanced predictor of symptoms compared to DOS at a busy clinical service with relative ease. The reduced index has the added convenience that for a stenosis severity of 50% and a moderate plaque GSM of 50, an index of approximately 1.0 is obtained, which increases with increasing stenosis severity and decreasing plaque GSM, and vice versa. Our study also has confirmed that the degree of stenosis was the strongest predictor of symptoms among the parameters studied, with the GSM and the SII providing approximately equivalent discriminatory power.

Further work is required to demonstrate the clinical benefit of these novel risk indices. This could be in the form of longitudinal studies looking prospectively at the development of cerebrovascular symptoms, in a cross-sectional comparison against plaque histology or other measures of plaque vulnerability, or studies utilising data from multiple centres.

## 7.7 Conclusions

This chapter defined a novel carotid plaque risk index, an intuitive method of combining quantitative measurements of plaque echogenicity, surface irregularities and DOS without the use of weighting factors optimised for the dataset. It was found that this risk index performs better than both DOS and a risk index which does include such optimized parameters. The clinical value of this risk index should be investigated in further studies.

# Chapter 8

# Summary, Discussion and Future Directions

## 8.1 Overview

This chapter summarises and discusses the contents of the previous chapters, highlighting key findings, identifying limitations, and future directions for research. A corresponding chapter by chapter summary is provided in Table 8.1.

## 8.2 Thesis Summary and Discussion

Stroke is a major healthcare problem. As well as causing premature death, it often leads to disability, leaving patients unable to carry out their daily activities and care for themselves. In Chapter 1, the carotid plaque was highlighted as a major cause of stroke, pointing out the need for further developments in relation to the characterisation of plaques. If plaques can be characterised better, treatment and preventative measures could be more appropriately tailored, leading to a reduction in the incidence and burden of stroke. It was also stated in Chapter 1 that the degree of carotid artery stenosis is routinely used to make treatment decisions, but carotid plaques associated with low or moderate degrees of stenosis can also cause stroke, and some severe stenoses can remain asymptomatic over many years. It has been long recognized that other parameters that describe the plaque, such as plaque morphology or dynamic behaviour, may enable further differentiation of the risk of stroke, helping to identify the vulnerable plaques. This is a reasonable expectation since the degree of stenosis quantifies the degree of arterial narrowing, and to some extent the amount of blood flow disturbances, but does not encapsulate any other information on the characteristics of plaques. Chapters 1 and 3 reported that the plaque greyscale median (GSM) may be potentially useful for identifying the vulnerable plaques. However, plaque GSM has remained mainly a research tool and has not been adopted in clinical practice, except, perhaps, in a qualitative sense. One of the reasons for this may have been the low reproducibility of GSM measurements across different studies. While most studies confirmed the negative correlation between plaque GSM and vulnerability, quantitative studies found different GSM figures for symptomatic and asymptomatic cases depending on the dataset and the

method of analysis used. In Chapter 3, it was suggested that one of the reasons for this may have been the fact that GSM measurements traditionally have been made on static or single frames of ultrasound images, typically obtained at arbitrary phases of the cardiac cycles. The first contribution to knowledge made in this thesis was the development of an effective means of tracking plaque boundaries over many ultrasound image frames (Chapters 2 and 3). This is a prerequisite for measuring the plaque GSM over many cardiac cycles as manual delineation of plaque boundaries over many image frames is prohibitively labour extensive, and is difficult to carry out without subjectivity. Chapter 3 showed that plaque outlines can be successfully tracked over image sequences of five seconds long or more, having as many as 300 frames per acquisition, with ease. This functionality also resulted in the second contribution made to knowledge in this thesis which was the measurement, for the first time, of the frame-by-frame variations in the plaque GSM over several cardiac cycles. Chapter 3 reported a mean inter-frame coefficient of variation of 5.2% (s.d. 2.5%) for the plaque GSM. These variations have been largely overlooked before, and the dynamic assessment of plaque GSM introduced in Chapter 3 could be a step forward towards reducing variations in GSM measurements across centres, thus helping make GSM a clinically relevant diagnostic tool.

Chapter 3 confirmed that the plaque GSM has a significant negative correlation to the presence of cerebrovascular symptoms, with symptomatic plaques having a significantly lower GSM on average than asymptomatic plaques. The arterial wall and surface tracking algorithm described in Chapter 2 formed an integral part of the novel method used to track plaque boundaries in Chapter 3, which made this possible.

In Chapter 4, a quantitative method for the measurement of carotid plaque surface irregularities was developed and a plaque surface irregularity index (SII) was described. SII demonstrated a significant association to the presence of cerebrovascular symptoms relating to the ipsilateral brain hemisphere. Previously, assessment of surface irregularities has been mainly qualitative, for example, categorising plaques subjectively as having a smooth surface or an irregular surface, while some studies used additional categories such as ulcerated and/or indeterminate [149,244-247]. The main limitations of these qualitative assessments have been their subjectivity, and the difficulty associated

with classifying plaques which have a moderate amounts of irregularities that cannot be classified as smooth or irregular with any certainty. Very few studies have carried out quantitative assessments; these included an assessment of the bending energy of the plaque surface [263], and the measurement of the principal curvatures of plaque surfaces in three dimensions [264-265]. The former did not find a difference in the bending energies of symptomatic and asymptomatic plaques, but plaque surfaces were manually delineated, which introduced an element of subjectivity into the process. Furthermore, the physical relevance of the bending energy of the plaque surface to the presence of cerebrovascular symptoms appear rather questionable. The studies which assessed the principal curvatures of plaque surfaces in three dimensions had more promising results; however, three dimensional ultrasound systems are not widely available and a two-dimensional assessment method would be more readily usable. Furthermore, curvature may not be the best method of measuring the roughness of the plaque surface, as it is, of course, a measure of curvature and not roughness. Although a rough plaque surface will exhibit spatial variations in curvature and, thus, the assessment of curvature has validity, curvatures in one direction can cancel curvatures in the opposite direction, resulting in a null overall curvature measurement for that surface. Chapter 4 contributed to knowledge by addressing the limitations of the existing studies, and providing a quantitative method for the assessment of carotid plaque surface irregularities in two dimensions that is directly related to the roughness of the plaque surface. Chapter 4 reported that the combination of the developed plaque surface irregularity index with the degree of carotid artery stenosis resulted in a more effective predictor of cerebrovascular symptoms compared to the degree of stenosis on its own.

Chapter 5 described an assessment of wall motion in the stenotic carotid artery, investigating whether stenosed carotid arteries with associated symptoms have different dilation characteristics compared to arteries without associated symptoms. Previously, the relationship between arterial dilation characteristics and the degree of stenosis [97], longitudinal distension gradient and the presence of symptoms had been studied [279], but there were no studies investigating whether the absolute and percentage dilation of arteries differ between arteries with and without symptoms. Chapter 5 found a mean absolute diameter change from diastole to systole of 0.45 mm (s.d. 0.17), and a mean

percentage diameter change of 6.9% (s.d. 3.1%), averaged across 45 stenosed carotid arteries. Absolute and percentage diameter changes did not have a statistically significant relationship to the degree of stenosis, greyscale plaque characteristics, or the presence of ipsilateral hemispheric symptoms. This was attributed to the opposing effects of (1) progressive atherosclerotic disease which tends to stiffen the arteries and reduce wall motion, and conversely (2) plaque rupture that may be caused by mechanical means which should increase in likelihood with increased amounts of wall motion. Contributions made to knowledge in this chapter included the first-ever correlation assessment between the dilation characteristics of the stenotic carotid artery and greyscale plaque characteristics, and the adding of new data to the literature on the absolute and percentage dilations of stenotic carotid arteries.

Chapter 6 described a quantitative investigation of carotid plaque motion. Displacement, velocity, and acceleration of plaques were studied relative to the ultrasound probe and relative to the tissues directly underlying the carotid plaque. Studies had previously investigated plaque motion using qualitative and quantitative methods, but the literature was relatively scarce [272]. Plaque motion is of prospective clinical interest, as motion may increase plaque vulnerability and be associated with a higher prevalence of symptoms [61,197-198,200,273-274,288]. However, the results of Chapter 6 did not support this hypothesis. Although motion parameters relative to the ultrasound probe could be reliably measured (average displacement magnitude was greater than 1 mm), motion relative to the underlying tissues suffered from low reproducibility (average displacement magnitude was less than 0.4 mm). The typical plaque displacements and velocities reported in Chapter 6 were in accordance with previous findings, but plaque acceleration had not previously been reported. The *in vitro* study further had further contribution by showing that motion magnitudes below 50 μm were not detected, while motion magnitudes in the range 50 to 100 μm had lower accuracy compared with motion magnitudes in the range 200 to 500 μm.

Chapter 7 was the culmination of the research project and described a novel ultrasound-based carotid plaque risk index. Two risk indices were introduced: a risk index incorporating the degree of stenosis with the plaque greyscale median and the quantitative measure of plaque surface irregularities, and a reduced index comprising

only the degree of stenosis and the GSM. These risk indices were shown to improve diagnostic performance compared to the degree of stenosis on its own, and an equivalent risk index constructed using logistic regression based methods with model parameters optimised for the data. The unique difference these risk indices have from those already described in the literature is the absence of any parameters that were optimised for the dataset, and their intuitive construction. The previous studies had described risk indices and other methods of assessing plaque vulnerability, incorporating weighting factors or other parameters optimized for the particular datasets studied. However, ultrasound plaque characteristics such as the GSM, and even the degree of stenosis, are subject to variations when measured by different centres and by using different methods [4]. Therefore, these variations may compromise the general validity and applicability of the previously described risk indices. The contributions made to knowledge in Chapter 7 were the development of risk indices that are not dataset dependent and thus, if confirmed in subsequent studies, may be employed by different centres without the re-optimisation of any weighting factors, and the first-ever description of a risk index that incorporates a quantitative measure of plaque surface irregularities.

**Table 8.1** - A summary of the thesis on a chapter by chapter basis including key findings, strengths and limitations.

| Chapter | Purpose and Aim | Key Findings | Limitations | Publications |
|---|---|---|---|---|
| 2 | To describe a method for tracking arterial walls in ultrasound image sequences. | Arterial lumens and plaque surfaces could be tracked in a variety of arterial configurations and image noise conditions. An increased immunity to image noise within the arterial lumen and a reduced susceptibility to region overflowing at boundary imperfections was found, when the method was compared against a conventional region growing technique. | Implementation was not optimised or designed to take advantage of the multi-core CPU architecture. However, even with the un-optimised implementation, processing times as fast as 33 ms/frame could be achieved for a large region-of-interest. | Kanber B, Ramnarine KV. A Probabilistic approach to computerized tracking of arterial walls in ultrasound image sequences. ISRN Signal Processing. 2012. |

| Chapter | Purpose and Aim | Key Findings | Limitations | Publications |
|---|---|---|---|---|
| 3 | To establish the presence and evaluate the extent of frame-by-frame variations in the plaque GSM. | A mean inter-frame coefficient of variation (COV) of 5.2% (s.d. 2.5%) was found for the plaque GSM and 4.2% (s.d. 2.9%) for the plaque area. Thirteen of the 27 plaques (48%) studied exhibited COV in GSM of greater than 5% whereas only 6 plaques (22%) had COV in plaque area of greater than 5%. There was no significant correlation between the COV of GSM and plaque area. | The use of two dimensional ultrasound and the absence of any attempts to fix the scan plane with respect to the plaque being imaged, other than those measures normally taken in the clinic (e.g. holding the probe fixed and asking the patient to remain still and breath-hold). | Kanber B, Hartshorne TC, Horsfield MA, Naylor AR, Robinson TG, Ramnarine KV. Dynamic variations in the ultrasound greyscale median of carotid artery plaques. Cardiovascular Ultrasound. 2013;11:21. |

| Chapter | Purpose and Aim | Key Findings | Limitations | Publications |
|---|---|---|---|---|
| 4 | To develop a quantitative method for the measurement of carotid plaque surface irregularities. | The mean surface irregularity index (SII) measured for plaques with associate ipsilateral hemispheric symptoms was significantly greater than for plaques without symptoms (1.89 radians/mm versus 1.67 radians/mm). There was no statistically significant association between the SII and the degree of stenosis (p = 0.30). SII predicted the presence of cerebrovascular symptoms with an accuracy of 66% (sensitivity 65%, specificity 67%) on its own and with an accuracy of 83% (sensitivity 96%, specificity 71%) in combination with the degree of stenosis. | The use of two dimensional ultrasound, and the cross-sectional study design using the presence of ipsilateral hemispheric symptoms to infer plaque vulnerability. | Kanber B, Hartshorne TC, Horsfield MA, Naylor AR, Robinson TG, Ramnarine KV. Quantitative assessment of carotid plaque surface irregularities and correlation to cerebrovascular symptoms. Cardiovascular Ultrasound. 2013;11:38. |

| Chapter | Purpose and Aim | Key Findings | Limitations | Publications |
|---------|-----------------|--------------|-------------|--------------|
| 5 | To quantify wall motion in stenotic carotid arteries and investigate any associations with the greyscale plaque characteristics, the degree of stenosis, and the presence of cerebrovascular symptoms. | The mean absolute diameter change from diastole to systole was 0.45 mm (s.d. 0.17), and the mean percentage diameter change was 6.9% (s.d. 3.1%). Absolute and percentage diameter changes did not have a statistically significant relationship to the degree of stenosis, greyscale plaque characteristics, or the presence of ipsilateral hemispheric symptoms (p > 0.05). | Diameter changes were measured before the proximal shoulder of the atherosclerotic plaque, but pulse pressures were not considered. However, this chapter focussed on motion aspects rather than stiffness and was part of our broader research aim to develop and define a plaque risk index based on ultrasound measurements. | Kanber B, Hartshorne TC, Horsfield MA, Naylor AR, Robinson TG, Ramnarine KV. Wall motion in the stenotic carotid artery: association with greyscale plaque characteristics, the degree of stenosis and cerebrovascular symptoms. Cardiovascular Ultrasound. 2013;11:37. |

| Chapter | Purpose and Aim | Key Findings | Limitations | Publications |
|---|---|---|---|---|
| 6 | To quantify plaque motion and investigate any relationships to the degree of stenosis, greyscale plaque characteristics, and the presence cerebrovascular symptoms. | Average motion magnitude was 1.2 mm, 0.35 mm relative to the periadventitial tissues. Maximum and mean plaque velocities were 4.7 and 1.3 mm/s relative to the ultrasound probe and 2.4 and 0.70 mm/s relative to the periadventitial tissues. Maximum and mean plaque accelerations were 69 and 22 $mm/s^2$ relative to the probe and 57 and 18 $mm/s^2$ relative to the periadventitial tissues. There were no significant differences, in relation to the presence of cerebrovascular symptoms, in any of the motion parameters. None of the motion parameters showed any significant relationship to the degree of stenosis, or the greyscale plaque characteristics. | A similar assessment using three dimensional ultrasound and radiofrequency data could provide additional benefit. Pulse pressures, which may affect the amount of plaque motion, were not considered. However, this chapter aimed to determine whether the motion of the plaque had a significant relationship to the presence of patient symptoms, rather than quantifying plaque mobility (i.e. motion per unit of pulse pressure). | Submitted. |

| Chapter | Purpose and Aim | Key Findings | Limitations | Publications |
|---------|-----------------|--------------|-------------|--------------|
| 7 | To determine the efficacy of a novel, ultrasound-based carotid plaque risk index (CPRI) in predicting the presence of cerebrovascular symptoms in patients with carotid artery stenosis. | The median CPRI of the symptomatic group was 23.2, while that of the asymptomatic group was 9.2. Diagnostic performance of CPRI exceeded that of the degree of stenosis, and an equivalent logistic regression based risk index with model parameters optimised to the dataset. CPRI demonstrated a better separation of the symptomatic and asymptomatic groups. | Further work is required to demonstrate the potential clinical benefit of this risk index. This could be in the form of longitudinal studies looking prospectively at the development of symptoms, or in a cross-sectional comparison against plaque histology or other measures of plaque vulnerability. | Submitted. |

## 8.3 Limitations

The main benefits of ultrasound over other imaging modalities is that it is widely available, low-cost, and convenient. Ultrasound examinations are quick to perform and do not involve the use of any ionizing radiation such as x-rays as is the case with x-ray angiography. Ultrasound, except for intra-vascular and contrast-enhanced ultrasound, which are not covered in this thesis, is non-invasive and the procedure has high patient acceptability. However, the complementary information that can be provided by other imaging modalities such as MRI, CT, PET, and others must not be overlooked.

The first limitation of the work described in this thesis is the use of cross-sectional, two dimensional ultrasound. One must remember that such examinations only provide a cross-sectional view of the three dimensional object that is the carotid plaque. The use of longitudinal cross-sectional imaging may result in carotid lesions to be missed, but this can be avoided by carrying out complementary transverse cross-sectional imaging, which is routine in the TIA clinic. An alternative would be to use three dimensional ultrasound. The techniques developed in this thesis would still be applicable if three dimensional techniques were to be used. The latter is becoming increasingly available and would undoubtedly provide additional benefit.

Plaque characterisation using the B-Mode greyscale images is also limited compared to a similar assessment using radiofrequency (RF) data, as the former goes through post-processing and discards phase information. This can limit the assessment of small motions such as intra-plaque motions or strains. However, B-Mode data is readily available from most clinical scanners while radiofrequency data typically requires the use of scanners specially equipped to output RF data. Thus, techniques that work with B-Mode ultrasound would be more easily adopted for clinical practice.

A further limitation arises from the study design: our clinical studies were cross-sectional with no follow-up. We have used the presence of patient symptoms to infer plaque vulnerability. Although this is a widely used method (since stroke risk is elevated following a symptomatic event) it is not ideal, since plaques which have not yet caused symptoms may also be vulnerable. An ideal clinical investigation would be that of a

longitudinal study, evaluating the parameters characterising the carotid plaque, and the associated risk indices, against the development of symptoms during a follow-up period. Such a clinical investigation will be suggested as a future direction for this research in the next section.

Another limitation of this project was that the my sample size was relatively small. The TIA clinic at the University Hospitals of Leicester sees many patients every week. However, several factors limited my sample size. First of these factors was that patient recruitment and data collection could only be done on occasional days when the clinic was not busy and without compromising the goodwill of the clinic staff. The second factor limiting my sample size was the absence of carotid artery plaques in many of the patients recruited. As this thesis is concerned with the development of methods to help identify the vulnerable plaque, patients without plaques had to be excluded from the study.

## 8.4 Future Directions

The future directions for this research will include the assessment of the developed risk indices, and parameters characterising the carotid plaque in prospective clinical trials. This would involve the measurement of plaque characteristics and the associated risk indices at baseline and (a) for patients not undergoing surgery, to follow-up patients for a set period and correlate results with the development of any cerebrovascular symptoms due to the carotid plaque and (b) for patients having surgery, to correlate results with the histological assessment of vulnerability of the surgically removed plaque specimens. It should also be explored whether other ultrasound-based methods such as a stratified GSM analysis (i.e. the analysis of plaque echogenicity with respect to the distance to the plaque surface) and the assessment of the mechanical properties of plaque and vessel wall using Shearwave Elastography can provide additional benefit. The methods developed in this thesis are also being used to study the endothelium-dependent, flow-mediated dilation of the brachial artery and in a study looking at aortic plaque characteristics in mice. There are also plans to further utilize these techniques to investigate arterial wall dynamics in a study of human spontaneous coronary artery dissection.

## 8.5 Conclusions

Stroke is a global health concern, and the carotid plaque is a major cause. The research described in this thesis has made unique contributions to knowledge by developing and describing efficient methods that enable tracking of plaque boundaries throughout ultrasound image sequences which underpin dynamic analyses of greyscale plaque characteristics. These analyses have lead to the identification of previously unexplored sources of variation in quantitative assessments of plaque echogenicity, and the first dynamically quantified analysis of plaque surface irregularities. Contributions were also made to arterial wall motion behaviour analysis in the stenotic carotid artery and the analysis of plaque motion throughout the cardiac cycle. The research also led to the development of two novel risk indices, which efficiently integrate quantified measures of plaque morphology with the degree of stenosis of the carotid artery. These risk indices, unlike the few existing risk indices described in the literature, do not require pre-determined weighting factors which have been optimised for the dataset. It is hoped that further research and clinical trials may lead to a reduction in the incidence and burden of stroke in patients with carotid artery stenoses with the use of these techniques.

# Chapter 9

# Appendix

## 9.1 Publications

1.     B. Kanber, K.V. Ramnarine. A Probabilistic Approach to Computerized Tracking of Arterial Walls in Ultrasound Image Sequences. ISRN Signal Processing 2012.


2.     B. Kanber, T.C. Hartshorne, M.A. Horsfield, A.R. Naylor, T.G. Robinson, K.V. Ramnarine. Dynamic Variations in the Ultrasound Greyscale Median of Carotid Artery Plaques. Cardiovascular Ultrasound 2013;11:21.


3.     B. Kanber, T.C. Hartshorne, M.A. Horsfield, A.R. Naylor, T.G. Robinson, K.V. Ramnarine. Wall motion in the stenotic carotid artery: association with greyscale plaque characteristics, the degree of stenosis and cerebrovascular symptoms. Cardiovascular Ultrasound 2013;11:37.


4.     B. Kanber, T.C. Hartshorne, M.A. Horsfield, A.R. Naylor, T.G. Robinson, K.V. Ramnarine. Quantitative assessment of carotid plaque surface irregularities and correlation to cerebrovascular symptoms. Cardiovascular Ultrasound 2013;11:38.


5.     B. Kanber, T.C. Hartshorne, M.A. Horsfield, A.R. Naylor, T.G. Robinson, K.V. Ramnarine. Quantitative Assessment of Plaque Motion in the Carotid Arteries using B-Mode Ultrasound. Submitted.


6.     B. Kanber, T.C. Hartshorne, M.A. Horsfield, A.R. Naylor, T.G. Robinson, K.V. Ramnarine. A Novel Ultrasound-Based Carotid Plaque Risk Index Associated with the Presence of Cerebrovascular Symptoms. Submitted.


7.     J.W. Garrard, P. Ummur, S. Nduwayo, B. Kanber, T.C. Hartshorne, K.P. West, D. Moore, A.R. Naylor, T.G. Robinson, K.V. Ramnarine. Shear-Wave Elastography vs.

Grayscale median in the assessment of carotid artery disease: A comparison with histology. Submitted.

8.   K.V. Ramnarine, J.W. Garrard, B. Kanber, S. Nduwayo, T.C. Hartshorne, R.B. Panerai, A.R. Naylor, T.G. Robinson. Shear Wave Elastography Imaging of Carotid Plaques: Clinical Potential. In preparation.

## 9.2 Conference Abstracts

1.   B. Kanber, T.C. Hartshorne, M.A. Horsfield, A.R. Naylor, T.G. Robinson, K.V. Ramnarine. Ultrasound greyscale median of carotid artery plaques: frame-by-frame variations. Proceedings of the British Medical Ultrasound Society's 44th Annual Scientific Meeting 2012.

2.   B. Kanber, T.C. Hartshorne, M.A. Horsfield, A.R. Naylor, T.G. Robinson, K.V. Ramnarine. Dynamic variations in the ultrasound greyscale median of carotid artery plaques. Cerebrovascular Diseases 2013;35(2):21.

3.   B. Kanber, T.C. Hartshorne, M.A. Horsfield, A.R. Naylor, T.G. Robinson, K.V. Ramnarine. Quantitative assessment of carotid plaque surface irregularities using ultrasound. Cerebrovascular Diseases 2013;35(2):22.

4.   J.W. Garrard, B. Kanber, S. Nduwayo, K. West, D. Moore, A.R. Naylor, T.G. Robinson, K.V. Ramnarine. Shear-wave Elastography vs. Greyscale Median in the assessment of carotid artery disease: A comparison with histology. Cerebrovascular Diseases 2013:35(2):40.

## 9.3 Presentations

1.   Novel Ultrasound Techniques to Identify The Vulnerable Carotid Plaque – Case Studies. Poster presentation at the CLAHRC for LNR Stakeholder Event, Leicester, UK, on 26 January 2012.

2.     Ultrasound greyscale median of carotid artery plaques: frame-by-frame variations. Oral presentation at the Annual General Meeting of the British Medical Ultrasound Society, Telford, UK, on 12 December 2012.

3.     Dynamic analysis of ultrasound image sequences to identify the vulnerable carotid plaque. Poster presentation at the Postgraduate Seminar Day, Leicester, UK, on 16 May 2013.

4.     Ultrasound quantification of a carotid plaque surface curvature index associated with cerebrovascular symptoms. Oral presentation at the Journal Club, Leicester, UK, on 17 May 2013.

5.     Dynamic variations in the ultrasound greyscale median of carotid artery plaques. Oral presentation at the 18th Meeting of the European Society of Neurosonology and Cerebral Haemodynamics, Porto, Portugal, on 25 May 2013.

6.     Quantitative assessment of carotid plaque surface irregularities using ultrasound. Oral presentation at the 18th Meeting of the European Society of Neurosonology and Cerebral Haemodynamics, Porto, Portugal, on 25 May 2013.

7.     A Novel Ultrasound-Based Carotid Plaque Risk Index Associated with the Presence of Cerebrovascular Symptoms. Poster presentation at Cardiovascular Theme Research Day: Immunity and Inflammation, Leicester, UK, on 9 May 2014.

## References

1.      Mayer FJ, Gruenberger D, Schillinger M, Mannhalter C, Minar E, Koppensteiner R, et al. Prognostic value of neutrophils in patients with asymptomatic carotid artery disease. Atherosclerosis. 2013;231:274-280.

2.      Libby P. Inflammation in atherosclerosis. Arteriosclerosis Thrombosis and Vascular Biology. 2012;32:2045-2051.

3.      Molloy J, Markus HS. Asymptomatic embolization predicts stroke and TIA risk in patients with carotid artery stenosis. Stroke. 1999;30:1440-1443.

4.      Thrush A, Hartshorne T. Peripheral vascular ultrasound : how, why, and when. 2nd ed. Edinburgh: Churchill Livingstone; 2005.

5.      Hollander M, Bots ML, Sol D, Iglesias A, Koudstaal PJ, Witteman JCM, et al. Carotid plaques increase the risk of stroke and subtypes of cerebral infarction in asymptomatic elderly: the Rotterdam study. Circulation. 2002;105:2872-2877.

6.      Rundek T, Arif H, Boden-albala B, Elkind MS, Paik MC, Sacco RL. Carotid plaque, a subclinical precursor of vascular events: the Northern Manhattan Study. Neurology. 2008;70:1200-1207.

7.      Autret A, Pourcelot L, Saudeau D, Marchal C, Bertrand P, De Boisvilliers S. Stroke risk in patients with carotid stenosis. Lancet. 1987;1:888-890.

8.      Spence JD, Eliasziw M, Dicicco M, Hackam DG, Galil R, Lohmann T. Carotid plaque area: a tool for targeting and evaluating vascular preventive therapy. Stroke. 2002;33:2916-2922.

9.      Ballotta E, Angelini A, Mazzalai F, Piatto G, Toniato A, Baracchini C. Carotid endarterectomy for symptomatic low-grade carotid stenosis. Journal of Vascular Surgery. 2013;59:25-31.

10.     Markus HS, Mackinnon A. Asymptomatic embolization detected by Doppler ultrasound predicts stroke risk in symptomatic carotid artery stenosis. Stroke. 2005;36:971-975.

11.     World Health Organization. The Atlas of Heart Disease and Stroke. 2004.

12.     National Audit Office. Progress in improving stroke care. 2010.

13.     Wolfe C, Rudd T. The Burden of Stroke / Stroke Alliance For Europe.; 2007.

14.     Stroke Association. Stroke Statistics (Factsheet); 2013.

15.     Ingall T. Stroke: incidence, mortality, morbidity and risk. Journal of Insurance Medicine. 2004;36:143-152.

16.     Suri JS, Kathuria C, Molinari F. Atherosclerosis disease management. New York: Springer; 2011.

17.     Underhill HR, Hatsukami TS, Cai J, Yu W, Demarco JK, Polissar NL, et al. A noninvasive imaging approach to assess plaque severity: the carotid atherosclerosis score. American Journal of Neuroradiology. 2010;31:1068-1075.

18.     Watanabe Y, Nagayama M, Suga T, Yoshida K, Yamagata S, Okumura A, et al. Characterization of atherosclerotic plaque of carotid arteries with histopathological correlation: vascular wall MR imaging vs. color Doppler ultrasonography (US). Journal of Magnetic Resonance Imaging. 2008;28:478-485.

19.     Bamford J, Sandercock P, Dennis M, Burn J, Warlow C. Classification and natural history of clinically identifiable subtypes of cerebral infarction. Lancet. 1991;337:1521-1526.

20.     Adams HP, Bendixen BH, Kappelle LJ, Biller J, Love BB, Gordon DL, et al. Classification of subtype of acute ischemic stroke. Definitions for use in a multicenter clinical trial. TOAST. Trial of Org 10172 in Acute Stroke Treatment. Stroke. 1993;24:35-41.

21.     Hill MD, Yiannakoulias N, Jeerakathil T, Tu JV, Svenson LW, Schopflocher DP. The high risk of stroke immediately after transient ischemic attack: a population-based study. Neurology. 2004;62:2015-2020.

22.     Lovett JK, Dennis MS, Sandercock PAG, Bamford J, Warlow CP, Rothwell PM. Very early risk of stroke after a first transient ischemic attack. Stroke. 2003;34:E138-e140.

23.     Johnston SC, Rothwell PM, Nguyen-huynh MN, Giles MF, Elkins JS, Bernstein AL, et al. Validation and refinement of scores to predict very early stroke risk after transient ischaemic attack. Lancet. 2007;369:283-292.

24.     Khashram M, Vasudevan TM, Donnell A, Lewis DR. Correlation of the ABCD2 score with the Degree of Internal Carotid Artery Stenosis: An Observational Pilot Study. Annals of Vascular Surgery. 2013.

25.     Wolfe CD. The impact of stroke. British Medical Bulletin. 2000;56:275-286.

26.     Von Sarnowski B, Schminke U, Tatlisumak T, Putaala J, Grittner U, Kaps M, et al. Prevalence of stenoses and occlusions of brain-supplying arteries in young stroke patients. Neurology. 2013;80:1287-1294.

27.     Gemmete JJ, Davagnanam I, Toma AK, Brew S, Ganesan V. Arterial ischemic stroke in children. Neuroimaging Clinics of North America. 2013;23:781-798.

28.     Sacco RL. Newer risk factors for stroke. Neurology. 2001;57:S31-S34.

29.     Van Den Oord SCH, Van Der Burg J, Akkus Z, Bosch JG, Van Domburg RT, Sijbrands EJG, et al. Impact of gender on the density of intraplaque neovascularization: A quantitative contrast-enhanced ultrasound study. Atherosclerosis. 2014;233:461-466.

30.     Elkind MS, Sacco RL. Stroke risk factors and stroke prevention. Seminars in Neurology. 1999;18:429-440.

31.     Misita CP, Moll S. Antiphospholipid antibodies. Circulation. 2005;112:E39-e44.

32.     Brey RL, Stallworth CL, McGlasson DL, Wozniak MA, Wityk RJ, Stern BJ, et al. Antiphospholipid antibodies and stroke in young women. Stroke. 2002;33:2396-2400.

33.     Brey RL. Antiphospholipid antibodies in young adults with stroke. Journal of Thrombosis and Thrombolysis. 2005;20:105-112.

34.     Homocysteine Studies Collaboration. Homocysteine and risk of ischemic heart disease and stroke: a meta-analysis. Journal of the American Medical Association. 2002;288:2015-2022.

35.     Lindsberg PJ, Grau AJ. Inflammation and infections as risk factors for ischemic stroke. Stroke. 2003;34:2518-2532.

36.     Marnane M, Prendeville S, McDonnell C, Noone I, Barry M, Crowe M, et al. Plaque Inflammation and Unstable Morphology Are Associated With Early Stroke Recurrence in Symptomatic Carotid Stenosis. Stroke. 2014.

37.     Rocque BG, Jackson D, Varghese T, Hermann B, McCormick M, Kliewer M, et al. Impaired cognitive function in patients with atherosclerotic carotid stenosis and correlation with ultrasound strain measurements. Journal of the Neurological Sciences. 2013;322:20-24.

38.     North American Symptomatic Carotid Endarterectomy Trial Collaborators. Beneficial effect of carotid endarterectomy in symptomatic patients with high-grade carotid stenosis. The New England Journal of Medicine. 1991;325:445-453.

39.     European Carotid Surgery Trialists' Collaborative Group. MRC European Carotid Surgery Trial: interim results for symptomatic patients with severe (70-99%) or with mild (0-29%) carotid stenosis. Lancet. 1991;337:1235-1243.

40.     Williams MA, Nicolaides AN. Predicting the normal dimensions of the internal and external carotid arteries from the diameter of the common carotid. European Journal of Vascular Surgery. 1987;1:91-96.

41.     Bladin CF, Alexandrov AV, Murphy J, Maggisano R, Norris JW. Carotid Stenosis Index. A new method of measuring internal carotid artery stenosis. Stroke. 1995;26:230-234.

42.     Cumming MJ, Morrow IM. Carotid artery stenosis: a prospective comparison of CT angiography and conventional angiography. AJR. American Journal of Roentgenology. 1994;163:517-523.

43.     Rothwell PM, Gibson RJ, Slattery J, Sellar RJ, Warlow CP. Equivalence of measurements of carotid stenosis. A comparison of three methods on 1001 angiograms. European Carotid Surgery Trialists' Collaborative Group. Stroke. 1994;25:2435-2439.

44.     Beach KW, Bergelin RO, Leotta DF, Primozich JF, Sevareid PM, Stutzman ET, et al. Standardized ultrasound evaluation of carotid stenosis for clinical trials: University of Washington Ultrasound Reading Center. Cardiovascular Ultrasound. 2010;8:39.

45.     Moneta GL, Edwards JM, Chitwood RW, Taylor LM, Lee RW, Cummings CA, et al. Correlation of North American Symptomatic Carotid Endarterectomy Trial (NASCET) angiographic definition of 70% to 99% internal carotid artery stenosis with duplex scanning. Journal of Vascular Surgery. 1993;17:152-157.

46.     Zierler RE, Strandness DE. Standness's duplex scanning in vascular disorders. 4th ed. Philadelphia, London: Lippincott Williams & Wilkins; 2010.

47.     Oates CP, Naylor AR, Hartshorne T, Charles SM, Fail T, Humphries K, et al. Joint recommendations for reporting carotid ultrasound investigations in the United Kingdom. European Journal of Vascular and Endovascular Surgery. 2008;37:251-261.

48.     Carnicelli AP, Stone JJ, Doyle A, Chowdhry AK, Mix D, Ellis J, et al. Cross-sectional area for the calculation of carotid artery stenosis on computed tomographic angiography. Journal of Vascular Surgery. 2013;58:659-665.

49.     Stary HC, Chandler AB, Glagov S, Guyton JR, Insull W, Rosenfeld ME, et al. A definition of initial, fatty streak, and intermediate lesions of atherosclerosis. A report from the Committee on Vascular Lesions of the Council on Arteriosclerosis, American Heart Association. Circulation. 1994;89:2462-2478.

50.     Stary HC, Chandler AB, Dinsmore RE, Fuster V, Glagov S, Insull W, et al. A definition of advanced types of atherosclerotic lesions and a histological classification of atherosclerosis. A report from the Committee on Vascular Lesions of the Council on Arteriosclerosis, American Heart Association. Circulation. 1995;92:1355-1374.

51.     Salem MK, Sayers RD, Bown MJ, West K, Moore D, Nicolaides A, et al. Patients with recurrent ischaemic events from carotid artery disease have a large lipid core and low GSM. European Journal of Vascular and Endovascular Surgery. 2012;43:147-153.

52.     Baroncini LAV, Filho AP, Ramos SG, Martins AR, Murta LO. Histological composition and progression of carotid plaque. Thrombosis Journal. 2007;5:4.

53.     European Carotid Plaque Study Group. Carotid artery plaque composition--relationship to clinical presentation and ultrasound B-mode imaging. European Journal of Vascular and Endovascular Surgery. 1995;10:23-30.

54.     Rakebrandt F, Crawford DC, Havard D, Coleman D, Woodcock JP. Relationship between ultrasound texture classification images and histology of atherosclerotic plaque. Ultrasound in Medicine & Biology. 2001;26:1393-1402.

55.     Golledge J, Greenhalgh RM, Davies AH. The symptomatic carotid plaque. Stroke. 2000;31:774-781.

56.     Saam T, Hetterich H, Hoffmann V, Yuan C, Dichgans M, Poppert H, et al. Meta-analysis and systematic review of the predictive value of carotid plaque hemorrhage on cerebrovascular events by magnetic resonance imaging. Journal of the American College of Cardiology. 2013;62:1081-1091.

57.     Ijäs P, Saksi J, Soinne L, Tuimala J, Jauhiainen M, Jula A, et al. Haptoglobin 2 allele associates with unstable carotid plaque and major cardiovascular events. Atherosclerosis. 2013;230:228-234.

58.     Nighoghossian N, Derex L, Douek P. The vulnerable carotid artery plaque: current imaging methods and new perspectives. Stroke. 2005;36:2764-2772.

59.     Carr S, Farb A, Pearce WH, Virmani R, Yao JS. Atherosclerotic plaque rupture in symptomatic carotid artery stenosis. Journal of Vascular Surgery. 1996;23:755-n 765.

60.     Woodcock JP. Characterisation of the atheromatous plaque in the carotid arteries. Clinical Physics and Physiological Measurement. 1989;10 Suppl A:45-49.

61.     Iannuzzi A, Wilcosky T, Mercuri M, Rubba P, Bryan FA, Bond MG. Ultrasonographic correlates of carotid atherosclerosis in transient ischemic attack and stroke. Stroke. 1995;26:614-619.

62.     Heiland VM, Forsell C, Roy J, Hedin U, Gasser TC. Identification of carotid plaque tissue properties using an experimental-numerical approach. Journal of the Mechanical Behavior of Biomedical Materials. 2013;27:226-238.

63. Rothwell PM, Villagra R, Gibson R, Donders RC, Warlow CP. Evidence of a chronic systemic cause of instability of atherosclerotic plaques. Lancet. 2000;355:19-24.

64. Hellings WE, Moll FL, De Kleijn DPV, Pasterkamp G. 10-years experience with the Athero-Express study. Cardiovascular Diagnosis and Therapy. 2012.

65. Hellings WE, Peeters W, Moll FL, Piers SRD, Van Setten J, Van Spek D, et al. Composition of carotid atherosclerotic plaque is associated with cardiovascular outcome: a prognostic study. Circulation. 2010;121:1941-1950.

66. Dunmore BJ, McCarthy MJ, Naylor AR, Brindle NPJ. Carotid plaque instability and ischemic symptoms are linked to immaturity of microvessels within plaques. Journal of Vascular Surgery. 2007;45:155-159.

67. Shah PK. Molecular mechanisms of plaque instability. Current Opinion in Lipidology. 2007;18:492-499.

68. Clarke MCH, Figg N, Maguire JJ, Davenport AP, Goddard M, Littlewood TD, et al. Apoptosis of vascular smooth muscle cells induces features of plaque vulnerability in atherosclerosis. Nature Medicine. 2006;12:1075-1080.

69. Clarke MCH, Littlewood TD, Figg N, Maguire JJ, Davenport AP, Goddard M, et al. Chronic apoptosis of vascular smooth muscle cells accelerates atherosclerosis and promotes calcification and medial degeneration. Circulation Research. 2008;102:1529-1538.

70. Bennett MR. Apoptosis of vascular smooth muscle cells in vascular remodelling and atherosclerotic plaque rupture. Cardiovascular Research. 1999;41:361-368.

71. Yu E, Calvert PA, Mercer JR, Harrison J, Baker L, Figg NL, et al. Mitochondrial DNA damage can promote atherosclerosis independently of reactive oxygen species through effects on smooth muscle cells and monocytes and correlates with higher-risk plaques in humans. Circulation. 2013;128:702-712.

72. Hankey GJ, Warlow CP, Sellar RJ. Cerebral angiographic risk in mild cerebrovascular disease. Stroke. 1990;21:209-222.

73. Gomez CR. Carotid plaque morphology and risk for stroke. Stroke. 1990;21:148-151.

74. Houser OW, Sundt TM, Holman CB, Sandok BA, Burton RC. Atheromatous disease of the carotid artery. Correlation of angiographic, clinical, and surgical findings. Journal of Neurosurgery. 1974;41:321-331.

75. Croft RJ, Ellam LD, Harrison MJ. Accuracy of carotid angiography in the assessment of atheroma of the internal carotid artery. Lancet. 1980;1:997-1000.

76. Eikelboom BC, Riles TR, Mintzer R, Baumann FG, Defillip G, Lin J, et al. Inaccuracy of angiography in the diagnosis of carotid ulceration. Stroke. 1983;14:882-885.

77. Schaar JA, Mastik F, Regar E, Uil D, Cornelis A, Gijsen FJ, et al. Current diagnostic modalities for vulnerable plaque detection. Current Pharmaceutical Design. 2007;13:995-1001.

78. Xu D, Hippe DS, Underhill HR, Oikawa-wakayama M, Dong L, Yamada K, et al. Prediction of High-Risk Plaque Development and Plaque Progression With the Carotid Atherosclerosis Score. JACC. Cardiovascular Imaging. 2014.

79. Chu B, Kampschulte A, Ferguson MS, Kerwin WS, Yarnykh VL, Brien KD, et al. Hemorrhage in the atherosclerotic carotid plaque: a high-resolution MRI study. Stroke. 2004;35:1079-1084.

80. Li Z, Howarth SPS, Tang T, Graves MJ, U-king-im J, Trivedi RA, et al. Structural analysis and magnetic resonance imaging predict plaque vulnerability: a study comparing symptomatic and asymptomatic individuals. Journal of Vascular Surgery. 2007;45:768-775.

81. Hatsukami TS, Ross R, Polissar NL, Yuan C. Visualization of fibrous cap thickness and rupture in human atherosclerotic carotid plaque in vivo with high-resolution magnetic resonance imaging. Circulation. 2000;102:959-964.

82. Geroulakos G, Ramaswami G, Nicolaides A, James K, Labropoulos N, Belcaro G, et al. Characterization of symptomatic and asymptomatic carotid plaques using high-resolution real-time ultrasonography. The British Journal of Surgery. 1993;80:1274-1277.

83. Balu N, Chu B, Hatsukami TS, Yuan C, Yarnykh VL. Comparison between 2D and 3D high-resolution black-blood techniques for carotid artery wall imaging in clinically significant atherosclerosis. Journal of Magnetic Resonance Imaging. 2008;27:918-924.

84. Fayad ZA, Fuster V. Clinical imaging of the high-risk or vulnerable atherosclerotic plaque. Circulation Research. 2001;89:305-316.

85. Van Der Meer FJ, Faber DJ, Perrée J, Pasterkamp G, Baraznji Sassoon D, Van Leeuwen TG. Quantitative optical coherence tomography of arterial wall components. Lasers in Medical Science. 2005;20:45-51.

86.     Yabushita H, Bouma BE, Houser SL, Aretz HT, Jang I, Schlendorf KH, et al. Characterization of human atherosclerosis by optical coherence tomography. Circulation. 2002;106:1640-1645.

87.     Graebe M, Pedersen SF, Højgaard L, Kjaer A, Sillesen H. 18FDG PET and ultrasound echolucency in carotid artery plaques. JACC. Cardiovascular Imaging. 2010;3:289-295.

88.     Tawakol A, Fayad ZA, Mogg R, Alon A, Klimas MT, Dansky H, et al. Intensification of statin therapy results in a rapid reduction in atherosclerotic inflammation: results of a multicenter fluorodeoxyglucose-positron emission tomography/computed tomography feasibility study. Journal of the American College of Cardiology. 2013;62:909-917.

89.     Schaar JA, Regar E, Mastik F, McFadden EP, Saia F, Disco C, et al. Incidence of high-strain patterns in human coronary arteries: assessment with three-dimensional intravascular palpography and correlation with clinical presentation. Circulation. 2004;109:2716-2719.

90.     Schaar JA, Van Der Steen AFW, Mastik F, Baldewsing RA, Serruys PW. Intravascular palpography for vulnerable plaque assessment. Journal of the American College of Cardiology. 2006;47:C86-C91.

91.     Baldewsing RA, Schaar JA, De Korte CL, Mastik F, Serruys PW, Van Steen D, et al. Intravascular Ultrasound Elastography: A Clinician's Tool for Assessing Vulnerability and Material Composition of Plaques. Studies in Health Technology and Informatics. 2005;113:75-96.

92.     Schaar JA, De Korte CL, Mastik F, Baldewsing R, Regar E, De Feyter P, et al. Intravascular palpography for high-risk vulnerable plaque assessment. Herz. 2003;28:488-495.

93.     McCormick M, Varghese T, Wang X, Mitchell C, Kliewer MA, Dempsey RJ. Methods for robust in vivo strain estimation in the carotid artery. Physics in Medicine and Biology. 2012;57:7329-7353.

94.     Shi H, Mitchell CC, McCormick M, Kliewer MA, Dempsey RJ, Varghese T. Preliminary in vivo atherosclerotic carotid plaque characterization using the accumulated axial strain and relative lateral shift strain indices. Physics in Medicine and Biology. 2008;53:6377-6394.

95.     Allen JD, Ham KL, Dumont DM, Sileshi B, Trahey GE, Dahl JJ. The development and potential of acoustic radiation force impulse (ARFI) imaging for carotid artery plaque characterization. Vascular Medicine. 2011;16:302-311.

96.     Couade M, Pernot M, Prada C, Messas E, Emmerich J, Bruneval P, et al. Quantitative assessment of arterial wall biomechanical properties using shear wave imaging. Ultrasound in Medicine & Biology. 2011;36:1662-1676.

97.     Ramnarine KV, Hartshorne T, Sensier Y, Naylor M, Walker J, Naylor AR, et al. Tissue Doppler imaging of carotid plaque wall motion: a pilot study. Cardiovascular Ultrasound. 2003.

98.     Jansen K, Van Soest G, Van Der Steen AFW. Intravascular Photoacoustic Imaging: A New Tool for Vulnerable Plaque Identification. Ultrasound in Medicine and Biology. 2014.

99.     Wang B, Karpiouk A, Yeager D, Amirian J, Litovsky S, Smalling R, et al. In vivo intravascular ultrasound-guided photoacoustic imaging of lipid in plaques using an animal model of atherosclerosis. Ultrasound in Medicine & Biology. 2013;38:2098-2103.

100.    Jansen K, Van Der Steen AFW, Van Beusekom HMM, Oosterhuis JW, Van Soest G. Intravascular photoacoustic imaging of human coronary atherosclerosis. Optics Letters. 2011;36:597-599.

101.    Sethuraman S, Aglyamov SR, Smalling RW, Emelianov SY. Remote temperature estimation in intravascular photoacoustic imaging. Ultrasound in Medicine & Biology. 2007;34:299-308.

102.    Emelianov S, Wang B, Su J, Karpiouk A, Yantsen E, Sokolov K, et al. Intravascular ultrasound and photoacoustic imaging. Proceedings of the IEEE Engineering in Medicine and Biology Society. 2009;2008:2-5.

103.    Jansen K, Wu M, Van Der Steen AFW, Van Soest G. Lipid detection in atherosclerotic human coronaries by spectroscopic intravascular photoacoustic imaging. Optics Express. 2013;21:21472-21484.

104.    Karpiouk AB, Wang B, Amirian J, Smalling RW, Emelianov SY. Feasibility of in vivo intravascular photoacoustic imaging using integrated ultrasound and photoacoustic imaging catheter. Journal of Biomedical Optics. 2013;17:96008-96001.

105.    Allen TJ, Hall A, Dhillon AP, Owen JS, Beard PC. Spectroscopic photoacoustic imaging of lipid-rich plaques in the human aorta in the 740 to 1400 nm wavelength range. Journal of Biomedical Optics. 2012;17:061209.

106.     Sethuraman S, Amirian JH, Litovsky SH, Smalling RW, Emelianov SY. Ex vivo Characterization of Atherosclerosis using Intravascular Photoacoustic Imaging. Optics Express. 2007;15:16657-16666.

107.     Wang B, Su JL, Amirian J, Litovsky SH, Smalling R, Emelianov S. Detection of lipid in atherosclerotic vessels using ultrasound-guided spectroscopic intravascular photoacoustic imaging. Optics Express. 2010;18:4889-4897.

108.     Wang B, Su J, Amirian J, Litovsky SH, Smalling R, Emelianov S. On the possibility to detect lipid in atherosclerotic plaques using intravascular photoacoustic imaging. Proceedings of the IEEE Engineering in Medicine and Biology Society. 2010;2009:4767-4770.

109.     Sethuraman S, Amirian JH, Litovsky SH, Smalling RW, Emelianov SY. Spectroscopic intravascular photoacoustic imaging to differentiate atherosclerotic plaques. Optics Express. 2008;16:3362-3367.

110.     Jansen K, Van Der Steen AFW, Wu M, Van Beusekom HMM, Springeling G, Li X, et al. Spectroscopic intravascular photoacoustic imaging of lipids in atherosclerosis. Journal of Biomedical Optics. 2014;19:026006.

111.     Wang B, Emelianov S. Thermal intravascular photoacoustic imaging. Biomedical Optics Express. 2011;2:3072-3078.

112.     Barbut D, Yao FS, Lo YW, Silverman R, Hager DN, Trifiletti RR, et al. Determination of size of aortic emboli and embolic load during coronary artery bypass grafting. The Annals of Thoracic Surgery. 1997;63:1262-1267.

113.     Topakian R, King A, Kwon SU, Schaafsma A, Shipley M, Markus HS, et al. Ultrasonic plaque echolucency and emboli signals predict stroke in asymptomatic carotid stenosis. Neurology. 2011;77:751-758.

114.     Wilson LS, Neale ML, Talhami HE, Appleberg M. Preliminary results from attenuation-slope mapping of plaque using intravascular ultrasound. Ultrasound in Medicine & Biology. 1994;20:529-542.

115.     Bridal SL, Fornés P, Bruneval P, Berger G. Correlation of ultrasonic attenuation (30 to 50 MHz and constituents of atherosclerotic plaque. Ultrasound in Medicine & Biology. 1997;23:691-703.

116.     Noritomi T, Sigel B, Swami V, Justin J, Gahtan V, Chen X, et al. Carotid plaque typing by multiple-parameter ultrasonic tissue characterization. Ultrasound in Medicine & Biology. 1997;23:643-650.

117.     Nair A, Kuban BD, Tuzcu EM, Schoenhagen P, Nissen SE, Vince DG. Coronary plaque classification with intravascular ultrasound radiofrequency data analysis. Circulation. 2002;106:2200-2206.

118.     Waters KR, Bridal SL, Cohen-bacrie C, Levrier C, Fornès P, Laugier P. Parametric analysis of carotid plaque using a clinical ultrasound imaging system. Ultrasound in Medicine & Biology. 2003;29:1521-1530.

119.     Shi H, Varghese T, Dempsey RJ, Salamat MS, Zagzebski JA. Relationship between ultrasonic attenuation, size and axial strain parameters for ex vivo atherosclerotic carotid plaque. Ultrasound in Medicine & Biology. 2008;34:1666-1677.

120.     He W, Zhang H, Shi C, Chen J, Gao J. Fly through ultrasound imaging in assessment of carotid atherosclerosis: a pictorial essay. Clinical Imaging. 2013;37:811-820.

121.     Weinstein R. Noninvasive carotid duplex ultrasound imaging for the evaluation and management of carotid atherosclerotic disease. Hematology/Oncology Clinics of North America. 1992;6:1131-1139.

122.     Kingstone LL, Torres C, Currie G. A Systematic Literature Review of Ultrasonography for Morphology and Characterization of Vulnerable Carotid Artery Plaques. Journal for Vascular Ultrasound. 2012;36:191-198.

123.     Geroulakos G, Hobson RW, Nicolaides A. Ultrasonographic carotid plaque morphology in predicting stroke risk. British Journal of Surgery. 1996;83:582-587.

124.     Gray-weale AC, Graham JC, Burnett JR, Byrne K, Lusby RJ. Carotid artery atheroma: comparison of preoperative B-mode ultrasound appearance with carotid endarterectomy specimen pathology. The Journal of Cardiovascular Surgery. 1988;29:676-681.

125.     Lal BK, Hobson RW, Pappas PJ, Kubicka R, Hameed M, Chakhtoura EY, et al. Pixel distribution analysis of B-mode ultrasound scan images predicts histologic features of atherosclerotic carotid plaques. Journal of Vascular Surgery. 2002;35:1210-1217.

126.     Lal BK, Hobson RW, Hameed M, Pappas PJ, Padberg FT, Jamil Z, et al. Noninvasive identification of the unstable carotid plaque. Annals of Vascular Surgery. 2006;20:167-174.

127.    Poepping TL, Rankin RN, Holdsworth DW. Flow patterns in carotid bifurcation models using pulsed Doppler ultrasound: effect of concentric vs. eccentric stenosis on turbulence and recirculation. Ultrasound in Medicine & Biology. 2010;36:1125-1134.

128.    Tsiaparas NN, Golemati S, Andreadis I, Stoitsis J, Valavanis I, Nikita KS. Assessment of carotid atherosclerosis from B-mode ultrasound images using directional multiscale texture features. Measurement Science and Technology. 2012.

129.    Elatrozy T, Nicolaides A, Tegos T, Griffin M. The objective characterisation of ultrasonic carotid plaque features. European Journal of Vascular and Endovascular Surgery. 1998;16:223-230.

130.    Geroulakos G, Domjan J, Nicolaides A, Stevens J, Labropoulos N, Ramaswami G, et al. Ultrasonic carotid artery plaque structure and the risk of cerebral infarction on computed tomography. Journal of Vascular Surgery. 1994;20:263-266.

131.    Tegos TJ, Stavropoulos P, Sabetai MM, Khodabakhsh P, Sassano A, Nicolaides AN. Determinants of carotid plaque instability: echoicity versus heterogeneity. European Journal of Vascular and Endovascular Surgery. 2001;22:22-30.

132.    El-barghouty N, Geroulakos G, Nicolaides A, Androulakis A, Bahal V. Computer-assisted carotid plaque characterisation. European Journal of Vascular and Endovascular Surgery. 1995;9:389-393.

133.    El-barghouty N, Nicolaides A, Bahal V, Geroulakos G, Androulakis A. The identification of the high risk carotid plaque. European Journal of Vascular and Endovascular Surgery. 1996;11:470-478.

134.    Grønholdt ML, Nordestgaard BG, Schroeder TV, Vorstrup S, Sillesen H. Ultrasonic echolucent carotid plaques predict future strokes. Circulation. 2001;104:68-73.

135.    Polak JF, Shemanski L, Leary DH, Lefkowitz D, Price TR, Savage PJ, et al. Hypoechoic plaque at US of the carotid artery: an independent risk factor for incident stroke in adults aged 65 years or older. Cardiovascular Health Study. Radiology. 1998;208:649-654.

136.    Mathiesen EB, Bønaa KH, Joakimsen O. Echolucent plaques are associated with high risk of ischemic cerebrovascular events in carotid stenosis: the tromsø study. Circulation. 2001;103:2171-2175.

137.    Sabetai MM, Tegos TJ, Nicolaides AN, Dhanjil S, Pare GJ, Stevens JM. Reproducibility of computer-quantified carotid plaque echogenicity: can we overcome the subjectivity? Stroke. 2000;31:2189-2196.

138.    Biasi GM, Froio A, Diethrich EB, Deleo G, Galimberti S, Mingazzini P, et al. Carotid plaque echolucency increases the risk of stroke in carotid stenting: the Imaging in Carotid Angioplasty and Risk of Stroke (ICAROS) study. Circulation. 2004;110:756-762.

139.    Pavela J, Ahanchi S, Steerman SN, Higgins JA, Panneton JM. Grayscale median analysis of primary stenosis and restenosis after carotid endarterectomy. Journal of Vascular Surgery. 2013.

140.    Biasi GM, Sampaolo A, Mingazzini P, De Amicis P, El-barghouty N, Nicolaides AN. Computer analysis of ultrasonic plaque echolucency in identifying high risk carotid bifurcation lesions. European Journal of Vascular and Endovascular Surgery. 1999;17:476-479.

141.    Seo Y, Watanabe S, Ishizu T, Moriyama N, Takeyasu N, Maeda H, et al. Echolucent carotid plaques as a feature in patients with acute coronary syndrome. Circulation Journal. 2006;70:1629-1634.

142.    Holdsworth RJ, McCollum PT, Bryce JS, Harrison DK. Symptoms, stenosis and carotid plaque morphology. Is plaque morphology relevant? European Journal of Vascular and Endovascular Surgery. 1995;9:80-85.

143.    Aburahma AF, Wulu JT, Crotty B. Carotid plaque ultrasonic heterogeneity and severity of stenosis. Stroke. 2002;33:1772-1775.

144.    Kardoulas DG, Katsamouris AN, Gallis PT, Philippides TP, Anagnostakos NK, Gorgoyannis DS, et al. Ultrasonographic and histologic characteristics of symptom-free and symptomatic carotid plaque. Cardiovascular Surgery. 1996;4:580-590.

145.    Van Damme H, Vivario M. Pathologic aspects of carotid plaques: surgical and clinical significance. International Angiology. 1993;12:299-311.

146.    Ruiz-ares G, Fuentes B, Martínez-sánchez P, Martínez-martínez M, Díez-tejedor E. Utility of the assessment of echogenicity in the identification of symptomatic carotid artery atheroma plaques in ischemic stroke patients. Cerebrovascular Diseases. 2012;32:535-541.

147.    Elatrozy TS, Zarka ZA, Griffin M, Tegos T, Nicolaides A. The way to standardize reporting on carotid plaque echodensity: application of image processing techniques. Presented at the 8th Mediterranean congress of angiology and vascular surgery, Alexandria, 31 May-3 April 1997.

148.    Elatrozy T, Nicolaides A, Tegos T, Zarka AZ, Griffin M, Sabetai M. The effect of B-mode ultrasonic image standardisation on the echodensity of symptomatic and asymptomatic carotid bifurcation plaques. International Angiology. 1998;17:179-186.

149.    De Bray JM, Baud JM, Dauzat M. Consensus Concerning the Morphology and the Risk of Carotid Plaques. Cerebrovascular Diseases. 1997;7:289-296.

150.    Van Swijndregt ADM, Elbers HRJ, Moll FL, De Letter J, Ackerstaff RGA. Ultrasonographic characterization of carotid plaques. Ultrasound in Medicine and Biology. 1998;24:489-493.

151.    Joakimsen O, Bønaa KH, Stensland-bugge E. Reproducibility of ultrasound assessment of carotid plaque occurrence, thickness, and morphology. The Tromsø Study. Stroke. 1997;28:2201-2207.

152.    Wilhjelm JE, Grønholdt ML, Wiebe B, Jespersen SK, Hansen LK, Sillesen H. Quantitative analysis of ultrasound B-mode images of carotid atherosclerotic plaque: correlation with visual classification and histological examination. IEEE Transactions on Medical Imaging. 1999;17:910-922.

153.    Christodoulou CI, Pattichis CS, Pantziaris M, Nicolaides A. Texture-based classification of atherosclerotic carotid plaques. IEEE Transactions on Medical Imaging. 2003;22:902-912.

154.    Golemati S, Tegos TJ, Sassano A, Nikita KS, Nicolaides AN. Echogenicity of B-mode sonographic images of the carotid artery: work in progress. Journal of Ultrasound in Medicine. 2004;23:659-669.

155.    Lind L, Andersson J, Rönn M, Gustavsson T. The echogenecity of the intima-media complex in the common carotid artery is closely related to the echogenecity in plaques. Atherosclerosis. 2007;195:411-414.

156.    Droste DW, Karl M, Bohle RM, Kaps M. Comparison of ultrasonic and histopathological features of carotid artery stenosis. Neurological Research. 1997;19:380-384.

157.    Grønholdt ML, Wiebe BM, Laursen H, Nielsen TG, Schroeder TV, Sillesen H. Lipid-rich carotid artery plaques appear echolucent on ultrasound B-mode images and may be associated with intraplaque haemorrhage. European Journal of Vascular and Endovascular Surgery. 1998;14:439-445.

158.    Golledge J, Cuming R, Ellis M, Davies AH, Greenhalgh RM. Carotid plaque characteristics and presenting symptom. British Journal of Surgery. 1998;84:1697-1701.

159.	Liapis CD, Kakisis JD, Kostakis AG. Carotid stenosis: factors affecting symptomatology. Stroke. 2001;32:2782-2786.

160.	Grogan JK, Shaalan WE, Cheng H, Gewertz B, Desai T, Schwarze G, et al. B-mode ultrasonographic characterization of carotid atherosclerotic plaques in symptomatic and asymptomatic patients. Journal of Vascular Surgery. 2005;42:435-441.

161.	Kalogeropoulos A, Terzis G, Chrysanthopoulou A, Hahalis G, Siablis D, Alexopoulos D. Risk for transient ischemic attacks is mainly determined by intima-media thickness and carotid plaque echogenicity. Atherosclerosis. 2006;192:190-196.

162.	Ding S, Zhang M, Zhao Y, Chen W, Yao G, Zhang C, et al. The role of carotid plaque vulnerability and inflammation in the pathogenesis of acute ischemic stroke. The American Journal of the Medical Sciences. 2008;336:27-31.

163.	Rosenkranz M, Wittkugel O, Waiblinger C, Thomalla G, Krutzelmann A, Havemeister S, et al. Cerebral embolism during carotid artery stenting: role of carotid plaque echolucency. Cerebrovascular Diseases. 2009;27:443-449.

164.	Dósa E, Hirschberg K, Apor A, Járányi Z, Entz L, Acsády G, et al. Echolucent or predominantly echolucent femoral plaques predict early restenosis after eversion carotid endarterectomy. Journal of Vascular Surgery. 2010;51:345-350.

165.	Staub D, Partovi S, Schinkel AFL, Coll B, Uthoff H, Aschwanden M, et al. Correlation of carotid artery atherosclerotic lesion echogenicity and severity at standard US with intraplaque neovascularization detected at contrast-enhanced US. Radiology. 2011;258:618-626.

166.	Kolkert JL, Meerwaldt R, Loonstra J, Schenk M, Van Der Palen J, Van Dungen D, et al. Relation between B-mode Gray-scale Median and Clinical Features of Carotid Stenosis Vulnerability. Annals of Vascular Surgery. 2013.

167.	Irie Y, Katakami N, Kaneto H, Takahara M, Nishio M, Kasami R, et al. The utility of ultrasonic tissue characterization of carotid plaque in the prediction of cardiovascular events in diabetic patients. Atherosclerosis. 2013;230:399-405.

168.	Singh AS, Atam V, Jain N, Yathish BE, Patil MR, Das L. Association of carotid plaque echogenicity with recurrence of ischemic stroke. North American Journal of Medical Sciences. 2013;5:371-376.

169.	Moore WS, Boren C, Malone JM, Roon AJ, Eisenberg R, Goldstone J, et al. Natural history of nonstenotic, asymptomatic ulcerative lesions of the carotid artery. Archives of Surgery. 1978;113:1352-1359.

170. Fisher M, Paganini-hill A, Martin A, Cosgrove M, Toole JF, Barnett HJM, et al. Carotid plaque pathology: thrombosis, ulceration, and stroke pathogenesis. Stroke. 2005;36:253-257.

171. Sitzer M, Müller W, Siebler M, Hort W, Kniemeyer HW, Jäncke L, et al. Plaque ulceration and lumen thrombus are the main sources of cerebral microemboli in high-grade internal carotid artery stenosis. Stroke. 1995;26:1231-1233.

172. Aburahma AF, Kyer PD, Robinson PA, Hannay RS. The correlation of ultrasonic carotid plaque morphology and carotid plaque hemorrhage: clinical implications. Surgery. 1998;124:721-n 726.

173. Kuk M, Wannarong T, Beletsky V, Parraga G, Fenster A, Spence JD. Volume of Carotid Artery Ulceration as a Predictor of Cardiovascular Events. Stroke. 2014.

174. Prati P, Tosetto A, Casaroli M, Bignamini A, Canciani L, Bornstein N, et al. Carotid plaque morphology improves stroke risk prediction: usefulness of a new ultrasonographic score. Cerebrovascular Diseases. 2011;31:300-304.

175. Handa N, Matsumoto M, Maeda H, Hougaku H, Kamada T. Ischemic stroke events and carotid atherosclerosis. Results of the Osaka Follow-up Study for Ultrasonographic Assessment of Carotid Atherosclerosis (the OSACA Study). Stroke. 1995;26:1781-1786.

176. Eliasziw M, Streifler JY, Fox AJ, Hachinski VC, Ferguson GG, Barnett HJ. Significance of plaque ulceration in symptomatic patients with high-grade carotid stenosis. North American Symptomatic Carotid Endarterectomy Trial. Stroke. 1994;25:304-308.

177. Rothwell PM, Gibson R, Warlow CP. Interrelation between plaque surface morphology and degree of stenosis on carotid angiograms and the risk of ischemic stroke in patients with symptomatic carotid stenosis. On behalf of the European Carotid Surgery Trialists' Collaborative Group. Stroke. 2000;31:615-621.

178. Rosenkranz M, Russjan A, Goebell E, Havemeister S, Thomalla G, Cheng B, et al. Carotid plaque surface irregularity predicts cerebral embolism during carotid artery stenting. Cerebrovascular Diseases. 2012;32:163-169.

179. Pedro LM, Fernandes J, Pedro MM, Gonçalves I, Dias NV, Fernandes R, et al. Ultrasonographic risk score of carotid plaques. European Journal of Vascular and Endovascular Surgery. 2002;24:492-498.

180.    Carra G, Visonà A, Bonanome A, Lusiani L, Pesavento R, Bortolon M, et al. Carotid plaque morphology and cerebrovascular events. International Angiology. 2003;22:284-289.

181.    Ten Kate GL, Van Dijk AC, Van Den Oord SCH, Hussain B, Verhagen HJM, Sijbrands EJG, et al. Usefulness of contrast-enhanced ultrasound for detection of carotid plaque ulceration in patients with symptomatic carotid atherosclerosis. The American Journal of Cardiology. 2013;112:292-298.

182.    Barry R, Pienaar C, Nel CJ. Accuracy of B-mode ultrasonography in detecting carotid plaque hemorrhage and ulceration. Annals of Vascular Surgery. 1990;4:466-470.

183.    Bluth EI, McVay LV, Merritt CR, Sullivan MA. The identification of ulcerative plaque with high resolution duplex carotid scanning. Journal of Ultrasound in Medicine. 1988;7:73-76.

184.    Hennerici M, Baezner H, Daffertshofer M. Ultrasound and arterial wall disease. Cerebrovascular Diseases. 2003;17 Suppl 1:19-33.

185.    Stoitsis J, Golemati S, Nikita KS, Nicolaides AN. Characterization of carotid atherosclerosis based on motion and texture features and clustering using fuzzy c-means. Proceedings of the IEEE Engineering in Medicine and Biology Society. 2007;2:1407-1410.

186.    Asvestas P, Golemati S, Matsopoulos GK, Nikita KS, Nicolaides AN. Fractal dimension estimation of carotid atherosclerotic plaques from B-mode ultrasound: a pilot study. Ultrasound in Medicine & Biology. 2002;28:1129-1136.

187.    Kakkos SK, Griffin MB, Nicolaides AN, Kyriacou E, Sabetai MM, Tegos T, et al. The size of juxtaluminal hypoechoic area in ultrasound images of asymptomatic carotid plaques predicts the occurrence of stroke. Journal of Vascular Surgery. 2013;57:609-618.

188.    Acharya UR, Sree SV, Krishnan MMR, Molinari F, Saba L, Ho SYS, et al. Atherosclerotic risk stratification strategy for carotid arteries using texture-based features. Ultrasound in Medicine & Biology. 2012;38:899-915.

189.    Tsiaparas NN, Golemati S, Andreadis I, Stoitsis JS, Valavanis I, Nikita KS. Comparison of multiresolution features for texture classification of carotid atherosclerosis from B-mode ultrasound. IEEE Transactions on Information Technology in Biomedicine. 2011;15:130-137.

190.    Mougiakakou SGR, Golemati S, Gousias I, Nicolaides AN, Nikita KS. Computer-aided diagnosis of carotid atherosclerosis based on ultrasound image statistics, laws' texture and neural networks. Ultrasound in Medicine & Biology. 2006;33:26-36.

191.    Thornhill RE, Lum C, Jaberi A, Stefanski P, Torres CH, Momoli F, et al. Can Shape Analysis Differentiate Free-floating Internal Carotid Artery Thrombus from Atherosclerotic Plaque in Patients Evaluated with CTA for Stroke or Transient Ischemic Attack? Academic Radiology. 2014;21:345-354.

192.    Sztajzel R, Momjian S, Momjian-mayor I, Murith N, Djebaili K, Boissard G, et al. Stratified gray-scale median analysis and color mapping of the carotid plaque: correlation with endarterectomy specimen histology of 28 patients. Stroke. 2005;36:741-745.

193.    Ogata J, Masuda J, Yutani C, Yamaguchi T. Rupture of atheromatous plaque as a cause of thrombotic occlusion of stenotic internal carotid artery. Stroke. 1990;21:1740-1745.

194.    Moon WK, Lo C, Huang C, Chen J, Chang R. Computer-aided diagnosis based on speckle patterns in ultrasound images. Ultrasound in Medicine & Biology. 2012;38:1251-1261.

195.    Zhang PF, Su HJ, Yao GH, Wu W, Zhang M, Liu CX, et al. Plaque volume compression ratio, a novel biomechanical index, is independently associated with ischemic cerebrovascular events. Journal of Hypertension. 2009;27:348-356.

196.    Golemati S, Sassano A, Lever MJ, Bharath AA, Dhanjil S, Nicolaides AN. Carotid artery wall motion estimated from B-mode ultrasound using region tracking and block matching. Ultrasound in Medicine & Biology. 2003;29:387-399.

197.    Bang J, Dahl T, Bruinsma A, Kaspersen JH, Nagelhus Hernes TA, Myhre HO. A new method for analysis of motion of carotid plaques from RF ultrasound images. Ultrasound in Medicine & Biology. 2003;29:967-976.

198.    Kashiwazaki D, Yoshimoto T, Mikami T, Muraki M, Fujimoto S, Abiko K, et al. Identification of high-risk carotid artery stenosis: motion of intraplaque contents detected using B-mode ultrasonography. Journal of Neurosurgery. 2013;117:574-578.

199.    Chan KL. Two approaches to motion analysis of the ultrasound image sequence of carotid atheromatous plaque. Ultrasonics. 1993;31:117-123.

200.    Meairs S, Hennerici M. Four-dimensional ultrasonographic characterization of plaque surface motion in patients with symptomatic and asymptomatic carotid artery stenosis. Stroke. 1999;30:1807-1813.

201.    Dahl T, Bang J, Ushakova A, Lydersen S, Myhre HO. Parameters describing motion in carotid artery plaques from ultrasound examination: A reproducibility study. Ultrasound in Medicine & Biology. 2004;30:1133-1143.

202.    Akkus Z, Ramnarine KV. Dynamic assessment of carotid plaque motion. Ultrasound. 2010;18:140-147.

203.    Momjian-mayor I, Kuzmanovic I, Momjian S, Bonvin C, Albanese S, Bichsel D, et al. Accuracy of a novel risk index combining degree of stenosis of the carotid artery and plaque surface echogenicity. Stroke. 2012;43:1260-1265.

204.    Tahmasebpour HR, Buckley AR, Cooperberg PL, Fix CH. Sonographic examination of the carotid arteries. Radiographics. 2005;25:1561-1575.

205.    Martin AJ, Ryan LK, Gotlieb AI, Henkelman RM, Foster FS. Arterial imaging: comparison of high-resolution US and MR imaging with histologic correlation. Radiographics. 1997;17:189-202.

206.    Naylor AR. You May Delay, but Time Will Not. Stroke. 2014.

207.    Webb S. The Physics of medical imaging. Institute of Physics Publishing; 1988.

208.    McGahan JP, Goldberg BB. Diagnostic ultrasound. 2nd ed. New York; London: Informa Healthcare; 2008.

209.    Wells PNT. Physical principles of ultrasonic diagnosis. London: Academic Press; 1969.

210.    Duck FA, Baker AC, Starritt HC. Ultrasound in medicine. Philadelphia, Pa: Institute of Physics Publishing; 1998.

211.    Culjat MO, Goldenberg D, Tewari P, Singh RS. A review of tissue substitutes for ultrasound imaging. Ultrasound in Medicine & Biology. 2010;36:861-873.

212.    Laland J. US data for solids (web resource: http://traktoria.org/files/sonar/passive_materials/acoustic_impedace_of_some_solids.htm).

213.    European Federation of Societies for Ultrasound in Medicine. Safety of ultrasound. Journal of Perinatal Medicine. 1984;12:289-290.

214.    Bromer RH, Mitchell JB, Soares N. Response of human hematopoietic precursor cells (CFUc) to hyperthermia and radiation. Cancer Research. 1982;42:1261-1265.

215.    World Federation for Ultrasound in Medicine. WFUMB Symposium on Safety of Ultrasound in Medicine: Conclusions and recommendations on thermal and non-thermal mechanisms for biological effects of ultrasound. Ultrasound in Medicine & Biology. 1998;24:1-55.

216.    Safety Group of the British Medical Ultrasound Society. Guidelines for the safe use of diagnostic ultrasound equipment. BMUS Bulletin. 2000.

217.    Kanber B, Ramnarine KV. A Probabilistic Approach to Computerized Tracking of Arterial Walls in Ultrasound Image Sequences. ISRN Signal Processing. 2012.

218.    Selzer RH, Mack WJ, Lee PL, Kwong-fu H, Hodis HN. Improved common carotid elasticity and intima-media thickness measurements from computer analysis of sequential ultrasound frames. Atherosclerosis. 2001;154:185-193.

219.    Wendelhag I, Liang Q, Gustavsson T, Wikstrand J. A new automated computerized analyzing system simplifies readings and reduces the variability in ultrasound measurement of intima-media thickness. Stroke. 1997;28:2195-2200.

220.    Beux F, Carmassi S, Salvetti MV, Ghiadoni L, Huang Y, Taddei S, et al. Automatic evaluation of arterial diameter variation from vascular echographic images. Ultrasound in Medicine & Biology. 2002;27:1621-1629.

221.    Cheng D, Schmidt-trucksäss A, Cheng K, Burkhardt H. Using snakes to detect the intimal and adventitial layers of the common carotid artery wall in sonographic images. Computer Methods and Programs in Biomedicine. 2002;67:27-37.

222.    Newey VR, Nassiri DK. Online artery diameter measurement in ultrasound images using artificial neural networks. Ultrasound in Medicine & Biology. 2002;28:209-216.

223.    Chen C, Chou Y, Chen CSK, Cheng J, Ou Y, Yeh F, et al. Cell-competition algorithm: a new segmentation algorithm for multiple objects with irregular boundaries in ultrasound images. Ultrasound in Medicine & Biology. 2005;31:1647-1664.

224.    Hii A, Hann CE, Chase JG, Van Houten EEW. Fast normalized cross correlation for motion tracking using basis functions. Computer Methods and Programs in Biomedicine. 2006;82:144-156.

225.    Cardinal MR, Meunier J, Soulez G, Maurice RL, Therasse E, Cloutier G. Intravascular ultrasound image segmentation: a three-dimensional fast-marching method based on gray level distributions. IEEE Transactions on Medical Imaging. 2006.

226.    Golemati S, Stoitsis J, Sifakis EG, Balkizas T, Nikita KS. Using the Hough transform to segment ultrasound images of longitudinal and transverse sections of the carotid artery. Ultrasound in Medicine & Biology. 2007;33:1918-1932.

227.    Mendizabal-ruiz G, Rivera M, Kakadiaris IA. A probabilistic segmentation method for the identification of luminal borders in intravascular ultrasound images. IEEE Conference on Computer Vision and Pattern Recognition. 2008.

228.    Yang X, Ding M, Lou L, Yuchi M, Qiu W, Sun Y. Common Carotid Artery Lumen Segmentation in B-mode Ultrasound Transverse View Images. International Journal of Image Graphics and Signal Processing. 2011;5:15-21.

229.    Bellman RE, Dreyfus SE. Applied dynamic programming, by Richard E. Bellman and Stuart E. Dreyfus. Princeton, N.J., Princeton University Press; 1962.

230.    Noble JA, Boukerroui D. Ultrasound Image Segmentation: A Survey. IEEE Transactions on Medical Imaging. 2006;25:987-1010.

231.    Ramnarine KV, Kanber B, Panerai RB. Assessing the performance of vessel wall tracking algorithms: the importance of the test phantom. Journal of Physics Conference Series. 2004;1:199-204.

232.    Claridge MW, Bate GR, Dineley JA, Hoskins PR, Marshall T, Adam DA, et al. A reproducibility study of a TDI-based method to calculate indices of arterial stiffness. Ultrasound in Medicine & Biology. 2007;34:215-220.

233.    Teirlinck CJP, Bezemer RA, Kollmann C, Lubbers J, Hoskins PR, Ramnarine KV, et al. Development of an example flow test object and comparison of five of these test objects, constructed in various laboratories. Ultrasonics. 1998;36:653-660.

234.    Ramnarine KV, Nassiri DK, Hoskins PR, Lubbers J. Validation of a new blood-mimicking fluid for use in Doppler flow test objects. Ultrasound in Medicine & Biology. 1998;24:451-459.

235.    Ramnarine KV, Hoskins PR, Routh HF, Davidson F. Doppler backscatter properties of a blood-mimicking fluid for Doppler performance assessment. Ultrasound in Medicine & Biology. 1999;25:105-110.

236.    Germond L, Bonnefous O, Loupas T. Quantitative assessment of the artery dilation measurements with an arterial phantom. IEEE Ultrasonics Symposium. 2001.

237.    Matlab Central File Exchange. Region Growing (2D/3D greyscale). 2011.

238.    Kanber B, Hartshorne TC, Horsfield MA, Naylor AR, Robinson TG, Ramnarine KV. Dynamic variations in the ultrasound greyscale median of carotid artery plaques. Cardiovascular Ultrasound. 2013;11:21.

239.    Olshansky B, Collins SM, Skorton DJ, Prasad NV. Variation of left ventricular myocardial gray level on two-dimensional echocardiograms as a result of cardiac contraction. Circulation. 1984;70:972-977.

240.    Grant EG, Benson CB, Moneta GL, Alexandrov AV, Baker JD, Bluth EI, et al. Carotid artery stenosis: gray-scale and Doppler US diagnosis--Society of Radiologists in Ultrasound Consensus Conference. Radiology. 2003;229:340-346.

241.    Jansen M, Van Alfen N, Nijhuis Van Der Sanden MWG, Van Dijk JP, Pillen S, De Groot IJM. Quantitative muscle ultrasound is a promising longitudinal follow-up tool in Duchenne muscular dystrophy. Neuromuscular Disorders. 2012;22:306-317.

242.    Lewis JP. Fast Normalized Cross-Correlation. Vision Interface. 1995.

243.    Kanber B, Hartshorne TC, Horsfield MA, Naylor AR, Robinson TG, Ramnarine KV. Quantitative assessment of carotid plaque surface irregularities and correlation to cerebrovascular symptoms. Cardiovascular Ultrasound. 2013;11:38.

244.    Leary DH, Holen J, Ricotta JJ, Roe S, Schenk EA. Carotid bifurcation disease: prediction of ulceration with B-mode US. Radiology. 1987;162:523-525.

245.    Muraki M, Mikami T, Yoshimoto T, Fujimoto S, Tokuda K, Kaneko S, et al. New criteria for the sonographic diagnosis of a plaque ulcer in the extracranial carotid artery. American Journal of Roentgenology. 2012;198:1161-1166.

246.    Schminke U, Motsch L, Hilker L, Kessler C. Three-dimensional ultrasound observation of carotid artery plaque ulceration. Stroke. 2000;31:1651-1655.

247.    Sitzer M, Müller W, Rademacher J, Siebler M, Hort W, Kniemeyer HW, et al. Color-flow Doppler-assisted duplex imaging fails to detect ulceration in high-grade internal carotid artery stenosis. Journal of Vascular Surgery. 1996;23:461-465.

248.    Steinke W, Hennerici M, Rautenberg W, Mohr JP. Symptomatic and asymptomatic high-grade carotid stenoses in Doppler color-flow imaging. Neurology. 1992;42:131-138.

249.    Young N, Soo YS, Fischer P. Comparison of duplex ultrasound with angiography in assessment of carotid bifurcation disease. Australasian Radiology. 1992;36:54-58.

250.	Aburahma AF, Covelli MA, Robinson PA, Holt SM. The role of carotid duplex ultrasound in evaluating plaque morphology: potential use in selecting patients for carotid stenting. Journal of Endovascular Surgery. 1999;6:59-65.

251.	Kessler C, Von Maravic M, Brückmann H, Kömpf D. Ultrasound for the assessment of the embolic risk of carotid plaques. Acta Neurologica Scandinavica. 1995;92:231-234.

252.	Manolio TA, Burke GL, Leary DH, Evans G, Beauchamp N, Knepper L, et al. Relationships of cerebral MRI findings to ultrasonographic carotid atherosclerosis in older adults : the Cardiovascular Health Study. CHS Collaborative Research Group. Arteriosclerosis Thrombosis and Vascular Biology. 1999;19:356-365.

253.	Pedro LM, Pedro MM, Gonçalves I, Carneiro TF, Balsinha C, Fernandes R, et al. Computer-assisted carotid plaque analysis: characteristics of plaques associated with cerebrovascular symptoms and cerebral infarction. European Journal of Vascular and Endovascular Surgery. 2000;19:118-123.

254.	Ding S, Zhang M, Zhao Y, Chen W, Yao G, Zhang C, et al. The role of carotid plaque vulnerability and inflammation in the pathogenesis of acute ischemic stroke. American Journal of the Medical Sciences. 2008;336:27-31.

255.	Denzel C, Fellner F, Wutke R, Bazler K, Müller K, Lang W. Ultrasonographic analysis of arteriosclerotic plaques in the internal carotid artery. European Journal of Ultrasound. 2003;16:161-167.

256.	Gaunt ME, Brown L, Hartshorne T, Bell PR, Naylor AR. Unstable carotid plaques: preoperative identification and association with intraoperative embolisation detected by transcranial Doppler. European Journal of Vascular and Endovascular Surgery. 1996;11:78-82.

257.	Rubin JR, Bondi JA, Rhodes RS. Duplex scanning versus conventional arteriography for the evaluation of carotid artery plaque morphology. Surgery. 1987;102:749-755.

258.	Widder B, Paulat K, Hackspacher J, Hamann H, Hutschenreiter S, Kreutzer C, et al. Morphological characterization of carotid artery stenoses by ultrasound duplex scanning. Ultrasound in Medicine and Biology. 1990;16:349-354.

259.	Wolverson MK, Bashiti HM, Peterson GJ. Ultrasonic tissue characterization of atheromatous plaques using a high resolution real time scanner. Ultrasound in Medicine and Biology. 1983;9:599-609.

260. Comerota AJ, Katz ML, White JV, Grosh JD. The preoperative diagnosis of the ulcerated carotid atheroma. Journal of Vascular Surgery. 1990;11:505-510.

261. European Carotid Plaque Study Group. Carotid artery plaque composition--relationship to clinical presentation and ultrasound B-mode imaging. European Journal of Vascular and Endovascular Surgery. 1995;10:23-30.

262. Prabhakaran S, Rundek T, Ramas R, Elkind MSV, Paik MC, Boden-albala B, et al. Carotid plaque surface irregularity predicts ischemic stroke: the northern Manhattan study. Stroke. 2006;37:2696-2701.

263. Tegos TJ, Kalomiris KJ, Sabetai MM, Kalodiki E, Nicolaides AN. Significance of sonographic tissue and surface characteristics of carotid plaques. American Journal of Neuroradiology. 2001;22:1605-1612.

264. Chiu B, Beletsky V, Spence JD, Parraga G, Fenster A. Analysis of carotid lumen surface morphology using three-dimensional ultrasound imaging. Physics in Medicine and Biology. 2009;54:1149-1167.

265. Fenster A, Blake C, Gyacskov I, Landry A, Spence JD. 3D ultrasound analysis of carotid plaque volume and surface morphology. Ultrasonics. 2006;44 Suppl 1:E153-E157.

266. Kanber B, Hartshorne TC, Horsfield MA, Naylor AR, Robinson TG, Ramnarine KV. Wall motion in the stenotic carotid artery: association with greyscale plaque characteristics, the degree of stenosis and cerebrovascular symptoms. Cardiovascular Ultrasound. 2013;11:37.

267. Ramnarine KV, Garrard JW, Dexter K, Nduwayo S, Panerai RB, Robinson TG. Shear wave elastography assessment of carotid plaque stiffness: in-vitro reproducibility study. Ultrasound in Medicine and Biology (in Press). 2013.

268. Dijk JM, Van Der Graaf Y, Grobbee DE, Banga JD, Bots ML. Increased arterial stiffness is independently related to cerebrovascular disease and aneurysms of the abdominal aorta: the Second Manifestations of Arterial Disease (SMART) Study. Stroke. 2004;35:1642-1646.

269. Leone N, Ducimetière P, Gariépy J, Courbon D, Tzourio C, Dartigues J, et al. Distension of the carotid artery and risk of coronary events: the three-city study. Arteriosclerosis Thrombosis and Vascular Biology. 2008;28:1392-1397.

270. Agabiti-rosei E, Muiesan ML. Carotid atherosclerosis, arterial stiffness and stroke events. Advances in Cardiology. 2006;44:173-186.

271.   Rothwell PM. Carotid artery disease and the risk of ischaemic stroke and coronary vascular events. Cerebrovascular Diseases. 2000;10 Suppl 5:21-33.

272.   Lenzi GL, Vicenzini E. The ruler is dead: an analysis of carotid plaque motion. Cerebrovascular Diseases. 2006;23:121-125.

273.   Kashiwazaki D, Yoshimoto T, Mikami T, Muraki M, Fujimoto S, Abiko K, et al. Identification of high-risk carotid artery stenosis: motion of intraplaque contents detected using B-mode ultrasonography. Journal of Neurosurgery. 2013;117:574-578.

274.   Kume S, Hama S, Yamane K, Wada S, Nishida T, Kurisu K. Vulnerable carotid arterial plaque causing repeated ischemic stroke can be detected with B-mode ultrasonography as a mobile component: Jellyfish sign. Neurosurgical Review. 2011;33:419-430.

275.   Giannattasio C, Failla M, Emanuelli G, Grappiolo A, Boffi L, Corsi D, et al. Local effects of atherosclerotic plaque on arterial distensibility. Hypertension. 2001;38:1177-1180.

276.   Lee KW, Wood NB, Xu XY. Ultrasound image-based computer model of a common carotid artery with a plaque. Medical Engineering & Physics. 2004;26:823-840.

277.   Hsu H, Chen Y, Sheu WH, Sheng W, Chao A. Comparison of brachial artery flow-mediated vasodilatation in symptomatic and asymptomatic patients with carotid arterial stenosis. The American Journal of Cardiology. 2002;90:814-816.

278.   Paini A, Boutouyrie P, Calvet D, Zidi M, Agabiti-rosei E, Laurent S. Multiaxial mechanical characteristics of carotid plaque: analysis by multiarray echotracking system. Stroke. 2006;38:117-123.

279.   Beaussier H, Naggara O, Calvet D, Joannides R, Guegan-massardier E, Gerardin E, et al. Mechanical and structural characteristics of carotid plaques by combined analysis with echotracking system and MR imaging. JACC. Cardiovascular Imaging. 2011;4:468-477.

280.   Long Q, Xu XY, Ramnarine KV, Hoskins P. Numerical investigation of physiologically realistic pulsatile flow through arterial stenosis. Journal of Biomechanics. 2001;34:1229-1242.

281.   Meagher S, Poepping TL, Ramnarine KV, Black RA, Hoskins PR. Anatomical flow phantoms of the nonplanar carotid bifurcation, part II: experimental validation with Doppler ultrasound. Ultrasound in Medicine & Biology. 2007;33:303-310.

282. Watts DM, Sutcliffe CJ, Morgan RH, Meagher S, Wardlaw J, Connell M, et al. Anatomical flow phantoms of the nonplanar carotid bifurcation, part I: computer-aided design and fabrication. Ultrasound in Medicine & Biology. 2007;33:296-302.

283. Schmidt-trucksäss A, Grathwohl D, Schmid A, Boragk R, Upmeier C, Keul J, et al. Structural, functional, and hemodynamic changes of the common carotid artery with age in male subjects. Arteriosclerosis Thrombosis and Vascular Biology. 1999;19:1091-1097.

284. Kanters SD, Elgersma OE, Banga JD, Van Leeuwen MS, Algra A. Reproducibility of measurements of intima-media thickness and distensibility in the common carotid artery. European Journal of Vascular and Endovascular Surgery the Official Journal of the European Society for Vascular Surgery. 1998;16:28-35.

285. Godia EC, Madhok R, Pittman J, Trocio S, Ramas R, Cabral D, et al. Carotid artery distensibility: a reliability study. Journal of Ultrasound in Medicine Official Journal of the American Institute of Ultrasound in Medicine. 2007;26:1157-1165.

286. Falk E. Why do plaques rupture? Circulation. 1992;86:III30-III42.

287. Hennerici MG. The unstable plaque. Cerebrovascular Diseases. 2004;17 Suppl 3:17-22.

288. Ogata T, Yasaka M, Wakugawa Y, Kitazono T, Okada Y. Morphological classification of mobile plaques and their association with early recurrence of stroke. Cerebrovascular Diseases. 2011;30:606-611.

289. Gastounioti A, Golemati S, Stoitsis JS, Nikita KS. Carotid artery wall motion analysis from B-mode ultrasound using adaptive block matching: in silico evaluation and in vivo application. Physics in Medicine and Biology. 2013;58:8647-8661.

290. Nasrabadi H, Pattichis MS, Fisher P, Nicolaides AN, Griffin M, Makris GC, et al. Measurement of motion of carotid bifurcation plaques. Proceedings of the IEEE International Conference on Bioinformatics & Bioengineering. 2012.

291. Teirlinck CJ, Bezemer RA, Kollmann C, Lubbers J, Hoskins PR, Ramnarine KV, et al. Development of an example flow test object and comparison of five of these test objects, constructed in various laboratories. Ultrasonics. 1998;36:653-660.

292. Ramnarine KV, Anderson T, Hoskins PR. Construction and geometric stability of physiological flow rate wall-less stenosis phantoms. Ultrasound in Medicine & Biology. 2001;27:245-250.

293. Ramnarine KV, Garrard JW, Dexter K, Nduwayo S, Panerai RB, Robinson TG. Shear wave elastography assessment of carotid plaque stiffness: in vitro reproducibility study. Ultrasound in Medicine & Biology. 2013;40:200-209.

294. Garrard JW, Ramnarine KV. Shear-Wave Elastography in Carotid Plaques: Comparison with Grayscale Median and Histological Assessment in an Interesting Case. Ultraschall in der Medizin. 2013.

295. Mayberg MR, Wilson SE, Yatsu F, Weiss DG, Messina L, Hershey LA, et al. Carotid endarterectomy and prevention of cerebral ischemia in symptomatic carotid stenosis. Veterans Affairs Cooperative Studies Program 309 Trialist Group. Journal of the American Medical Association. 1991;266:3289-3294.

296. Naylor AR, Rothwell PM, Bell PRF. Overview of the principal results and secondary analyses from the European and North American randomised trials of endarterectomy for symptomatic carotid stenosis. European Journal of Vascular and Endovascular Surgery. 2003;26:115-129.

297. Rothwell PM, Eliasziw M, Gutnikov SA, Fox AJ, Taylor DW, Mayberg MR, et al. Analysis of pooled data from the randomised controlled trials of endarterectomy for symptomatic carotid stenosis. Lancet. 2003;361:107-116.

298. Rothwell PM, Goldstein LB. Carotid endarterectomy for asymptomatic carotid stenosis: asymptomatic carotid surgery trial. Stroke. 2004;35:2425-2427.

299. Executive Committee for the Asymptomatic Carotid Atherosclerosis Study. Endarterectomy for asymptomatic carotid artery stenosis. Journal of the American Medical Association. 1995;273:1421-1428.

300. Halliday A, Mansfield A, Marro J, Peto C, Peto R, Potter J, et al. Prevention of disabling and fatal strokes by successful carotid endarterectomy in patients without recent neurological symptoms: randomised controlled trial. Lancet. 2004;363:1491-1502.

301. Naylor AR. Time to rethink management strategies in asymptomatic carotid artery disease. Nature Reviews Cardiology. 2012;9:116-124.

302. Chambers BR, Donnan GA. Carotid endarterectomy for asymptomatic carotid stenosis. The Cochrane Database of Systematic Reviews. 2005.

303. Conrad MF, Baloum V, Mukhopadhyay S, Garg A, Patel VI, Cambria RP. Progression of asymptomatic carotid stenosis despite optimal medical therapy. Journal of Vascular Surgery. 2013;58:128-35.E1.

304.    Hobson RW, Weiss DG, Fields WS, Goldstone J, Moore WS, Towne JB, et al. Efficacy of carotid endarterectomy for asymptomatic carotid stenosis. The Veterans Affairs Cooperative Study Group. The New England Journal of Medicine. 1993;328:221-227.

305.    Mayo Asymptomatic Carotid Endarterectomy Study Group. Results of a randomized controlled trial of carotid endarterectomy for asymptomatic carotid stenosis. Mayo Clinic Proceedings. 1992;67:513-518.

306.    Naylor AR, Golledge J. High risk plaque, high risk patient or high risk procedure? European Journal of Vascular and Endovascular Surgery. 2006;32:557-560.

307.    Mas J, Chatellier G, Beyssen B, Branchereau A, Moulin T, Becquemin J, et al. Endarterectomy versus stenting in patients with symptomatic severe carotid stenosis. The New England Journal of Medicine. 2006;355:1660-1671.

308.    Yadav JS, Wholey MH, Kuntz RE, Fayad P, Katzen BT, Mishkel GJ, et al. Protected carotid-artery stenting versus endarterectomy in high-risk patients. The New England Journal of Medicine. 2004;351:1493-1501.

309.    Ammirati E, Magnoni M, Camici PG. Need for new non-invasive imaging strategies to identify high-risk asymptomatic patients with carotid stenosis. International Journal of Cardiology. 2013;168:4342–4343.

310.    Spence JD. Asymptomatic carotid stenosis. Circulation. 2013;127:739-742.

311.    Afonso D, Seabra J, Suri JS, Sanches JM. A CAD system for atherosclerotic plaque assessment. Proceedings of the Annual International Conference of the IEEE Engineering in Medicine and Biology Society. 2013;2012:1008-1011.

312.    Nicolaides AN, Kakkos SK, Kyriacou E, Griffin M, Sabetai M, Thomas DJ, et al. Asymptomatic internal carotid artery stenosis and cerebrovascular risk stratification. Journal of Vascular Surgery. 2011;52:1486-1496.

313.    Kyriacou E, Nicolaides A, Pattichis CS, Petroudi S, Pattichis M, Griffin M, et al. First and second order statistical texture features in carotid plaque image analysis: preliminary results from ongoing research. Proceedings of the Annual International Conference of the IEEE Engineering in Medicine and Biology Society. 2012;2011:6655-6658.

314.    Mayor I, Momjian S, Lalive P, Sztajzel R. Carotid plaque: comparison between visual and grey-scale median analysis. Ultrasound in Medicine & Biology. 2003;29:961-966.

315.    Seabra J, Pedro LM, Fernandes JFE, Sanches J. Ultrasound Plaque Enhanced Activity Index for Predicting Neurological Symptoms. Pattern Recognition and Image Analysis. 2011;6669:184-191.

316.    Piliouras N, Kalatzis I, Theocharakis P, Dimitropoulos N, Cavouras D. Development of the probabilistic neural network–cubic least squares mapping (PNN–LSM3) classifier to assess carotid plaque's risk. Pattern Recognition Letters. 2004;25:249-258.

317.    Seabra J, Pedro LM, Fernandes J, Sanches J. Ultrasonographic characterization and identification of symptomatic carotid plaques. Proceedings of the Annual International Conference of the IEEE Engineering in Medicine and Biology Society. 2011;2010:6110-6113.

318.    Kyriacou EC, Petroudi S, Pattichis CS, Pattichis MS, Griffin M, Kakkos S, et al. Prediction of high-risk asymptomatic carotid plaques based on ultrasonic image features. IEEE Transactions on Information Technology in Biomedicine. 2013;16:966-973.

319.    Acharya UR, Mookiah MRK, Vinitha Sree S, Afonso D, Sanches J, Shafique S, et al. Atherosclerotic plaque tissue characterization in 2D ultrasound longitudinal carotid scans for automated classification: a paradigm for stroke risk assessment. Medical & Biological Engineering & Computing. 2013;51:513-523.